The University Of Sheffield.

Bacterial nitric oxide metabolism in the pathogenesis of meningococcal sepsis

A Thesis Submitted for the Degree of Doctor of Philosophy

Author: Md. Risat ul Haque

Supervisor: Professor Robert Charles Read

Department of Infection and Immunity
University of Sheffield Medical School
University of Sheffield
United Kingdom
September 2015

Declaration

The research presented in this thesis is the work of the candidate with the following exceptions:

Chapter 3: Intraperitoneal injection of bacteria, handling of animal and euthanisation of mice were kindly carried out by Dr Jay Laver.

Chapter 5: Human primary airway epithelial cells (HPECs) were kindly provided by Dr Cornelia Blume and Natalie Smithers.

Acknowledgements

I cann't help but to write a big acknowledgement section as it would be very unfair to submit this thesis without acknowledging the people who have helped me to get to this stage. First and foremost I would like to thank my mentor, guide, supervisor and a man of fatherly stature to me, Professor Rob Read for everything you have done for me. I would never have got here without your help and support. Most importantly for believing in me till the end when I did not want to myself. Then special thanks must go to Dr Jay Laver for introducing me to the titillating and tantalising world of nitric oxide. Your support and supervision during my project was pivotal for me in reaching this stage. A super special thanks must go to Dr Martina Daly and the postgraduate research and innovation team at the University of Sheffield for dealing with my extenuating circumstances. I would like to wholeheartedly thank the University of Sheffield for awarding me the Scholarship for pursuing this project which has been a life changing experience for me. Then I would like to thank Dr Ed Guccione, my Cloning Guru and also a wonderful person for your support. I don't know how much I have been able to make use of your training but I can assure you I have tried my best regardless of the circumstances! I must give special thanks to Katie Cooke for ordering so many staff for me during my project. I would also like to heartfully thank all the technicians and managers (the unsung heroes/heroines of Science) at the Sheffield Medical School whom I have annoyed many times especially during the big move to Southampton. For taking the daily share of mad scientist's agony and the rarest moment of glory (if there was any!) I would like to thank my friends at the Department of Infection and Immunity, Dr Laura Harrison, Dr Lorena Preciado-Llanes, Dr Richard Jones, Dr Manal Almahmeed, Dr Martin Bewley, Dr Tessabelle Sultana, Dr Jamil Jubrail, Dr Jennifer Parker, Jenny, Daniel, Tom. Then I would like to especially thank Dr Cornelia Blume at Southampton for introducing me to the world of Asthma and COPD!! Thank you very much for all the help you have given me. Special thanks must also go to Dr Emily Swindle and Natalie Smithers for your kind help. I am really grateful to Sara Hughes and Dr Ray Allan at NHS Southampton for introducing me to the world of biofilm. I would like to thank all the people in the Department of 'Molecular Microbiology' at the University of Southampton for your help with special mention to Dr Andrew Vaughan, Dr Colette O'Neill, Emma, Anish, Zoe, Dr Myron Christodoulides. I would also take this opportunity to thank Prof Gow, Prof Stansfield and Prof Brown at Aberdeen for giving me the opportunity to do science in your labs. I would not have been here without your guidance that I received during those projects.

I would like to thank my friend Erhan (Ibis!) who have always stood beside me regardless of the circumstances. I know our friendship will remain firm no matter what direction we take in life. Then I would heartfully like to thank Rashed bhai, Kayes bhai, Sabah, David, Imran, Simon, Alia Apu and Arif bhai for letting me stay in your house when I was badly in need of shelter. When I was suffering from depression, I was fortunate to have epic people like Rahat bhai, Sadat bhai, Parosh bhai, Cherry bhabi, Sami bhai, Salehin, Gazi bhai, Tipu uncle and Dr Hafiz who have sacrificed their own time to provide me support. It is said adversity exposes your genuine well-wishers. I could not have felt it more and will always be grateful in life for the support you provided at that time. I would like to thank my special friends from the school with whom not only have I shared some wonderful memories but also from whom I have learnt so many inspirational things in life. I would also like to thank all the people from my school administration who have worked round the clock to nurture us. I am also grateful to the men and women I have come across around the world for teaching me so many important things in life.

Then the people I have considered as my guardian during my stay in the UK, Raju uncle and Rushmi aunty for time and again keeping up with my bizarre circumstances! I would have been no way near this stage if it was not for your sacrifice and support. I would also like to thank my wonderful relatives who have been so nice towards me and were beside me whenever necessary. Special thanks must go to my grandmother for being so supportive throughout my journey. It's turn for the people who matter most to me on this planet. Dad, sometimes I wish if I had 10% of your vision, calmness under pressure, integrity and intelligence. You are a true inspiration to me and thanks for showing us all that you can achieve anything in your life no matter where you begin from. It is said that having a sister is one of the best blessings you can have. Nobody can appreciate it more than me. I am really proud of the way you have nurtured yourself despite receiving minimal support. Despite a considerable age difference, I really enjoy the banters with you and looking forward to more of those!! First thing that comes to my mind when I think about my mom, how can someone be so simple and innocent! You would never know how much I have missed your supportive voice over the phone for the last couple of years. I love you ma, truly, madly, deeply! This work is dedicated to you.

Table of contents

1 Chapter 1: Introduction 18

1.1 History and a brief overview of Neisseria meningitidis 18
1.2 Genetics of Neisseria meningitidis 21
1.3 Classification of Neisseria meningitidis 21
1.4 Transmission, carriage and epidemiology of Neisseria meningitidis 22
1.5 Clinical representation and diagnosis of meningococcal disease 25
1.6 Pathological events of meningococcal sepsis 26
1.6.1 Increased vascular permeability 26
1.6.2 Pathophysiological vasodilation and vasoconstriction 26
1.6.3 Intravascular thrombosis and coagulation 27
1.6.4 Severe myocardial dysfunction 27
1.7 Mechanisms of colonisation and cellular invasion by N. meningitidis 28
1.8 Nitric oxide: a brief history and overview 33
1.9 Formation of NO and S-nitrosothiol 35
1.10 S-nitrosohaemoglobin: an important protein in vasodilation 39
1.11 Biological roles of NO 39
1.11.1 NO as EDRF 39
1.11.2 NO in infection and as an antimicrobial agent 40
1.12 Respiratory pathway of Neisseria meningitidis 42
1.13 Essential enzymes and proteins of meningococcal respiratory pathway 45
1.13.1 AniA (Nitrite Reductase) 45
1.13.2 NorB (Nitric oxide reductase) 46
1.13.3 NsrR (Nitrite sensing repressor protein) 47
1.13.4 FNR- (Fumarate and nitrite reductase regulator) 47
1.13.5 NarQ/NarP- Nitrite response sensor/regulator 48
1.14 Regulation of transcriptional control of meningococcal partial denitrification pathway 48
1.15 Importance of meningococcal NO metabolism on host-pathogen interactions 52
1.16 Aims and Objectives 54

2 Chapter 2: Materials and Methods 55

2.1 Reagents 55
2.1.1 Antifoaming agent FG-10 55
2.1.2 Complete, Mini EDTA-free protease inhibitor cocktail tablets 55
2.1.3 Drabkin's solution 55
2.1.4 Human holo transferrin (hHTF) 55
2.1.5 Polymerase chain reaction primers 55
2.2 Buffers 55
2.2.1 Phosphate buffered saline (PBS) at pH 7.4 55
2.2.2 S-nitrosothiol compatible lysis buffer 55
2.2.3 50 mM Phosphate buffer + 1 mM DTPA, pH 7.4 56
2.3 Solutions 56
2.3.1 100 mM Sulphanilamide in 2 N HCl 56
2.3.2 50 mM Mercury (II) chloride ($HgCl_2$) 56
2.3.3 Hanks Balanced Salt Solution (HBSS) without Ca^{2+} or Mg^{2+} 56
2.3.4 Tri-iodide (I_3^-) reaction mixture 56
2.3.5 Preparation of S-nitrosoglutathione (GSNO) 56

2.3.6 RF1 solution for competent cell 57
2.3.7 RF2 solution for competent cell 57
2.3.8 Spermine NONOate 57
2.4 Bacterial Culture Techniques 57
2.4.1 Columbia Blood Agar 57
2.4.2 GC Agar 57
2.4.3 LB Media 57
2.4.4 LB Agar 58
2.4.5 Mueller Hinton Broth 58
2.4.6 Maintenance and growth of bacterial cultures 58
2.4.7 Propagation of viable N. meningitidis 61
2.4.8 Broth Culture of N. meningitidis 61
2.4.9 Counting and manipulation of bacterial numbers for experiments 61
2.5 Infection of mice and preparation of liver lysates and whole blood samples from the murine model of fulminant meningococcal sepsis 62
2.5.1 Infection of mice 62
2.5.2 Severity score for meningococcal sepsis 62
2.5.3 Preparation of liver lysates 64
2.5.4 Preparation of plasma from C57BI/6 mouse blood 64
2.5.5 Preparation of stabilisation solution for SNO haemoglobin 64
2.5.6 Preparation of SNO haemoglobin from mouse blood 65
2.5.7 Measurement of heme concentration 65
2.6 Chemiluminescence Techniques 66
2.6.1 Analysis of S-nitrosothiol, nitrite (NO_2^-) and nitrate (NO_3^-) concentrations 66
2.6.1.1 Calibration of GSNO solutions of known concentration 66
2.6.1.2 Ozone-based Chemiluminescence 66
2.6.2 Measurement of samples by triiodide (I_3^-) dependant, ozone-based chemiluminescence 67
2.6.3 Measurement of samples by Vanadium (III) Chloride (VCl_3) dependant ozone-based chemiluminescence 67
2.6.4 Injection of samples into the purging vessel 68
2.6.5 Analysing chemiluminescence data using the Origin 8.1 program 68
2.7 Statistics 68
2.8 Immunological Techniques 69
2.8.1 IL-8 and TNFα cytokine measurement by ELISA 69
2.9 Cell Culture Techniques 70
2.9.1 Consumables 70
2.9.2 Reagents 70
2.9.3 Preparation of reagents for ALI medium 70
2.9.3.1 Collagen I solution (1:100) 70
2.9.3.2 BSA stock (1.5mg/ml) for 2x ALI medium 70
2.9.3.3 Preparation of 2x BEGM medium 71
2.9.3.4 Recipe for preparation of DMEM for 1x ALI medium 71
2.9.3.5 Preparation of Retinoic acid (all-trans RA) $5x10^{-5}$ M (50 µM) 71
2.9.3.6 Preparation of 1x ALI media 72
2.9.4 Methods for the establishment and maintenance of ALI cultures 72
2.9.4.1 Collection of HPEC after bronchoscopy 72
2.9.4.2 Preparation of a cell suspension 72
2.9.4.3 Preparation of the transwell trays (Day 0) 72
2.9.4.4 Taking transwells to air-liquid interphase day 1 73

2.9.4.5 Points to consider for growing and maintaining ALI culture 73
2.9.4.6 Continuous feeding of ALI cultures DAY 2-21 onwards 73
2.9.4.7 Transepithelial resistance (TER) measurement (day 7, 14, 21) 74
2.9.4.8 Counting the cells prior to the experiment 75
2.10 Biochemical Techniques 75
2.10.1 Measurement of NO_2^- by Griess Assay 75
2.10.2 Glutathione peroxidase assay 77
2.10.3 Measurement of Transepithelial cell resistance (TER) 77
2.10.4 Determination of Protein Concentration 78
2.11 Molecular Biology Techniques 78
2.11.1 Preparation of DH5α Cells 78
2.11.2 Transformation of E. coli DH5α competent cells with DNA 78
2.11.3 Primers 79
2.11.4 Preparation of Isocloning buffer 82
2.11.5 DNA quantification by NanoDrop 82
2.11.6 Bacterial genomic DNA extraction 83
2.11.7 PCR Purification 84
2.11.8 Plasmid DNA extraction 84
2.11.9 Restriction digest 85
2.11.10 DNA Ligation 85
2.11.11 Phosphatase treatment 86
2.11.12 Broth culture transformation of N. meningitidis 86
2.11.13 Spot transformation of N. meningitidis 87
2.11.14 Agarose gel electrophoresis 87
2.11.15 PCR reactions 87
2.11.15.1 Colony PCR 87
2.11.15.2 My Taq Red Mix 88
2.11.15.3 ACCUZYME DNA polymerase 89
2.11.15.4 NEB Phusion^R high-fidelity Master Mix with HF buffer 90
2.11.15.5 Q5 High Fidelity DNA Polymerase 91
3 Chapter 3: Role of denitrification of *N. meningitidis* in the homeostasis of NO metabolites in a murine model of early fulminant meningococcal sepsis 92
3.1 Introduction 92
3.2 Ozone based chemiluminescence and NO analyser 94
3.3 Measurement of NO metabolites by chemiluminescence 97
3.4 Considerations for preparation of biological samples for chemiluminescence 100
3.5 Results 102
3.5.1 Establishing a murine model of early fulminant meningococcal sepsis 102
- *A high bacterial inocula (10^9) causes severe bacteraemia in a murine model of meningococcal septicaemia within 6 hour 102*
- *NO metabolite concentrations in liver homogenate and whole blood are not differentially affected by meningococcal NO detoxification 102*

3.5.1.1 Rationale and methods 102
3.5.1.2 Results 104
3.5.2 Refining the murine model of acute meningococcal sepsis 112
- *Inclusion of human holo transferrin induces prolonged sepsis with a lower dosage of bacterial inocula (10^7) 112*

- *Bacterial NO denitrification pathway does not affect the production of NO metabolites in liver and whole blood* *112*
- *Bacterial burden correlates with increased Plasma SNO, increased hepatic NO_2^- and decreased hepatic NO_x* *112*

3.5.2.1 Rationale and methods *112*
3.5.2.2 Results *114*
3.5.3 Attempting to bolster the SNO signal from the murine model of meningococcal sepsis with LPS *121*

- *Inclusion of LPS along with human holo transferrin increases the sepsis severity* *121*
- *In the presence of LPS and human holo transferrin, bacterial infection still does not result in a differential profile of NO metabolites with regards to NO denitrification machinery in whole blood and liver* *121*

3.5.3.1 Rationale and methods *121*
3.5.3.2 Results *122*
3.6 Discussion ***128***

4 Chapter 4: Creation and characterisation of a set of denitrification gene mutants (Δ*aniA*/Δ*norB*, Δ*nsrR*/Δ*norB*, Δ*aniA*/Δ*norB*/Δ*nsrR*) **133**

4.1 Introduction ***133***
4.2 Results ***134***
4.2.1 Creation of ΔaniA/ΔnorB/ΔnsrR (ΔTriple) mutant *134*
4.2.1.1 Rationale and methods *134*
4.2.1.2 Results *137*
4.2.2 Creation of ΔaniA/ΔnorB and ΔnsrR/ΔnorB double mutants *144*
4.2.2.1 Rationale and methods *144*
4.2.2.2 Results *144*
4.2.3 Investigation of polar effect of gene deletion of norB in the newly created ΔaniA/ΔnorB/ΔnsrR *148*
4.2.3.1 Rationale and methods *148*
4.2.3.2 Results *149*
4.2.4 Growth characteristics of strains in aerobic condition *151*
4.2.4.1 Rationale and methods *151*
4.2.4.2 Results *151*
4.2.5 Characterisation of metabolism of the mutant strains in presence of $NaNO_2$ *153*
4.2.5.1 Rationale and methods *153*
4.2.5.2 Results *153*
4.2.6 Characterisation of metabolism by mutant strains in the presence of an NO donor, Spermine NONOate *157*
4.2.6.1 Rationale and methods *157*
4.2.6.2 Results *157*
4.3 Discussion ***160***

5 Chapter 5: Effect of meningococcal NO metabolism on the regulation of barrier function and innate immune response in human primary bronchial airway epithelial cells **165**

5.1 Introduction ***165***
5.2 Differentiated, human primary bronchial airway epithelial cell at air-liquid interface (HPEC-ALI) ***166***
5.2.1 HPEC-ALI as physical barrier *167*

5.2.2 HPEC-ALI as chemical barrier 169
5.2.3 HPEC-ALI as an immunological barrier 169
5.3 Results 171
5.3.1 Infection of HPEC-ALI with N. meningitidis results in a decreased TER and increased cytokine release but meningococcal NO metabolism does not differentially regulate the TER and cytokine release 171
5.3.1.1 Rationale and methods 171
5.3.1.2 Results 172
5.3.2 Induction of HPEC-ALI with a slow releasing NO donor SNAP (S-Nitroso-N-acetyl-DL-Penicillamine) does not affect the TER and cytokine profile of HPEC-ALI in relation to meningococcal NO denitrification pathway 181
5.3.2.1 Rationale and methods 181
5.3.2.2 Results 182
5.4 Discussion 188
6 Chapter 6: Effect of meningococcal denitrification on biofilm formation *in vitro* 191
6.1 Introduction 191
6.2 Bacterial biofilm formation and NO 191
6.3 Results 193
6.3.1 The absence of denitrification pathway affects meningococcal biofilm formation in vitro 193
6.3.1.1 Rationale and methods 193
6.3.1.2 Results 194
6.3.2 Reverse complementation of ΔaniA under the control of an IPTG inducible promoter 198
6.3.2.1 Rationale and methods 198
6.3.2.2 Results 199
6.3.3 aniA activity is not restored in the newly created IPTG inducible ΔaniA/aniA^{IPTG+} strain 204
6.3.3.1 Rationale and methods 204
6.3.3.2 Results 204
6.3.4 Reverse complementation of aniA under the control of its endogenous promoter 207
6.3.4.1 Rationale and methods 207
6.3.4.2 Results 208
6.3.5 aniA activity is restored in the ΔaniA/aniA^{+} strain where aniA was complemented along with its endogenous promoter and upstream regulatory elements 215
6.3.5.1 Rationale and methods 215
6.3.5.2 Results 215
6.4 Discussion 218
7 Chapter 7: General Discussion 221
8 Chapter 8: References 227

Please refer to the attached CD-ROM for accessing the comprehensive data set from this project

Table of Figures

Figure 1.1 A) Image of diplococcus *Neisseria meningitidis* and B) Picture of a patient suffering from meningococcal infection 20
Figure 1.2 Epidemiology of the meningococcal disease 24
Figure 1.3 Depiction of colonisation and invasion by *N. meningitidis.* 31
Figure 1.4 Outer membrane structures of *N. meningitidis* important for the bacterial interaction with the epithelial cells and pathogenesis. 32
Figure 1.5 Mechanisms of NO, SNO production and decomposition. 37
Figure 1.6 Reaction and impact of NO at various concentrations in biology. 38
Figure 1.7 Denitrification pathway and meningococcal respiratory chain 44
Figure 1.8 Sophisticated environmental and transcriptional regulation of denitrification pathway of *N. meningitidis*. 51
Figure 2.1 Progression of HPEC-ALI culture over a period of 21 days. 74
Figure 2.2 Chemical interactions involved in the measurement of NO_2^- using the Griess Reagent System. 76
Figure 3.1 A cartoon summarising the apparatus set up for NO measurement by ozone based chemiluminescence. 96
Figure 3.2 Schematic summarising the processes involved in the measurement of NO metabolites by I_3^- based chemiluminescence. 99
Figure 3.3 Workflow of experimental procedures for the measurement of NO metabolites in a murine model of early fulminant meningococcal sepsis 107
Figure 3.4 Severity scoring data in 7-10 week old female C57BI6 mice infected with 10^9 bacteria/mouse suspended in PBS over the course of 6 hours A) PBS B) Wt and C) Δ*norB.* 108
Figure 3.5 Viable bacteria recovered from inocula (A), whole blood output (B), and liver lysates (C) after experiment in murine model infected with 10^9 bacteria/mouse in PBS for 6 hours. 109
Figure 3.6 Measurement of plasma NOx (A), NO_2^- (B), SNO (C) and SNO-Hb (D) in mice infected with 10^9 bacteria + PBS for 6 hours. 110
Figure 3.7 Measurement of Liver NO_2^- (A), SNO (B) in mice infected with 10^9 bacteria suspended in PBS for 6 hours. 111
Figure 3.8 Confirmation of meningococcal sepsis by severity scoring in 7-10 weeks old female C57BI6 mice infected with 10^7 bacteria/mouse suspended in PBS + 8 mg hTf for 8 hours A) Wt, B) Δ*norB* and C) *nsrR.* 116
Figure 3.9 Viable bacteria recovered from inocula (A), whole blood output (B) and liver lysates output (C) in the murine model infected with PBS + 8 mg hTf + 10^7 bacteria/mouse for 8 hours. 117
Figure 3.10 Measurement of plasma NO_x (A), NO_2^- (B), SNO (C) and SNO-Hb (D) in mice infected with PBS + 8 mg hTf + 10^7 bacteria for 8 hours. 118
Figure 3.11 Measurement of Liver NO_x (A), NO_2^- (B), SNO (C) in mice infected with 10^7 bacteria suspended in PBS + 8 mg hTf for 8 hours. 119
Figure 3.12 Statistically significant correlation between recovered bacterial burden and Plasma SNO A), Liver lysate NO_2^- B) and Liver lysate NO_x C) in the PBS + hTf + 10^7 bacteria/mouse supplemented sepsis model. 120

Figure 3.13 Confirmation of meningococcal sepsis by severity scoring in 7-10 weeks old female C57BI6 mice infected with 10^6 bacteria/mouse suspended in PBS + 25000 EU/g LPS + 8 mg hTf for 6 hours A) LPS + Htf, B) Wt, C) Δ*norB*, D) Δ*aniA* and E) HkWt (Heat killed Wt) 124
Figure 3.14 Viable bacteria recovered from inocula (A), whole blood output (B), and liver lysates output (C) in murine model infected with bolus injection of PBS + 25000 EU/g LPS + 8 mg human holo transferrin + 10^6 bacteria/mouse for 6 hours. 125
Figure 3.15 Measurement of plasma NOx (A), NO_2^- (B), SNO (C) and SNO-Hb (D) in mice infected with PBS + 25000 EU/g LPS + 8 mg hTf + 10^6 bacteria for 6 hours. 126
Figure 3.16 Measurement of Liver SNO (A) and NO_2^- (B) in mice infected with 10^6 bacteria suspended in PBS + 8 mg hTf + 25000 EU/g LPS for 6 hours. 127
Figure 4.1 Overview of Isothermal Assembly Cloning (ISA) method for generating Kanamycing resistant *norB* cassette in pGEM-3zf plasmid. 138
Figure 4.2 PCR amplification of *norBF1*, *norBF2* fragments and Kanamycin cassette. 139
Figure 4.3 Confirmation of HincII Digestion of pGEM-3zf plasmid. 140
Figure 4.4 Diagnostic PCR screening for selecting positive clones of the pGEM–3zf NK plasmid after transformation of isocloning ligation mix into the DH5α competent cells. 141
Figure 4.5 PCR amplification of *norBF1-Kan-norBF2* cassette from pGEM–3zf NK plasmid. 142
Figure 4.6 PCR confirmation of Δ*aniA/*Δ*norB/*Δ*nsrR (*Δ*Triple)* mutant creation. 143
Figure 4.7 PCR confirmation of Δ*aniA/*Δ*norB* mutant creation. 146
Figure 4.8 PCR confirmation of Δ*nsrR/*Δ*norB* mutant creation. 147
Figure 4.9 Investigation of polar effect of *norB* inactivation in Δ*aniA/*Δ*norB/*Δ*nsrR* on downstream GpxA activity. 150
Figure 4.10 Growth curve of the newly constructed mutant strains under normal aerobic condition. 152
Figure 4.11 Characterisation of the functional inactivation of the newly generated mutant strains in the presence of 5 mM $NaNO_2$. 155
Figure 4.12 Transition from oxidative respiration to denitrification in four identical cultures of *N. meningitidis* Wt MC58. 156
Figure 4.13 Characterisation of the functional inactivation of the newly generated mutant strains in the presence of 50 µM SpermineNONOate. 159
Figure 5.1 Differentiated bronchial airway epithelial cells with tight junction complex. 168
Figure 5.2 Methods for measuring TER, TNFα and IL-8 after infecting the HPEC-ALI culture with denitrification mutants of *N. meningitidis.* 175
Figure 5.3 Measurement of A) TER and B) Correlation graph for TER vs Ouput viable count of the differentiated HPEC-ALI infected with Wt, Δ*aniA/*Δ*norB*, Δ*aniA/*Δ*norB/*Δ*nsrR* (MOI 1-100). 176
Figure 5.4 Measurement of A) TNFα and B) Correlation graph for TNFα vs Output viable count of the differentiated HPEC-ALI infected with Wt, Δ*aniA/*Δ*norB,* Δ*aniA/*Δ*norB/*Δ*nsrR* (MOI 1-100). 177
Figure 5.5 Measurement of IL-8 release from the apical compartment of the differentiated HPEC-ALIs infected with Wt, Δ*aniA/*Δ*norB,* Δ*aniA/*Δ*norB/*Δ*nsrR* (MOI 1-100). 178
Figure 5.6 Measurement of IL-8 release from the basolateral compartment of the differentiated HPEC-ALIs infected with Wt, Δ*aniA/*Δ*norB,* Δ*aniA/*Δ*norB/*Δ*nsrR* (MOI 1-100). 179

Figure 5.7 A) Input and B) Output viable count from the differentiated HPEC-ALI infected with Wt, Δ*aniA/*Δ*norB*, Δ*aniA/*Δ*norB/*Δ*nsrR* at MOI 1-100. 180
Figure 5.8 Measurement of TER of the differentiated HPEC-ALI infected with Wt, Δ*aniA/*Δ*norB,* Δ*aniA/*Δ*norB/*Δ*nsrR* (MOI 100) in the presence of 500 µM SNAP. 183
Figure 5.9 Measurement of TNFα of the differentiated HPEC-ALIs infected with Wt, Δ*aniA/*Δ*norB,* Δ*aniA/*Δ*norB/*Δ*nsrR* (MOI 100) in the presence of 500 µM SNAP. 184
Figure 5.10 Measurement of IL-8 release from apical supernatants of the differentiated HPEC-ALIs infected with Wt, Δ*aniA/*Δ*norB,* Δ*aniA/*Δ*norB/*Δ*nsrR* (MOI 100) in the presence of 500 µM SNAP. 185
Figure 5.11 Measurement of IL-8 release from basal supernatants of the differentiated HPEC-ALIs infected with Wt, Δ*aniA/*Δ*norB,* Δ*aniA/*Δ*norB/*Δ*nsrR* (MOI 100) in the presence of 500 µM SNAP. 186
Figure 5.12 A) Input and B) Output viable count from the differentiated HPEC-ALI infected with Wt, Δ*aniA/*Δ*norB,* Δ*aniA/*Δ*norB/*Δ*nsrR* at MOI 100 in the presence of 500 µM SNAP. 187
Figure 6.1 Role of meningococcal denitrification on biofilm formation *in vitro* (24 hour) ..196
Figure 6.2 Role of meningococcal denitrification on biofilm formation *in vitro* (48 hour). .197
Figure 6.3 Testing of pGCC4 plasmid for reverse complementing Δ*aniA* under the control of an IPTG inducible promoter. 200
Figure 6.4 Diagnostic PCR for the selection of pGCC4::$aniA^{IPTG+}$ plasmid containing *aniA* coding region under the control of lac promoter 201
Figure 6.5 Amplification of *aspC* to *lctP* region along with *aniA* coding sequence under lac promoter from pGCC4::$aniA^{IPTG3+}$ for transforming into Δ*aniA*. 202
Figure 6.6 PCR confirmation of *aniA* restoration in Δ*aniA/*$aniA^{IPTG+}$ 203
Figure 6.7 Functional characterisation of the newly generated IPTG inducible Δ*aniA/*$aniA^{IPTG+}$ in the presence of $NaNO_2$ in microaerobic condition. 205
Figure 6.8 Functional characterisation of the newly generated IPTG inducible Δ*aniA/*$aniA^{IPTG+}$ in the presence of $NaNO_2$ in aerobic condition. 206
Figure 6.9 Testing of pGCC5 plasmid for complementing Δ*aniA* under the control of its endogenous promoter. 209
Figure 6.10 Sequence selected for reverse complementation of *aniA* along with its endogenous promoter and upstream regulatory protein (FNR, NsrR, FUR, NarP) binding sites. 210
Figure 6.11 Diagnostic restriction digest for selecting positive pGCC5::*aniA* plasmid. 211
Figure 6.12 Amplification of *aspC* to *lctP* region containing *aniA* with its upstream promoter region using pGCC5 :: $aniA^{2+}$ as template for transforming into Δ*aniA*. 212
Figure 6.13 Confirmation of positive colonies from the reverse complemented Δ*aniA/*$aniA^{+}$ under its native promoter by colony PCR. 213
Figure 6.14 PCR confirmation of the reverse complementation of Δ*aniA/*$aniA^{+}$ under its endogenous promoter region. 214
Figure 6.15 Functional characterisation of the newly generated complemented strain Δ*aniA/*$aniA^{+}$ in the presence of 5 mM $NaNO_2$ in microaerobic condition. 216
Figure 6.16 Transition from oxidative respiration to denitrification in the three out of four identical cultures of Δ*aniA/*$aniA^{+}$ 217

List of Tables

Table 2.1 Strains used for this project 58
Table 2.2 List of plasmids from the project 59
Table 2.3 Severity score assessment 63
Table 2.4 Recipe for preparation of BEGM for ALI media 71
Table 2.5 Recipe for preparation of DMEM for ALI medium 71
Table 2.6 Primers used for this project 79
Table 2.7 Preparation of Isothermal Buffer 82
Table 2.8 Preparation of Isothermal assembly buffer for final Isocloning reaction 82
Table 2.9 Recipe for Restriction digest 85
Table 2.10 Recipe for DNA ligation 85
Table 2.11 Control for ligation reactions 86
Table 2.12 PCR mix for My Taq Mix 88
Table 2.13 PCR cycling conditions for My Taq PCR 88
Table 2.14 PCR mix for Accuzyme polymerase 89
Table 2.15 PCR cycling conditions for Accuzyme DNA polymerase 89
Table 2.16 PCR mix for NEB phusion polymerase 90
Table 2.17 PCR cycling condition for NEB Phusion polymerase 90
Table 2.18 PCR recipe for Q5 DNA polymerase 91
Table 2.19 PCR cycling condition for Q5 DNA Polymerase 91
Table 3.1 Summary of NO metabolites output from mice infected with 10^9 bacteria/mouse suspended in PBS for 6 hours. Values are given as median, with interquartile range (IQR) in parentheses 106
Table 3.2 Summary of NO metabolites output from mice infected with 10^7 bacteria/mouse in presence of 8 mg hTf for 8 hours. Values are given as median, with interquartile range (IQR) in parentheses. 115
Table 3.3 Summary of NO metabolites measured from mice infected with 10^6 bacteria/mouse in presence of LPS + 8 mg hTf for 6 hours. (Values are given as median, with interquartile range (IQR) in parentheses) 123
Table 5.1 Input viable count 174
Table 5.2 Output viable count 174

Abstract

Neisseria meningitidis is the causative agent of fatal meningococcal sepsis in humans, characterised by high bacterial loads in blood, and collapse of the microcirculatory system. The organism is adapted to colonise the human nasopharynx, an environment which is oxygen poor but rich in nitric oxide (NO), a gas vital for the regulation of essential physiological processes such as vasorelaxation, antimicrobial and innate immune responses by the host. Furthermore, during sepsis caused by meningococcaemia, high concentrations of nitrite can be measured in the blood, derived from activated circulating monocytes and endothelial cells. Meningococci express a partial denitrification pathway comprising of a nitrite reductase (AniA) and a nitric oxide reductase (NorB) to survive and thrive in an oxygen deficient niche such as the nasopharynx. The *aniA* and *norB* genes are negatively regulated by an NO sensitive repressor, NsrR. Studies from our group have shown that NorB is critical for counteracting the antimicrobial and innate immune response of the host. As NO based regulation requires a tightly regulated equilibrium, this could have far reaching consequences on the NO mediated signalling processes, and is likely to be relevant to survival of the organism within NO-enriched nasopharyngeal mucosae and blood.

Previously, it was shown that bacterial NO detoxification reduces the concentration of host-cell S-nitrosothiol (SNO), a vital post-translational modification akin to phosphorylation, in murine macrophages *in vitro*. To investigate if similar meningococcal NO metabolism mediated SNO depletion persists *in vivo,* we established a murine model of early acute meningococcal sepsis. We showed that bacterial burden correlates positively with plasma SNO and hepatic NO_2^- but negatively with hepatic NO_x. However, bacterial NO metabolism did not differentially modulate SNO and other NO metabolite profile of murine blood and liver tissue.

Since there is no information to date on the effect of multiple meningococcal denitrification genes (*aniA* and *norB*) on the cellular pathology of meningococcal sepsis, we constructed and characterised a combination of NO metabolising gene mutants (Δ*aniA/*Δ*norB*, Δ*nsrR/*Δ*norB*, Δ*aniA/*Δ*norB/*Δ*nsrR*) using the isocloning method.

Differentiated human primary bronchial airway epithelial cells cultured at an air-liquid interface (HPEC-ALI) are polarised cells with tight junctions, possessing similar characteristics to the nasopharyngeal epithelial cells with which meningococci have to interact during colonisation and pathogenesis. HPEC-ALIs were infected with the newly created mutants (Δ*aniA/*Δ*norB* and Δ*aniA/*Δ*norB/*Δ*nsrR*) to examine the role of bacterial NO

metabolism on the barrier function and immune response, functions known to be modulated by high concentrations of NO present in the airway epithelium. We demonstrated bacterial burden inversely correlates with the barrier function (TER) but positively with the cytokine profile (IL-8, TNFα). However, meningococcal denitrification does not have any differential role in the regulation of barrier function and cytokine profile of the HPEC-ALIs in the experimental system we used.

The role of meningococcal denitrification in biofilm formation *in vitro* was also investigated. Preliminary data showed when biofilm formation was induced by nutrient starvation, Δ*aniA/*Δ*norB* showed a significantly reduced biofilm forming ability compared to the Wt strain measured by the crystal violet staining. To investigate the role of *aniA* in differential regulation of biofilm formation, reverse complemented strains (Δ*aniA/aniA*$^{IPTG+}$ and Δ*aniA/aniA*$^{+}$) were created. Characterisation data showed functional activation was restored in Δ*aniA* when *aniA* was complemented along with the upstream regulatory elements such as the endogenous promoter (Δ*aniA/aniA*$^{+}$) but not when *aniA* coding region was complemented under the control of an IPTG inducible lac promoter (Δ*aniA/aniA*$^{IPTG+}$).

Abbreviations

ALI	Air-liquid interphase
APP	Adhesion and penetration protein
ATP	Adenosine triphosphate
AUC	Area Under Curve
BEGM	Bronchial epithelial cell growth medium
BH4	Tetrahydrobiopterin
CEACAM	Carcinoembryonic antigen cell adhesion molecule
CFU	Colony forming units
cGMP	Cyclic guanosine monophosphate
CSF	Cerebrospinal fluid
CV	Crystal Violet
DMEM	Dulbecco's modified eagle's medium
DNA	Deoxyribonucleic acid
DNICs	Dinitrosyl-iron complexes
DTPA	Diethylene triamine pentaacetic acid
DTT	Dithiothreitol
EDRF	Endothelium derived relaxing factor
EDTA	Ethylenediaminetetraacetic acid
ELISA	Enzyme linked immunosorbent assay
eNOS	Endothelial nitric oxide synthase
FAD	Flavin adenine dinucleotide
FCS	Foetal calf serum
fHbp	Factor H binding protein
FMN	Flavin mononucleotide
FNR	Fumarate and nitrate-reductase repressor
FUR	Ferric uptake regulator
FWD	Forward primer
GD	Genomic DNA
Gpx	Glutathione peroxidase
GTN	Glyceryl trinitrate
GSNO	S-nitrosoglutathione
GSNOR	S-nitrosoglutathione reductase
GTP	Guanosine triphosphate
HBSS	Hanks Balanced Salt Solution
HI-FCS	Heat-inactivated foetal calf-serum
HkWt	Heat killed Wild type
HPEC	Human primary airway epithelial cells
HRP	Horse radish peroxidase
hTf	Human holo transferrin
IFNɣ	Interferon-ɣ
IL	Interleukin
iNOS	Inducible nitric oxide synthase
i/p	Intraperitoneally
IPTG	Isopropyl β-D-1-thiogalactopyranoside
IQR	Interquartile range
ISA	Isothermal assembly cloning
LOS	Lipooligosaccharides
LPS	Lipopolysaccharides

MIC	Minimum inhibitory concentration
MDM	Monocyte derived macrophages
MHB	Mueller hinton broth
MLST	Multi-locus sequence typing
MOI	Multiplicity of infection
NadA	*Neisseria* adhesin A
NADPH	Nicotinamide adenine dinucleotide phosphate
NED	N-1-napthylethylenediamine
NEM	N-Ethylmaleimide
NhhA	*Neisseria hia/hsf* homolog A
nNOS	Neuronal nitric oxide synthase
NO	Nitric oxide
NO_2^-	Nitrite
NO_3^-	Nitrate
NO_x	NO metabolites
NOA	Nitric oxide Analyser
NOS	Nitric oxide synthase
NsrR	Nitrite sensing repressor protein
OD	Optical density
OMP	Outer membrane protein
$ONOO^-$	Peroxynitrite
Opa	Opacity associated protein
PAMP	Pathogen associated molecular pattern
PBS	Phosphate buffer saline
PCR	Polymerase chain reaction
PMT	Photomultiplier tube
PMSF	Phenylmethanesulfonylfluoride
RBC	Red blood cell
REV	Reverse primer
RNA	Ribonucleic acid
sGC	Soluble guanyl cyclase
SEM	Standard error of the mean
SNAP	S-nitroso-N-acetylpenicillamine
SNO	S-nitrosothiol
SNO-Hb	S-nitrosohaemoglobin
TER	Transepithelial electrical resistance
Tfp	Type IV pili
TLR	Toll like receptor
TNFα	Tumor like necrosis factor alpha
TSB	Tryptic soy broth
Wt	Wild type

1 Chapter 1: Introduction

1.1 History and a brief overview of *Neisseria meningitidis*

Disease similar to the meningococcal infection dates back to the 16th century. Vieusseux first described the disease in 1805 when an outbreak occurred in Geneva, Switzerland (Vieusseux, 1805). In 1806 the disease was reported in Medfield, USA by physicians Lothario Danielson and Elias Mann (Danielson, 1806). Existence of the oval shaped micrococci in cerebrospinal fluid (CSF) was described by Italian pathologists Marchiafava and Celli in 1884 (Marchiafava, 1884). Austrian bacteriologist, Anton Weichselbaum first isolated the bacterium from the CSF of a patient with meningitidis and termed it as '*Diplococcus intracellularis*' (Weichselbaum, 1887). Human lumbar puncture, a routinely used technique for culture based diagnosis of meningococcal infection was described in 1893 (Quincke, 1893). Kiefer grew meningococci from the nasopharynx of the patients suffering from meningococci and also from the people who were in close contact with the patients (Kiefer, 1896). Early investigators were perplexed by the presence of meningococci in the nasopharynx of the healthy people. However, this observation first confirmed the non-symptomatic carriage of the organism in nasopharynx. In 1909, Dopter extracted an organism which had similar properties to the meningococci which failed to agglutinate to antibody made against other strains found in CSF. Subsequently these organisms were termed as parameningococci. Hence, Dopter is credited of having revealed the first example of meningococcal serogrouping (Dopter, 1909). Serum therapy was used to treat meningococcal infection (Flexner, 1913) until the introduction of sulphonamide in 1937 for treating asymptomatic carriage (Schwentker *et al,* 1984) . This reduced the mortality rate from 70% to 30%. Sulphonamide resistant meningococci was reported within the Naval recruits at San Diego (Bristow *et al,* 1965). However, the first vaccine against meningococcal serogroup C was introduced in the 1960s due to the development of resistance against sulphonamides (Artenstein *et al,* 1970). Conjugate polysaccharide vaccines developed against the capsular component have provided good protection against serogroup A, C, W-135 and Y (Trotter & Ramsay, 2007). Development of vaccine against serogroup B meningococcal disease has been a challenge for a long time. This is due to the fact that polysaccharide of serogroup B meningococcal capsule closely mimics the human tissue antigen such as NCAM (neural cell adhesion molecule). Due to this molecular mimicry, the antibody against capsule in serogroup B is poorly immunogenic and does not induce a protective response (Finne *et al,* 1987; Nedelec *et al,* 1990). Multiple vaccine candidates were identified using the reverse vaccinology (Rappuoli, 2001) which involved the screening of whole genome sequence of serogroup B

meningococci for finding novel antigens other than the capsule (Pizza *et al*, 2000). After subsequent serological and immunological characterisation, novel surface exposed antigens were identified. Using these components, a novel vaccine was developed against serogroup B which is marketed as Bexsero (also known as 4CMenB). Bexsero consists of four main components, 1) Factor H binding protein (fHbp), 2) *Neisseria* heparin binding antigen (NHBA), 3) *Neisserial* adhesin A (NadA) 4) New Zealand MenB vaccine (MenZB) (Serruto *et al*, 2012). Other ingredients that make up the vaccine are aluminium hydroxide, histidine, sodium chloride, sucrose and water. The vaccine was licenced for use in Europe in January 2013 (Bai *et al*, 2011). A formal decision to include Bexsero as part of the child immunisation scheme in UK was made in the late March 2015 (http://www.bbc.co.uk/news/health-32101921) and became a part of the routine vaccination schedule in September 2015 (http://www.bbc.co.uk/news/health-34084999). TRUMENBA, produced by Pfizer, a vaccine against serogroup B was approved by the Food and Drug Administration (FDA) authority in October 29, 2014 for use in USA (http://www.cdc.gov/meningococcal/outbreaks/vaccine-serogroupb.html). It constitutes of two variants of the factor H binding protein (fHbp). After evaluating the global data from initial trials, Bexsero was approved in USA in January 2015 (http://www.fda.gov/BiologicsBloodVaccines/Vaccines/ApprovedProducts/ucm431446.htm). A recent study by our group demonstrated that inoculation of live *Neisseria lactamica* into young university student reduces the carriage and acquisition of *N. meningitidis* at a rate higher than the existing glycoconjugate vaccines (Deasy *et al*, 2015). This outcome could inform a new way of fighting meningococcal disease using bacterial medicine. Despite evidences of good protection, the efficacy of these novel vaccines/treatments have to be monitored over a large population and a long period of time given the plasticity of meningococcal genome have the potential to render these treatment regimes non-functional and obsolete in the long run (Deasy *et al*, 2015; Evans *et al*, 2011).

The genus '*Neisseria*' was first coined by bacteriologist Albert Neisser (Ligon, 2005). Although *Nesseria spp* are primarily human commensals, some species have been reported to be found in animals such as *Neisseria ovis* in sheep (Lindqvist, 1960), *Neisseria dentiae* in cows (Sneath & Barrett, 1996). Out of 14 *Neisseria* species that exclusively colonise human mucosal surfaces, *N. gonorrhoeae* and *N. meningitidis* are clinically important pathogens responsible for causing significant morbidity and mortality around the globe. In addition, harmless and non pathogenic commensal *N. lactamica* has also received significant medical attention as several studies have reported an inverse correlation between colonisation of *N.*

lactamica and pathogenic *N. meningitidis*. *N. meningitidis* (also known as ‘’the meningococcus’’) is a Gram negative heterotrophic bacterium belonging to the family of *Neisseriaceae* and is exclusively found in human nasopharynx which provides a stable ecological niche for the organism. It is predominantly diplococcus **(Figure 1.1 A).** At any given time the organism can colonise the nasopharynx of up to 35% of the healthy individuals and can be transmitted from one person to another by respiratory droplets (Caugant & Maiden, 2009). By adopting yet undetermined mechanism the organism can enter the bloodstream and cause pathology in the forms of meningitidis and septicaemia **(Figure 1.1 B).** However, the occurrence of invasive disease is rare because it represents an evolutionary dead end for the bacteria which normally is a successful coloniser of the human nasopharynx. The organism is fastidious in nature and has a limited lifespan *ex vivo*. It is non motile, aerobic and catalase producing. Like other bacteria, it is surrounded by lipid containing outer membrane protein (OMP). It grows optimally at 37°C with 5% CO_2 supplementation on various nutrient plates such as Columbia blood agar, Chocolate agar, GC agar and Mueller- Hinton agar (used in this study). The bacterium is an oxidase positive diplococcus (0.6 µm x 0.8 µm) which can be either encapsulated or unencapsulated (Rouphael & Stephens, 2012). The cocci can be found as single cells, tetrads or pairs. Glucose and maltose are utilised by the bacterium as carbon sources (Beno *et al,* 1968; Exley *et al,* 2005). Antimicrobial susceptibility test is performed by using Etest strip, broth microdilution or by minimal inhibitory concentration (MIC) determination. Laboratory personnel dealing with the organism must work in a biological safety cabinet and have protective vaccination. Antibiotic resistance is not widespread in the organism with the exception of sulphonamide. However, emergence of ciprofloxacin resistant meningococci have been reported in North America (Wu *et al,* 2009).

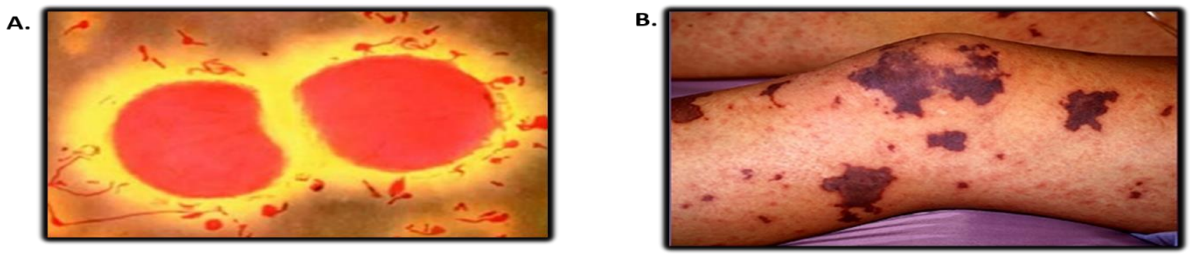

Figure 1.1 A) Image of diplococcus *Neisseria meningitidis* and B) Picture of a patient suffering from meningococcal infection

(http://bioweb.uwlax.edu/bio203/s2008/bingen_sama/shape%20of%20neisseria.jpg)
(http://carrington.edu/blog/medical/vaccines/meningococcal-disease-and-meningococcal-vaccine/)

1.2 Genetics of *Neisseria meningitidis*

Possession of a plastic genome is one of the main evolutionary features of *N. meningitidis*. This property provides the organism an additional advantage over other pathogens to colonise the nasopharynx and cause pathology by evading or subverting immune response. To date a number of genome sequences of *N. meningitidis* strains have been unravelled, such as Z2491 (Serogroup A, ST4, 2,184,406 bp length) (Parkhill *et al,* 2000), MC58 (Serogroup B, ST-32, 2,272,351 bp length) (Tettelin *et al,* 2000), FAM18 (Serogroup C, ST-11, 2,194,961 bp length) (Bentley *et al,* 2007) and NMB-CDC (Serogroup B, ST-8). Genome sequences reveal that the chromosome length of *N. meningitidis* is around 2.0-2.2 megabases containing about 2000 genes (Schoen *et al,* 2008). Apart from the IHT-A1 region which harbours the genes for capsule biosynthesis there is no defined core pathogenome for the organism. This might indicate that the virulence is clonal group dependent. Genetic islands coding for virulence factors and hypothetical surface proteins are present in the meningococcal genome. These islands are often acquired by horizontal transfer events between *N. meningitidis*, *N. gonorrhoeae*, commensal *Neisseria spp* and other bacterial species such as *Haemophilus* (Davidsen & Tonjum, 2006; Kroll *et al*, 1998; Linz *et al*, 2000). Presence of 2000 copies of uptake signal sequence in meningococcal genome facilitates the uptake of foreign DNA by transformation (Kroll *et al,* 1998; Smith *et al*, 1999). Meningococci shares 90% sequence homology with *N. lactamica* and *N. gonorrhoeae*. Events of genetic recombination is evidenced by the presence of repetitive sequences, IS elements and polymorphic regions which make up about 10% of the genome.

1.3 Classification of *Neisseria meningitidis*

N. meningitidis is classified by serological typing and serogrouping (Frasch *et al,* 1985 ; Slaterus, 1961). Unlike *N. gonorrhoeae*, *N. meningitidis* is an organism with capsular polysaccharide. On the basis of immune reactivity and capsular structure, meningococci can be divided into 13 serogroups (A, B, C, E-29, H, I, K, L, W-135, X, Y, Z and Z' (29E) (Branham, 1953). However, six serogroups (A, B, C, W-135, X, Y) account for more than 90% of the clinical cases of meningococcal disease (Pollard, 2004). Capsular structure of serogroup B, C, Y and W-135 consists of sialic acid linked to glucose or galactose (Bhattacharjee *et al,* 1975) and N-acetyl mannosamine-1-phosphate is the main component of serogroup A capsule (Liu *et al,* 1971).

The most abundant outer membrane protein for meningococci is porin. The two porins expressed by the organism are PorA and PorB (PorB2, PorB3). PorB expression facilitates serotyping whereas variability in PorA gene helps serosubtyping (Frasch *et al,* 1985). Unlike lipopolysaccharides found in members of the other Gram negative bacterial family, meningococcal outer membrane consists of lipo-oligosaccharides (LOS). It is composed of lipid A and a short chain of 8-12 saccharide units but lacks multiple sugar residues of LPS. It is responsible for the endotoxin activity. Immunotyping of meningococci is performed by the antigen recognition of 12 different immunogroups by the variability of their LOS antigens (Scholten *et al,* 1994). Molecular typing has been the choice of method for identifying and categorising various meningococcal strains, clonal groups and meningococcal genomes. Several molecular methods are used for typing such as multilocus enzyme electrophoresis (MLEE) (Weis & Lind, 1998), pulse-field gel electrophoresis (PFGE) (Bevanger *et al,* 1998), PCR (Mothershed *et al,* 2004) and multilocus sequence typing (MLST). MLST is the most widely used and accepted modern technique for classifying various meningococcal strains into different sequence types. This is done on the basis of nucleotide sequence polymorphisms associated in the selected housekeeping genes (Maiden *et al,* 1998). Around 10000 sequence types are listed in the *Neisseria* Multi Locus Sequence Typing website (http://pubmlst.org/neisseria/) (Jolley & Maiden, 2010).

1.4 Transmission, carriage and epidemiology of *Neisseria meningitidis*

N. meningitidis can be transmitted from person to person by contacting respiratory droplets. Although the disease is most common in the infants, highest carriage of the organism is found in the young adults such as university students (Ala'aldeen *et al,* 2011). At any given time the bacteria can colonise 10% of the given population excluding situation such as epidemics (Caugant *et al,* 1994). Social behaviours such as kissing, bedroom-sharing, cigarette smoking and close contact environment such as the one encountered during Hajj pilgrimage can lead up to higher asymptomatic carriage of the organism in adolescents (Christensen *et al,* 2010; MacLennan *et al,* 2006; Soriano-Gabarro *et al,* 2011; Wilder-Smith *et al,* 2003).

There are around 1.2 million cases of meningococcal disease worldwide resulting in the death of 135000 people per annum (Rouphael & Stephens, 2012). Age group, population, geographical location and different bacterial serogroup play important roles in dictating the severity of meningococcal disease. A few genetically well defined clonal complexes are responsible for meningococcal disease (Maiden *et al,* 1998). About 90% of the disease worldwide is caused by serogroups A, B and C. In recent times, incidences of disease caused by serogroup A have been low in the developed world despite outbreaks in the early part of 20th century in USA (Rosenstein *et al,* 2001). However, Serogroup A has been responsible for the largest outbreak of meningococcal disease in the sub-Saharan African region spanning 21 countries from Ethiopia to Senegal also known as the 'meningitis belt' (Hart & Cuevas, 1997). This has caused the death of around 30000 people out of 300000 affected. In this region epidemic occurs every 8-10 years (Stephens *et al,* 2007). Although the reasons behind development of these outbreaks are poorly understood, environmental factors such as dust and excessive humidity could be responsible (Greenwood *et al,* 1984; Molesworth *et al,* 2003). Serogroup A meningococcal disease has also been reported in Asian countries such as China, India, Nepal and Russia (Stephens *et al,* 2007; Wang *et al,* 1992). Serogroup B accounts for the majority of endemics in the developed world, causing 80% of the disease in Europe and 30%-40% in USA. In England and Wales, serogroup B has accounted for most of the laboratory confirmed meningococcal infection from 2004 – 2014 **(Figure 1.2).** There was a large outbreak of MenB in New Zealand in 1991 (Martin *et al,* 1998). In USA serogroup C has been responsible for the 30% of the disease (Jackson *et al,* 1995). Serogroup W epidemic was reported in the pilgrims returning from Hajj in 2001 (Wilder-Smith *et al,* 2003). In addition, emergence of pathology with serogroup W has also been reported in Latin America, Africa (Stephens *et al,* 2007). Although rare in other regions around 1300 cases of Serogroup X meningococcal disease has been found in African meningitis belt during 2006-2010 (Xie *et al,* 2013). Due to waning maternal antibodies, the highest rate of MenB disease is prevalent in infants under the age of one (Cartwright *et al,* 2001).Worldwide data show that young children are the most vulnerable group for meningococcal infection but in endemics older children and adolescents are more prone to risk.

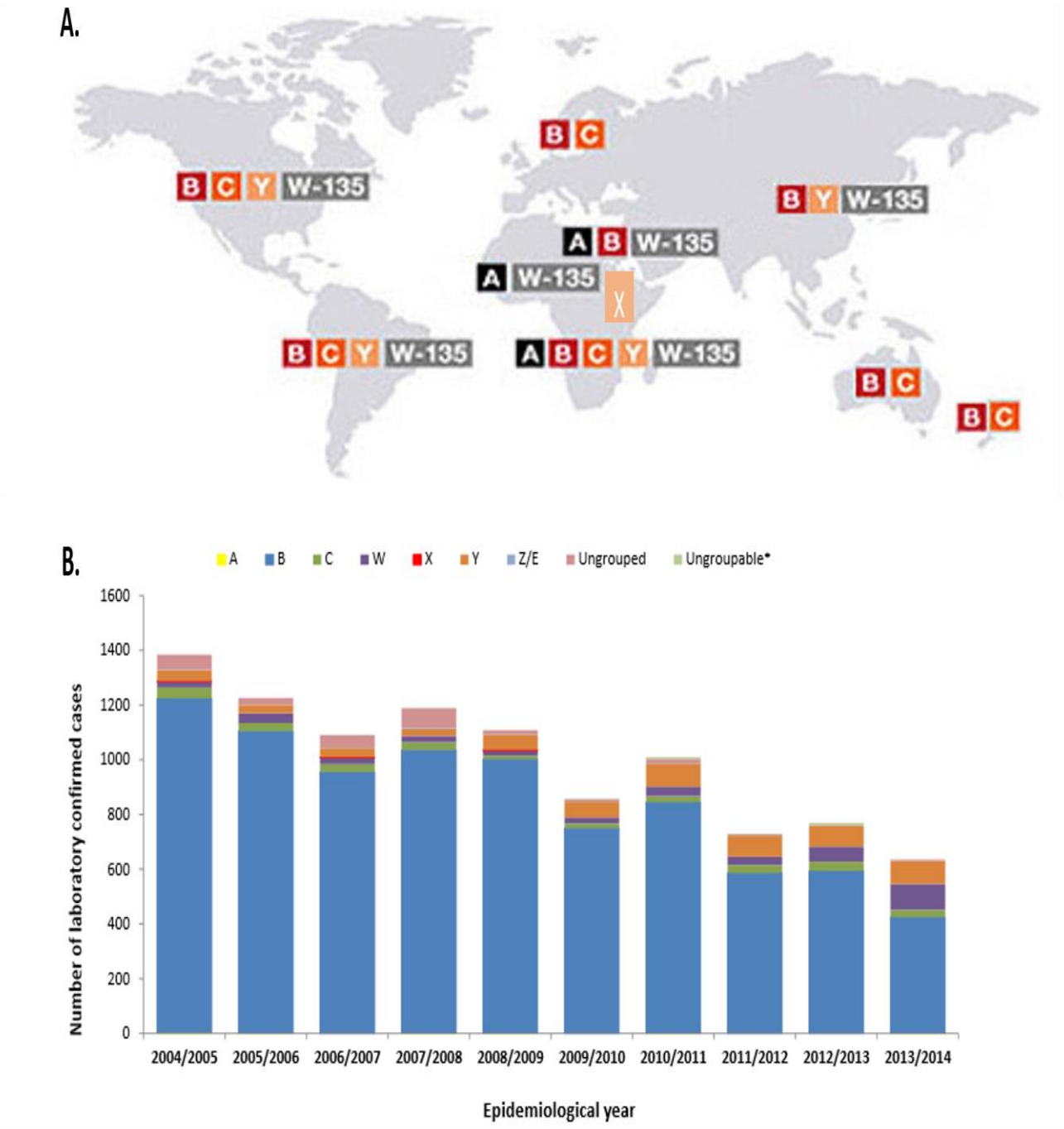

Figure 1.2 Epidemiology of the meningococcal disease

A) Worldwide geographical distribution of pathogenic major serogroups (A, B, C, W-135, X and Y) of meningococci (http://www.meningitis.com/US/media/uploads/map_2.jpg)

B) Prevalence of the laboratory confirmed meningococcal disease and their serogroups in England and Wales from 2004-2014. (https://www.gov.uk/government/uploads/system/uploads/attachment_data/file/397913/hpr0315_imd.pdf).

1.5 Clinical representation and diagnosis of meningococcal disease

Meningococcal disease is a clinical emergency which can kill a person of any age within hours. A study from hospital emergency room reported that about one-third of the fatalities happen within the first 6 hours of admission and about two-thirds within the first 18 hours (van Deuren *et al*, 2000). The clinical spectrum of the disease is diverse. Sepsis and meningitis are the two most common forms of representation of the meningococcal disease. Acute pyogenic meningitis accounts for 75% of the patients for meningococcal disease (Brandtzaeg & van Deuren, 2012). It is caused by the inflammation of meninges. Approximately 40% of the patients suffering from meningitis would have bacteraemia. However, 10% of the patient would have bacteraemia without meningitis (Al-Tawfiq *et al*, 2010; Dankert, 2004). In rare circumstances, patients would have mild meningococcal bacteraemia which can be treated without using any antibiotic (Sullivan & LaScolea, 1987). Outcome of the meningococcal disease is dependent on multiple factors such as age of the patient and infecting clonal complex (Read *et al*, 2003). The most extreme outcome of meningococcal disease is purpura fulminas which is characterised by haemorrhagic infraction and intravascular thrombosis of the skin. Even after successful treatment patients may suffer from sequelae such as deafness. Sequelae from meningococcal disease usually results from sepsis and could lead to organ amputation in the long run (Baraff *et al*, 1993).

In case of suspected meningococcal disease blood sample or CSF is collected. Samples are to be examined urgently as the treatment will differ on the basis of disease detection and severity. Samples are tested by blood culture, agglutination test or meningococcal PCR. For confirming meningitis, a lumber puncture is performed for isolating CSF. An advanced PCR technique combined with fluidic microarray (the Luminex xMAPTM technology) is also used for detecting bacteria in CSF in patients suspected with having meningitis. This is a robust method which uses PCR combined with flow cytometry, laser technology, digital signal processing, traditional chemistry and microspheres (Moller, 2012). Although gram staining is an efficient method for detecting meningococcal disease, the success of this process depends on the bacterial concentration present in the sample. Around 60%-90% of CSF specimen from meningococcal sample yield a positive result with gram staining (Dankert, 2004). Increased leukocytes (exceeding 1000 cells/mm^3) and decreased glucose concentration in leukocytes (<40 mg/dl) are also indicators of meningococcal disease (Wilks, 2003).

1.6 Pathological events of meningococcal sepsis

N. meningitidis reside in the nasopharynx of 5%-10% of the population without causing any pathological complications (Donovan & Blewitt, 2009). However, under unknown circumstances, the bacteria can penetrate through the nasopharyngeal mucosae and enter the bloodstream to cause meningococcal septicaemia and from there, traverse the endothelial blood-brain barrier and cause meningococcal meningitis. The overall mortality rate from meningococcal disease is around 8% (Rajapaksa & Starr, 2010). Survivors of meningitis and septicaemia can often suffer from neurological and physical abnormalities. Sepsis is defined as a systemic respiratory response syndrome in response to infection showing multiple clinical manifestations such as abnormal body temperature (>38°C or < 36°C), high heart rates (> 90 beats per minute), abnormal breathing (> 20 breaths/minute) or hyperventilation, abnormal leukocyte count (> 12000 cells/cubic mm or < 4000 cells/cubic mm or > 10% immature neutrophils) (Bone *et al,* 1992). The main pathological observation in septic patients is the perturbation of the tightly regulated microvasculature, in which Nitric oxide (NO) is a pivotal signalling molecule **(Section 1.11.1)** (Buerk, 2007). Increased vascular permeability, intravascular thrombosis and both the abnormal vasodilation and vasoconstriction can result in the failure of the circulatory system.

1.6.1 Increased vascular permeability

Early events in septicaemia are characterised by the increased vascular permeability in response to the exposure of meningococcal endotoxin and surface adhesion molecules. This results in an excessive activation of the innate immune system and subsequent recruitment of macrophages and neutrophils to the site of infection. Increased vascular permeability in response to meningococcal infection subsequently induces hypovolaemia, an event resulting from the aberrant loss of plasma albumin. Enzymatic degradation of the endothelial surface proteins such as glycosaminoglycans has been attributed for the capillary leakage by hypovolaemia (Klein *et al,* 1992; Oragui *et al,* 2000). This cascade of events subsequently results in respiratory failure, pulmonary oedema and a significant reduction in the cardiac output.

1.6.2 Pathophysiological vasodilation and vasoconstriction

To counteract respiratory failure mediated by hypovolaemia, compensatory vasoconstriction is induced to restore blood perfusion and cardiac output. This results in an initial restoration of homeostasis of microvasculature. However, in most of the severely affected patients intense

vasoconstriction persists. This results in the generation of pale, cold and ischaemic tissues, which can consequently lead to thrombosis and gangrene. In contrast, some of the patients experience an excessive vasodilation in response to the compensatory vasoconstriction following initial hypovolaemia. Consequently, hypotension is triggered with a marked drop in blood pressure. Excessive production of NO as encountered during sepsis due to high NOS activity could also contribute to excessive vasodilation leading to hypotension and inflammatory tissue damage (Kilbourn *et al*, 1997; Thiemermann, 1997). This could lead to multiple organ failure including kidneys, lungs, brain and heart.

1.6.3 Intravascular thrombosis and coagulation

One of the major characteristics of severe meningococcal sepsis is the development of purpura fulminas accompanied by intravascular thrombosis and haemorrhagic necrosis of skin and limbs (Brandtzaeg & van Deuren, 2012). Clot formation during normal vascular homeostasis is a process which requires spatiotemporal and precisely regulated coordination of three important pathways; the procoagulant, antithrombic and thrombolytic pathways. Severe disseminated thrombosis during meningococcal sepsis occurs as result of disruption in the regulation of these pathways. In response to endotoxin or inflammatory stimulus of meningococci, the procoagulant pathway is activated rapidly. The endothelium harbours various components of anticoagulation required for thromboresistance. For example NO and prostacyclin, inhibit platelet formation and heparin sulphate has antithrombic properties (Heyderman *et al*, 1992). However, the pathway for activating anticoagulating proteins such as antithrombin, protein C and protein S is severely impaired and down-regulated in the septic patients (Faust *et al*, 2001). Dysfunctional anticoagulating mechanism coupled with upregulation of tissue and procoagulating factors from monocytes and platelets result in widespread intravascular thrombosis. An impaired thrombolytic mechanism also contributes to this pathophysiology.

1.6.4 Severe myocardial dysfunction

Significant impairment in the activity of microvasculature following capillary leak and hypovolaemia, loss of circulating blood volume can subsequently lead to myocardial failure. Despite the compensatory vasoconstriction in order to restore the normal blood perfusion, persistent defect in myocardial contractility has been reported. Proinflammatory mediators such as TNFα, IL-1β, NO act as myocardial depressant factors (Kumar *et al*, 1999; Kumar *et al*, 1996). Other accompanying physiological events in sepsis such as acidosis, ischemia,

hypoglycaemia, hypocalcaemia and hypophosphataemia can also lead to the severe myocardial dysfunction (Pathan *et al,* 2003).

1.7 Mechanisms of colonisation and cellular invasion by *N. meningitidis*

Following acquisition by the inhalation of respiratory droplets, the meningococcus establishes contact with the mucosal epithelial cell of the nasopharynx **(Figure 1.3).** *N. meningitidis* has evolved a number of surface associated proteins and structures to facilitate its interaction with the host cell. These components play essential role in the colonisation process of meningococci. In addition, they also determine many important parameters in host-pathogen interaction such as tissue tropism and invasive versus carriage potential. Meningococcal adhesion to the host is a dynamic process involving complex interaction between the bacterial surface components and host receptors. The outcome of this interaction is dependent on the cooperation of multiple surface proteins **(Figure 1.4)** at different stages of infection and colonisation.

Type IV pili (Tfp) are responsible for mediating the initial attachment of *Neisseria* to the epithelium. Adhesive properties of capsulated meningococci are governed by pili which extend several thousand nanometres beyond the polysaccharide capsular structure (Pinner *et al,* 1991; Virji *et al,* 1992a). Non piliated strains of meningococci do not efficiently bind to the host cell (Nassif, 1999; Virji *et al,* 1991). Tfp is also important for facilitating the DNA uptake by *N. meningitidis* (Proft & Baker, 2009). It is a multimeric protein complex consisting of PilE protein. *pilE* deficient capsulated strains are incapable of binding to the host cell. Although CD46, a membrane bound cofactor protein, is considered to be the predominant receptor for Tfp binding (Kallstrom *et al,* 1997), CD46 independent binding of pili has also been reported (Kirchner *et al,* 2005). In *N. meningitidis* two types of PilC are found, PilC1 and PilC2. However, it is PilC1 which is essential for binding with epithelium as evidenced by the lack of binding by $PilC1^-$ isolates despite the expression of PilC2 (Nassif *et al,* 1994). Tfp is a dynamic structure which is being constantly remodelled. It can undergo posttranslational modification such as glycosylation. It has been suggested that meningococci can disseminate to a new location by detaching from the microcolony using glycosylated pili (Chamot-Rooke *et al,* 2011).

Porin is the predominant surface protein which is responsible for the diffusion of small metabolites such as ions through the pores. It can facilitate pathogenesis by modulating important processes such as immune stimulation, serum resistance and invasion (Massari *et al,* 2003). Three types of porins are found (PorA, PorB2 and PorB3) of which PorA is cation selective and PorB2 and PorB3 are anion selective. Unlike *N. gonorrhoeae* (Bauer *et al,* 1999),

there is no evidence for a direct effect of meningococcal porin on invasion process. But it is postulated that it can indirectly affect *Neisserial* entry into cells by modulating the nucleation process.

Sequencing has revealed a number of physiologically important novel surface structures such as autotransporters (App, MspA/AusI, NadA, NhhA), outer membrane proteins (Opa, Opc) **(Figure 1.4)** which have been implicated in the colonisation and invasion machinery of *N. meningitidis.*

The outer membrane opacity proteins give an opaque type phenotype to *N. meningitidis* when grown on the agar plates. Two types of OM opa proteins (Opa and Opc) are expressed by both pathogenic and commensal meningococci. Eight transmembrane β-strands and four surface bound loops make up the structure of Opa protein. It is expressed by multiple genes and its regulation is subject to phase and antigenic variation (Callaghan *et al,* 2006). Opa binds to the multiple members of the CEACAM (Carcino-embryonic antigen related cell-adhesion molecule) receptor family (Dehio *et al,* 1998; Virji *et al,* 1996). Thus Opa facilitates the cellular attachment and invasion by interacting with the CEACAM receptors which are highly expressed during inflammation. Opc is only expressed by meningococci of all *Neisseria spp* and is encoded by a single gene. In non-capsulated meningococci Opc facilitates the adherence and invasion of endothelial cells independent of the activity of pili and Opa (Virji *et al,* 1993; Virji *et al*, 1992b; Virji *et al,* 1994). Both Opa and Opc can bind to HSPGs (Heparan sulfate proteoglycans) which are found on the cell surface (Virji *et al,* 1999; Virji *et al,* 1992b).

Neisseria adhesin A (NadA) of *N. meningitidis* is one of the members of trimeric autotransporter protein family. In particular it belongs to the Oca (Oligomeric coiled-coil adhesion) family which represents a group of autotransporters responsible for mediating the oligomerisation process by the presence of a coiled-coil motif (Desvaux *et al,* 2004). It is found in about 50% of the *N. meningitidis* strains including hypervirulent lineages such as ET5, ET37, cluster 4 but absent in lineage III and also in *N. gonorrhoeae,* commensal species such as *N. lactamica* (Comanducci *et al,* 2002). However, it is only found in 5% of the healthy carriage population (Comanducci *et al,* 2004). In addition, it is well conserved, induces strong bactericidal antibody response and helps the meningococci to bind to the epithelial cell (Capecchi *et al,* 2005). These observation supported the hypothesis that NadA is an important co-factor in the pathogenesis of group B meningococci and thus was incorporated as one of the four antigen components of the novel multicomponent Bexsero vaccine against the group B meningococci.

Neisseria hia homolog A (NhhA) is another member of the trimeric autotransporter family. It is composed of 590 amino acids and have been found in all meningococcal strains (Scarselli *et al,* 2006). It facilitates the adherence of meningococci to epithelial cells and protects the organism from phagocytosis and complement mediated killing (Sjölinder *et al,* 2008). By adopting these mechanisms, NhhA affects colonisation and invasion in *vivo*.

Adhesion and penetration protein (App) is an autotransporter protein which is present in all *Neisseria spp*. It is homologous to the Hap adhesin of *Haemophilus influenzae* (St Geme *et al,* 1994). It has autocatalytic serine protease activity and helps the meningococci to adhere to epithelial cell (Hadi *et al,* 2001; Serruto *et al,* 2003). It is suggested that App is involved in the early stage of colonisation until it is autocleaved and thereby could facilitate the dissemination of bacteria by promoting detachment. In addition, MspA/AusI and NaIP are other autotransporters with serine protease activity which have been shown to have adhesive properties during interaction with the epithelial cells (Turner *et al,* 2006; van Ulsen *et al,* 2006; van Ulsen *et al,* 2003).

It is noteworthy that surface structures such as App, NadA and NhhA have been found to be expressed and functional in capsulated meningococcal strains (Capecchi *et al,* 2005; Scarselli *et al,* 2006; Serruto *et al,* 2003). Some of the meningococcal surface proteins such as App, NhhA were found while comparing with homologues from other colonisers of the upper respiratory tract such as *Haemophilus influenzae*, *Bordetella pertussis.* These homologue proteins also play important roles in colonisation and invasion process in other bacteria. First step in establishing meningococcal colonisation is the attachment of the bacterium to the nasopharyngeal epithelial cells. Given that pili is the primary factor determining the attachment step, the outer membrane proteins and adhesins can act as auxiliary factors facilitating the colonisation process. Antibodies directed against App, NadA and NhhA have been found from the sera of convalescent patients and carrier population of meningococcal disease. A screen for finding novel vaccine candidates showed that antibodies generated against these surface proteins elicit bactericidal response (Pizza *et al,* 2000). These observations further highlight the relevance of the meningococcal surface proteins in modulating the colonisation and invasion process.

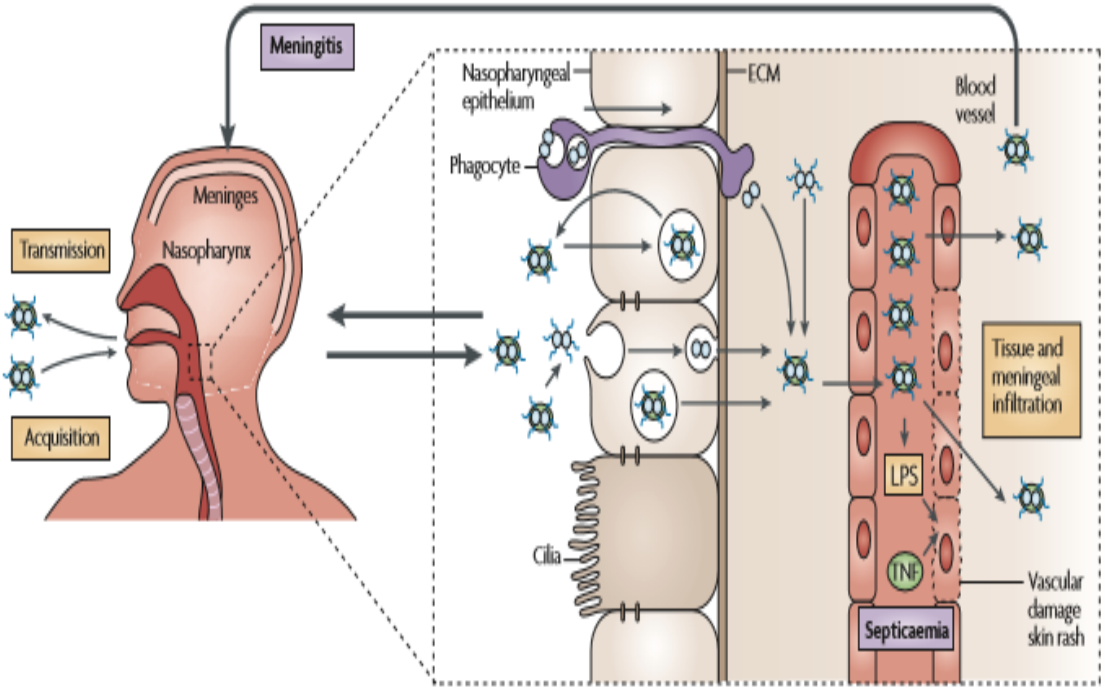

Figure 1.3 Depiction of colonisation and invasion by *N. meningitidis*.

Following acquisition by the inhalation of respiratory droplets, the meningococcus establishes contact with the mucosal epithelial cell of the nasopharynx. Apart from transcytosis, the meningococci can cross the epithelial barrier and enter bloodstream by disrupting the barrier function or by phagocytosis. However, bacteria are eliminated after crossing the epithelial barrier in asymptomatic carriage samples. Once in the bloodstream bacteria may thrive and multiply in the blood stream or disseminate throughout the body and the brain. Upon reaching brain it can cross the brain vascular endothelium and cause infection of the meninges and the CSF. Figure adapted from (Virji, 2009)

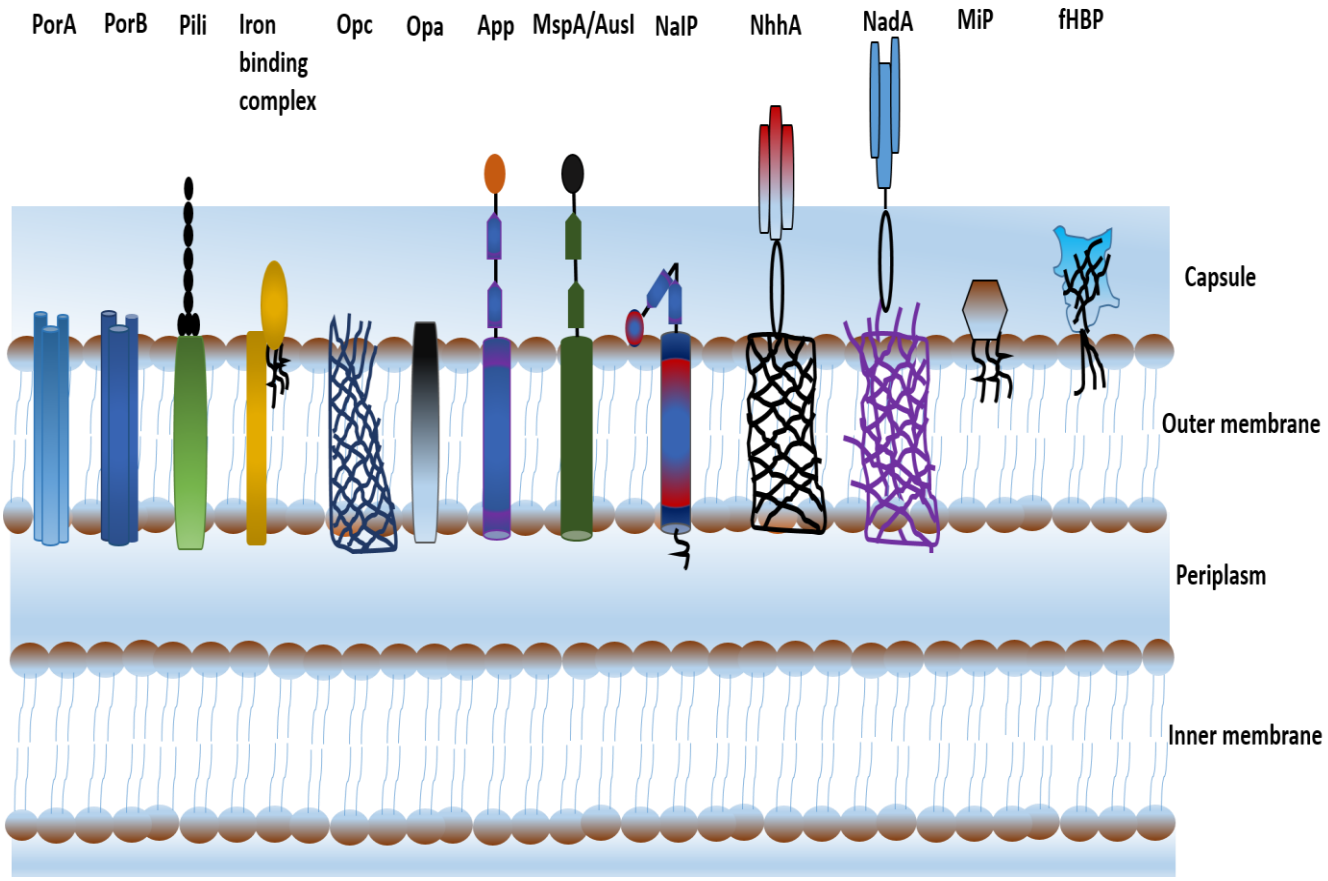

Figure 1.4 Outer membrane structures of *N. meningitidis* important for the bacterial interaction with the epithelial cells and pathogenesis.

Porins (PorA, PorB), Pili (Type IV pili), Iron binding complex (consists of TbpA and TbpB proteins), Outer membrane opacity proteins (Opa, Opc), App- (Adhesion and penetration protein), MsPA/ AusI (Autotransporter protein), NaIP (*Neisseria* autotransporter lipoprotein), NhhA (*Neisseria* hia/hsf homologue), NadA (*Neisseria* adhesion A), MiP (Macrophage infectivity potentiator), fHBP (Factor H binding protein)

1.8 Nitric oxide: a brief history and overview

English chemist Joseph Priestley first discovered NO in 1772 which he termed as 'nitrous air'. The use of NO for treating critical heart conditions without the appreciation of NO as EDRF (endothelium derived relaxation factor) can be traced back to the late 18th century. Physician Lauder Brunton showed the physiological role of NO derived compound such as nitrite by treating a patient suffering from angina with amyl nitrite in 1876 (Marsh & Marsh, 2000). However, he was not aware of the specific role and mechanism by which NO from nitrite reduced chest pain.

When prescribed GTN (also known as glyceryl trinitrate), a component of dynamite as treatment for angina pectoris, the discoverer of dynamite, Alfred Nobel in a letter addressed to his assistant, Ragnar Sohlman, mentioned that ''*My heart trouble will keep me here in Paris for another few days at least, until my doctors are in complete agreement about my immediate treatment. Isn't it the irony of fate that I have been prescribed GTN, to be taken internally! They call it Trinitrin, so as not to scare the chemist and the public''* (http://www.nobelprize.org/alfred_nobel/biographical/articles/ringertz/). Although NO harbouring vasodilatory compounds such as nitroprusside and nitroglycerine were shown to activate the sGCs (Arnold *et al,* 1977; Schultz *et al,* 1977), any possibility of NO mediated sGC activation was ignored as NO at that time was considered being a carcinogenic, pungent-smelling gas and an air pollutant (Fontijn *et al,* 1970). It was hard to accept for the scientific community that a harmful compound like NO would be pivotal for regulating an important physiological process such as vasodilation. The major breakthrough in unravelling the role of NO as EDRF came by two major discoveries. Firstly a substance from endothelium was found to be responsible for mediating vasorelaxation (Furchgott & Zawadzki, 1980). The substance was termed as EDRF. Secondly, NO was discovered independently by Ignarro and Moncada groups as the EDRF responsible for stimulating sGCs in smooth muscle cells to synthesise cGMP, thereby causing vasodilation (Ignarro *et al,* 1987; Moncada *et al,* 1988; Palmer *et al,* 1988). Their work was commended with the award of Nobel Prize in Physiology and Medicine in 1998. Since then NO has been proven to be an important molecule in physiology, microbiology, immunology, pharmacology and was declared as the 'Molecule of the Year' in 1992 (Culotta & Koshland, 1992).

NO is a colourless and simple diatomic gas consisting of one atom of nitrogen and one atom of oxygen. It is poorly soluble in water and does not undergo hydration reaction. NO is an uncharged molecule which can traverse the cellular boundary. Therefore, it can exert its

biological effect away from its origin. Due to the presence of an unpaired electron, it can act as a highly reactive free radical. It can interact with a diverse range of inorganic molecules such as transition metals, superoxide, oxygen, prosthetic groups such as heme or thiol groups of protein to form S-nitrosothiols (SNO), structural component of DNA such as pyrimidine bases, reaction with iron-sulphur cluster or zinc finger domains (Bogdan, 2001). Many of these target for NO reactions are important regulatory components such as transcription factors or parts of signalling cascades. Therefore, NO can affect heterogeneous and diverse range of biological processes (Murad, 2004). However, the biological chemistry of NO is complex and often controversial.

It has been challenging for the researchers to link micro-environmental NO chemistry with the biological effects mediated by NO. In particular, defining the parameters of redox chemistry in the regulation of NO mediated biological responses has proven to be challenging. It is also questionable how such a ubiquitously expressed and short lived molecule can selectively regulate a vast number of important cellular processes including cell signalling. Many investigators referred to the post translational modification of thiol containing cysteine proteins by the formation of S-nitrosthiol (SNO) as an answer to this caveat. S-nitrosylation involves the formation of SNO following the reaction of NO with a thiol of cysteine residue of protein in presence of an oxidising agent **(Section 1.9).** It has been proven to regulate a diverse range of cellular responses such as apoptosis, neurotransmission, cell signalling and gene expression (Seth & Stamler, 2010; Stamler *et al*, 2001). The process of S-nitrosylation is spatiotemporally regulated, reversible in nature and stimulus evoked (Stamler *et al*, 2001). The realisation of the opposite process, denitrosylation, involving the release of NO moiety from SNO has been relatively recent (Tannenbaum & White, 2006). Thus, S-nitrosylation can be compared with other important posttranslational modifications processes such as phosphorylation and ubiquitylation. Increased S-nitrosylation has been implicated in Parkinson's disease, neurotoxicity, cerebral ischemia (Foster *et al*, 2003; Lipton *et al*, 1998; Schonhoff *et al*, 2006). Denitrosylation is linked to clinical conditions such as asthma, vascular dysfunction, sickle cell diseases (Benhar *et al*, 2009). In addition, SNO homeostasis is also important in the pathogenesis of malignant hyperthermia, type 2 diabetes, haemorrhage (Foster *et al*, 2009; Sheng *et al*, 2010).

1.9 Formation of NO and S-nitrosothiol

The majority of NO production in mammalian cells is driven by the activity of Nitric Oxide synthase (NOS) enzymes (Hogg, 2000). NOS catalyses the L-arginine to citrulline conversion in an oxygen and NADPH dependent manner and produces NO **(Figure 1.5 A).** In higher eukaryotes three types of NOS isoforms have been identified; constitutively expressed neuronal and endothelial NOSs (nNOS and eNOS, respectively) and the inducible NOS (iNOS) (Nathan & Xie, 1994). NOS exert its function as a dimer. Each NOS monomer contains a C-terminal reductase domain and an N-terminal oxygenase domain. The C-terminal domain harbours binding sites for NADPH, flavoproteins such as Flavin adenine dinucleotide (FAD) and Flavin mononucleotide (FMN). N-terminal oxygenase domain contains heme, tetrahydrobiopterin (BH_4) and L-arginine binding site (Crane *et al,* 1997; Sennequier & Stuehr, 1996). The reaction of NO and citrulline production from L-arginine requires five electrons, co factors such as FAD, FMN, BH4, calmodulin (CAM), co-substrates such as NADPH and O_2. In reductase domain electron from NADPH is transferred to flavoproteins FAD, FMN. Subsequently, CAM binding facilitates the transfer of electrons to heme group and O_2 of oxygenase domain. For generation of one mole of NO from NOS, one mole of O_2 and 1.5 NADPH molecules are required (Nathan & Xie, 1994) (Stuehr *et al*, 1991).

Constitutively expressed, nNOS and eNOS are regulated by the intracellular concentration of calcium. They produce low levels of NO and are important for regulating vasorelaxation, cell growth and proliferation processes **(Figure 1.6).** In contrast, iNOS has been attributed to the production of high amounts of NO in response to stress and injury. Burst of NO induced by the iNOS **(Figure 1.6)** has been implicated to pathways relating to the cell cycle and apoptosis. NO reacts with O_2 to form NO_2^- in aqueous solution in the presence of oxygen. As NO reacts rapidly with metal centres to form Fe-nitrosyl complexes and superoxide radical (O_2^-) **(Figure 1.6),** the observed half life of the molecule in biological samples is only 3-5 seconds (Ignarro, 1990). Rapid reaction of NO with iron-containing proteins is one of the most prevalent interactions in the mammalian cells. The predominant oxidation product of NO is NO_3^- owing to the reaction of NO with metal-oxygen complexes (e.g. formation of met-haemoglobin and NO_3^- after reaction of NO with oxyhaemoglobin) (Ignarro *et al,* 1993).

Higher oxides of NO such as N_2O_3 react with thiol of cysteine protein to form SNO **(Figure 1.5 A).** The process is termed as S-nitrosylation. It is very important to note the selective nature of S-nitrosylation given that only some cysteine containing proteins are s-nitrosylated where the others are not. The generic structure SNO is R-S-N=O and the bond is a covalent one. In biological conditions, the kinetics of three main reactions can govern the formation and decomposition of RSNO: denitrosylation, transnitrosylation and thiolation (shown in **Figure 1.5**). Given that S-N bond dissociation energy is not favourable for the homolytic decomposition of RSNO (Bartberger *et al*, 2001), reversible reductive and enzymatic mechanisms are likely to be of more importance in SNO homeostasis. The denitrosylation reaction involves the release of NO from SNOs. Temperature, light, metal ions such as iron, copper and other metal ion containing proteins can reduce RSNO by releasing NO (Lipton *et al*, 1998; Stamler *et al*, 1997b). Several enzymes such as GSNO reductase, thioredoxins are also capable of releasing NO from the RSNOs (Liu *et al*, 2004; Sengupta *et al*, 2007). Transnitrosylative reactions involve the transfer of NO from one thiol group of a SNO to another thiol group and the process is reversible **(Figure 1.5 B).** Biochemistry of transnitrosylation has received much attention due its role in the regulation of cell signalling pathways (Seth & Stamler, 2010). This reaction results in the formation of another SNO and thereby provides a mechanism for auto S-nitrosylation mediated posttranslational protein modification. Nucleophillic interaction of sulphur (thiol) on RSNO results in the production of a nitroxyl and disulphide anion and the reaction is termed as S-thiolation **(Figure 1.5 D)** (Hogg, 2002). Given the formation of strong disulphide bonds, S-thiolated modifications provide more stability compared to transnitrosylation. It is postulated that SNO can act as NO, $NO^{\cdot}$ and NO^{+} donor under physiological condition. However, the mechanism and mode of transfer or release of NO from SNO is debatable and often controversial (Tannenbaum & White, 2006).

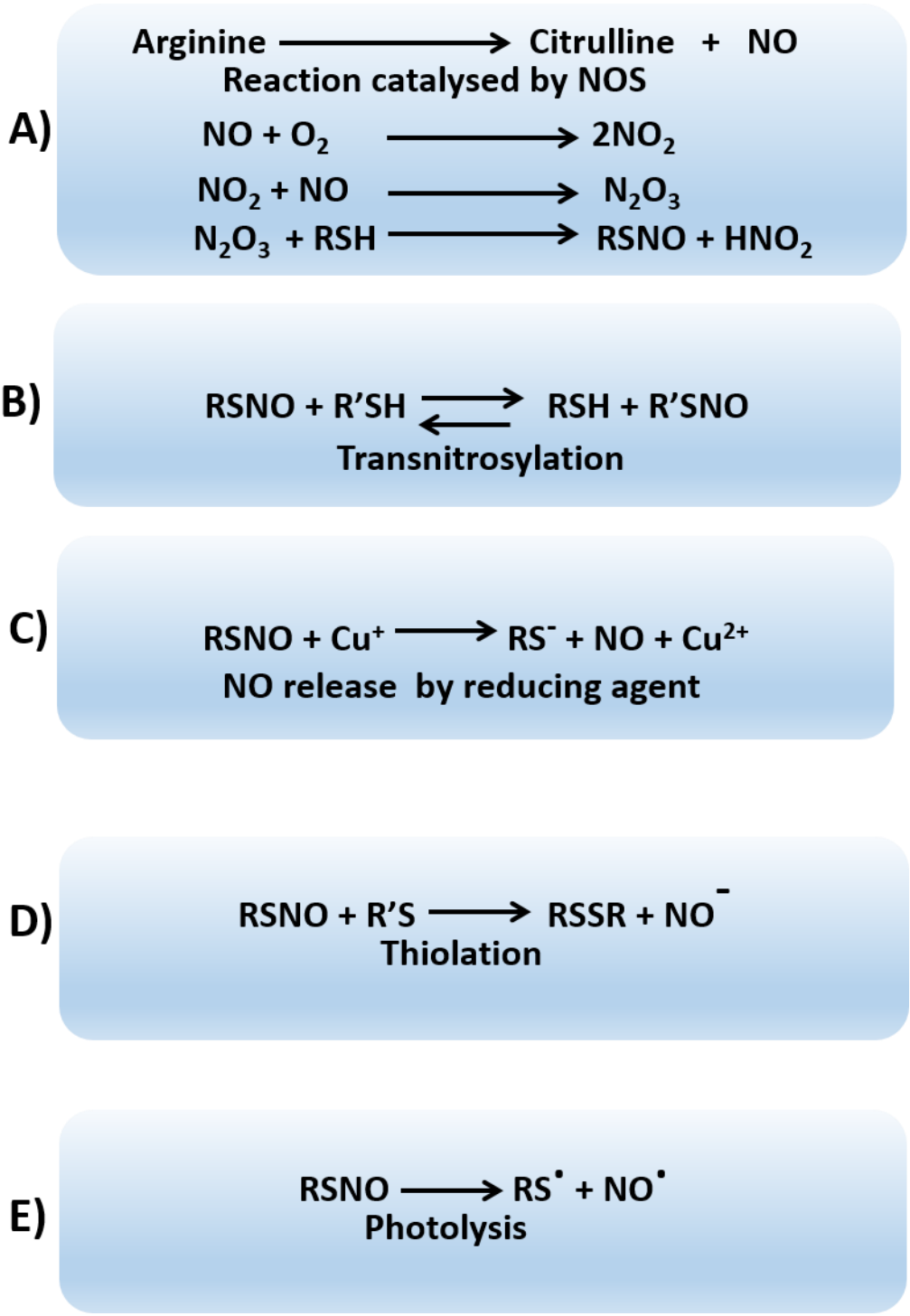

Figure 1.5 Mechanisms of NO, SNO production and decomposition.

A) NOS catalysed NO production from arginine leads to the production of higher NO oxides. N_2O_3 can induce S-nitrosylation reaction. **B)** Transnitrosylation involves the transfer of NO group from one SNO group to another. **C)** NO release reaction results in the liberation of NO and is governed by a reducing agent such as Copper (Cu) **D)** Thiolation is the nucleophilic interaction of thiols with NO of SNO-proteins. **E)** Light mediated photolysis of SNO results in the production of free radical $NO^{\cdot}$

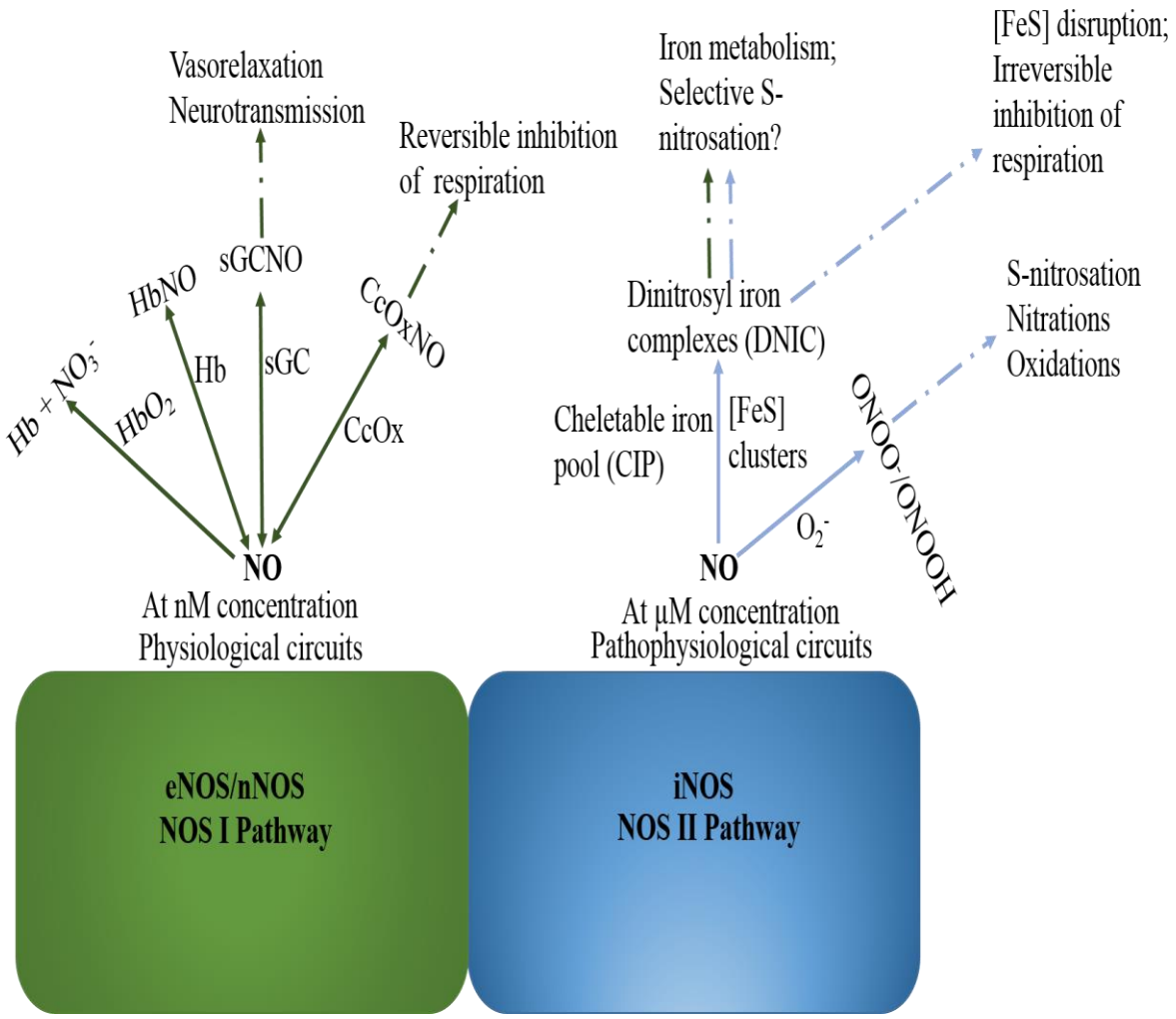

Figure 1.6 Reaction and impact of NO at various concentrations in biology.

At physiological concentrations (nM) (generated by eNOS/nNOS activity), NO reacts with heme proteins such as oxyhaemoglobin/haemoglobins, (HbO_2/Hb), soluble guanylate cyclase (sGC) and cytochrome c oxidase (CcOx) which affect important processes such as vasorelaxation, neurotransmission, respiration. In the presence of high concentrations (µM) of NO (as encountered following the iNOS activity) in pathophysiological conditions, it reacts with superoxide anion radical (O_2^-) and iron sulphur clusters [FeS] to exert biological effects such as immune response, respiration, apoptosis. Adapted from (Toledo & Augusto, 2012).

1.10 S-nitrosohaemoglobin: an important protein in vasodilation

Haemoglobin is the tetrameric protein component of the RBC that transports oxygen (O_2) from lungs to tissue. S-nitrosohaemoglobin (SNO-Hb) has been implicated directly in the SNO mediated hypoxic vasodilation (Stamler *et al*, 1997a). In oxygenated conditions, haemoglobin tetramer is endogenously s-nitrosylated by FeNO of haemoglobin at the cysβ93 position. The oxygenated structure of Hb is termed as 'R' (relaxed, high O_2 affinity). Following deoxygenation of haemoglobin, the NO group from SNO-Hb is released along with O_2 resulting in bioactive NO signal transduction leading to vasodilation. The deoxygenated Hb is termed as 'T' (tensed, low O_2 affinity). Therefore after allosteric transition from R to T state, SNO-Hb from RBCs can transport NO to the compartments of low PO_2 to increase O_2 delivery coupled with NO dispension at microvascular sites (Allen & Piantadosi, 2006; Jia *et al*, 1996). S-nitrosylation driven allosteric regulation of haemoglobin has been validated by different biochemical methods such as photolysis, mass spectrometry and chemiluminescence (Jia *et al.*, 1996, Gow *et al.*, 1998 and Lipton *et al.*, 2001). However, Schimdt and co-workers (1996) argued against the principle of FeNO-SNO transfer in SNO-Hb where they used a triiodide based chemiluminescence for measuring SNO-Hb following cyanide pre-treatment (Schmidt *et al*, 1996). In another analysis Gaston *et al* (2003) questioned the credibility of technique pointing out that tri iodide based chemiluminescence is not suitable for SNO mediated allosteric regulation analysis. Given the redox based complexity of haemoglobin protein, the role of SNO-Hb in vascular regulation still remains a fertile area of research.

1.11 Biological roles of NO

1.11.1 NO as EDRF

Soluble guanyl cyclase is the natural receptor for NO and only a small concentration of NO (5-10 nM) can activate the enzyme. It is mainly found in two major isoforms, $\alpha_1\beta_1$ and $\alpha_2\beta_1$. The latter isoform is found in brain whereas $\alpha_1\beta_1$ has a wider distribution across different tissues (Friebe & Koesling, 2003). Despite difference in spatial expression, there is no difference in their catalytic activity, substrate affinity for NO binding. Although homodimers ($\alpha_1\alpha_1$ and $\beta_1\beta_1$) of sGC has been identified, they are functionally inactive (Zabel *et al*, 1999). Therefore, only heterodimers can catalyse the formation of cGMP from GTP. The subunits are divided into three domains: a C terminal catalytic domain, a middle part and an N-terminal region. It's the N-terminal region that harbours the prosthetic heme group. Presence of this heme group is mandatory for the activation of enzyme by NO. A histidine residue at His-105 position acts as the proximal ligand by binding with the heme. This is pivotal for the NO mediated activation

of the sGC as deletion of his-105 results in abrogation of NO induced activation. (Wedel *et al,* 1994). The NO sensitive heme of sGC exhibits an absorbance maximum at 431 nm. This indicates the presence of a five coordinated ferrous heme group with a histidine acting as axial ligand at the fifth coordinating position (Stone & Marletta, 1994). NO binds to the sixth coordinating and form a NO-Fe^{2+}- His complex. Subsequent breakdown of Fe^{2+}- His complex results in formation of a five coordinated heme-nitrosyl complex with the following reaction of NO with heme.

Fe (II) + NO → Fe (II) - NO

The above cascade of events initiate a conformational change in the structure of sGC enzyme, thereby increasing the conversion of GTP to cGMP by approximately 200 fold (Humbert *et al,* 1990). Studies from Marletta group has shown that sGCs belongs to a recently identified group of proteins termed as 'heme nitric oxide/ oxygen binding protein' (H-NOX) found in both prokaryotes and eukaryotes (Olea *et al,* 2010). The H-NOX domain of sGC is only selective for NO. Structural studies of prokaryotic O_2 binding H-NOX domain have shown that the presence of a hydrogen bonding network in the distal pocket is essential for stable binding to O_2. Sequential mutagenesis of distal pocket amino acids demonstrated that single tyrosine is required for O_2 binding and hydrogen bond formation (Boon *et al,* 2005). However, the mammalian sGCs lack such a tyrosine in its heme pocket, eliminating O_2 as a ligand for heme. Thus in aerobic environment, sGCs can selectively use NO as a ligand to produce cGMP and regulate important biological processes such as vasorelaxation. cGMP stimulates a cGMP-dependent protein kinase that activates myosin light chain phosphatase, the enzyme that dephosphorylates myosin light chains resulting in smooth muscle relaxation.

1.11.2 NO in infection and as an antimicrobial agent

Since NO entered the immunology field in the late 1980s, scientists have been perplexed by the dual role of the molecule in both inhibiting and stimulating immune response. It is produced by a large number of immune cells such as macrophages, T cells, B cells, natural Killer cells. There have been contradictory reports on the levels of iNOS expression in human macrophages (Bogdan, 2001; Schneemann & Schoedon, 2002). When measured by chemiluminescence in our laboratory, the amount of NO detected from MDM is low and it is subsequently converted to nitrite (Stevanin *et al,* 2005). However other studies have demonstrated the presence of iNOS protein and mRNA expression, from human macrophages (Fang, 1997; Weinberg *et al,* 1995). Presence of NO in MDM was also confirmed by the increased 4-amino-5-methylamino-2'7'-

difluorofluorescein (DAF-FM) after infection with *N. meningitidis (*Tunbridge *et al,* 2006). Contrary to previous view that iNOS is the key mediator in immune response, other constitutive NOS such as nNOS, eNOS have been found to be produced by the immune cells during infection (Bogdan, 2001). The diffusible nature of NO means it can exert immune response away from its origin. Redox environment and other stimuli can also trigger NO generation in immune cells independent of the NOS mediated pathway. NO harbouring molecules such as low molecular weight SNO (GSNO) can act as long distance NO carriers (Gaston *et al,* 2003). NO can be liberated from GSNO spontaneously or following cleavage by ectoenzyme gamma-glutamyl transpeptidase (GGT) present on the human T and B lymphocytes (Henson *et al,* 1999). In acidic conditions present in phagocytes, stable product of NOS activity, NO_2^- can be converted to NO. Hemeproteins such as cytochrome P450, peroxidases can oxidise N-hydroxy-L-arginine present in the cells to citrulline and NO (Wu & Morris, 1998).

NO at high concentration as such encountered in an infection situation is normally cytotoxic or inhibitory for microbes (De Groote & Fang, 1995). However, the extent of antimicrobial action depends on multiple factors such as spatiotemporal generation of NO, sensitivity of the organism to NO, ability to detoxify NO by organism. Molecular targets affected by NO include DNA, proteins and lipids. NO can reversibly inhibit cytochrome c oxidase, the terminal enzyme of mitochondrial respiratory chain, leading to the inhibition of cellular respiration (Cleeter *et al,* 1994). Zinc is an essential element of living organism and also a vital component of proteins such as NOS. In addition it helps to stabilise the protein structures. NO can displace zinc from the metallothionein of *E.coli* (Binet *et al,* 2002) and mobilise the zinc in *Salmonella enterica* (Schapiro *et al,* 2003). Most of the antimicrobial effects of NO result not from the direct effect of NO but by the activity of reactive nitrogen intermediates formed by the NO oxidation products. Such examples include formation of peroxynitrite ($OONO^-$) and SNO. Peroxynitrite ($OONO^-$) is formed when NO rapidly reacts with the superoxide (O_2^-). They are very reactive compounds which can interact with a variety of biological of targets. Peroxynitrite affects transcription after reacting with the DNA sugar phosphate backbone, cell membrane degradation after reacting with lipid, and cause cysteine oxidation and tyrosine nitration after reacting with the metal-centres and amino acid residues (Pacher *et al,* 2007). In aerobic condition, NO can deaminate DNA via the intermediate of SNO production N_2O_3 (Wink *et al,* 1991) **(Figure 1.5A)**. NO derived reactive nitrogen species inhibit essential microbial enzymes such as ribonucleotide reductase and aconitase by reacting with the iron group present in these enzymes (Burgner *et al,* 1999). NO can exert lethal effects on microbes indirectly by its

immunomodulatory actions such as T-cell activation/inhibition, cytokine regulation, autoimmune response (McInnes & Liew, 2002).

During sepsis high levels of NO from iNOS may contribute to hypotension and inflammatory tissue damage (Kilbourn *et al,* 1997). Indeed, decreased mortality and microvascular reactivity has been observed in iNOS deficient animal model or conditions where iNOS activity has been inhibited by commercial inhibitor or scavengers (Hollenberg *et al,* 2000; Kim & Greenburg, 2002). In contrast, other groups have reported contradictory findings using similar approaches where a reduced iNOS activity resulted in unaltered or increased mortality in sepsis (Laubach *et al*, 1995; Lopez *et al,* 2004). Therefore NO may play both detrimental and protective role during the course of sepsis. This implies any NO mediated observation in sepsis has to be interpreted from the context the experimental system used.

1.12 Respiratory pathway of *Neisseria meningitidis*

N. meningitidis is typically considered as an obligate aerobe. It utilises oxygen as the terminal electron acceptor. It is incapable of anaerobic growth which could be due to the possession of only the aerobic (class I) ribonucleotide reductase (Rock *et al,* 2005). It can grow microaerobically using the partial denitrification pathway (Anjum *et al*, 2002). This would make evolutionary sense as the only natural habitat of the organism, nasopharynx is oxygen poor but rich in NO (Lundberg *et al*, 1994; Lundberg & Weitzberg, 1999). Routine isolation of both aerobic and anaerobic bacteria further strengthens this argument (Brook, 2003).

Denitrification is the step-wise reduction of nitrate (NO_3^-) to dinitrogen (N_2) gas. Conversion from NO_3^- to N_2 is split into four reactions, each catalysed by a specific metalloenzyme complex **(Figure 1.7 A)** (Tavares *et al,* 2006). Firstly NO_3^- is converted to NO_2^- catalysed by nitrate reductase. Subsequently NO_2^- is reduced to NO by nitrite reductase. NO is converted to N_2O by nitric oxide reductase and lastly nitrous oxide reductase converts N_2O to N_2. In denitrifying bacteria, denitrification pathway is linked to the respiratory chain. NO oxide substrates at each step serve as alternative sink for electrons and support bacterial growth by coupling with oxidative respiration (Zumft, 1997). *In vivo*, NO_2^- is produced both by the activity of the nitrate reducing bacteria present in mouth, pharynx and also by oxidation of NO which is used as a signalling molecule (Lundberg *et al,* 2004; Rock *et al*, 2005).

Unlike other full denitrifiers such as *Paracoccus denitrificans*, *Pseudomonas aeruginosa*, *Ralstonia metallidaruns* etc, *N. meningitidis* is classified as a partial denitrifier as it contains only two genes of the whole denitrification pathway **(Figure 1.7 A).** Whole genome sequence

of *N. meningitidis* has revealed the presence of two divergently transcribed genes coding for *aniA*, a copper containing nitrite reductase **(Section 1.13.1)**, and *norB*, a nitric oxide reductase **(Section 1.13.2)** (Tettelin *et al*, 2000). These two genes are separated by having an intergenic region of 370 bp and are subject to complex regulation by multiple transcriptional activators, repressors **(Figure 1.8).**

Homologues for respiratory complexes I, II and II are found in *N. meningitidis*. Therefore, electrons could enter the respiratory chain through a proton translocating NADH dehydrogenase or a succinate dehydrogenase. Subsequently these electrons could be transferred to the cytochrome bc1 complex by ubiquinone **(Figure 1.7 B)** (Rock & Moir, 2005). It is to be noted that *N. meningitidis* possess only one terminal reductase capable of utilising oxygen. The reductase is known as cytochrome cbb_3 oxidase and was first identified in *Bradyrhizobium japonicum*. It is a membrane bound heme copper oxidase (Preisig *et al*, 1996). It has high affinity for oxygen and is involved with oxygen limited conditions (Pitcher & Watmough, 2004). This property enables *N. meningitidis* to adapt to microaerobic condition. However, meningococcal cbb_3 active site can bind to both O_2 and NO. This implies that during the denitrification process, the oxidase can be competitively inhibited by the generation of NO, intermediate product of denitrification. In presence of high NO and O_2 concentrations, these two compounds can react to form peroxynitrite which can damage the cbb_3 (Brown & Cooper, 1994; Sharpe & Cooper, 1998).

Respiration by oxygen reduction is preferable over nitrite as the redox potential of O_2/H_2O (+820 mV) is higher than that of NO_2^-/NO (+348 mV) (Conrad, 1990). So, O_2 has higher affinity for electron over NO_2^-. In addition, higher energy is liberated by proton translocation by the flow of electrons towards oxidase physiologically in comparison to the reduction of NO_2^-. The translocated protons are used for generating ATP for the organism. Hence both in presence of O_2 and NO_2^-, reduction of O_2 is preferable in most of the cases due to the generation of more energy in the form of ATP. NADH is the major source of electrons for both the O_2 and NO_2^- mediated respiratory pathways. Ubiquinone is reduced to ubiquinol in quinone pool present in the inner membrane by receiving electrons from NADH. NorB enzyme or bc_1 complex directly oxidises ubiquinol by receiving electron and reducing NO to N_2O in the process. A number of intermediate cytochromes transfer electrons from bc_1 complex terminal oxidases to AniA and cbb_3 **(Figure 1.7 B).**

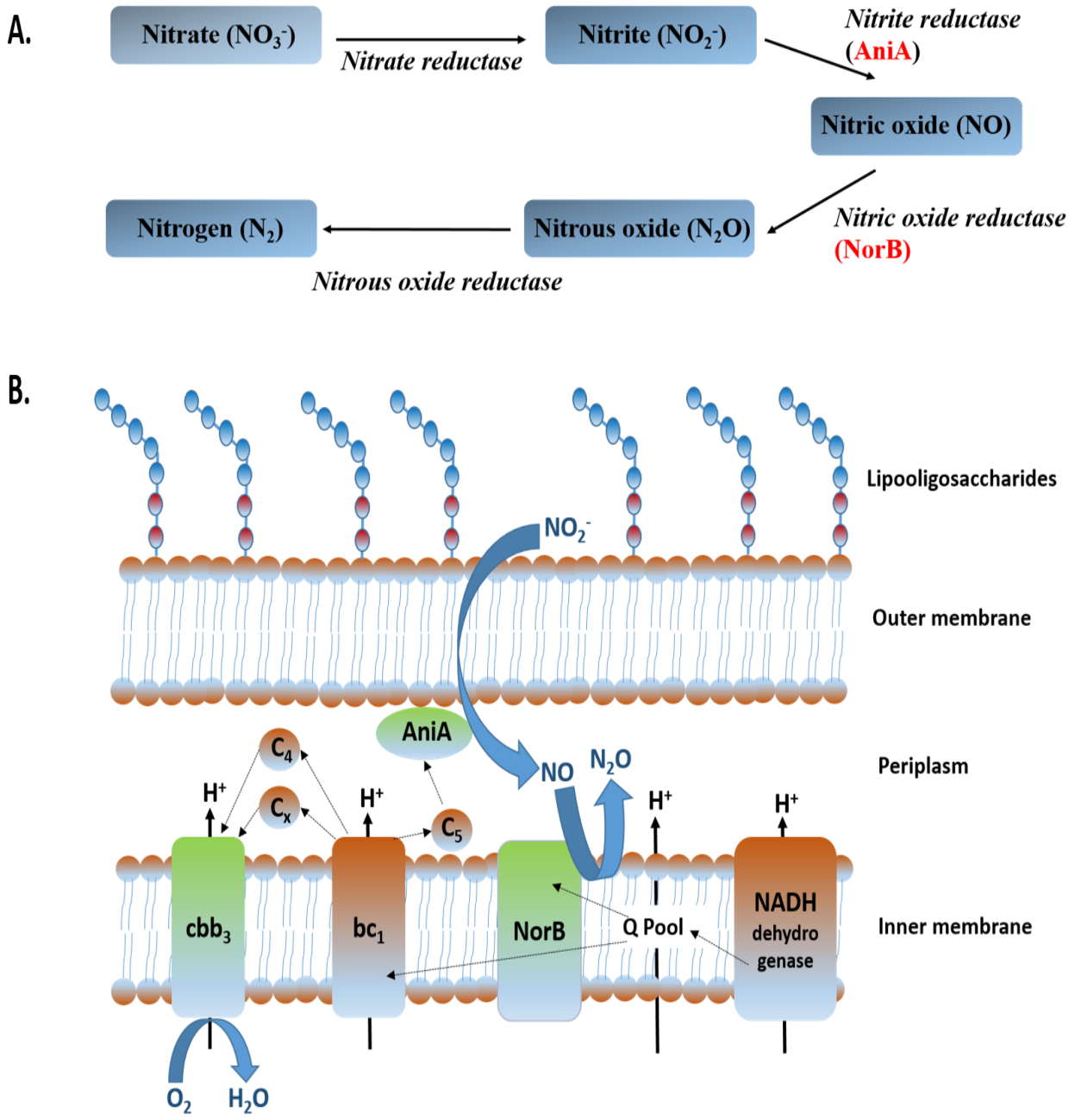

Figure 1.7 Denitrification pathway and meningococcal respiratory chain

A) Denitrification pathway- Gradual reduction of NO_3^- to N_2 where each step is catalysed by a denitrification enzyme. The enzymes encoded by *N. meningitidis* are highlighted in red. **B) A cartoon summarising the respiratory chain of *N. meningitidis***- Respiratory substrates (NO_2^-, NO, O_2) are indicated in blue, corresponding thick blue arrays link them to the corresponding reducing enzymes in green gradient (AniA, NorB and cbb_3). Electron transporters are highlighted in light orange gradient and electron flow is depicted by black arrows.

1.13 Essential enzymes and proteins of meningococcal respiratory pathway

1.13.1 AniA (Nitrite reductase)

AniA was identified as Pan1 (54 kDa), major protein expressed by *N. gonorrhoeae* in anaerobic conditions. The terminal electron acceptor supporting anaerobic growth was identified as nitrite in gonococcus (Knapp & Clark, 1984). Later using specific antibody, presence of Pan1 was confirmed in the patients suffering from gonorrhoea (Clark *et al,* 1987) and similar proteins were found in other *Neisseria* spp such as in *N. meningitidis* (Hoehn & Clark, 1990). Pan1 was renamed as AniA (anaerobically induced protein A) after cloning and sequencing (Hoehn & Clark, 1992a). Study by the same group also confirmed it as an outer membrane protein by identifying it as a lipoprotein (Hoehn & Clark, 1992b). Bacterial nitrite reductase can be of two types which are distinguishable by their prosthetic groups: the copper containing nitrite reductases (CuNIR) and the cytochrome cd1-type reductases containing two haem groups. Low level similarity of AniA to that of copper containing nitrite reductase was first reported in 1995 (Berks *et al,* 1995). AniA was confirmed as the copper containing inducible nitrite reductase when an insertional mutation in the *aniA g*ene rendered the anaerobic growth of gonococcus severely impaired (Mellies *et al,* 1997). Importance of *aniA* as gonococcal virulence factor was further realised when a study showed that overexpression of *aniA* can afford protection against the killing following exposure to human serum (Cardinale & Clark, 2000). Crystal structure and sequence comparison of nitrite reductases from 15 other bacteria have revealed that AniA is a class II CuNIR sharing 45% sequence identity with the nitrite reductase from the archaebacterium *Haloarcula marismortui* (Boulanger & Murphy, 2002). Meningococcal AniA is coded by NMB1623 and is 1173 bp in length. It has been shown to be important for the bacterial growth in oxygen limited conditions (Rock & Moir, 2005). It can accept electrons from the c type cytochrome (C_5) **(Figure 1.7 B)** (Deeudom *et al,* 2008). However studies from different groups have confirmed the presence of mutation in the catalytic domain of meningococcal *aniA* whereas it is conserved in other *Neisseria spp*. A study conducted by Barth and colleagues reported that 13 of 41 (32%) sequenced meningococcal genome contains a frameshift mutation in the *aniA* region and the strain 053442 lacks *aniA* completely suggesting that the strain would be unable to perform denitrification (Barth *et al,* 2009). In addition, in *N. gonorrhoeae* and other related *Neisseria spp.,* AniA can receive electrons from C_5 and via a second route via the CcoP domain of cytochrome cbb_3. However, AniA of *N. meningitidis* only receives electrons from cytochrome C_5 as one of the CcoP domains is non functional due to a single nucleotide polymorphism (Aspholm *et al,* 2010). This is a meningococci specific

adaptation. All these strains retain functional *norB* **(Section 1.13.2)** providing the organism protection from the toxic effects of NO. Therefore, it has been suggested that *N. meningitidis* could be evolving towards becoming a NO tolerant aerobe from being a denitrifier (Moir, 2011).

$$\text{AniA}_{\text{(reduced)}} + NO_2^- + 2H^+ \rightarrow \text{AniA}_{\text{(oxidised)}} + NO + H_2O$$

1.13.2 NorB (Nitric oxide reductase)

NO reductases (NOR) are of three types, the cNOR (cytochrome *bc* type complex), qNOR (the cytochrome b type complex lacking the cytochrome c component) and a qNOR-type reductase that also includes Cu_A (qCu_ANOR). cNOR type reductases accept electrons from soluble protein donors and qNOR receives electrons from quinol. Identification of nitrous oxide as the end product of anaerobic respiration on nitrite (Lissenden *et al,* 2000) led to the identification of qNOR in *N. gonorrhoeae* (Householder *et al,* 2000). The NOR in *N. meningitidis* is a qNOR-type reductase which is encoded by NMB1622 (Wasser *et al,* 2002). The first *Neisserial* 84.3 kDa NorB was identified in *N. gonorrhoeae* and it shares high sequence identity with the soil bacterium *Ralstonia eutropha* (Householder *et al,* 2000). It catalyses the conversion of NO to N_2O by receiving electron from the quinone pool **(Figure 1.7 B).** Accumulation of high concentration of NO as a result of NO_2^- reduction by AniA has bactericidal activity as it inhibits aerobic respiration by binding to the cbb_3 oxidase competitively. Therefore, this enzyme is critical for bacterial growth during microaerobic condition. It is highly conserved across all *Neisseria* species. Activity of NorB is 2.5 to 3 times higher in *N. meningitidis* (240-256 nmol NO reduced per minute per OD_{600} unit) compared to *N. gonorrhoeae* (88-155 nmol NO reduced per minute per OD_{600} unit) (Barth *et al,* 2009). It has been shown to be important for the survival of the organism inside human MDMs and nasopharyngeal mucosa (Stevanin *et al,* 2005). Furthermore, it is also essential for regulation of apoptosis (Tunbridge *et al,* 2006) and cytokine and chemokine response of human MDMs (Stevanin *et al,* 2007).

$$\text{NorB}_{\text{(reduced)}} + NO + 2H^+ \rightarrow \text{NorB}_{\text{(oxidised)}} + N_2O + H_2O$$

1.13.3 NsrR (Nitrite sensing repressor protein)

NsrR (Nitrite sensing repressor protein) is an NO sensing Rrf2 type transcriptional repressor protein. It was first discovered in *Nitrosomonas europaea* (Beaumont *et al,* 2004). Since then it has been shown to be a mediator of expression of NO metabolising genes in different bacterial species such as *E. coli* (Bodenmiller & Spiro, 2006), *Salmonella* (Gilberthorpe *et al,* 2007) , *N. gonorrhoeae* (Overton *et al,* 2006) and *N. meningitidis* (Heurlier *et al,* 2008; Rock *et al,* 2007) etc. The protein sequence is well conserved across all *Neisseria* spp (Barth *et al,* 2009). Both *N. gonorrhoeae* and *N. meningitidis* use NsrR as a negative regulator of *aniA* and *norB* transcription (Overton *et al,* 2006; Rock *et al,* 2007). Binding site of NsrR is located 60 bp upstream of the *aniA* promoter. Three conserved cysteine residues in NsrR are responsible for sensing NO by coordinating with [2Fe- 2S] cluster (Isabella *et al,* 2008). These residues are conserved in all the *Neisseria* species (Barth *et al,* 2009). *E.coli* has a large NsrR regulon where it regulates the expression of 39 genes (Filenko *et al,* 2007). In contrast, NsrR regulon is small in *N. meningitidis* where it regulates the expression of only 5 genes (*aniA, norB, nirV, dnrN, mobA*) (Heurlier *et al,* 2008). *dnrN* encodes for a protein involved in the repair of nitrosative damage to iron-sulfur clusters) and *nirV* (a putative nitrite reductase assembly protein).

1.13.4 FNR- (Fumarate and nitrite reductase regulator)

Expression of *aniA* is primarily mediated by O_2 sensing FNR protein. FNR is a transcriptional activator and homologue of the fumarate and nitrate reductase repressor protein. It was first discovered in *E. coli* (Lambden & Guest, 1976) and is a member of FNR-CRP superfamily of transcriptional regulators (Korner *et al,* 2003).

Structural prediction of FNR in comparison with similar transcriptional regulator such as CRP of *E. coli* (Weber & Steitz, 1987) reveal that it can be divided into three regions depending on the function; a C-terminal DNA binding domain, a helix responsible for facilitating the dimerization of the FNR monomer and an N-terminal domain harbouring an iron-sulphur (FeS) centre for oxygen sensing. The FeS centre is found as [4Fe – 4S] in anoxic condition but converted to [2Fe-2S] upon exposure to oxygen (Barth *et al,* 2009).

FNR is termed as the master regulator of *aniA* expression. By binding directly with O_2, FNR regulates the expression of nine transcriptional units in *N. meningitidis* (Bartolini *et al,* 2006). In closely related pathogen, *N. gonorrhoeae* it regulates the expression of fourteen genes but downregulate six genes (Whitehead *et al,* 2007). FNR regulated genes are involved in anaerobic respiration and carbon metabolism. Both in gonococcus and meningococci, FNR is

pivotal for AniA activity as evidenced by diminished NO_2^- reduction by *fnr* mutants (Lissenden *et al,* 2000; Rock *et al,* 2005; Rock *et al,* 2007).

In addition, *N. meningitidis* serogroup B *fnr* mutant strains are attenuated in mouse and rat models (Bartolini *et al,* 2006). Although normally regarded as an oxygen sensitive regulator of *aniA*, it can also be regulated by NO (Heurlier *et al,* 2008). The $[4Fe\text{-}4S]^{2+}$ cluster of FNR reacts with NO to form dinitrosyl-iron complexes (DNICs) which reduces the affinity of FNR to bind its DNA sequence (Cruz-Ramos *et al,* 2002). Unlike other facultative anaerobe such as *E. coli,* meningococcal FNR retains substantial DNA binding activity even under aerobic condition due to the absence of an anaerobic ribonucleotide reductase (Rock *et al,* 2007). Therefore FNR allows limited transcription of promoters it regulates such as *aniA* under aerobic condition (Heurlier *et al,* 2008). Paradoxically *aniA* can be expressed even in the presence of 70%-80% oxygen saturation when no NsrR is present. This implies that meningococcal FNR is insensitive to oxygen when compared with FNR from *E. coli*. In addition, binding to its cognate DNA also makes the protein less sensitive to oxygen (Edwards *et al,* 2010).

1.13.5 NarQ/NarP- Nitrite response sensor/regulator

The first NarQ-NarP regulator was discovered in *E.coli* (Stewart & Parales, 1988). The two component signal transduction pathway is responsible for regulating the expression of *aniA* in *Neisseria*. NarP is a cytoplasmic protein but NarQ is located at the inner membrane. As a part of the two component system, it regulates the expression of target genes when the sensor phosphorylates the regulator. In *N. gonorrhoeae,* NarP increases the expression of *aniA* (Overton *et al,* 2006). Both oxygen and nitrite availability induces *aniA* activity in *N. meningitidis* (Rock *et al,* 2005). Despite the presence of NarQ/NarP, FNR is an absolute requirement for the activity of *aniA* in meningococci (Rock *et al,* 2005). Therefore, increased nitrite reduction activity of *N. meningitidis* is only commenced after when there is a low concentration of oxygen and a high concentration of nitrite.

1.14 Regulation of transcriptional control of meningococcal partial denitrification pathway

The transition from aerobic to microaerobic growth in *N. meningitidis* is sophisticated and regulated by a variety of genes, stimuli and transcription factors **(summarised in Figure 1.8).** Both *aniA* and *norB* are divergently transcribed from promoters sharing a common intergenic region which has putative binding sites for NsrR, AsrR, Fur, NarP and FNR. Amount of

available NO in the environment is one of the main determinants of expression of denitrification genes. Both constitutive and inducible NO responsive systems are operated by meningococci to protect the cells from nitrosative damage and continue denitrification to support growth. Cytochrome c' (CycP) is the part of constitutive NO detoxification system. In photosynthetic denitrifying bacterium *Rhodobacter capsulatus* it provides protection against NO in aerobic and microaerobic condition but is not involved in denitrification pathway (Cross *et al*, 2000; Cross *et al*, 2001). Likewise meningococcal CycP can bind to NO (Huston *et al*, 2005) and can presumably offer some protection against NO mediated toxicity prior to a burst of NO (Anjum *et al*, 2002). Similar regulation operates in the closely related organism *N. gonnorhoeae* where CycP protects the organism against NO during transition to denitrification, a time before the accumulation of high NO for *norB* activity (Turner *et al*, 2005). In low NO concentration (< 1µM), limited *aniA* is expressed by the oxygen tolerant FNR **(Section 1.13.4).** NsrR repressor **(Section 1.13.3)** is still bound to the operon at this stage. In environment such as a lack of oxygen and in the presence of NO_2^-, *aniA* activity is increased to enable the bacteria to utilise NO_2^- as the respiratory substrate to supplement its growth. Conversion from NO_2^- to NO results in an accumulation of NO. As NO concentration increases to a high level (~1 µM), NsrR is inactivated. Repression of NsrR regulon is relieved as it comes off the DNA. This enables the transcription of genes from *norB* and *dnrN* promoters and also increases activity of *aniA* promoter. Meningococcal *dnrN* is homologous to YftE protein in *E. coli* where it is essential for maintaining and repairing the iron-sulphur cluster upon exposure to NO (Justino *et al*, 2007). Regulation of *dnrN* by *nsrR* would indicate that *dnrN* helps to maintain iron-sulphur clusters in proteins such as FNR and thereby eliminating the need to synthesise new FNR proteins in nitrosative stress conditions. So, in response to high NO, denitrification increases to support bacterial growth and NO detoxification helps to protect bacteria from the NO mediated toxicity arising from the exposure to high NO concentration **(Section 1.11.2).** This kind of regulation has significant implication for the adaptability of organism to nasopharynx as constitutively high levels of NO is detected from human nasopharynx (Andersson *et al*, 2002; Lundberg *et al*, 1995). NO produced from the immune cells such as macrophages can also contribute to the pool of NO present in nasopharynx. Therefore, the NsrR regulon could be switched on at all times in nasopharyngeal environment due to high physiological concentration of NO.

When NO concentration increases further (>1 µM), NO binds to $[4Fe\text{-}4S]^{2+}$ cluster of FNR and forms dinitrosyl-iron-cysteine complex (DNIC) (Cruz-Ramos *et al*, 2002). Consequently FNR

is inactivated due to its reduced affinity for DNA from *aniA* promoter region and *aniA* transcription is completely diminished. However, *norB* and *dnrN* expression still remain high due to the *nsrR* inactivation. Reduced *aniA* expression and continued high *norB, dnrN* prevent the NO mediated toxicity by preventing accumulation of intermediate NO and continued NO detoxification. In response to varying concentration of NO, sensitivity of FNR and NsrR to NO helps to spatiotemporally regulate the optimal expression of denitrification/detoxification genes to support bacterial growth as well as to allow NO detoxification.

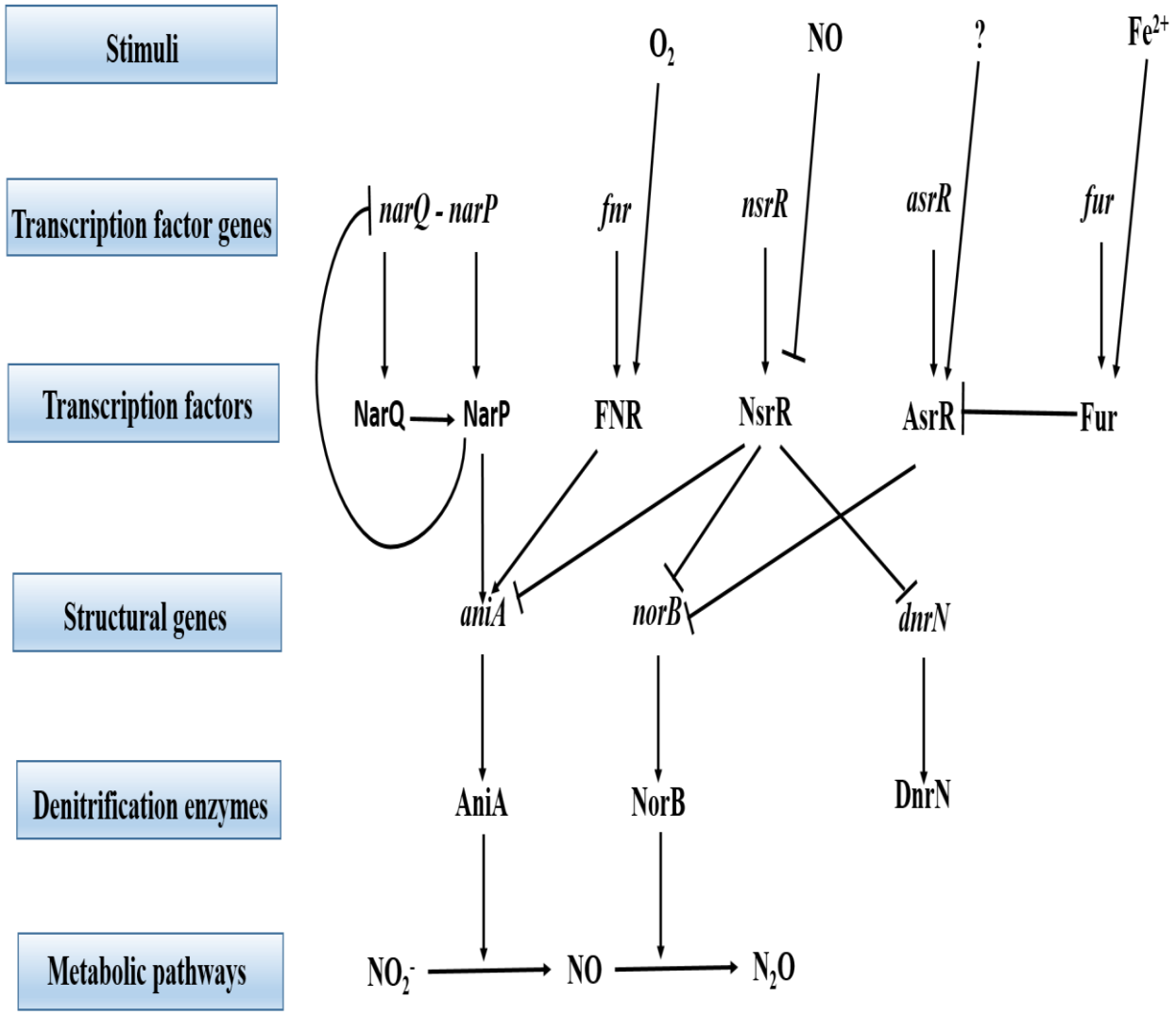

Figure 1.8 Sophisticated environmental and transcriptional regulation of denitrification pathway of *N. meningitidis*.

Different stimuli, transcription factors, enzymes regulating the truncated denitrification pathway of *N. meningitidis* are shown. (For further description of the components the reader is referred to section 1.13- 1.14)

1.15 Importance of meningococcal NO metabolism on host-pathogen interactions

While studying any infectious disease, it is important to consider both host and pathogen holistically. Sophisticated interaction between invading microbe and host determine the progression and outcome of the disease. This is more applicable in the case of *N. meningitidis* which is normally a harmless commensal in 10% -35 % of the adults. When the interplay between host and commensal is disrupted by various factors, commensal can go on to become a pathogen. *N. meningitidis* has developed a set of exquisite mechanisms such as LOS, capsule, adhesins, factor H binding protein to evade the immune response and cause systemic infection. It still remains a paradox that why such a commensal would develop a range of mechanisms to trigger hyperimmune response as it would represent an evolutionary dead end for this accidental pathogen.

By conducting a number of studies our group has shown the importance of NO detoxification pathway of *N. meningitidis* as a virulence factor. NorB and to a lesser extent CycP are essential for the survival of *N. meningitidis* inside human MDM and organ culture of human nasopharyngeal mucosa. The effect was diminished when iNOS was inhibited by L-arginine analogue, (L-NMMA), N (G)-monomethyl- L-arginine (Stevanin *et al,* 2005). Therefore, *N. meningitidis* counteracts NO mediated toxicity in phagocytic cells such as MDM by expressing *norB*. Incubation of resting macrophage with an exogenous NO donor, SNAP (S-nitroso-N-acetylpenicillamine) alters the cytokine and chemokine profile (Stevanin *et al,* 2007). Same work showed that infection of MDM for 20 hours with Δ*norB* significantly increased the production of TNFα, IL-8, IL-10, IL-12 but lowered the production of CCL5 compared to Wt infected MDM. This implies bacterial NO detoxification can differentially modulate the cytokine profile of immune cells such as MDMs.

Apoptosis is an important process initiated by the immune cells to kill the invading microbes. NO has dichotomous role in the regulation of apoptosis as it has both stimulatory and inhibitory effects on cell death. Infection of human MDM with either Δ*norB* or Δ*cycP* for 20 hours leads to a significant increase in the number of MDM undergoing apoptosis compared to Wt infection (Tunbridge *et al,* 2006). This would help the bacteria to survive longer inside the phagocytic cells in an infection situation.

A study from our group has demonstrated that NO detoxification of *N. meningitidis* reduces the SNO formation in the murine macrophage cell line J774.2 (Laver *et al,* 2010). Murine

macrophage cell lines were stimulated with LPS and IFNɣ for 18 hours to induce iNOS activity. NO detoxification machinery was able to reduce the formation of SNO by metabolising iNOS induced NO. Similar SNO depletion mechanism was observed with NO detoxifying flavohemoglobin (Hmp) gene mutants of *Escherichia coli* and *Salmonella enterica*. This would have far reaching consequences in the regulation of cellular processes as SNO is a tightly regulated signalling molecule. Therefore, any reduction in local SNO concentration by active bacterial NO metabolism as demonstrated by Laver and his colleagues has the potential to cause pathology in clinics. This work was particularly important for this thesis as it provided the foundation for Chapter 3 which investigated if the similar observation is noticed *in vivo* in a murine model of acute fulminant meningococcal sepsis.

1.16 Aims and Objectives

This thesis set out to establish an animal model of early acute meningococcal sepsis in which we can measure NO metabolites in a reproducible manner. Subsequently, it will be exploited to examine if SNO depletion by the active NO detoxification of *N. meningitidis* in the murine J774.2 cell line (Laver *et al,* 2010) can be replicated *in vivo* **(Chapter 3).**

To date we have used isogenic single mutants of meningococcal denitrification genes for studying the cellular pathology of sepsis. Since NO is subject to sophisticated redox based regulation in biology and meningococcal denitrification is a multifactorial process **(Figure 1.8)** defect in multiple genes could have profound impact on the cellular pathology of meningococcal sepsis. Therefore, it was decided to generate and characterise a panel of denitrification mutants (Δ*aniA*/Δ*norB*, Δ*nsrR*/Δ*norB*, Δ*aniA*/Δ*norB*/Δ*nsrR*) which will serve as important tools in studying the contribution of meningococcal denitrification pathway to pathogenesis **(Chapter 4).**

Differentiated human primary bronchial airway epithelial cell cultured at an air-liquid interphase (HPEC-ALI) is a differentiated and polarised epithelial layer forming tight junctions sharing similar characteristics with the nasopharyngeal epithelial cells. Meningococci have to interact with the nasopharyngeal epithelium during colonisation and pathogenesis. NO is present in high concentrations in the airway epithelium where it is an important regulator of many important processes such as barrier function and immune response of the airway epithelium. Therefore, we decided to investigate if meningococci could use its denitrification pathway to modulate barrier function and immune response of the HPEC-ALIs **(Chapter 5).**

As nasopharynx is an NO rich habitat, meningococcal denitrification would be essential for the survival and successful colonisation of the organism in nasopharynx. Biofilm formation could be one of the strategies employed by the meningococci to colonise nasopharynx. In the closely related pathogen *N. gonorrhoeae,* the denitrification pathway plays an important role in biofilm formation both *in vitro* and *in vivo*. So it was decided to examine the role of meningococcal denitrification pathway on biofilm formation *in vitro* **(Chapter 6).**

Details on the experimental rationale and methods are mentioned in each chapter.

2 Chapter 2: Materials and Methods

2.1 Reagents

2.1.1 Antifoaming agent FG-10

Antifoaming agent FG-10 30x concentrate was supplied by Dow Corning. This was diluted with dH_2O to a working concentration prior to usage.

2.1.2 Complete, Mini EDTA-free protease inhibitor cocktail tablets

Complete mini EDTA-free protease inhibitor tablets were purchased from Roche.

2.1.3 Drabkin's solution

In 1000 ml of distilled water, 200 mg $K_3Fe^{III}(CN)_6$, 50 mg KCN (FW 65.12, Aldrich Chemicals), 140 mg (KH_2PO_4), 0.5 ml of Sterox SE were added to make Drabkin's solution.

2.1.4 Human holo transferrin (hHTF)

Each bolus of injection into the mice where appropriate contained 8 mg of hHTF purchased from Sigma-Aldrich, UK.

2.1.5 Polymerase chain reaction primers

PCR primers were purchased from Eurofins and Sigma-Aldrich. After receiving the primers from the company they were briefly centrifuged and mixed with the specified amount of molecular biology water (as mentioned on the primer label) to give a final concentration of 100 µM. Then they were diluted by 10 fold to have a final concentration of 10 µM and stored in the freezer for future applications.

2.2 Buffers

2.2.1 Phosphate buffered saline (PBS) at pH 7.4

Phosphate buffered saline was produced in-house by the addition of 10 PBS tablets (Thermo Fisher Scientific, USA) to 1 L of dH_2O. Sterilisation of PBS in 500 ml aliquots were performed by autoclaving at 121°C for 15 minutes. The PBS contains NaCl (140 mM), Na_2HPO_4 (8.0 mM), $K_2H_2PO_4$ (1.5 mM) and KCl (2.7 mM), 50 mM Phosphate buffer + 1 mM Diethylenetriaminepentaacetic acid (DTPA) at pH 7.4.

2.2.2 S-nitrosothiol compatible lysis buffer

SNO compatible lysis buffer solution was prepared for processing the liver lysates. Sixty three mg of N-ethylmaleimide (NEM) was mixed with 5 ml of 50 mM phosphate buffer + 1 mM DTPA, 12.5 µl of 0.5 mM Phenylmethanesulphonyl flouride (PMSF) and ½ tablet of protease

inhibitor cocktail tablet. The solution was prepared by vortexing for 15 minutes in a light protected tube. For ensuring maximum efficacy, the buffer had to be prepared prior to the experiment and stored in the dark, on ice along the experimental procedures.

2.2.3 50 mM Phosphate buffer + 1 mM DTPA, pH 7.4

For preparing GSNO standards, 50 mM phosphate buffer was prepared. 3.87 ml of 1 M Na_2HPO_4 and 1.13 ml of 1 M NaH_2PO_4, 39.3 mg of DTPA were topped up with 100 ml of dH_2O and pH of the solution was adjusted to 7.4.

2.3 Solutions

2.3.1 100 mM Sulphanilamide in 2 N HCl

A total of 1.722 g of sulphanilamide was added to 100 ml of 2 N HCl to produce 100 mM sulphanilamide and stored at 4°C for later usage.

2.3.2 50 mM Mercury (II) chloride ($HgCl_2$)

Produced by dissolving 1.358 g of Mercury chloride in 100 ml of dH_2O.

2.3.3 Hanks Balanced Salt Solution (HBSS) without Ca^{2+} or Mg^{2+}

(Life Technologies Cat No: 14170-138)

2.3.4 Tri-iodide (I_3^-) reaction mixture

For each chemiluminescence experiment, fresh tri-iodide mixture was prepared in a light protected conical flask. 525 mg Potassium Iodide (KI), 336 mg dry Iodin (I_2) were dissolved in 21 ml dH_2O and 73.5 ml glacial acetic acid. The solution was mixed at least for 20 minutes by using a magnetic stirrer and stirring plate. The dark brown coloured final solution can be stored for 24 hours at room temperature without the loss of reactivity.

2.3.5 Preparation of *S*-nitrosoglutathione (GSNO)

In a small beaker containing 4 ml of ice-cold H_2O, 0.76 g of L-glutathione was added and mixed using a magnetic stirrer. Then 1.25 ml of ice-cold 2 N HCl was added with a concentration of $NaNO_2$ between 0.17 g and 0.2 g. The subsequent colour of the mixture was pink. The whole apparatus was stirred for 40 minutes in the cold room at 4°C. 10 ml of ice-cold acetone was added and the mixture was stirred further for 10 minutes to precipitate *S*-nitrosoglutathione (GSNO). Pink solid GSNO was separated using a vacuum flask and filter paper. The GSNO was washed with 10 ml of ice-cold acetone for the second time to precipitate any remaining GSNO. The freshly prepared GSNO on filter paper was placed in a light

shielding vacuum desiccator. Small quantities of GSNO were stored at -80°C in the light shielded microcentrifuge tubes following the overnight desiccation period.

2.3.6 RF1 solution for competent cell

For preparing 100 ml of RF1, 100 mM KCl (0.745 g), 50 mM $MnCl_2.4H_2O$ (0.98g), 30 mM K- acetate (0.29g), 10 mM $CaCl_2.2H_2O$ (0.246g), 15% (m/v) Glycerol were mixed and topped up to 100 ml sterile Milli-Q H_2O. Final pH of the solution was adjusted to 5.8 with acetic acid. Then the solution was used after filter sterilisation.

2.3.7 RF2 solution for competent cell

RF2 solution was prepared by adding 10 mM MOPS (50 mg), 10 mM KCl (15 mg), 75 mM $CaCl_2.2H_2O$ (369 mg), 15% (w/v) glycerol (3 g). pH was adjusted to 6.8 with NaOH. The final solution was filter sterilised before final use.

2.3.8 Spermine NONOate

Spermine NONOate was purchased from AG Scientific Inc., San Diego, CA. Concentration of 50 mM was prepared by suspending the compound in 0.01 M NaOH. Working concentration of 50 µM was used prepared by making 1 in 1000 dilution. The compound has a half-life of 39 minutes at 37°C at neutral pH.

2.4 Bacterial Culture Techniques

2.4.1 Columbia Blood Agar

Columbia blood agar supplemented with horse blood was purchased from Oxoid, UK.

2.4.2 GC Agar

GC Agar was produced by autoclaving 10.8 g of GC agar base powder (Oxoid, UK) in 300 ml dH_2O at 121°C for 15 minutes and was allowed to cool for 10 minutes. Following this step, agar solution was supplemented with 1% (v/v) Vitox supplement (Oxoid). For preparing Spectinomycin containing GC agar plates, the cooled solution was also supplemented with 50 µg/ml stock of spectinomycin (Sigma-Aldrich). Where appropriate other antibiotics were used at a concentration of Kanamycin 50 µg/ml, Chloramphenicol 0.75 µg/ml, Tetracycline 2.5 µg/ml and Erythromycin 2 µg/ml.

2.4.3 LB Media

For preparing 1000 ml of LB media, 10 g tryptone, 5 g yeast extract and 10 g NaCl were dissolved in 1000 ml deionised water. The solution was autoclaved for 20 minutes at 121°C.

2.4.4 LB Agar

With LB media **(Section 2.4.3),** 1% agar was added and the resulting solution was autoclaved for 20 minutes at 121°C. After autoclaving, the solution was cooled and poured on agar plates with the addition of antibiotics where appropriate. Antibiotic concentrations used were Ampicillin 100 µg/ml; Chloramphenicol 25 µg/ml; Kanamycin 50 µg/ml. For long term storage plates were stored at 4°C.

2.4.5 Mueller Hinton Broth

Mueller Hinton Broth was prepared by mixing 10.5 g of Mueller Hinton Broth powder (OXOID, UK) in 500 ml dH_2O, then autoclaving for 20 minutes at 121°C.

2.4.6 Maintenance and growth of bacterial cultures

For this work, a serogroup B *N. meningitidis* strain, originally isolated from an English patient suffering from meningococcal meningitis (McGuinness *et al*, 1991) was used (MC58). Full genome of this strain has been sequenced (Tettelin *et al*, 2000). Mutant derivatives of MC58; Δ*aniA*, Δ*norB* and Δ*nsrR* were generated by the disruption of *aniA* (NMB 1623), *norB* (NMB 1622) and *nsrR* (NMB0437) genes (Anjum *et al*, 2002; Rock *et al*, 2005; Rock *et al*, 2007). Insertion of the omega interposons, conferring resistance to an antibiotic rendered these genes inactive which were confirmed later by PCR analysis. Δ*nsrR/*Δ*aniA* was a kind gift from our collaborator (Dr James Moir, University of York). During the course of this project, the strains generated by author are mentioned in **Table 2.1** and detailed in **Chapter 4 and 6.**

Table 2.1 Strains used for this project

***N. meningitidis* strain**	**Genotype and antibiotic resistance**	**Reference**
MC 58	Wild type	(McGuinness *et al*, 1991)
Δ*aniA*	*aniA* :: $Spec^R$	Dr Jay Laver, PhD thesis
Δ*norB*	*norB* :: $Spec^R$	(Anjum *et al*, 2002)
Δ*nsrR*	*nsrR* :: $Spec^R$	(Rock *et al*, 2007)
Δ*nsrR*	*nsrR* :: Tet^R	(Heurlier *et al*, 2008)

Δ***nsrR/*Δ*aniA***	*nsrR/aniA* :: Tet^R/ $Spec^R$	(Heurlier *et al*, 2008)
Δ***aniA/*Δ*norB***	*aniA/norB* :: $Spec^R$/Kan^R	**Created by the author**
Δ***nsrR/*Δ*norB***	*nsrR/norB* :: Tet^R/Kan^R	**Created by the author**
Δ***aniA/*Δ*norB/*Δ*nsrR***	*aniA/norB/nsrR* :: $Spec^R$/Kan^R/Tet^R	**Created by the author**
Δ***aniA/aniA*$^+$**	*aniA/aniA*$^+$ :: $Spec^R$/Cm^R	**Created by the author**
Δ***aniA/aniA*$^{IPTG+}$**	*aniA/aniA*$^{IPTG+}$ :: $Spec^R$/Ery^R	**Created by the author**

Table 2.2 List of plasmids from the project

Plasmid name	Antibiotic resistance	Description	Source
pGEM-3zf	Amp^R	Plasmid with multiple cloning sites widely used for cloning	Commercially purchased
pJMK30	Kan^R	Plasmid containing 1.452 Kbp Kanamycin cassette	Kindly provided by Dr Jon Shaw, University of Sheffield
pGCC4	Kan^R	Plasmid permits ectopic complementation of a *Neisseria spp.* gene at an unlinked locus between	Kindly provided by Professor Christoph Tang,

		aspC and *lctP* region under the control of IPTG promoter with lac regulatory elements.	University of Oxford
pGCC5	Kan^R	Plasmid allows ectopic complementation of a *Neisseria spp.* gene along with its endogenous promoter between *aspC* and *lctP* region of *Neisseria*	Commercially purchased from Addgene
pGEM-3zf:: *ΔnorB*	Kan^R	2.5 Kbp *norB F1*-Kan-*norB F2* cloned into the pGEM-3zf	**Created by the author**
pGCC5 :: *aniA*$^{2+}$	Kan^R/Cm^R	Approximately 1.6 Kb *aniA* along with its endogenous promoter containing 300 bp upstream sequence was cloned into pGCC5 plasmid	**Created by the author**
pGCC4 :: *aniA*$^{IPTG3+}$	Kan^R/ Ery^R	1.173 Kb *aniA* gene coding sequence was cloned into pGCC4 plasmid under the control of an IPTG inducible promoter	**Created by the author**

2.4.7 Propagation of viable *N. meningitidis*

Frozen aliquots of viable bacteria were maintained in cryopreservation fluid (Protect™, TSC) at -80°C. Sterile loops were used to streak aliquots of frozen bacteria onto solid GC agar plates **(Section 2.4.2)** supplemented where applicable with appropriate antibiotic. Plates were incubated overnight in a CO_2 incubator at 37°C for at least 12 hours to produce colonies. Single colonies were chosen and propagated onto fresh plates with no less than three colonies being pooled to avoid the issues associated with phase variability of *N. meningitidis* surface structures.

2.4.8 Broth Culture of *N. meningitidis*

At least three single colonies were cultured in 10 ml Muller-Hinton broth (MHB) **(Section 2.4.5)** in 25 ml universal tubes. These cultures were agitated at 37°C, 5 % CO_2 by a plate mixer until an optical density of 0.25 at 600 nm (OD_{600nm}), representing log-phase bacterial growth, was reached.

2.4.9 Counting and manipulation of bacterial numbers for experiments

Tenfold serial dilution of culture, supernatants and liver lysates was performed to estimate the number of used bacteria according to the method established by Miles and Misra (Miles *et al*, 1938). Triplicate aliquots (10 µl) of each dilution were separately spotted on Columbia blood agar plates and left in a microbiological safety cabinet for 10 minutes to allow them to dry. Following overnight incubation at 37°C, 5 % CO_2, the mean number of colonies for each dilution were counted and corrected for the dilution factor and volume. Thus the mean of countable dilutions were averaged to estimate the number of bacteria present in the original suspension. This process was performed before and after the experiment to get an estimation of the input and output viable count. Using the viable counts of triplicate cultures at OD_{600nm}, the average number of viable bacteria per ml of culture was calculated as: wild type = 2.04 x 10^8 cfu/ml, *ΔaniA* = 1.15 x 10^8 cfu/ml, *ΔnsrR* = 2.74 x 10^8 cfu/ml and *ΔnorB* = 3.33 x 10^8 cfu/ml. These values were used to determine the volume of log phase culture (absorbance = 0.25 at OD_{600nm}) needed for an experiment requiring a defined number of bacteria. Viable counts using the Miles and Misra method were always performed on bacteria containing media or lysates. In order to provide a heat-killed control for metabolic activity, an aliquot of wild type bacteria, containing the same number of cells as the wild type inoculum, were incubated at 80°C in a dry heat block for 20 minutes.

2.5 Infection of mice and preparation of liver lysates and whole blood samples from the murine model of fulminant meningococcal sepsis

2.5.1 Infection of mice

Female C57BI/6 mice aged between 7-10 weeks were ordered from HARLAN, UK and maintained at the Field Laboratories, University of Sheffield. All the mice were acclimatised at least for a week before experiment and had access to the recommended laboratory rodent food and water. Health conditions of mice were monitored by the Field Laboratories staff, as per the guidelines of ASPA (Animal Scientific Procedures Act 1986). Prior to each experiment, mice were weighed to determine the maximum volume that could be injected (100 µl per g). The appropriate volume of bacterial culture (OD_{600nm} = 0.25) was isolated, washed twice in sterile PBS **(Section 2.2.1)** then resuspended into the relevant diluents: either LPS-free PBS, or LPS-free PBS supplemented with 8 mg human holo transferrin (hHTF) **(Section 2.1.4).** In experiments involving the administration of lipopolysaccharide (LPS), the LPS-free PBS was supplemented with *E. coli* LPS (Serogroup 026:B6, Sigma-Aldrich) such that 10 µl (1 unit) contained 25,000 endotoxin units (EU).

2.5.2 Severity score for meningococcal sepsis

Mice were intraperitoneally injected with the bacteria and were monitored for any departure from the normal well-being. In accordance with our infection protocol under the auspices of our Project Licence, the severity of sepsis was scored for each mouse at hourly intervals. Any mouse judged to score a cumulative score of 25 or a 5 in any one particular category was euthanized (see Score assessment, below). As severity of the disease progressed (cumulatively scoring 21 or more), the frequency of observation was increased. All mice were terminally anaesthetised with a 5 unit injection of 200 mM sodium pentobarbital. The exsanguination by cardiac puncture was performed following the confirmation of deep anaesthesia by the withdrawal of pedal reflex. A heparinised syringe containing 5 units of heparin per syringe was used for exsanguination. Throughout the entire procedure every effort was made to minimise the suffering of the mice.

Table 2.3 Severity score assessment

Score	Appearance	Activity (without stimulation)	Response to stimulation	Respiration	Response to handling	Behaviour in new setting
1	Normal	Normal	Normal	Normal	Normal	Normal
2	Partial piloerection	Slightly Subdued				
3	Partial piloerection, slightly hunched	Subdued	Slightly subdued	Slightly altered	Slightly docile	Curious but subdued
4	Marked piloerection, Hunched	Markedly subdued	Markedly subdued	Markedly altered	Docile	Lack of curiosity
5	Marked piloerection, Markedly Hunched	Immobile	No response	Labored	Impaired righting response	Immobile

Guidelines for overall severity assessment:

Cumulative score 6 = Normal

Cumulative score 7-8 = Mild

Cumulative score 9-18 = Moderate

Cumulative score 19-24 = Substantial (Observation frequency increased)

Cumulative Score 25-30 = Substantial (Mice should be culled)

As the severity scores increased, the frequency of observations also had to be increased. Mice had to be immediately culled when severity score of 5 was reached in any single category. Severity score adapted from (Khan *et al*, 2002).

2.5.3 Preparation of liver lysates

Mice liver were extracted from cadavers into light protected, 1.5 ml microcentrifuge tubes and weighed. In case of mouse with bacterial inoculation, the whole liver was washed in 20 ml of 0.25 % bile salts (Sodium taurocholate) for 30 seconds. This was done to kill any bacteria on the surface of the liver tissue. Following this step, mice livers were washed twice in 20 ml of sterile PBS in universal tube. Sterile tweezers were used to transfer the whole liver in different solution containing tubes. Liver was homogenised using a hand held rotor stator homogeniser (OMNI International, USA) in 4 ml of lysis buffer (50 mM phosphate buffer plus + 1 mM DTPA, 0.5 mM PMSF and ½ protease inhibitor cocktail tablet in each 5 ml) **(Section 2.2.2)** . 30 µl aliquot of each infected liver lysate was used for checking viable bacterial counts. The rest of the lysate was centrifuged at 500 g for 5 minutes using a Falcon 6/300 centrifuge and approximately 2 ml of supernatant was extracted. Another centrifugation step was performed at 16000 g for 3 minutes to remove any remaining pellet. Final supernatant was mixed in a 1 in 2 dilution with NEM containing lysis buffer (100 mM NEM, 50 mM phosphate buffer plus + 1 mM DTPA, 0.5 mM PMSF and ½ protease inhibitor cocktail tablet in each 5 ml), to give a final NEM concentration of 50 mM. The NEM buffer containing liver lysates were left on ice at least for 20 minutes to block the thiol residues present in the sample and stored in liquid nitrogen for later analysis.

2.5.4 Preparation of plasma from C57BI/6 mouse blood

Plasma was extracted after centrifuging the whole blood at 16000 g, 4°C for 5 minutes, the supernatant was diluted 2 fold in 50 mM phosphate buffer + 1mM DTPA + 100 mM NEM.

2.5.5 Preparation of stabilisation solution for SNO haemoglobin

SNO haemoglobin stabilisation solution was composed of 4 mM ferricyanide ($K_3Fe^{III}(CN)_6$), 10 mM N-ethylmaleimide (NEM), 100 µM diethylenetriaminepentaacetic acid (DTPA), and 1% nonidet-P-40 detergent (NP-40) in PBS.

2.5.6 Preparation of SNO haemoglobin from mouse blood

In the light protected tubes, 900 µl of stabilisation **(Section 2.5.5)** solution was aliquoted. It was important to use a light protected tube as light can break down SNO. Plasma was removed after centrifuging the whole blood at 13000 rpm for 5 minutes and 100 µl of red blood cell pellet was added into 900 µl stabilising solution. Sample was vortexed and stored in a light protected tube. A 9.5 ml bed volume G-25 sephadex column was thoroughly washed with degassed PBS (at pH 7-7.4) in a dark room. The column had two caps, one on the top and other in the bottom for controlling the entry and exit of the solution through the column. The PBS run through the column was collected in a liquid waste reservoir. The bottom cap column was put back. After defrosting and a vortexing step, 500 µl of 100 µl red blood cell plus 900 µl of stabilisation solution was added onto the G-25 Sephadex column by removing the top cap. Then the bottom cap was released and the lysed red blood cell mixture soaked the upper disc of the column. The bottom cap was put back and a volume of 3 ml of degassed PBS was added to the column. Then the bottom cap was removed and the PBS was allowed to run through the column. By the time 3 ml of PBS has soaked into the upper disc, the readily identifiable red band containing haemoglobin was at the bottom of the column. The haemoglobin was eluted by the addition of 700 µl of PBS and collected in a light protected tube. Immediately, the haemoglobin solution was placed on ice. An aliquot of 50 µl of haemoglobin was separated for measuring heme concentration with Drabkin's reagent. The remaining solution was split into two 270 µl fractions. One fraction was treated with 30 µl of 50 mM $HgCl_2$ **(Section 2.3.2).** The sample was vortexed and left at room temperature for 2 minutes. Then 30 µl of 5% acidified sulphanilamide **(Section 2.3.1)** was added to both the fractions and mixed thoroughly. In the purge vessel of NO analyser, 300 µl of sample was added in the triiodide solution. Injection volumes varied depending on the concentration of sample. Percentage of SNO per heme molecule was determined using the following equation:

Percent SNO per heme = (mM NO concentration determined using I_3^-/ mM Heme concentration from Drabkin's assay) x 100

2.5.7 Measurement of heme concentration

In a cuvette 50 µl haemoglobin solution per sample was placed and mixed with 950 µl Drabkin's solution **(Section 2.1.3).** In another cuvette 950 µl Drabkin's solution was pipetted as a blank. The solutions were incubated at room temperature after thorough mixing. The spectrophotometer was blanked with only Drabkin solution containing cuvette. The absorbance

was read at 540 nm wavelength. The haemoglobin concentration was determined using the equation below:

Concentration of heme (at mM) = (measured absorbance at 540 λ/ Extinction coefficient at 540λ= 11)

2.6 Chemiluminescence Techniques

2.6.1 Analysis of *S*-nitrosothiol, nitrite (NO_2^-) and nitrate (NO_3^-) concentrations

2.6.1.1 Calibration of GSNO solutions of known concentration

Small concentration of GSNO between 5 -10 mg was weighed in a microcentrifuge tube and dissolved in 50 mM phosphate buffer + 1 mM DTPA **(Section 2.2.3)** (referred as PB-DTPA) by vortexing. This generated a 100 mM solution and was allowed to settle on ice in a light protected environment. Spectrophotometry was used to accurately determine the GSNO concentration. The spectrophotometer was blanked at OD_{336nm} using 1 ml of PB-DTPA solution in a quartz cuvette (Shimadzu Europa, UK). Stock solution of GSNO was diluted 100 times in PB-DTPA solution without disturbing the settled solid. GSNO concentration in mM was finally determined by dividing this absorbance reading at OD_{336nm} by 0.77, the absorbance of 1 mM GSNO solution at OD_{336nm}. Due to the light-sensitivity of the *S*-nitrosothiol bond, all the solutions were stored on ice in a light protected environment. GSNO solutions and calibration curve were prepared fresh before the start of each experiment.

2.6.1.2 Ozone-based Chemiluminescence

All the nitric oxide (NO) measurements were performed using a Sievers Nitric Oxide Analyser (NOA) 280i (Sievers, Boulder, CA). All the parameters and procedures were identical for all NO measurements. NO was removed from the purging vessel by bubbling N_2 gas at a pressure of 1 bar and O_2 was supplied to the NOA at the same pressure. The pressure inside the purging vessel was adjusted before the start of each experiment to match that of atmospheric pressure. Throughout the measurements, cold water was run through the condenser. Before making any injections for NO measurement, the apparatus was run for at least 15 minutes to have a steady state low baseline signal. In case of NO_x measurement using Vanadium (III) chloride (VCl_3) solution, the purge vessel containing 4 ml VCl_3 in HCl solution was run for at least 30 minutes for establishing a low baseline signal. After injection of any sample, the purge vessel was rinsed thoroughly with dH_2O.

2.6.2 Measurement of samples by triiodide (I_3^-) dependant, ozone-based chemiluminescence

The tri-iodide solution **(Section 2.3.4)** was able to generate chemiluminescence signal from all reducible NO species apart from the nitrate (NO_3^-). All the samples and standards were pre-treated with 10% (v/v) sulphanilamide (in 2 N HCl) to remove contaminating NO_2^-. The reaction is triggered on ice and in light protected environment to prevent degradation of the *S*-nitrosothiol bond. *S*-nitrosothiol was measured by using a variety of reducing agents and samples were treated in three different ways to achieve this. Firstly, the untreated plasma and liver lysate were injected to measure the combined amount of nitrite (NO_2^-), nitrosyls, nitrosoamines and *S*-nitrosothiol (SNO) compounds present in the sample (collectively termed tri-iodide reactive NO species (NO_{I3-})). Secondly, sample was treated with 10% (v/v) 100 mM sulphanalimide in 2N HCl **(Section 2.3.1)** on ice for 10 minutes to complex free NO_2^-. This was achieved by the formation of a diazonium salt following the reaction between nitrite and acidified sulphanilamide, which cannot be reduced to NO when introduced to the I_3^- reagent. Finally, sample was treated first with 10 % (v/v) of a 50 mM $HgCl_2$ solution **(Section 2.3.2)** on ice for 10 minutes which was followed by the treatment with 10% (v/v) acidified sulphanilamide. Subtraction of the values of the concentration of NO_{I3-} measured in the latter two samples from the value of the concentration of NO_{I3-} measured in the first allows the determination of the concentrations of specific NO species.

2.6.3 Measurement of samples by Vanadium (III) Chloride (VCl_3) dependant ozone-based chemiluminescence

Acidified vanadium chloride solution was prepared by adding 0.8 g VCl_3 (MW: 157.30) to 100 ml of 1M HCl. A deep blue solution resulted. This reagent was strong enough to produce chemiluminescence signal from all reducible NO species including the nitrates (NO_3^-). 1M $NaNO_3$ solution was made by dissolving 0.43 g of $NaNO_3$ (MW: 83.99) in 5 ml dH_2O and 10 fold serial dilutions were made from 10 mM to 100 nM. A calibration curve was prepared by measuring NO from these solutions which was used to calculate the NO_x present in the sample. Solutions were always prepared fresh and stored in a light-protected environment when not in use. For NO_x measurement, the purging vessel had to be connected to a water bath set at 90°C. Four ml of acidified VCl_3 was added to the purge vessel and the apparatus had to be run for at least 30 minutes to establish a low stable baseline reading. Typically, 3-5 µl injections without any treatment were made for NO_x measurement.

2.6.4 Injection of samples into the purging vessel

Gas-tight microsyringes (Analytix, UK) were used to inject specific amounts of samples into the purging vessel. For measuring NO in liver lysates, typically 10-150 µl of liver lysates were injected. For each injection, a 10 µl headspace of air was taken for ensuring the maximum efficacy of injection. With complete depression of plunger, samples were injected as a bolus into the purging vessel. Duplicate injections were made depending on the availability of the sample. Microsyringes were washed three times with dH_2O between injections. To avoid contamination, the needle of the syringe was thoroughly dried before each injection was made.

2.6.5 Analysing chemiluminescence data using the Origin 8.1 program

The release of NO from its oxidised forms is stoichiometric in the purging vessel, meaning one molecule of NO is generated for every nitrogen atom in a sample (dependent upon the strength of the reducing agent employed). In the chemiluminometer, NO reacts with ozone in a high energy collision which releases a photon. These photons are detected by a photomultiplier tube, which produces an electric current. The voltage of the current is directly proportional to the number of photons detected, which in turn is directly proportional to the amount of NO released from the sample. Thus using the LIQUID program we generate a graph of mV against time, the Area Under Curve (AUC) which we can integrate and relate to a curve of areas generated from standards of known concentrations, in order to determine the concentration of NO produced in our purging vessel. The mean of AUC from duplicate injections of known concentration of $NaNO_2$ is used for measuring NO_2^-, NO_x and GSNO **(Section 2.6.1.1)** is used for measuring SNO. LIQUID program used to capture the data is reportedly less effective at integrating the area under smaller peaks than is Origin 8.1 (Laver *et al*, 2008), so it is the latter software we employ to smooth and subsequently integrate our data. We used a Savitzky-Golay filter with a gate size of 21 to smooth out the traces generated in our experiments. Post-integration, the concentration of NO measured in Hg-treated samples was multiplied by a factor of 1.1 to account for the addition 10 % (v/v) dilution.

2.7 Statistics

All the statistics were performed by using the GraphPad Prism 5 software. The statistical test used depended and varied on nature of experimental design and result. Chosen statistical tests are highlighted in the figure legends. If the skewness was double or equal to the standard error of skewness, non parametric test was used but if the skewness was less than double the standard error of skewness, parametric test was used.

2.8 Immunological Techniques

2.8.1 IL-8 and TNFα cytokine measurement by ELISA

For IL-8 and TNFα measurement human DuoSet ELISA development kit from R & D was used. Capture antibody (720 µg/ml) was reconstituted with 1ml PBS. For longer term storage antibody was kept in aliquots at -20°C freezer for up to 6 months. Before the assay, the antibody was diluted at the working concentration of 4 µg/ml in PBS. 3.6 µg/ml (63 µg/ml for TNFα) biotinylated goat anti-human IL-8 detection antibody was reconstituted in 1 ml of reagent diluent. Before assay, a working concentration of antibody was made at 20 ng/ml (350 ng/ml for TNFα) in reagent diluent. 100 ng/ml human IL-8 was reconstituted with 0.5 ml of water. TNFα (at 320 ng/ml) was reconstituted in 0.5 ml reagent diluent. The standard was let to set at room temperature for 15 minutes before storing it at -20°C freezer for long term storage. A standard solution of high concentration (2000 pg/ml) was prepared prior to the assay and a seven point standard curve was made using 2 fold dilution. Streptavidin- HRP, PBS, block buffer, substrate and stop solution were prepared according to manufacturer's instruction. Firstly, the ELISA plate had to be prepared. The required number of wells of 96 well ELISA plate were coated with 100 µl of capture antibody in each well. Plate was sealed and incubated overnight at room temperature. Following day, contents of the plate were discarded and washed with the wash buffer for three times. Each wash step was done by adding 400 µl of wash buffer. Plate was aspirated or inverted to remove any residual wash buffer left in the well before starting next was step. Then 300 µl of block buffer was added to each well and incubated at room temperature for 2 hours. 100 µl sample diluted in reagent diluent was added to the wells and the plate was incubated at 4°C overnight after sealing with an adhesive strip. Following day, the plate was washed three times with 400 µl of wash buffer. Any residual wash buffer had to be removed before proceeding to the next step. 100 µl of detection antibody at working concentration was added and the plate was incubated at room temperature for 2 hours. The plate was washed with wash buffer as before and aspirated thoroughly. Subsequently, 100 µl working concentration of Streptavidin-HRP was added and plate was incubated at room temperature for 30 minutes. Wash step was performed again for three times to remove any Streptavidin-HRP. After washing 100 µl of substrate solution was added to each well and incubated at room temperature for 30 minutes protecting from light. Then 50 µl of stop solution was added to each well and plate was gently tapped to ensure thorough mixing. The plate was read using a microplate reader set to 450 nm. Final analysis was performed after correcting for the background reading using the built in software.

2.9 Cell Culture Techniques

Culture and maintenance of human primary bronchial epithelial cells at air-liquid interphase (HPEC-ALI)

2.9.1 Consumables

- 20 ml polystyrene Universals (Greiner, Cat No: 201172)
- 5 ml stripettes (Fisher, Cat No: FB55483)
- 10 ml stripettes (Fisher, Cat No: FB55484)
- 25 ml stripettes (Fisher, Cat No: FB55485)
- Extended Fine Tip Pastette: alpha Laboratories, Cat No: LW4232
- Syringe driven sterile filter unit (Millex-GP, 0.22 µm, polyethersulfone, 33 mm, radio-sterilized): Millipore, Cat No: SLGP033RS
- 6.5 mm Transwell® with 0.4 µm Pore Polyester Membrane Insert, Sterile: Corning, Cat No 3470

2.9.2 Reagents

- Trypsin, 0.5% (10 x) with EDTA 4Na (Life Technologies, Cat No: 15400) diluted 1:10 with HBSS, aliquoted in 10 ml and stored at -20°C
- Fetal Bovine Serum (heat inactivated) (Life Technologies ,Cat No: 10108-165)
- RPMI 1640 medium without L-Glutamine (Life Technologies, Cat No:31870-025)
- Dulbecco's Modified Eagle Medium (DMEM) high glucose (Life Technologies, Cat No: 11960-085)
- Penicillin-Streptomycin (5000 IU/ml Penicillin, 5000 µg/ml Streptomycin) (Life Technologies, Cat No: 15070-063)
- Non Essential Amino Acids (x 100) w/o L-Glut: Life Technologies (Cat No: 11140-035)
- Sodium Pyruvate MEM 100 mM (Life Technologies, Cat No: 11360-039)
- L-Glutamine 200 mM (x 100) (Life Technologies, Cat No: 25030-024)
- BEGM BulletKit (contains BEBM and SingleQuots) (Lonza, Cat No: CC3170)
- Retinoic acid (RA) (Sigma, Cat No R2625) and BEGM SingleQuot Kit Suppl. & Growth Factors (Lonza, Cat No: CC-4175)

2.9.3 Preparation of reagents for ALI medium

2.9.3.1 Collagen I solution (1:100)

A volume of 30 µg/ml collagen I solution (PureCol, Advanced Biomatrix) was prepared by adding 0.5 ml of 3 mg/ml collagen I stock to 49.5 ml of sterile ddH_2O in a 50 ml conical tube.

2.9.3.2 BSA stock (1.5mg/ml) for 2x ALI medium

An amount of 100 mg/ml BSA (Bovine serum albumin, Sigma, Cat No: A3059-100G) stock was prepared by dissolving 1g BSA in 10 ml ddH_2O. The stock was filter sterilised using a low protein binding filter and 100 µl aliquots (0.5 ml microtubes) were prepared and stored at -20°C in TC3 freezer. Another 1.5 mg/ml BSA stock was prepared by adding 90 µl (100 mg/ml) to 5910 µl of BEBM (1/66.7 dilution). 600 µl aliquots were made and stored at -20°C in freezer.

2.9.3.3 Preparation of 2x BEGM medium

The singlequot vials should not be freeze/thawed. Making up 2x BEGM enables the singlequots to be used for both monolayer and ALI cultures. The following steps were followed:

In 250 ml sterile bottle, 244.5 ml of BEBM medium and the following reagents from BEGM singlequots were added **(Table 2.4).** After defrosting the singlequots were briefly centrifuged (12000 rpm, 1 min) to ensure all the contents are in the bottom of the vial and transferred to the 250 ml bottle. The contents in the 250 ml bottle were thoroughly mixed by pipetting up and down using a 25 ml pipette.

Table 2.4 Recipe for preparation of BEGM for ALI media

Reagent	Vol/250ml 2x BEGM (ml)
BEBM	244.5
Bovine Pituitary extract (BEGM singlequot)	2
hEGF (BEGM sinlgequot)	0.5
Insulin (BEGM sinlgequot)	0.5
Hydrocortisone (BEGM sinlgequot)	0.5
Transferrin (BEGM sinlgequot)	0.5
Triiodothyronine (BEGM sinlgequot)	0.5
Epinephrine (BEGM sinlgequot)	0.5
BSA (1.5 mg/ml)	0.5

2.9.3.4 Recipe for preparation of DMEM for 1x ALI medium

Table 2.5 Recipe for preparation of DMEM for ALI medium

Reagent	Vol/50 ml (ml)	Vol/250 ml (ml)	Vol/500 ml (ml)
DMEM	48	240	480
Non-essential amino acids	0.5	2.5	5.0
Sodium pyruvate	0.5	2.5	5.0
Penicillin/streptomycin (100X)	0.5	2.5	5.0
L-glutamine (100X)	0.5	2.5	5.0

A minimum of 50 ml of DMEM was prepared and stored in 50ml conicals

2.9.3.5 Preparation of Retinoic acid (all-trans RA) $5x10^{-5}$ M (50 µM)

The primary stock solution was made by dissolving 50 mg retinoic acid (MW 300) in 16.67 ml DMSO in a darkened room to exclude UV light to give a final concentration of 3 mg/ml (10 mM). 25 µl of aliquots were made and stored in a bag wrapped in tin foil at -80°C freezer. To make a working stock solution 20 µl of the primary stock was diluted in 4 ml DMSO to have

a final concentration of 50 µM (5 x 10^{-5} M) and stored in 60 µl aliquots at -20°C in a light tight container. Care was taken not to thaw and freeze the aliquots.

2.9.3.6 Preparation of 1x ALI media

BEGM is an expensive media which cannot be used further after addition of the retinoic acid. So only the amount required was made up. The amount of media required was worked out (300 µl/transwell + a couple of mls for pipetting losses). Into a 25/50 ml universal tube half the total volume of ALI DMEM **(Section 2.9.3.4)** and half the total volume of 2 x ALI BEGM **(Section 2.9.3.3)** was added. Just before usage, a vial of retinoic acid (50 µM was thawed) **(Section 2.9.3.5)** was added in 1 µl per ml of 1 x ALI media. It is to be noted that retinoic acid is unstable and light sensitive. While using it was protected from light under all circumstances and repeated thaw/freeze cycles had to be avoided.

2.9.4 Methods for the establishment and maintenance of ALI cultures

2.9.4.1 Collection of HPEC after bronchoscopy

Human primary bronchial epithelial cells (HPEC) were obtained from the healthy volunteers by epithelial brushing. All the procedures were approved by the Southampton and South West Hampshire Research Ethics Committee. Passage 1→2 of HPEC was used for generating air-liquid interphase cultures.

2.9.4.2 Preparation of a cell suspension

The cells were trypsinised and resuspended in 10% FBS/RPMI. They were pelleted after centrifugation and the supernatant was discarded. Pellet was resuspended in 1-2 ml of BEGM. After cell counting with haemocytometer **(Section 2.9.4.8)**, the suspension was diluted at 0.35 x 10^6 cells/ml in BEGM.

2.9.4.3 Preparation of the transwell trays (Day 0)

Collagen I solution (1:100) from stock of 3 mg/ml = 30 µg/ml in sterile double distilled water was prepared. 100 µl/well was added into apical compartment of required transwell of 24-well plates. The collagen was let to polymerise in 37°C incubator for 30 minutes. Collagen was removed with fine-tip sterile pastette. In transwell 200 µl of the 0.35 x 10^6 cells/ml was pipetted (0.7 x 10^5 cells/well). 0.5 ml of BEGM was added to the basal compartment of each transwell. 1 ml HBSS was added to empty wells to minimise evaporation. Each plate was thoroughly labelled with the date, donor code and phenotype and incubated overnight (at 37°C, 5% CO_2) to form a confluent monolayer.

2.9.4.4 Taking transwells to air-liquid interphase day 1

A minimum of 50 ml of 2 x ALI and DMEM was prepared. If there were lots of cells in culture then 250 ml of media each was prepared as per recipe at the end of protocol. Tubes were labelled with name and date. The amount of ALI medium needed was calculated (4 ml /each 12-well transwell plate; (12 x 0.3 ml = 3.6 ml) in 50 ml conicals. Just before use an aliquot of RA (5 x 10^{-5} M) **(Section 2.9.3.5)** was defrosted by placing in hand or wrapped in foil. With special care 1:1 (v/v) DMEM : 2 x ALI medium to required volume was prepared. Then 1µl of 50 µM RA stock for each ml of ALI medium **(Section 2.9.3.6)** was added immediately prior to the use. The conical was wrapped with aluminium foil. This was done to protect the ALI media from light as RA is UV sensitive. Using a fine-tip sterile pastette first basal then apical media was removed from the transwell by not disturbing the cell layer. In the basal compartment 300 µl of 1 x ALI media underneath the transwell was added. No media was added to the apical compartment. The plate was incubated at 37°C.

2.9.4.5 Points to consider for growing and maintaining ALI culture

On day 1 the cultures should be 95%-100% confluent. If they are subconfluent the cells are fed as described above and they may become confluent over the following few days. Persistent subconfluent cultures indicate that the cells are becoming quiescent and are less likely to differentiate. After the first few days a confluent cell layer may appears to form 'holes' that give a lace curtain appearance. This will not inhibit differentiation and these areas will regress over time. The cells start to visibly produce mucus at around 7 days. Ciliated cells should start to appear from day 14-19 but may not be visible under an inverted microscope if there is mucus impeding their beat. Cells are generally used for assays from day 19-21. However, leaving the cultures left for longer (e.g. another week) generally increases the percentage of ciliated cells. Transepithelial resistance can be determined using chop-stick electrodes of voltohmmeter EVOM. Basal resistance = approx. 150 Ω, resistance of differentiated cultures = approx. 400 Ω – 2500 Ω.

2.9.4.6 Continuous feeding of ALI cultures DAY 2-21 onwards

From freezer 2 x ALI culture media and DMEM media was taken out and required volumes of 1 x ALI medium without RA into 50 ml conicals were made. The media was warmed by leaving at 37°C for at least 20 minutes. Just before feeding the cells, the required amount of RA (1µl/ml) was added into 1 x ALI media immediately before replacing media. The RA was

protected from UV light by wrapping it with aluminium foil. Using a fine-tip sterile pastette, the basal media was removed from the transwell. Any excess mucus accumulating on the surface of apical layer along with any additional media was removed from approximately day 7 onwards. Care was taken not to dislodge the cell layer. 300 µl of 1 x ALI media underneath the transwell in the basal compartment was added.

2.9.4.7 Transepithelial resistance (TER) measurement (day 7, 14, 21)

TER was measured on day 7, 14 and 21 to check the epithelial barrier integrity **(Section 2.10.3).** In 5 ml bijoux tube 5 ml of HBSS was aliquoted and warmed at 37°C incubator for 30 minutes. Chopsticks from the TER machine was sterilised by placing in a 25 ml conical with IMS. Any excess mucus from the apical compartment of the transwells was removed. Pre-warmed 100 µl of HBSS was added to the apical compartment and incubated at 37°C for 15 minutes. Chopstick of TER machine was removed from IMS and let to evaporate. The electrodes were dipped into HBSS. After drying, the electrodes were positioned at a 90° angel to the base of the plate, with the longest electrode on the outside (basal) and shortest electrode on the inside (apical) side of the transwell insert. After recording TER, basal medium was removed along with HBSS from the apical compartment with fine-tipped pastette. Freshly prepared 1x ALI was added into the basal compartment. TER reading was taken again.

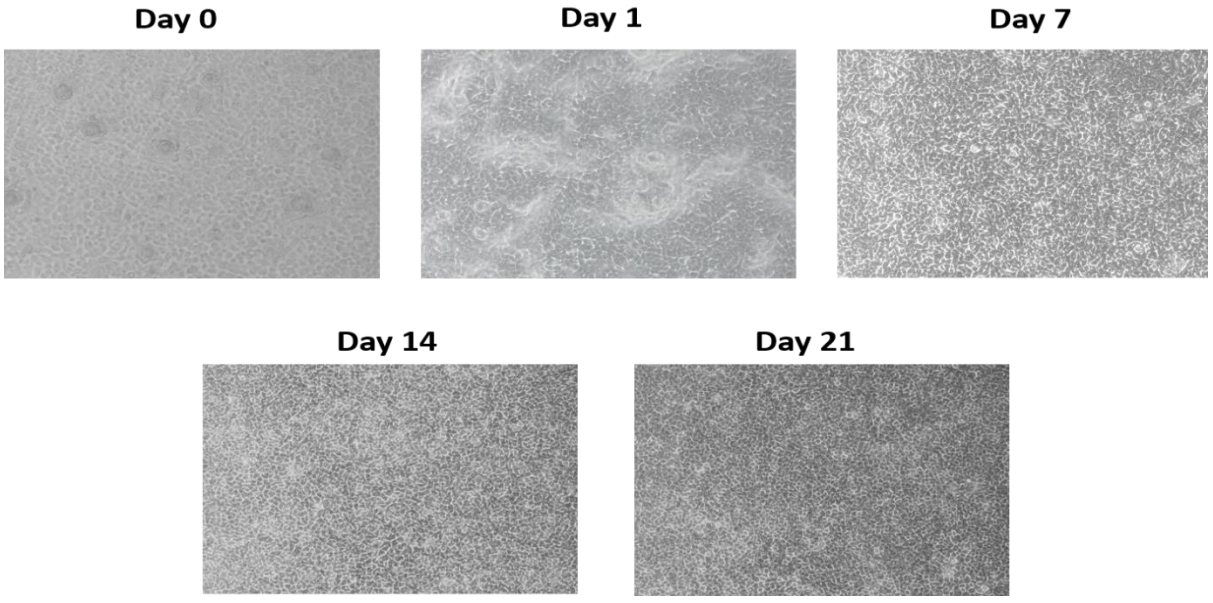

Figure 2.1 Progression of HPEC-ALI culture over a period of 21 days.

After bronchoscopy HPEC were seeded for generating ALI culture. As can be seen with the progression to day 14 and day 21 density of the cell population increased which was depicted by high TER reading. (Image kindly provided by Dr Emily Swindle, University of Southampton). Image taken by Light microscopy.

2.9.4.8 Counting the cells prior to the experiment

A well containing ALI culture was used for counting the cells using haemocytometer. 1 ml of prewarmed HBSS was applied on top of the transwell and was let to overflow. On the apical side of the well 200 µl trypsin and in the basal compartment 300 µl trypsin was added. The plate was left in the incubator for 5-10 minutes. The detachment of the cells was monitored by microscope by pipetting up and down. After trypsinisation, all cells/trypsin were added to 100 µl FBS in the Eppendorf. The trypsinised well was rinsed to dissolve the total cells in 1 ml volume. The cells were repeatedly pipetted up and down and vortexed to break down any clump to interfere with cell counting. Since the cells have tendency to settle to the bottom, pipetting and vortexing had to be performed just before counting the cells. This step was pivotal as clumped cells in solution would provide an inaccurate cell count. A total 50 µl of cell suspension was mixed with 10 µl of (0.4 %) trypan blue solution and 40 µl of HBSS. These mixtures were mixed thoroughly. An aliquot of 10 µl was used to perform cell count using haemocytometer. A small volume of trypan blue containing sample was added to the space between the surface of the counting chamber and the underside of the glass coverslip. Average of total number of cells in specified four grids of haemocytometer was multiplied by 10^4 to get the number of cells ml^{-1} in the suspension. Approximately 0.2-0.7 x 10^6 cells were found from one transwell and this count was used to determine the required MOI for infection.

2.10 Biochemical Techniques

2.10.1 Measurement of NO_2^- by Griess Assay

Measurement of NO_2^- in batch culture was performed by Griess Assay Kit (Promega). The assay relies on the Griess reaction which was first described by Peter Griess (Griess, 1879). Kit came with Sulfanilamide (1% sulphanilamide in 5% phosphoric acid), NED solution (0.1% N-1-napthylethylenediamine) and nitrite standard.

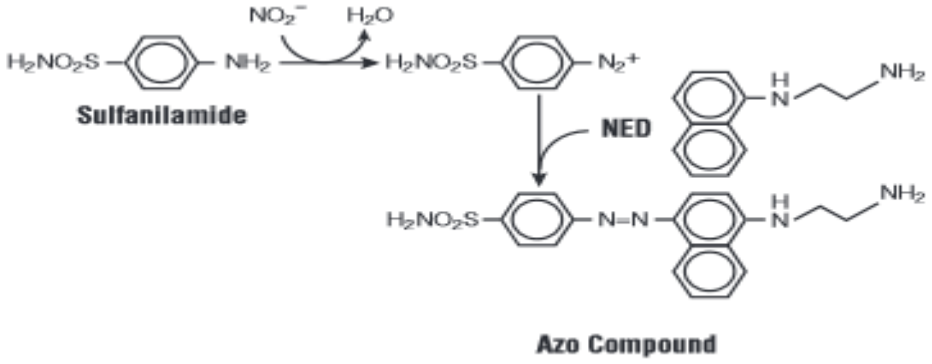

Figure 2.2 Chemical interactions involved in the measurement of NO_2^- using the Griess Reagent System.

Sulfanilamide reacts with NO_2^- present in the sample and forms a diazonium salt. The reaction of this salt with Azo dye (NED) leads to the development of pink colour which is detected by a spectrophotometer at an absorbance between 520-550 nm. *(http://www.promega.co.uk/~/media/Files/Resources/Protocols/Technical%20Bulletins/0/Griess%20Reagent%20System%20Protocol.pdf)*

The media from 5 mM $NaNO_2$ containing growth curve was diluted 1 in 200/300 growth media prior to the assay. Media from 50 µM SperNO growth curve was measured after making 1 in 2 dilution. Supplied 0.1 M $NaNO_2$ standard was diluted 1000 fold in MHB to prepare 100 µM nitrite standard. 100 µl of 100 µM nitrite was plated in triplicates in a 96 well flat bottom plate. This solution was serially diluted (1 in 2) 6 times by transferring 50 µl of sample to prepare 50, 25, 12.5, 6.25, 3.13, 1.56 µM solution. 50 µl of sample was discarded from the 1.56 µM standard. In separate 3 wells, 50 µl MHB were added and this was counted 0 as standard. Half an hour before the assay Sulfanilamide and NED were equilibriated at the room temperature protected from light. 50 µl of each sample was added to the well in triplicates. Using a multichannel pipettor, 50 µl of acidified sulphanilamide was added to each experimental well and the plate was incubated at room temperature for 5-10 minutes protected from light. After that 50 µl of NED was added to each well and incubated at room temperature for 5-10 minutes. Purple colour will start to form immediately. Within 30 minutes absorbance was read at OD_{540nm}. Reading from standard 0 well was considered as background and was subtracted from each output. Average absorbance reading from nitrite standards was plotted against concentration to draw the standard curve. Absorbance readings of the samples were determined from the standard curve.

2.10.2 Glutathione peroxidase assay

The Glutathione peroxidase (Gpx) is an enzyme that plays a pivotal role in counteracting oxidative damage. In this project Gpx activity was determined using a commercial kit according to the manufacturer's instruction (Abcam ab 102530). This kit measured Gpx indirectly through enzymatic consumption of NADPH. Reduced glutathione (GSH) is converted to oxidized glutathione (GSSG) by Gpx. Supplied glutathione reductase reduces GSSG back to GSH by utilising NADPH which can be easily detected at 340nm. The decrease in NADPH consumption is directly proportional to Gpx activity. Meningococcal overnight cultures were lysed by sonication. The supernatant was collected by centrifuging the cells at 10000 g for 15 minutes at 4°C. 50 µl samples were used for the assay in a 96 well plate. NADPH was used as a standard for Gpx activity detection. NADPH were prepared in concentrations (0, 20, 40, 60, 80, 100 nmol/well) and added to the 96 well plates. A volume of 5 µl Gpx was topped up to 50 µl with assay buffer and used as a positive control. A volume of 40 µl reaction mix was prepared by adding 33 µl assay buffer, 3 µl 40 mM NADPH, 2 µl GR, 2 µl GSH. To each test sample 40 µl reaction mix was added and incubated for 15 minutes to allow GSSG depletion. Then OD_{340nm} reading was taken by a 96 well plate reader. After that 10 µl of cumene hydroperoxide was added and the plate was incubated for 40 minutes protected from light. Absorbance reading was taken again at OD_{340nm}. For calculating the final Gpx activity in mU/ml, NADPH reduction between t =0 and t = 40 minutes were determined by subtraction and adjusted with sample volume and timepoint (40 minute). Initial experiments showed that beyond 40 minutes timepoint, the Gpx signal is significantly diminished and therefore 40 minutes timepoint was used for the Gpx measurement.

2.10.3 Measurement of Transepithelial cell resistance (TER)

During the maintenance of HPEC-ALI cultures, the differentiation state of the cells is confirmed by TER readings. Before and after infection TER of HPEC-ALI was measured. TER measurement was performed by an EVOM Voltohmmeter (World precision instruments) with chopstick electrodes. Chopsticks from the TER machine was sterilised by placing in a 25 ml conical with IMS. Pre-warmed 100 µl of HBSS was added to the apical compartment and incubated at 37°C for 15 minutes. Chopstick of TER machine was removed from IMS and let to evaporate. The electrodes were dipped into 25 ml HBSS containing conical. After drying, the electrodes were positioned at a 90° angel to the base of the plate, with the longest electrode on the outside (basal) and shortest electrode on the inside (apical) side of the transwell insert. TER reading on display was recorded. The electrodes had to be kept steady while taking the

measurement to get results devoid of noise. Readings before and after the experiments are used to measure TER (Ω). TER reading after experiment was divided by TER reading before the experiment to get a ratio. Then the ratio found was normalised to the TER ratio of the control well (No bacteria) to get the final TER reading.

2.10.4 Determination of Protein Concentration

Protein concentration of plasma, bacterial cell lysates and liver lysates were calculated using the RC DC protein Assay kit (Bio Rad, USA), according to the manufacturer's instruction. In this colorimetric assay, protein concentrations were calculated in reference to a bovine serum albumin (BSA) standard curve. BSA standard curve was prepared fresh by making dilutions from 1.5 mg/ml to 0 mg/ml and colour change was quantified at OD_{750nm} using a spectrophotometer.

2.11 Molecular Biology Techniques

2.11.1 Preparation of DH5α Cells

One distinct colony from freshly grown DH5α cells (NEB C2987) was inoculated in sterile 25 ml LB media **(Section 2.4.3)** overnight at 37°C. In the following morning 500 µl of overnight culture was mixed with 100 ml of LB media in a 500 ml flask and incubated in a shaker incubator at 37°C. The culture was grown exactly up to the mid log phase (OD_{600nm} = 0.5) and transferred to two 50 ml centrifuge tubes. The mid log phase (OD_{600nm} = 0.5) was critical for the efficacy of the competent cells. Therefore, the OD_{600nm} was more frequently observed after the culture reached at OD_{600nm} 0.2-0.3. After incubation on ice for 15 minutes, the cells were centrifuged at 15 Kg at 4°C for 15 minutes. The supernatant was carefully poured off and resuspended in 50 ml RF1 **(Section 2.3.6)** per tube. Following 15 minute incubation on ice, the cells were centrifuged as before. Pellets from two tubes were combined in 8 ml RF2 **(Section 2.3.7)** and incubated on ice for 20 minutes. The cells were aliquoted in eppendorf tubes and stored at -80°C. It was pivotal to maintain aseptic environment throughout the whole process.

2.11.2 Transformation of *E. coli* DH5α competent cells with DNA

Competent cells **(Section 2.11.1)** were thawed on ice just prior to the use. Approximately 1-5 µl of DNA from ligation reaction **(Section 2.11.10)** was chilled in a clean 1.5 ml microcentrifuge tube. Around 150-200 µl of competent cells were added to DNA. The tube was flicked 4-5 times to mix the cells and DNA. Vortexing was avoided as a way of mixing as it could damage the competent cells. The mixture was incubated on ice for 30 minutes. The tube was heat shocked at 42°C for 30 seconds without mixing. Prewarmed and sterile 800 µl

of LB media was added to the tube and was incubated at 37°C for 60 minutes at 250 rpm. After 1 hour, 100 µl of this mixture was spread plated on prewarmed LB agar plates containing appropriate antibiotics **(Section 2.4.4)**. The remainder of the mixture from tube was centrifuged and resuspended in 100 µl LB media and spread plated on a separate LB agar plate. All the plates were incubated 37°C overnight and screened for positive colonies the following day.

2.11.3 Primers

Table 2.6 Primers used for this project

Primers	Sequence	Description
norB F1-FWD	***GAGCTCGGTACCCGGGGATCCTCTAGAGTC <u>ACGGCAGCGTCGTCATCAGC</u>***	This primer contained 30 bp sequence homologous to the pGEM-3zf before the HincII restriction site plus 20 bp from the beginning of the part (underlined) of chosen 524 bp *norB* sequence
norB F1-REV	***AAGCTGTCAAACATGAGAACCAAGGAGAAT <u>ACCCTGGCCTTCGACGGTGT</u>***	The reverse primer contained 30 bp adapter sequence which was homologous to the reverse complement of the start of the Kan cassette from pJMK30 plus 20 bp of the reverse complement of the last part (underlined) of the chosen 524 bp *norB* sequence
norB F2-FWD	***GAATTGTTTTAGTACCTAGCCAAGGTGTGC <u>ACTGCCTCCACTTTGGCCGC</u>***	The forward primer contained a 30 bp sequence homologous to the last 30 bp of pJMK30 plus 20 bp from the start (underlined) of the chosen 522 bp of *norB* sequence
norB F2-REV	***AGAATACTCAAGCTTGCATGCCTGCAGGTC <u>CTGAATCGCGCCGACAGGCA</u>***	The reverse primer contained sequence homologous to the last 30 bp of pGEM-3zf after the HincII restriction site plus 20 bp from the reverse complement (underlined) of last part of chosen 522 bp *norB* sequence

Kan- FWD	***ATTCTCCTTGGTTCTCATGTTTGACAGCTTAT***	Forward primer for amplifying the Kan cassette from pJMK30
Kan-REV	***GCACACCTTGGCTAGGTACTAAAACAATTCAT***	Reverse primer for amplifying the Kan cassette from pJMK30
aniA_RUH1_FWD	***TGCCTGATTTGCCGAAGCCCT***	Forward primer for amplifying the 1.3 Kb of *aniA* region
aniA_RUH1_REV	***AAGCAGCAGGAGCTGCACCG***	Reverse primer for amplifying the 1.3 Kb of *aniA* region
norB_RUH2_FWD	***TACTTGCTGTTTGCCGTTCT***	Forward primer for amplifying the 2.0 Kb of *norB* coding region
norB_RUH2_REV	***GCAGCCAGAAGCCCCAAGTC***	Reverse primer for amplifying the 2.0 Kb of *norB* coding region
nsrR_RUH3_FWD	***CGATGCCTTTCTTCCGGCGT***	Forward primer for amplifying the 1.4 Kb of *nsrR* region
nsrR_RUH3_REV	***CCTCATCAAGCAGGCGGTTG***	Reverse primer for amplifying the 1.4 Kb of *nsrR* region
AniA_compl_RUH8_FWD	***ACGATACAGACGTCTACCGCGCAAATAAAC***	Forward primer for PCR amplifying the *aniA* coding sequence along with its 300 bp upstream regulatory region and 100 bp downstream of the coding stop codon with *AatII* restriction site underlined
AniA_compl_RUH8_REV	***GGACTGCGATGCATATCAATCTTCCGAAAG***	Reverse primer for PCR amplifying the *aniA* coding sequence along with its 300 bp upstream regulatory region and 100 bp downstream of the coding stop codon with *NsiI* restriction site underlined
Comp1_check_RUH14_lctP/aspC_FWD	***ATGGCACTTTTCCTCAGCATATTCC***	Forward primer for PCR amplifying the region from *aspC* to *lctP* of pGCC5 plasmid
Comp1_check_RUH14_lctP/aspC_REV	***CTATACTTTCACGATGCTTTCACAC***	Reverse primer for PCR amplifying the region from *aspC* to *lctP* of pGCC5 plasmid

Comp_check_RUH19_aniA1	***TACCGCGCAAATAAACATTTGTTC***	Sequencing primer for checking the first 800 bp of reverse complemented *aniA* sequence along with its 300 bp upstream endogenous promoter region
Comp_check_RUH20_aniA2	***ACAACGTCGACTTCCACGCGGCTA***	Sequencing primer for checking the last 800 bp of reverse complemented *aniA* sequence along with its endogenous promoter region
Ampli_aniA_Comp_Forward	***CGTTGTAC<u>TTAATTAA</u>ATGAAACGCCAAGC CTTAGC***	Forward primer for PCR amplifying the *aniA* coding region with *PacI* restriction site (Underlined)
Ampli_aniA_Comp_Reverse	***CGTTGTAC<u>GGCCGGCC</u>TTAATAAACGCTTT TTTCGGATGCAGAGG***	Reverse primer for PCR amplifying the *aniA* coding region with *FseI* restriction site (Underlined)
Ampli-pGCC4Forward	***CTATGAAAGGTTGGGCTTCGGAATC***	Forward primer for PCR amplifying the *aspC* to *lctP* region of pGCC4 plasmid
Ampli-pGCC4Reverse	***GTCATCCGCAAATGGCTGGC***	Reverse primer for PCR amplifying the *aspC* to *lctP* region of pGCC4 plasmid
pGCC4_diagnostic_Fwd	***GCATTCAGGCGTAGTAATGATGCG***	Forward primer for PCR amplifying the 1.224 Kb region of pGCC4 containing lac promoter regulatory elements
pGCC4_diagnostic_Rev	***CAGTTGATCGGCGCGAGATTTAATC***	Reverse primer for PCR amplifying the 1.224 Kb region of pGCC4 containing lac promoter regulatory elements
Sequencing Primer aniA 1	***GCCGACATCATAACGGTTCTGGCAAA***	Primer for sequencing the integrated *aniA* sequence along with the upstream *lacI* promoter region of pGCC4
Sequencing Primer aniA 2	***GCCAACAAGAACCATCCGTTCTG***	Primer for sequencing the integrated *aniA* sequence along with the upstream

		lacI promoter region of pGCC4
aniA_Fwd_start	***ATGAAACGCCAAGCCTTAGC***	Forward primer for PCR amplifying the *aniA* coding region
aniA_Rev_end	***TTAATAAACGCTTTTTTCGGATGCAGAGG***	Reverse primer for PCR amplifying the *aniA* coding region

2.11.4 Preparation of Isocloning buffer

Table 2.7 Preparation of Isothermal Buffer

1 ml (µl)	3 ml (µl)	6 ml (µl)	Components	Mw		g	µg
500	1500	3000	**1M Tris-HCl pH 7.5**	121.14	50 ml	6.06	
25	75	150	**2M MgCl2.6H20**	203.30	2 ml	0.81	
10	30	60	**100 mM dGTP**	N/A	N/A	N/A	N/A
10	30	60	**100 mM dCTP**	N/A	N/A	N/A	N/A
10	30	60	**100 mM dTTP**	N/A	N/A	N/A	N/A
10	30	60	**100 mM dATP**	N/A	N/A	N/A	N/A
50	150	300	**1M DTT**	154.25	1 ml	0.15	154.3
0.25 g	0.75 g	1.5 g	**PEG-8000**	N/A	N/A		
50	150	300	**100 mM NAD**	663.45	250 µl	0.02	16.6
335	1005	2010	**dH_2O**				

Table 2.8 Preparation of Isothermal assembly buffer for final Isocloning reaction

Components	5 tubes (µl)	10 tubes (µl)
5X isothermal assembly buffer	20	40
Dilute T5 Exonuclease (Dilute 8x – 1 µl to 7 µl 1x ISA buffer)	0.5	1
Phusion polymerase	1.25	2.5
Taq ligase	10	20
H_2O	43.3	86.5

The resulting final buffer was aliquoted into 15 µl volumes and stored in -20°C.

2.11.5 DNA quantification by NanoDrop

DNA was quantified by NanoDrop ND-1000 spectrophotometer (NanoDrop Technologies, Inc). The sample retention system in NanoDrop contains two surfaces, the upper and lower

optical surface. 2 µl of deionized water was added to the lower optical surface. The lever arm was closed to bath the upper optical surface several times. Both the optical surfaces were cleaned with Kimwipe. From the dropdown menu of NanoDrop software, nucleic acid module was selected. On the lower optical surface carefully 2 µl clean water was pipetted. Care had to be taken to avoid touching the optical surface with pipette tip. The level arm was brought down gently to touch the water and lower optical surface. The button 'initialize' from NanoDrop software was pressed. This step approximately lasted for 10 seconds. Both the surfaces were wiped with clean Kimwipe. A volume of 2 µl of DNA sample to be measured was pipetted carefully on the lower optical surface and liver arm was lowered gently to touch the sample. Reading was taken after pressing 'measure' button from the software. Alongside the DNA concentration reading, the 260/280 ratio reading was noted. A ratio between 1.8 and 2.0 was normally considered as an acceptable measure for DNA purity.

2.11.6 Bacterial genomic DNA extraction

A commercial bacterial genomic DNA extraction kit was used (Omega bio-tek, USA). Three single colonies of bacteria were incubated in the Mueller hinton broth overnight at 37°C, 5% CO_2. No more than 3 ml culture or $1x10^9$ cells were centrifuged at 4000 x g for 10 minutes at room temperature. The media was discarded and 100 µl TE buffer was added to the pellet. The pellet was resuspended completely by vortexing. After addition of 10 µl lysozyme, the bacteria were incubated at 37°C for 10 minutes. 100 µl BTL buffer and 20 µl proteinase K solution were mixed with the sample and vortexed thoroughly. The sample was incubated at 55° C water bath shaking every 20 minutes for 1 hour. Then 5 µl RNase A was added and the tube was inverted several times to mix. After incubating at room temperature for 5 minutes, the sample was centrifuged at 10000 x g for 2 minutes to pellet any undigested component. The supernatant was transferred to a fresh 1.5 mL microcentrifuge tube. Special care was taken not to dislodging the pellet. To the supernatant 220 µl BDL buffer was added and incubated at 65°C for 10 minutes. 220 µl of 100% ethanol was added and vortexed for minimum 20 seconds at maximum speed. A HiBind DNA mini column (Omega Bio-Tek) was inserted into a 2 mL collection tube. The entire sample was transferred to the mini column along with any formed precipitate. After centrifugation at 10000 g for 1 minute the filtrate and collection tube were discarded. 500 µl HBC buffer was added after transferring the column to a new collection tube. After centrifuging at 10000 g for 1 minute the filtrate was discarded and the collection tube was reused for two 700 µl DNA buffer wash. After the second DNA buffer wash, the empty column was centrifuged for 2 minutes at 10000 x g to get rid of any unwanted content on the column. The

column was inserted into a new 1.5 ml microcentrifuge tube. Preheated (at 65°C) elution buffer was added to the middle of the column and let to sit for 5 minutes at room temperature. DNA was eluted in the microcentrifuge tube after centrifuging at 10000 x g for a minute. After quantification with a NanoDrop spectrophotometer **(Section 2.11.5),** the DNA was stored at -20°C with appropriate labelling.

2.11.7 PCR Purification

The PCR products were purified with Qiagen PCR purification kit before any cloning step to remove any carry over products from PCR reaction and restriction digest. Total 5 volume of Buffer PB was added to 1 volume of PCR sample and mixed thoroughly. A QIAquick spin column was placed in a 2 ml collection tube in the kit. The whole sample was applied to the column and centrifuged at 17900 x g (13000 rpm) for 30 to 60 seconds. The flow through was discarded and the column was placed back in the collection tube. For washing, the column was centrifuged after adding 750 µl of Buffer PE. For getting rid of any unwanted residue of PCR purification, the column was centrifuged for another minute. Then the column was placed in a clean 1.5 ml microcentrifuge tube. 50µl elution buffer was added to the centre of column and left at room temperature for 5 minutes. After centrifugation, the sample was collected and preserved in -20°C.

2.11.8 Plasmid DNA extraction

Plasmid DNA extraction kit from Qiagen was used. To extract plasmid from bacterial cultures one colony of plasmid from respective LB plate was inoculated in 5 ml of LB media. Antibiotics were added where appropriate: Ampicillin 100 µg/ml, Kanamycin 50 µg/ml, Erythromycin 300 µg/ml. The overnight culture was pelleted by centrifugation at 8000 rpm for 3 minutes at room temperature. Bacterial pellet was transferred to a microcentrifuge tube after resuspending in 250 µl Buffer P1. The sample was mixed with 250 µl Buffer P2 and vortexed. After adding 350 µl Buffer N3 sample was centrifuged at 13000 rpm for 10 minutes. The supernatant was applied on to a QIAprep spin column and centrifuged for a minute and the flow through was discarded. The column was discarded again after adding 750 µl Buffer PE. The column was centrifuged twice to wash all the residual buffer and was let to stand for 5 minutes at room temperature. Lastly, the plasmid was eluted by adding preheated 50 µl elution buffer to the centre of the column. After measuring the quality and quantity by using the NanoDrop spectrophotometer **(Section 2.11.5),** the plasmid was stored in the -20°C.

2.11.9 Restriction digest

The restriction enzymes for cloning were carefully selected by avoiding the ones with star activity. Then the following recipe was used for setting up the restriction digest. Enzymes were purchased from Promega or NEB. Digests were set up according to the manufacturer's instruction using the following protocol as standard:

Table 2.9 Recipe for Restriction digest

Components	20 µl reaction (For Promega enzymes)	50 µl reaction (For NEB enzymes)
DNA	1 µg	1 µg
Restriction enzyme	1 µl (For double digest 2 µl, 1µl for each enzyme)	1 µl (For double digest 2 µl, 1µl for each enzyme)
Restriction digest buffer	2 µl 10X buffer	5 µl of 10X buffer
BSA (if recommended)	Up to 3 µl 10x buffer	
Nuclease free water	Up to 20 µl	Up to 50 µl

The enzyme was the last item added to the mixture and taken out of the freezer just immediately before addition. Incubation time of digestion time depended on manufacturer's instructions. For sequential double digest, product was digested with enzyme requiring low salt buffer first using the above recipe. Then product was digested with 2nd restriction enzyme with addition of 1 µl of restriction enzyme, 5 µl buffer and 32 µl nuclease free water. After digestion enzymes were heat inactivated according to manufacturer's instruction for each enzyme. Restriction digested product was run by 1% Agarose gel (Section 2.11.14) for digestion confirmation.

2.11.10 DNA Ligation

All the ligations were carried out by NEB's T4 DNA ligase (M0202). The reaction was set up as follow:

Table 2.10 Recipe for DNA ligation

Components	20 µl Reaction
10X DNA Ligase Buffer	2 µl
Vector DNA : Insert	1:1, 1:3, 1:5 and 1:10 ratio
Nuclease free water	Up to 20 µl

T4 DNA Ligase	1 µl

The mixture was pipetted gently and incubated at 16°C overnight in a thermocycler.

Table 2.11 Control for ligation reactions

Control	Ligase	Interpretation
Uncut vector	-	Checks for the viability of the competent cells and efficacy of the antibiotic resistance of the agar plates.
Cut vector	-	Background colonies due to undigested vector.
Cut vector	+	Background colonies due to recircularisation of vector in particular useful for verifying phosphatase treated vector.
Water or insert	+	Presence of any colony indicates the contamination of intact plasmid in ligation or transformation agents.
Cut vector + insert	+	Grown colonies likely to contain the desired cloned sequence and have to be screened for the presence of right sequence by diagnostic PCR, restriction digest and sequencing.

2.11.11 Phosphatase treatment

Where appropriate the plasmid vector had to be treated with phosphatase to remove 5′ phosphate group. Therefore, the chance of vector re-circularisation following ligation step was minimised. During this project, Antarctic Phosphatase (NEB, M0289S) was used. Following double digestion, 5 µl of Antarctic phosphatase reaction buffer (x10) and 1 µl Antarctic phosphatase enzyme were added. The reaction mix was incubated at 37°C for 1 hour.

2.11.12 Broth culture transformation of *N. meningitidis*

Cells from frozen stocks of *N. meningitidis* were plated on GC Agar plate (with 2% Vitox supplement) containing appropriate antibiotic in the CO_2 incubator at 37°C. Colonies from overnight plate were inoculated in 2 ml of liquid MHB containing 10 mM $MgCl_2$ at OD_{550nm} ~ 0.1. Two micrograms of DNA was added to the culture followed by a 6 hour incubation period at 37°C with shaking. After this incubation period, 100 µl of pure culture, undiluted or diluted

1/10, 1/100 and 1/1000 were spread on GC Agar plates containing appropriate antibiotic **(Section 2.4.2).** Recombinant colonies normally appeared after 48 hour period of incubation at 37°C in the presence of 5% CO_2.

2.11.13 Spot transformation of *N. meningitidis*

An overnight (around 16 hour) growth culture of *N. meningitidis* was grown on a GC agar plate **(Section 2.4.2).** A square of 1x1 cm was drawn on the back of GC Agar plate using a marker pen and a small amount (barely visible) of the overnight culture was streaked onto this square. The DNA to be transformed was spotted onto the bacteria on the square and the plates were incubated at 37°C with 5% CO_2 for 8 hours. Following incubation period, the whole bacterial population within the square was plated on a fresh GC agar plate containing appropriate antibiotics. Single colonies from the plates were picked after 48 hours and were restreaked onto fresh antibiotic containing plates. Prior to testing by colony PCR **(Section 2.11.15.1)** this process was repeated again to prevent selecting false positives from non incorporated DNA used for the transformation. This also ensured the stability of antibiotic resistance over longer period of time before screening.

2.11.14 Agarose gel electrophoresis

Genetically manipulated DNA was checked by separating them on agarose gel. For visualising normal bands 1% gel was run. The larger bands (5.0 -10.0 Kb) were checked on a lower percentage (0.6%) gel. 0.5 g of agarose was melted in 50 ml of 1 x TAE buffer to produce 1% agarose gel. For visualising DNA bands, 0.1 µg ml^{-1} ethidium bromide was added to the agarose gel solution before pouring. The gel was set in an appropriate gel tank which was carefully sealed around by tapes to prevent any possible leakage. The gel tank was transferred to a horizontal tank and submerged in 1 x TAE buffer. All the PCR product to be run were mixed with 5 X DNA loading buffer (Qiagen) to a final solution of 1 X 5 ul of PCR product which was loaded on the gel along with 1 Kb DNA Hyperladder I (Bioline). The gel was run at 90 V for an hour using a Bio Rad powerpack. A dual intensity transilluminator (UVP) was used for the ultraviolet visualisation of the DNA bands.

2.11.15 PCR reactions

2.11.15.1 Colony PCR

For performing confirmatory PCR, colonies from appropriate antibiotic containing plates were picked by pipette tip and dissolved in 20 µl RNase free water (Qiagen). 5 µl of this mix was plated on appropriate antibiotic containing plate and the rest was denatured by a PCR machine

at 95°C for 5 minutes. This solution was used as a template for subsequent PCR. My Taq^{TM}Red mix (Bioline) **(Section 2.11.15.2)** was used to screen for positive colonies.

2.11.15.2 My Taq Red Mix

My Taq Red Mix (MyTaq^{TM}, BIO-25043, Bioline) contains a very efficient and rapid Taq polymerase. The mix contains all the essential components for optimum PCR such as Taq buffer, dNTPs, $MgCl_2$, enhancers and stabilizers. Therefore, the mix was added with the template and primers directly. After PCR, samples can be directly loaded on to the Agarose gel as the My Taq mixture contains red loading dye which does not interfere with the PCR process.

Table 2.12 PCR mix for My Taq Mix

Components	Amount
Template	100 ng
Primers (10 µM) each	1 µl
My Taq Mix, 2x	12.5 µl
Water	Up to 25 µl
Total	25 µl

Table 2.13 PCR cycling conditions for My Taq PCR

Step	Temperature	Time	Cycles
Initial denaturation	95°C	1 minute	1
Denaturation	95°C	15 second	25-35
Annealing	Variable (Depended on the primers used, normally calculated from primer Tm calculators from website)	15 second	
Extension	72°C	30 second per Kb	

2.11.15.3 ACCUZYME DNA polymerase

ACCUZYME™ is a very high yield DNA polymerase (BIO-21051, Bioline). It's a thermostable and high-fidelity enzyme producing blunt end amplicons of up to 5 Kb in length. It possesses 5′→ 3′ polymerase and 3′ → 5′ exonuclease activity. Mg^{2+} containing 10X reaction buffer helps to optimise a range of PCR conditions.

Table 2.14 PCR mix for Accuzyme polymerase

Components	Amount
10 X AccuBuffer	5 µl
50 mM $MgCl_2$	Optional
100 mM dNTP	0.5 – 1 µl
Template	As required
Primers 20 mM each	1 µl
ACCUZYME DNA polymerase 2.5 U/µl	1 – 3 µl
Water (ddH_2O)	Up to 50 µl
Total	50 µl

Table 2.15 PCR cycling conditions for Accuzyme DNA polymerase

Step	Temperature	Time	Cycles
Initial denaturation	95°C – 98°C	3 minute	1
Denaturation	95°C – 98°C	15 second	25-30 cycle
Annealing	55°C – 60°C (Variable, depended on the primers of the reaction)	15 second	
Extension	72°C	1.5-2 minute/Kb	

2.11.15.4 NEB Phusion^{R} high-fidelity Master Mix with HF buffer

NEB high-fidelity phusion polymerase (NEB, M0531S) is important for applications in which the target DNA sequence has to be correctly amplified. It's a thermostable polymerase that has an error rate of 50% lower than that of *Taq* polymerase. It possesses 5′→ 3′ polymerase and 3′ → 5′ exonuclease activity. The following reaction mix and cycling conditions were used:

Table 2.16 PCR mix for NEB Phusion polymerase

Component	Concentration
5 X Phusion HF or GC buffer	10 µl
10 mM dNTPs	1 µl
10 µM forward primer	2.5 µl
10 µM reverse primer	2.5 µl
Template DNA	Variable
DMSO	(1.5 µl)
Phusion DNA polymerase	0.5 µl
Nuclease free-water	Up to 50 µl
Total	50 µl

Table 2.17 PCR cycling condition for NEB Phusion polymerase

Step	Temperature	Time
Initial denaturation	98°C	30 second
25-35 cycles	98°C 45°-72°C (Was calculated using the Tm calculator available in the NEB website) 72°C	5-10 second 10-30 second 15-30 second per Kb
Final extension	72°C	5-10 minute
Hold	4°-10°C	10 minute

2.11.15.5 Q5 High Fidelity DNA Polymerase

Q5 High-Fidelity DNA polymerase (M0491S, NEB) is a high fidelity polymerase from NEB which has 12 times lower error rate compared to the *Pfu* (*Pyrococcus furiosus*) and 100 fold lower than the *Taq* DNA polymerase. It is a thermostable DNA polymerase with 3′ – 5′ exonuclease activity. The following reaction conditions were used:

Table 2.18 PCR recipe for Q5 DNA polymerase

Components	50 µl reaction	Final Concentration
5 x Q5 reaction buffer	5 µl	1 x
10 mM dNTPs	1 µl	200 µM
10 µM Forward Primer	1.25 µl	500 nM
10 µM Reverse Primer	1.25 µl	500 nM
Template DNA	Variable (Genomic DNA 1 ng – 1 µg, Plasmid DNA 1 pg – 1 ng)	<1000 ng
Q5 High Fidelity DNA Polymerase	0.25 µl	0.02 U/µl
Nuclease free water	Up to 50 µl	

Table 2.19 PCR cycling condition for Q5 DNA Polymerase

Step	Temp	Time
Initial Denaturation	98°C	30 second
18-20 cycles	98°C	5-10 second
	50°C - 72°C (Was calculated using the Tm calculator from the NEB website)	10-30 second
	72°C	20-30 second/Kb
Final Extension	72°C	2 minute

3 Chapter 3: Role of denitrification of *N. meningitidis* in the homeostasis of NO metabolites in a murine model of early fulminant meningococcal sepsis

3.1 Introduction

Meningococcal sepsis is a complex systemic inflammatory condition which causes significant morbidity and mortality around the world. The mortality rate for those diagnosed with fulminant meningococcal sepsis (FMS) is up to 50% although recent advancements in medicine have helped to lower the death rates (Booy *et al,* 2001). Pathophysiology in sepsis is characterized by a rapid burst of pro-inflammatory immune response. Subsequently, increased vascular permeability, intravascular thrombosis and both abnormal vasodilation and vasoconstriction can result in the failure of circulatory system, leading to multiple organ failure and death (Klein *et al,* 1992; Oragui *et al,* 2000) **(for details see Section 1.6).** Unlike other forms of sepsis caused by gram negative bacteria, FMS causes severe pathology within few hours which can lead to death. Despite aggressive resuscitation and treatment with drugs and fluid, the mortality rate from meningococcal sepsis remains high.

One of the main features of sepsis is failure of the tightly regulated microvasculature. NO is a pivotal signalling molecule for maintaining vascular homeostasis and hemodynamics **(Section 1.11.1).** Therefore, NO could be a key molecule whose disruption might affect the pathophysiological course of meningococcal sepsis. In septic patients there is a high correlation between sepsis severity and detectable levels of lipooligosaccharides (LOS), endotoxin present in the cell wall of *N. meningitidis* (Brandtzaeg *et al,* 1992). Likewise there is a strong association between bacterial genomic load and severity of meningococcal disease (Darton *et al,* 2009). Bacterial LOS induces iNOS production at a very high rate. During sepsis high levels of NO from iNOS may contribute to hypotension and inflammatory tissue damage (Kilbourn *et al,* 1997; Thiemermann, 1997).

There have been a number of studies that reported a positive correlation between infection and amounts of circulating nitrogen oxides such as NO_2^- and NO_3^- in sepsis. Children with septic syndrome such as hypotension have high levels of NO_2^- and NO_3^- in serum (Wong *et al,* 1995). Similar analysis in the CSF of meningitis patients reported a 3 fold increase in NO_3^- and almost 50 fold increase in NO_2^- (Visser *et al,* 1994). In children, meningococcal sepsis is characterised by high bacterial titres in blood and sepsis severity correlates with an increased production of circulating nitric oxides, including NO_2^- and NO_3^- (Baines *et al,* 1999). High plasma levels of

NO_2^-/NO_3^- is found in new born infants with sepsis (Shi *et al*, 1993) and adult patients in intensive care unit (Gomez-Jimenez *et al*, 1995; Ochoa *et al*, 1991). Formation of SNO, termed S-nitrosylation, is an important form of post-translational protein modification akin to phosphorylation and is important for regulating myriad cellular processes such as vasodilation, apoptosis, neurotransmission, cell signalling and gene expression (Allen & Piantadosi, 2006; Seth & Stamler, 2010; Stamler *et al*, 2001). **Previous studies from our group have shown that NorB-mediated NO detoxification by *N. meningitidis* reduces the concentration of host-cell SNO (Laver *et al,* 2010). This could have far reaching consequences for homeostasis of the pathways regulated by SNO such as SNO-Hb mediated vascular regulation. Following deoxygenation of blood, NO bound to conserved cysteine of SNO-Hb is dispensed at microvascular sites leading to vasodilation (Section 1.10). This process couples deoxygenation of haemoglobin to vasodilation. If a similar SNO depletion effect can be observed *in vivo* following meningococcal infection, then it is plausible that SNO repletion may be a viable therapy for treatment of meningococcal sepsis. Supplementation with *S*-nitrosoglutathione (GSNO) has been shown to be effective in repairing cerebrovascular damage in an animal model of haemorrhage (Sehba *et al,* 2007). We hypothesise that bacterial NO denitrification during sepsis interferes with the amount of NO metabolites, including SNO, within the organs of the host *in vivo* and contributes toward pathogenesis. To test this we decided to establish a murine model of early acute meningococcal sepsis and to do a comparative analysis of NO metabolites produced in response to bacterial infection by *N. meningitidis*. By using both a wild type strain (MC58) and mutants with different insertionally-inactivated NO denitrification genes, we intend to investigate whether bacterial mechanisms of NO detoxification are able to impact on systemic levels of NO metabolites.**

3.2 Ozone based chemiluminescence and NO analyser

One of the most enduring and sensitive techniques for measuring NO is the ozone based chemiluminescence. Quantification of NO is performed by gas-phase chemiluminescence detection using ozone (O_3). Singlet oxygen molecules react readily with a variety of gases such as NO, NO_2, SO_2 and CO. In contrast, ozone reacts more rapidly with NO due to lower activation energy of the reaction. In the gas phase, O_3 reacts with NO and generates NO_2 in an excited state (NO_2*) **(Reaction 1)**. The excited NO_2* returns to the ground state either by colliding with another molecule, or by the release of a photon. Photon release is detected in the red and near infrared region of the spectrum (Gorimar, 1985). The amount of NO present in the sample is directly proportional to the emission of light. The whole reaction is pressure and temperature sensitive.

$NO + O_3 \rightarrow NO_2^* + O_2 \rightarrow NO_2 + O_2 + h\nu$…….(1)

Although the first chemiluminescence based NO analyser was developed in 1970 (Fontijn *et al*, 1970), the basic design of the apparatus has remained unaltered. The Sievers 280i Nitric Oxide Analyser used for this study consists of a reaction cell, an ozone generating pump and a cooled photomultiplier tube **(Figure 3.1).** Ozone is supplied to the machine in excess, ensuring that O_3 does not become a limiting factor in the generation of NO_2*. The samples are drawn to the reaction cell through a vacuum of gas-impermeable reaction tube. Reaction with O_3 takes place inside the vacuum, ensuring minimal mechanical quenching of excited NO_2*. The vacuum also acts to stabilise NO by removing O_2, which could react with NO to form NO_2. Since NO_2 does not emit light following interaction with O_3, the presence of the vacuum therefore prevents loss of signal strength. The NO analyser is built in with a specific and very sensitive photomultiplier tube capable of detecting light in the near-infrared range. This is pivotal to the accurate detection of signal from reaction vessel as red and infrared light generated from the relaxation of NO_2* is of very low intensity. It enables individual photons from the light to be detected on a photosensitive surface and causes the release of electrons which are accelerated in an electron multiplier field comprising of several dynodes. The cumulative action of multiple dynodes leads to the generation of several million electrons from a single photon. These electrons are drawn to the anode resulting in the production of a current pulse by the accumulation of charges. The current is used by NO analyser to detect amount of NO present in the sample. The signal by current pulse is digitalised and relayed to a computer attached to the machine. It is plotted as the intensity of signal (mV) against time using the user friendly LIQUID software. As the reaction of NO with O_3 takes place in the gas phase, NO

present in the liquid samples have to be stripped into gas phase. High partition coefficient of NO helps the voluntary diffusion of NO from liquid to gas phase. To aid this process an inert gas, nitrogen (N_2) is passed through the liquid sample in the purge vessel. In addition, this helps to maintain an oxygen depleted environment inside the purge vessel and thereby preventing the formation of NO_2 from NO.

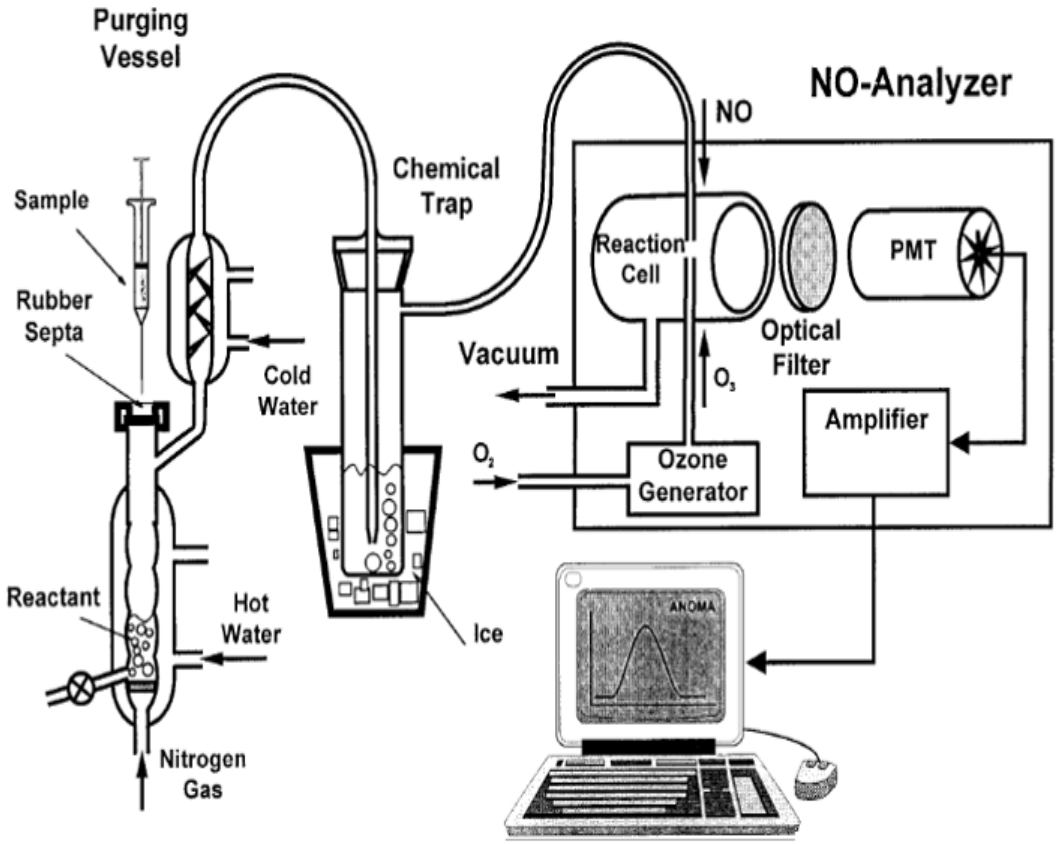

Figure 3.1 A cartoon summarising the apparatus set up for NO measurement by ozone based chemiluminescence.

Sample is added on to the reactant (reducing agent) inside the purge vessel. Generated NO diffuses into the headspace above the reactant through NaOH trap and pulled into the NO analysed by an external vacuum. NO reacts with the O_3 from ozone generator and light emitted in the reaction is detected, amplified and converted into electrical signal by photomultiplier tube (PMT). The final output displayed on the monitor of attached computer. The data is analysed by specialised LIQUID software. Figure reproduced from (Samouilov & Zweier, 1998)

3.3 Measurement of NO metabolites by chemiluminescence

For measuring NO metabolites such as NO_2^-, NO_x and SNO, samples were reduced using a variety of reducing agents. The most commonly used method for measuring SNO is triiodide (I_3^-) based chemiluminescence. The method was first used for measuring low molecular weight SNO (Samouilov & Zweier, 1998). Later adaption of the method enabled the measurement of larger molecular weight SNO such as SNO-albumin (Marley *et al,* 2000). In a series of reactions **(Reactions 2-6),** the NO moiety from SNO is released by reduction at a stoichiometry of 1:1. During the process, the reaction chamber is maintained at 30°C by connection to a circulating water bath, and acidic vapours are neutralised in an acid-vapour trap. The I_3^- solution **(Section 2.3.4)** can yield a chemiluminescence signal from all NO species except nitrate (NO_3^-). Therefore, signal coming from the reduction of each NO species has to be separated for determining the concentration of any particular NO moiety. This is achieved by splitting the samples into aliquots and treating them with different reagents, in order to remove or otherwise render the moiety/moieties inert that would otherwise contribute to the chemiluminescence signal **(Figure 3.2)**. Treatment of sample with acidified sulphanilamide complexes the NO_2^- present in the sample, incorporating it into a stable diazonium compound that can no longer be reduced into NO by I_3^- solution. Treatment of samples with $HgCl_2$ releases a nitrosonium ion (NO^+) from SNO, which replaces NO group present in SNO with Hg^+ ion. After measuring the output from differentially treated samples, it is possible to subtract the signals derived from each measurement from the overall (untreated) signal, enabling the operator to calculate the concentration of a given NO compound. A detail overview of the process in presented in **Figure 3.2.**

$I_2 + I^- \rightarrow I_3^-$ .....**(2)**

$I_3^- + 2RSNO \rightarrow 3I^- + 2RS + 2NO^+$ …...**(3)**

$2NO^+ + 2I^- \rightarrow 2NO + I_2$ …….**(4)**

$RSNO \rightarrow RS\bullet + NO$ …….**(5)**

$2RS\bullet \rightarrow RSSR$ ……..**(6)**

To measure higher NO oxides such as NO_3^- by ozone-based chemiluminescence, a stronger reducing agent is required. An acidified, saturated VCl_3 solution is used to liberate NO from NO_3^- **(Reaction 7).** The solution reduces all oxidised NO metabolites (NO_x) such as NO_2^-, S-nitrosocompounds, N-nitrosamines and Fe-nitrosyls, producing NO. The reaction takes place

at 95°C in the purge vessel. The acid vapour trap is particularly important when making these measurements, and contains 1 M NaOH to neutralise the hot acidic vapour from the acidified VCl_3 solution **(Section 2.6.3).**

$2NO_3^- + 3V^{3+} + 2H_2O \rightarrow 2NO + 3VO_2^+ + 4H^+$……**(7)**

An anti-foaming agent **(Section 2.1.1)** is used to prevent excessive foam formation, which is often encountered while measuring NO_x with acidified VCl_3. Excess foam can interfere with the chemiluminescence signal.

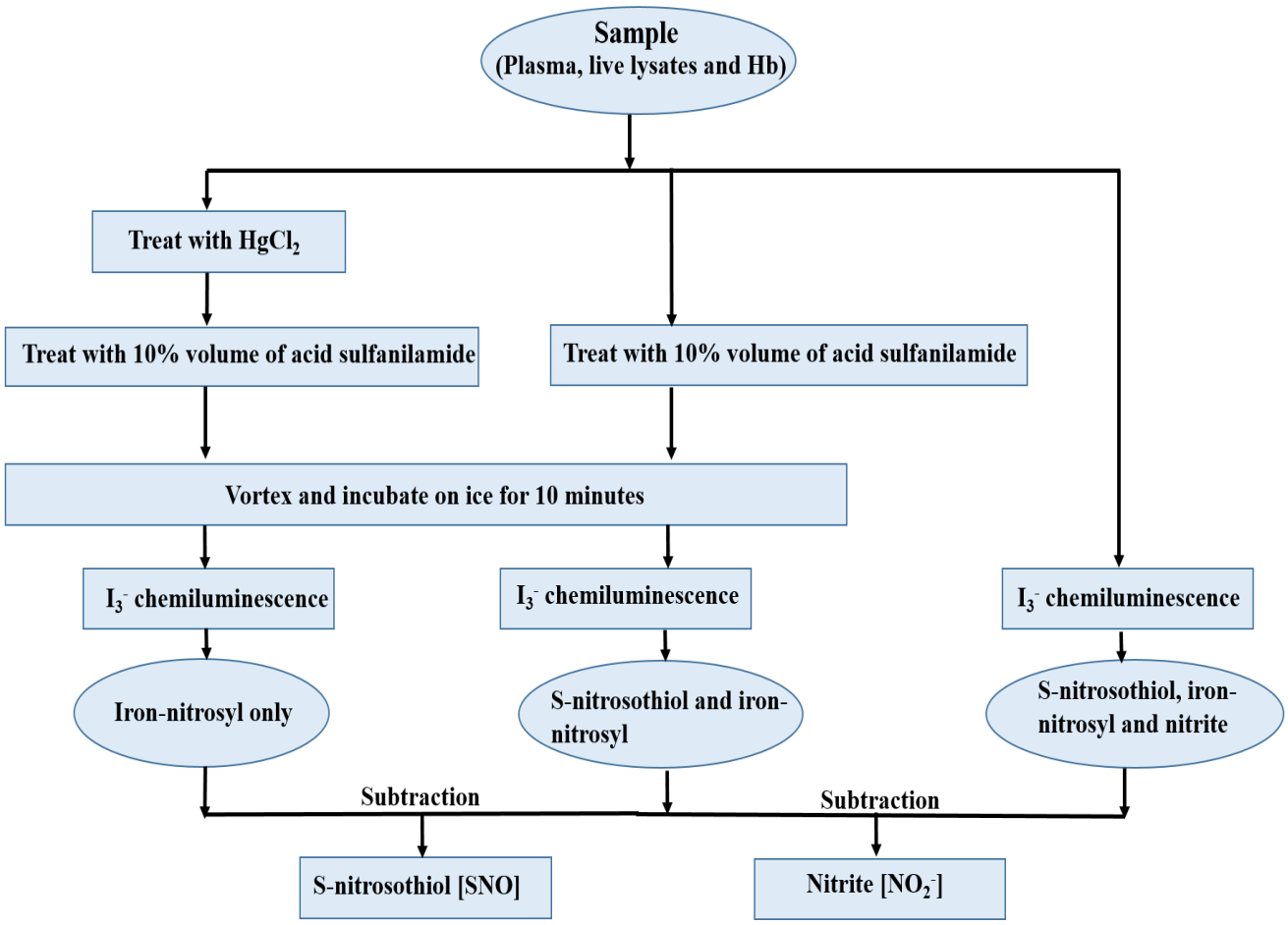

Figure 3.2 Schematic summarising the processes involved in the measurement of NO metabolites by I_3^- based chemiluminescence.

Samples were split into different parts and treated with different compounds prior to I_3^- based chemiluminescence. Measurement of each compound achieved different objectives: $HgCl_2$ released NO from SNO present in the sample. Acidified sulfanilamide converted NO_2^- present in the samples into a non I_3^- reactive diazonium salt. Concentrations calculated for treated samples (adjusted for extra dilution) were deducted from the concentration calculated for untreated samples, allowing the concentration of SNO and NO_2^- to be elucidated. Adapted from (Yang *et al*, 2003)

3.4 Considerations for preparation of biological samples for chemiluminescence

Careful preparation of biological samples is pivotal for accurate measurement of NO metabolites by chemiluminescence. Sonication is a widely used method for cell lysis. However, exposure of low molecular weight thiols to ultrasonication in presence of air leads to the production of S-nitrosocompounds (Stepuro *et al*, 2000). This property eliminates ultrasonication as a choice of method for cell lysis. Detergents are normally avoided to lyse cells for NO measurement by chemiluminescence due to their propensity to form excessive foams in the purge vessel. However, no such problem was encountered with NP-40, the detergent used for cell lysis during this study.

N-ethylmaleimide (NEM), an alkylating agent; is used in the lysis buffer to block any free thiol residue in the samples. NEM is a thiol-reactive substance, and prevents artefactual SNO formation in the lysates. Samples were incubated on ice for 10 minutes for this reaction to happen. In addition, the lysis solution contained protease inhibitor cocktail and phenylmethanesulfonate (PMSF), a serine-protease inhibitor, to prevent protein degradation. This step was crucial as all the SNO readings were normalised to protein concentration in those samples.

The NO-heme adduct iron-nitrosyl-hemoglobin ($HbFe^{II}NO$) is formed through the reversible reaction between NO and haemoglobin. The resulting $HbFe^{II}NO$ can bind to thiol on cysteine-93 of the β-globin chain to form S-nitrosohaemoglobin (SNO-Hb). After collecting whole blood it was centrifuged and plasma from the upper layer was stored in a separate tube. From the bottom of the pellet red blood cells were moved and rapidly collected in a stabilisation solution **(Section 2.5.5).** SNO-Hb had to be stabilised as it degrades rapidly in red blood cell environment in a temperature and redox dependant manner (Gladwin *et al*, 2002). SNO-Hb stabilising solution consisted of potassium ferricyanide ($K_3Fe^{III}(CN)_6$), N-ethylmaleimide (NEM), diethylenetriaminepentaacetic acid (DTPA) and 1% NP-40 detergent in PBS. The potassium ferricyanide component redox inactivated the heme group by forming cyanomethemoglobin. Red blood cell membranes were rapidly solubilised and lysed by NP-40 detergent which released any membrane bound S-nitrososthiol. NEM blocked the free thiol groups on the lysates and contaminating copper and trace metals were chelated with DTPA.

In addition, all the samples were preserved in light protected tubes and stored in liquid nitrogen to keep degradation of NO metabolites such as SNO to a minimal level. Repeated freeze-thawing also was avoided.

3.5 Results

3.5.1 Establishing a murine model of early fulminant meningococcal sepsis

Section Summary:

- ***A high bacterial inocula (10^9) causes severe bacteraemia in a murine model of meningococcal septicaemia within 6 hour***
- ***NO metabolite concentrations in liver homogenate and whole blood are not differentially affected by meningococcal NO detoxification***

3.5.1.1 Rationale and methods

It was necessary to establish a murine model capable of producing fulminant meningococcal sepsis in a reproducible manner. This model was to be used to measure NO metabolites such as SNO, NO_2^- and NO_x. Previous studies from our lab have shown that NO detoxification of *N. meningitidis* prevents the formation of S-nitrosothiol in a murine macrophage cell line J774.2 (Laver *et al,* 2010). The initial aim of this study was to establish a model to investigate if the observation can be replicated *in vivo.*

Preliminary experiments revealed that a dosage of 10^{10} bacteria per mouse elicited highly severe sepsis from the mice. Dosages from 10^6-10^8 bacteria per mouse were too low to establish bacteraemia (data not shown). Inocula of 10^9 bacteria per mouse, however was able to reproducibly induce sepsis, which was confirmed by the recovery of viable meningococci from murine blood and liver lysates. Preliminary experiments also showed that detectable levels of SNO are found in murine blood and liver but not from kidney and spleen (data not shown). High levels of iNOS mRNA have been detected from septic rat (Hom *et al,* 1995). NO signalling is critically important in the regulation of SNO proteins in blood such as SNO-albumin and SNO-Hb (Stamler, 2004). Substantial iNOS activity (Knowles *et al,* 1990) and presence of an extensive S-nitrosoproteome (Lopez-Sanchez *et al,* 2008) have been reported in the murine liver. As such, the decision was made to measure NO metabolites exclusively in blood and from liver.

To investigate whether the activity of the nitric oxide reductase (NorB) of the meningococcus had any effect on circulating and/or hepatic concentrations of NO metabolites in the acute cases of murine meningococcal sepsis, C57Bl/6 mice (Harlan, UK) were inoculated intraperitoneally (i/p) with a bolus of 10^9 wild type or *ΔnorB* mid-log phase bacteria suspended in 10 units (100

µl) of sterile PBS **(Section 2.5.1).** Mice were monitored continually and were scored hourly on the severity of infection **(Section 2.5.2).** The frequency of scoring was increased from hourly to half-hourly upon individual mice reaching a cumulative severity score of 19 or more. Upon reaching the end point of the experiment, mice were terminally anaesthetised using an i/p injection of sodium pentobarbitone (5 units/mouse). Mid-place anaesthesia was confirmed by the loss of pedal withdrawal-reflex. Blood was collected by exsanguination through cardiac puncture and whole liver was excised. After collecting the whole blood it was centrifuged and plasma from the upper layer was stored in a separate tube. From the bottom of the pellet red blood cells were moved and rapidly collected in a stabilisation solution **(Section 2.5.5).** After stabilisation, the mix was filtered through a Sephadex G25 sizing column to remove low molecular weight SNO and elute the SNO-Hb. The SNO-Hb solution was split into two fractions. The first fraction was treated with $HgCl_2$ to liberate nitrosonium ion (NO^+) from SNO. Subsequently it was treated with acidified sulphanilamide to eliminate any contaminating NO_2^- through the formation of diazonium salt. Second fraction was treated with acidified sulphanilamide to remove NO_2^-. Difference in readings between two fractions corresponded to the amount of SNO-Hb in the sample **(Figure 3.2).** The reading was normalised to percentage of SNO per heme molecule determined using Drabkin's solution **(Section 2.5.7).** Whole liver was treated with 0.25% bile salt to remove external bacteria and homogenised using a hand held rotor-stator homogeniser in SNO compatible lysis buffer **(Section 2.5.3 and Figure 3.3).**

After appropriate preparation of plasma **(Section 2.5.4),** SNO-Hb **(Section 2.5.6)** and liver lysates **(Section 2.5.3)** samples, they were measured by I_3^- based chemiluminescence **(Section 2.6.2).** For SNO measurement samples were normalised to the protein concentration of the lysate **(Section 2.10.4).** Plasma NO_x was measured by acidified VCl_3 **(Section 2.6.3).** All the measurements were subsequently analysed by using the Origin software **(Section 2.6.5).** A summarised schematic for the experimental procedure is presented in **Figure 3.3**.

3.5.1.2 Results

Each infected mouse demonstrated an increasing severity of infection over time, with the severity limit being equalled or exceeded in each infected mouse at 6 hour **(Figure 3.4 B and C).** Injection with a bolus of PBS alone did not result in the generation of sepsis symptoms, and the mice were phenotypically unaffected **(Figure 3.4 A).** There was no significant difference in the severity of sepsis between mice infected with wild type bacteria and mice infected with Δ*norB* bacteria (Area under curve analysis, $p = 0.58$).

Sepsis was confirmed by serial tenfold dilution of either blood or liver homogenate in PBS, followed by viable count **(Figure 3.5).** There was no statistically significant difference between the viable counts of the inocula between Wt = 5.9×10^8 cfu/ml (IQR = $5.1 \times 10^8 – 8.3 \times 10^8$) and Δ*norB* = 5.89×10^8 cfu/ml (IQR = $4.58 \times 10^8 – 8.22 \times 10^8$) infected mice. Recovery of viable bacteria from blood and liver homogenates was possible for both wt and Δ*norB*-infected mice, however there was no statistically significant difference in the viable count recovered from whole blood and liver lysates between Wt and Δ*norB* infected mice.

Mice infected with Δ*norB* showed significantly higher plasma NO_x concentrations (160.9 µM (IQR = 112.8 - 237.3)) compared to the PBS control group (18.74 µM (IQR = 5.69 – 63.39)) **(Figure 3.6 A).** This was not seen in case of the NO_2^- output **(Figure 3.6 B).** Infection with either wild type or Δ*norB* strain led to a significant increase in the concentration of plasma SNO (Wt = 58.49 nM (IQR = 33.92 – 73.17); Δ*norB* = 59.32 nM (IQR = 51.33 – 73.60)), as compared to PBS-injected mice (19.79 nM (IQR= 14.18 – 38.61) (**p* <0.05). There was no statistically significant difference between Wt and Δ*norB* infected mice **(Figure 3.6 C).** A similar observation was made for SNO-Hb measurements, which were significantly elevated in the RBC of infected mice as compared to those injected with PBS alone. Mice infected with wt strain contained 3.2×10^{-3} % SNO per heme (IQR =1.96×10^{-3} % - 4.52×10^{-3} % SNO per heme) and mice infected with Δ*norB* bacteria produced 3.38×10^{-3} % SNO per heme (IQR= 2.22×10^{-3} % - 6.84×10^{-3} % SNO per heme). The concentration of SNO-Hb in PBS-injected mice was 6.3×10^{-4} % SNO per heme (IQR= 4.13×10^{-4} % - 1.19×10^{-3} % SNO per heme) (**p*<0.01) **(Figure 3.6 D).**

The concentration of SNO measured in liver homogenates, produced from the liver of wt-infected mice was 3.006 pmol/mg (IQR= 2.40 - 4.78) and in liver homogenates produced from the liver of Δ*norB*-infected mice was 3.32 pmol/mg (IQR = 2.36 - 4.49) **(Figure 3.7)**. While

these concentrations are not significantly different from one another, infected mice exhibited a significantly higher concentration of liver homogenate SNO than did PBS-injected controls, (0.63 pmol/mg (IQR= 0.06 – 1.09)) (**p*<0.01). A similar pattern was observed in the concentrations of liver homogenate NO_2^-, insofar as there was a general increase in the concentration of this metabolite in the livers of infected mice as compared to PBS-injected controls, but in this instance the increase was not statistically significant.

Table 3.1 details the breakdown of the concentrations of various NO metabolites measured in both murine blood and liver homogenates.

Table 3.1 **Summary of NO metabolites output from mice infected with 10^9 bacteria/mouse suspended in PBS for 6 hours. Values are given as median, with interquartile range (IQR) in parentheses**

NO metabolites	PBS	Wt	Δ*norB*
Plasma NO_x	18.74 µM (5.69 - 63.87)	153.5 µM (131.4 – 176.7)	160.9 µM (112.8 – 237.3)
Plasma NO_2^-	1.12 x 10^3 nM (5.74 x 10^2 – 3.71 x 10^3)	1.6 x 10^3 nM (1.1 x 10^3 – 1.84 x 10^3)	1.46 x 10^3 nM (1.14 x 10^3 – 1.68 x 10^3)
Plasma SNO	19.79 nM (14.18 – 38.61)	58.49 nM (33.92 – 73.17)	59.32 nM (51.33 – 73.60)
SNO-Hb	6.3 x 10^{-4} % SNO per heme (4.13x10^{-4} % – 1.19 x 10^{-3} %)	3.2 x 10^{-3} % SNO per heme (1.96 x 10^{-3} % – 4.52 x 10^{-3} %)	3.37 x 10^{-3} % SNO per heme (2.22 x 10^{-3} % – 6.84 x 10^{-3}%)
Liver SNO	0.63 pmol/mg (0.06 – 1.089)	3.006 pmol/mg (2.41 – 4.78)	3.32 pmol/mg (2.36 – 4.49)
Liver NO_2^-	18.27 pmol/mg (12.79 – 29.64)	63.17 pmol/mg (18.63 – 85.00)	69.26 pmol/mg (31.72 – 103.7)

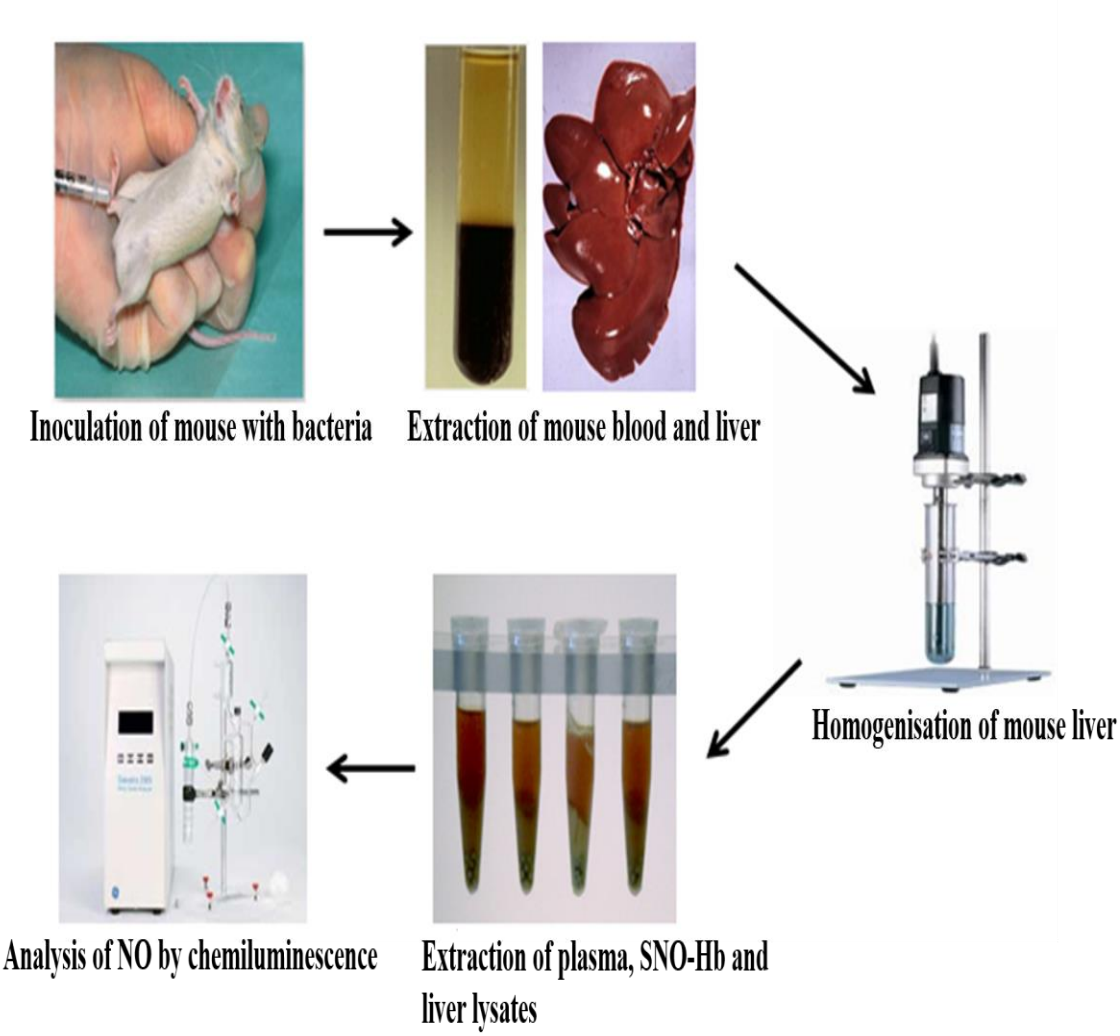

Figure 3.3 Workflow of experimental procedures for the measurement of NO metabolites in a murine model of early fulminant meningococcal sepsis.

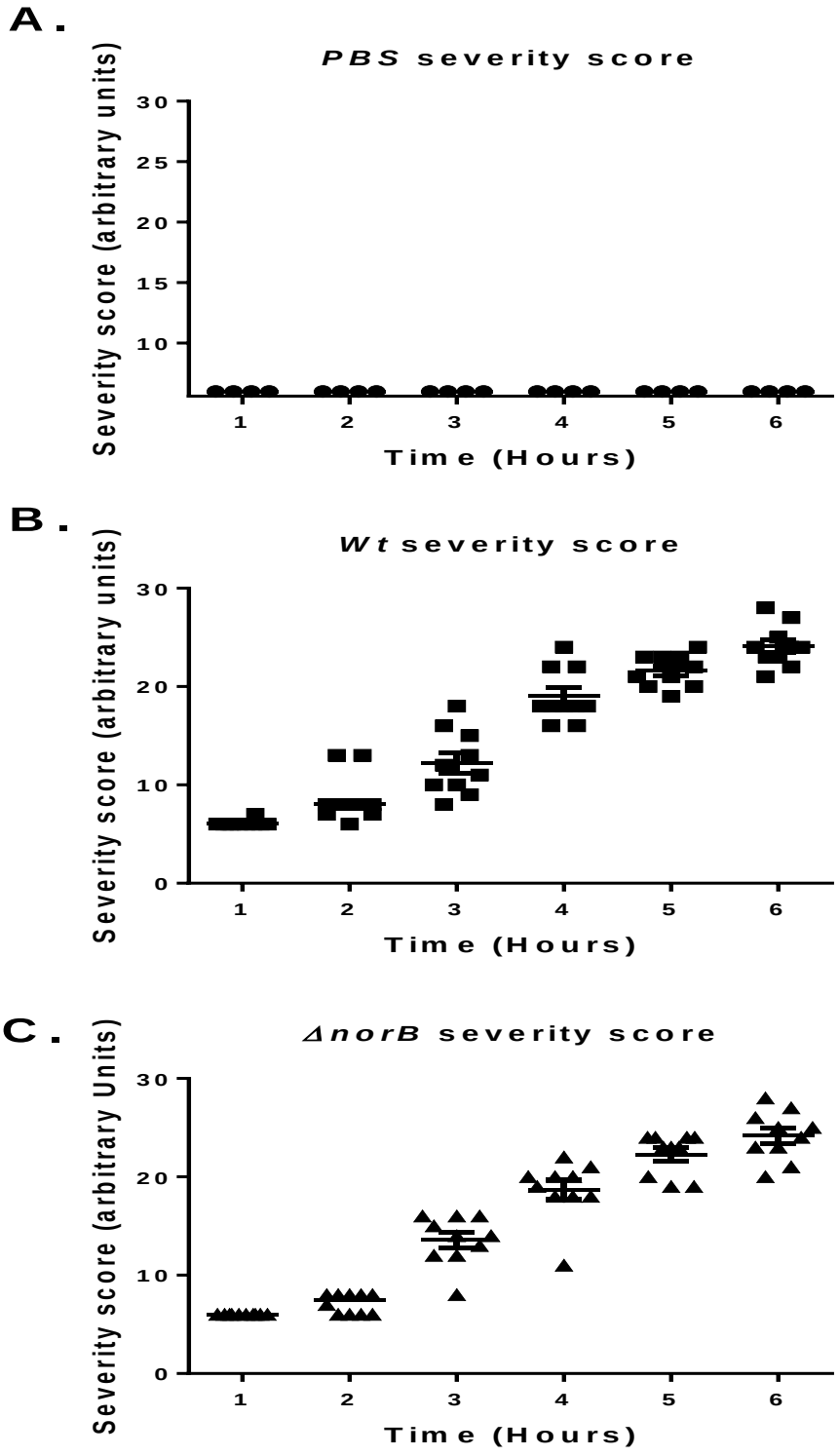

Figure 3.4 Severity scoring data in 7-10 week old female C57BI6 mice infected with 10^9 bacteria/mouse suspended in PBS over the course of 6 hours A) PBS B) Wt and C) Δ*norB*.

Following intraperitoneal injection mice were monitored for severity every hour according to the sepsis severity scoring guideline **(Section 2.5.2).** Total score 9-18 = moderate, 19- 24 = substantial (monitored every 30 minutes), 25-30= substantial (mice had to be culled). Bars denote median. One way ANOVA with Dunn's post test.

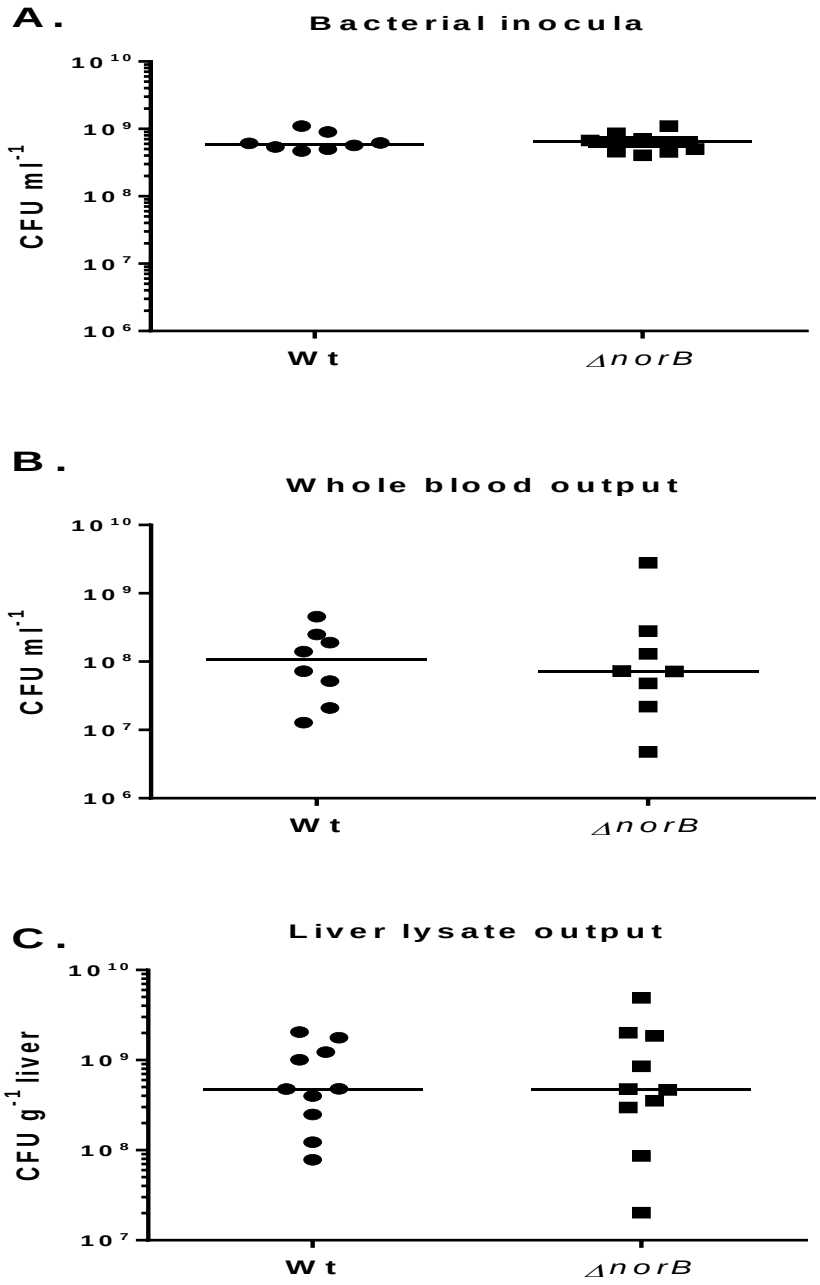

Figure 3.5 Viable bacteria recovered from inocula (A), whole blood output (B), and liver lysates (C) after experiment in murine model infected with 10^9 bacteria/mouse in PBS for 6 hours.

Samples were serially diluted and triplicate of 10 µl aliquots of each dilution were separately spotted on CBA plates, left in a microbiological safety cabinet for 10 minutes to allow them to air-dry. Following overnight incubation at 37°C, 5% CO_2, the mean number of colonies for each dilution were counted and corrected for the dilution factor and volume. Thus the mean of countable dilutions were averaged to estimate the number of bacteria present in the original suspension. Viable counts of bacteria recovered from mice liver lysates infected with *Neisseria*. Liver lysate viable counts were normalised to CFU/g of excised liver (wet weight). Bars denote median. For statistical analysis, Unpaired t-test was used.

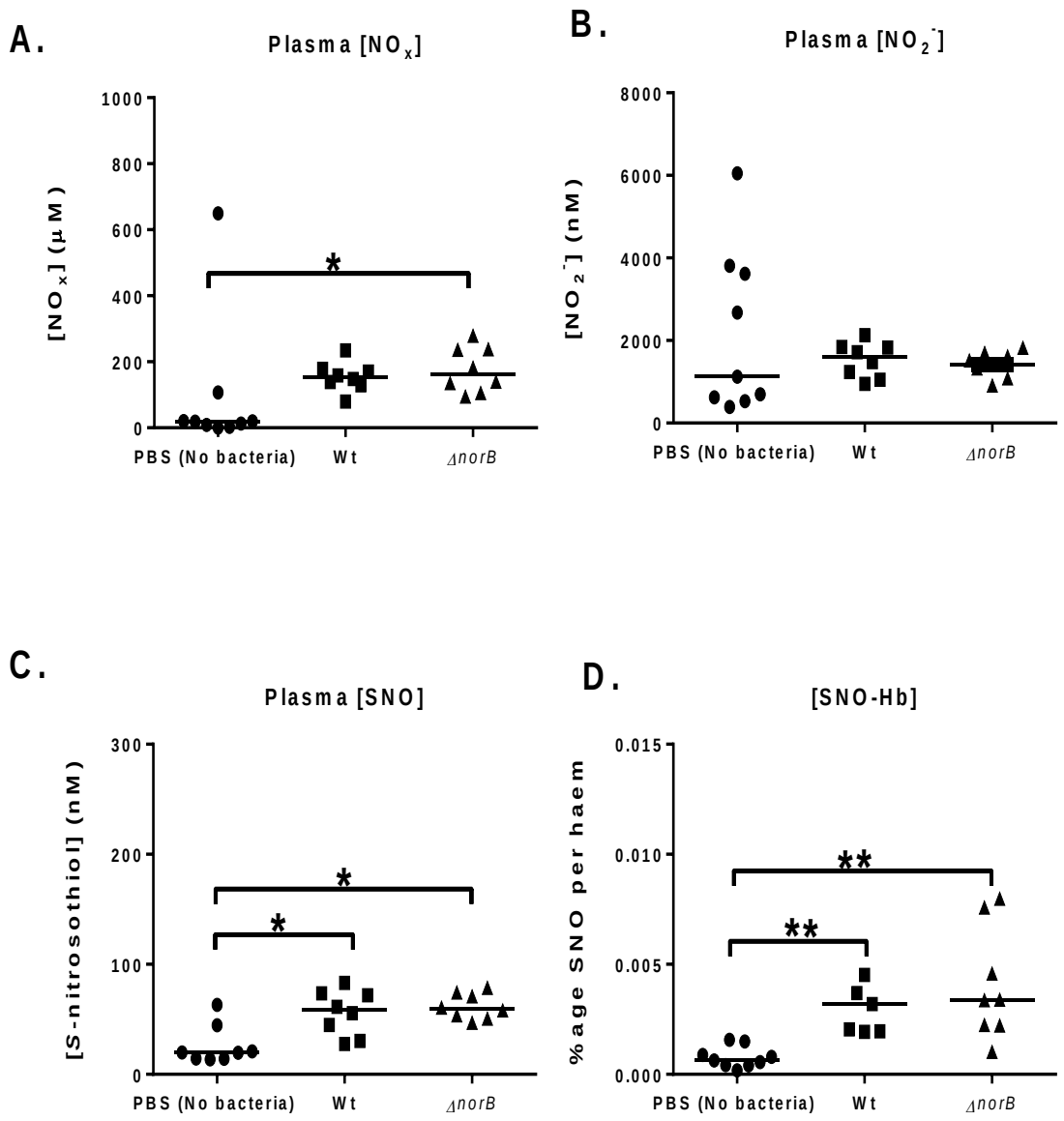

Figure 3.6 Measurement of plasma NOx (A), NO_2^- (B), SNO (C) and SNO-Hb (D) in mice infected with 10^9 bacteria + PBS for 6 hours.

NO metabolites were measured in red blood cell after bolus injection of endotoxin free PBS + Wild type/*ΔnorB N. meningitidis* (10^9 bacteria/mouse) into 7-10 weeks old female C57BI6 mice. NO_x **(A)** was measured by acidified VCl_3 at 90°C **(Section 2.6.3).** NO_2^- **(B)** and SNO **(C)** were measured by I_3^- dependent, Ozone-based chemiluminescence with reference to a GSNO standard curve **(Section 2.6.2).** SNO-Hb **(D)** was normalised to heme % **(Section 2.5.6- 2.5.7).** Bars denote median. For statistical analysis, One way ANOVA with Dunns test was performed using Graphpad Prism (v5). *p<0.05, **p<0.01.

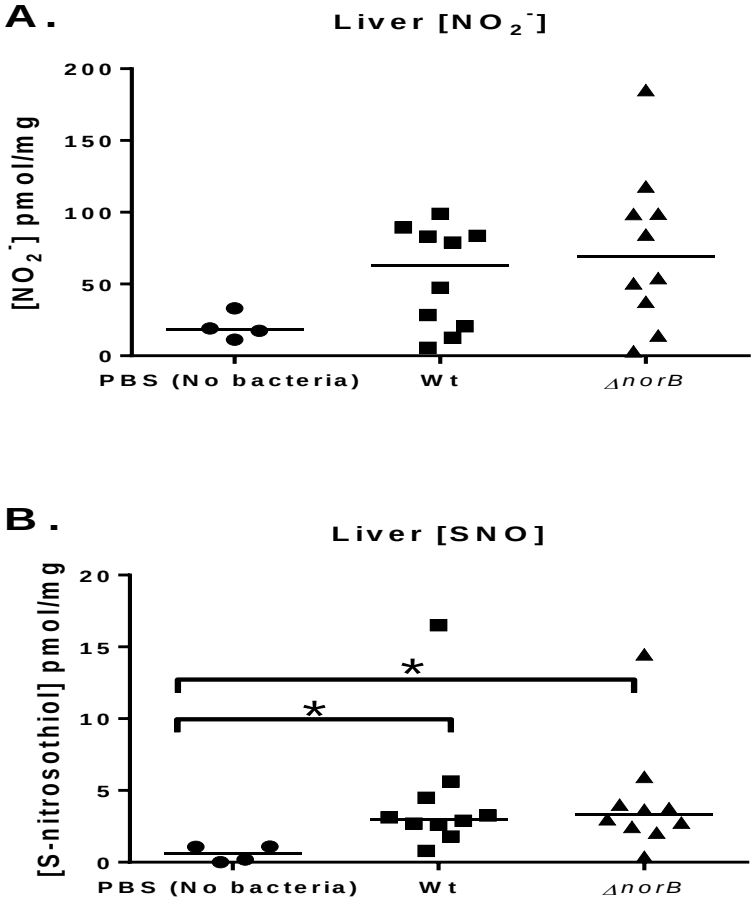

Figure 3.7 Measurement of Liver NO_2^- (A), SNO (B) in mice infected with 10^9 bacteria suspended in PBS for 6 hours.

Liver lysates were processed by a hand held rotor stator homogeniser **(Section 2.5.3).** NO metabolites **(A and B)** were measured by I_3^- dependent, Ozone-based chemiluminescence with reference to a GSNO standard curve **(Section 2.6.2)**. Bars denote median. For statistical analysis One way ANOVA with Dunns post test was performed. *p<0.05

3.5.2 Refining the murine model of acute meningococcal sepsis

Section Summary:

- ***Inclusion of human holo transferrin induces prolonged sepsis with a lower dosage of bacterial inocula (10^7)***
- ***Bacterial NO denitrification pathway does not affect the production of NO metabolites in liver and whole blood***
- ***Bacterial burden correlates with increased Plasma SNO, increased hepatic NO_2^- and decreased hepatic NO_x***

3.5.2.1 Rationale and methods

Despite successfully establishing a model of reproducible meningococcal sepsis, the bacterial inoculum was relatively high (10^9 bacteria/mouse) **(Section 3.5.1.1)**. One consequence of a large inoculum was the rapid increase in severity score, such that the severity became substantial within 5 hour and equalled or exceeded our severity limits within 6 hour **(Figure 3.4).** A previous *in vitro* study in J774 murine macrophages showed that iNOS expression is mandatory for *norB* mediated SNO depletion (Laver *et al*, 2010). Given that synthesis of iNOS and the accumulation of iNOS-derived NO take time, it would be preferable for the model to be run over a longer time period.

A large bacterial inoculum was necessary to induce sepsis in our original model, most likely due to the inaccessibility of iron in the murine system **(Figure 3.4 - 3.7)**. *N. meningitidis* accesses iron by binding to the human transferrin, achieved through the expression of outer membrane receptor proteins termed as transferrin binding proteins (TbpA and TbpB) (Renauld-Mongenie *et al*, 2004). However, these proteins are highly specific for human transferrin, and *N. meningitidis* is unable to bind to and liberate free iron from murine transferrin (Gorringe *et al*, 2005). Importantly, it has been shown that the iron responsive Fur protein binds to the intergenic promoter region between *aniA* and *norB* (Delany *et al*, 2004) and acts as an activator of the denitrification regulon **(Figure 1.8).** In addition, another study reported that Fur is responsible for *aniA* activation in *N. meningitidis* (Edwards *et al*, 2012). It might therefore be crucial for efficient expression of the denitrification genes in our model.

Previous studies have shown that injection of 8 mg of human holo transferrin (human holoTf) into mice results in the physiological levels of circulating human holoTf for up to 24 hour (Yi *et al*, 2003). Therefore, mice supplemented with human holoTf could mimic a human model of sepsis more closely and enable bacteria to thrive for longer by utilising transferrin. As the aim of the investigation was to examine bacterial metabolism-mediated alterations in the concentration of NO-related species, a longer sepsis protocol was favourable to allow sufficient time for NOS activity. As such, it was decided that the bacterial inocula should be supplemented with 8 mg human holoTf.

Initial range finding experiments for determining appropriate bacterial inocula in presence of holoTf were carried out using 10^6-10^9 bacteria/mouse. Severity score showed that a dose of 10^7 bacteria/mouse can cause bacteraemia in the presence of human holoTf. Therefore, the bacterial dose used for i/p injection was lowered to 10^7 bacteria/mouse from previously used 10^9 bacteria/mouse for these set of experiments. Along with Wt and Δ*norB*, another isogenic mutant, Δ*nsrR*, which negatively regulates the denitrification genes such as *aniA* and *norB* (Heurlier *et al*, 2008) was used. Strain Δ*nsrR* would serve as condition where denitrification genes could be upregulated in absence of *nsrR* mediated repression as evidenced by previous studies (Rock *et al*, 2007). Sepsis progression was monitored by severity scoring as described before **(Section 3.5.1.1).** Mice were exsanguinated after the cumulative severity score was equalled or exceeded. After processing the plasma **(Section 2.5.4),** SNO-Hb **(Section 2.5.6)** and liver lysates samples **(Section 2.5.3)** were measured by I_3^- dependent chemiluminescence **(Section 2.6.2)**. NO_x was measured by acidified VCl_3 **(Section 2.6.3)**.

3.5.2.2 Results

As can be seen from **Figure 3.8**, sepsis was prolonged to 8 hour, an increase of 33% on the previous length of 6 hour **(Figure 3.4).** Infection with different strains did not make any difference to either progression or severity of sepsis. Importantly, there was no significant difference in the inocula from the strains used for this study **(Figure 3.9).** Relatively high number of bacteria was recovered from whole blood and liver lysate despite using a lower dose inocula, 10^7 bacteria/mouse **(Figure 3.9 B and 3.9 C).**

Regardless of the NO metabolites (SNO, NO_x, NO_2^-, SNO-Hb) quantified no significant difference was found in relation to the presence of bacterial NO denitrification machinery **(Figure 3.10 and Figure 3.11 and Table 3.2)**

Non parametric Spearman correlation test was performed to investigate the correlation between bacterial burden and NO metabolites. In response to bacterial infection, there was a positive correlation between whole blood output viable count and plasma SNO (p = 0.03), a positive correlation between liver lysate output viable count and liver NO_2^- (p = 0.002) and a negative correlation between liver lysate output viable count and liver NO_x (p = 0.022**) (Figure 3.12)**

Table 3.2 **Summary of NO metabolites output from mice infected with 10^7 bacteria/mouse in presence of 8 mg hTf for 8 hours. Values are given as median, with interquartile range (IQR) in parentheses.**

NO metabolites	Wt	Δ*norB*	Δ*nsrR*
Plasma NO_x	129.9 µM (92.67 – 154.4)	105.6 µM (77.20 – 142.7)	106.1 µM (90.39 – 162.7)
Plasma NO_2^-	1.15 x 10^3 nM (9.94×10^2 –1.61 x 10^3)	1.31 x 10^3 nM (1.14 x 10^3 – 2.35 x 10^3)	2.32 x 10^3 nM (1.10 x 10^3 – 3.61 x 10^3)
Plasma SNO	38.59 nM (21.33 – 54.40)	38.68 nM (32.31 – 58.04)	50.44 nM (34.86 – 120.1)
SNO-Hb	1.49 x 10^{-3} % SNO per heme (1.20 x 10^{-3} % –2.72 x 10^{-3} %)	2.09 x 10^{-3} % SNO per heme (1.46 x 10^{-3} % – 3.32 x10^{-3} %)	2.04 x 10^{-4} % SNO per heme (1.46 x 10^{-3} % – 3.17 x 10^{-3} %)
Liver NO_x	3.29 x 10^3 pmol/mg (1.58 x 10^3 – 4.62 x 10^3)	2.87 x 10^3 pmol/mg (1.32 x 10^3 – 3.91 x 10^3)	2.17 x 10^3 pmol/mg (1.37 x 10^3 – 3.09 x 10^3)
Liver NO_2^-	172 pmol/mg (48.40 – 270)	169 pmol/mg (62.35 – 344.0)	200 pmol/mg (58.05 – 327.5)
Liver SNO	3.78 pmol/mg (1.74 – 5.59)	1.2 pmol/mg (0.94 - 4.44)	2.97 pmol/mg (0.91 – 7.60)

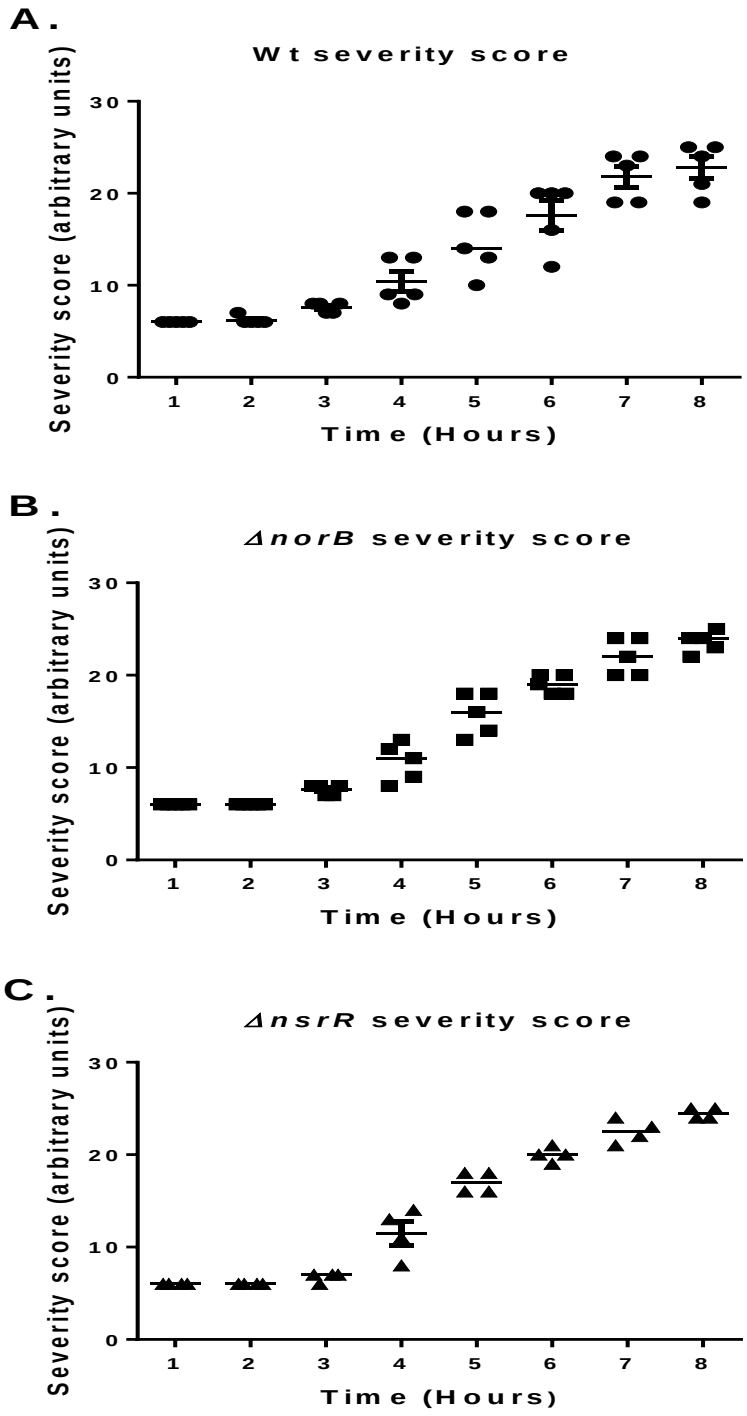

Figure 3.8 Confirmation of meningococcal sepsis by severity scoring in 7-10 weeks old female C57BI6 mice infected with 10^7 bacteria/mouse suspended in PBS + 8 mg hTf for 8 hours A) Wt, B) Δ*norB* and C) Δ*nsrR*.

Following intraperitoneal injection mice were monitored for severity every hour according to the sepsis severity scoring guideline **(Section 2.5.2).** Total score 9-18 = moderate, 19- 24 = substantial (monitored every 30 minutes), 25-30= substantial (mice had to be culled). Bars denote median.

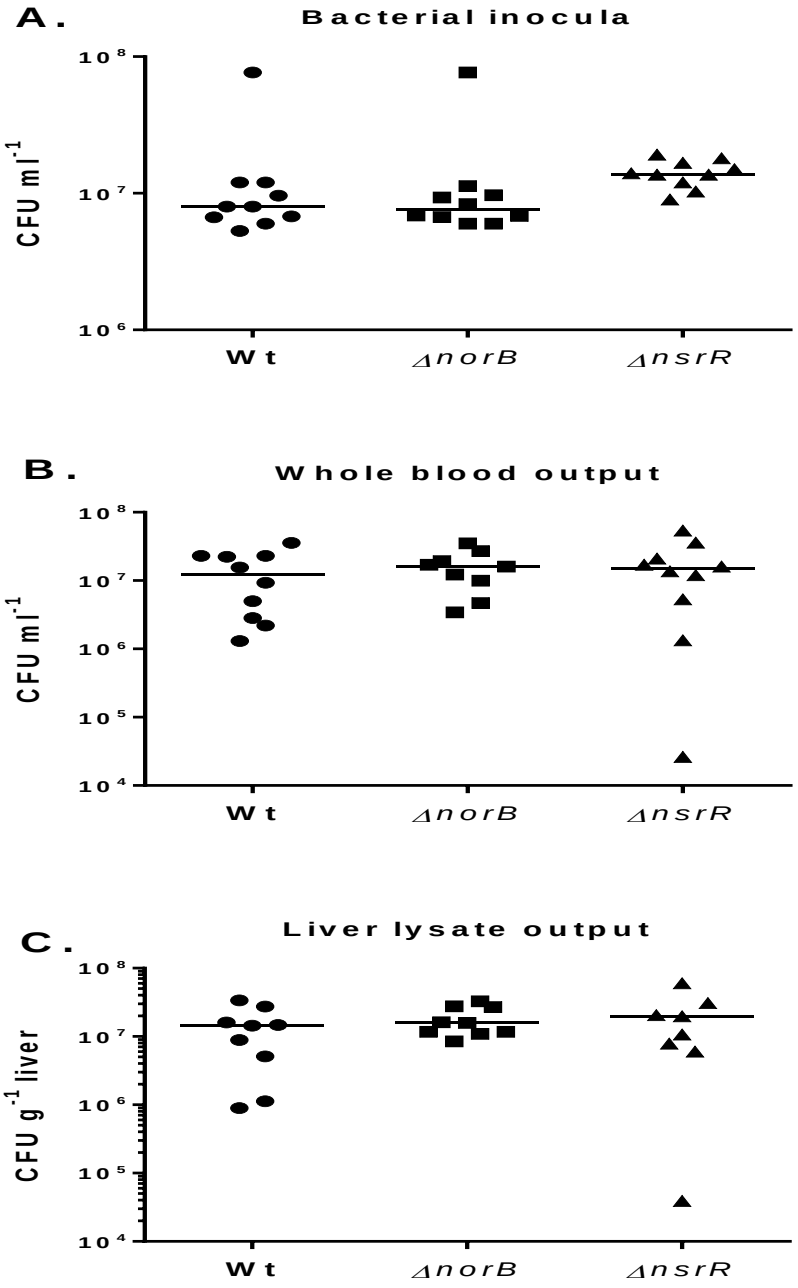

Figure 3.9 Viable bacteria recovered from inocula (A), whole blood output (B) and liver lysates output (C) in the murine model infected with PBS + 8 mg hTf + 10^7 bacteria/mouse for 8 hours.

Samples were serially diluted and triplicate of 10 µl aliquots of each dilution were separately spotted on CBA plates, left in a microbiological safety cabinet for 10 minutes to allow them to air-dry. Following overnight incubation at 37˚C, 5% CO_2, the mean number of colonies for each dilution were counted and corrected for the dilution factor and volume. Thus the mean of countable dilutions were averaged to estimate the number of bacteria present in the original suspension. Viable counts of bacteria recovered from mice liver lysates infected with *Neisseria*. Liver lysate viable counts were normalised to CFU/g of excised liver (wet weight). Bars denote median. For statistical analysis, One way ANOVA with Dunn's post test.

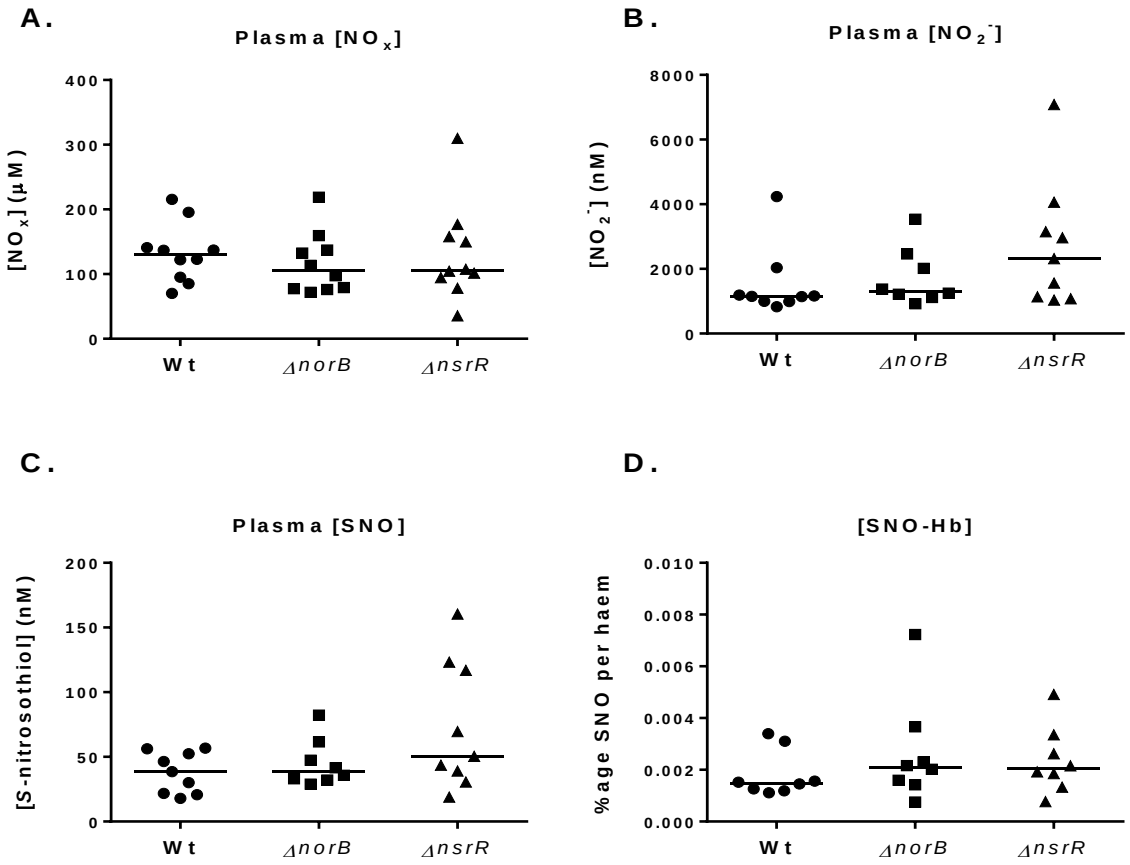

Figure 3.10 Measurement of plasma NO_x (A), NO_2^- (B), SNO (C) and SNO-Hb (D) in mice infected with PBS + 8 mg hTf + 10^7 bacteria for 8 hours.

NO metabolites were measured after bolus injection of PBS + Wild type/*ΔnorB/ΔnsrR N. meningitidis* (10^7 bacteria/mouse) into 7-10 weeks old female C57BI6 mice. NO_x **(A)** was measured by acidified VCl_3 at 90°C **(Section 2.6.3).** NO_2^- **(B),** SNO **(C)** were measured by I_3^- dependent, ozone-based chemiluminescence with reference to a GSNO standard curve **(Section 2.6.2)**. SNO-Hb **(D)** was normalised to heme % **(Section 2.5.6- 2.5.7).** Bars denote median. For statistical analysis, One way ANOVA with Dunn's post test was performed.

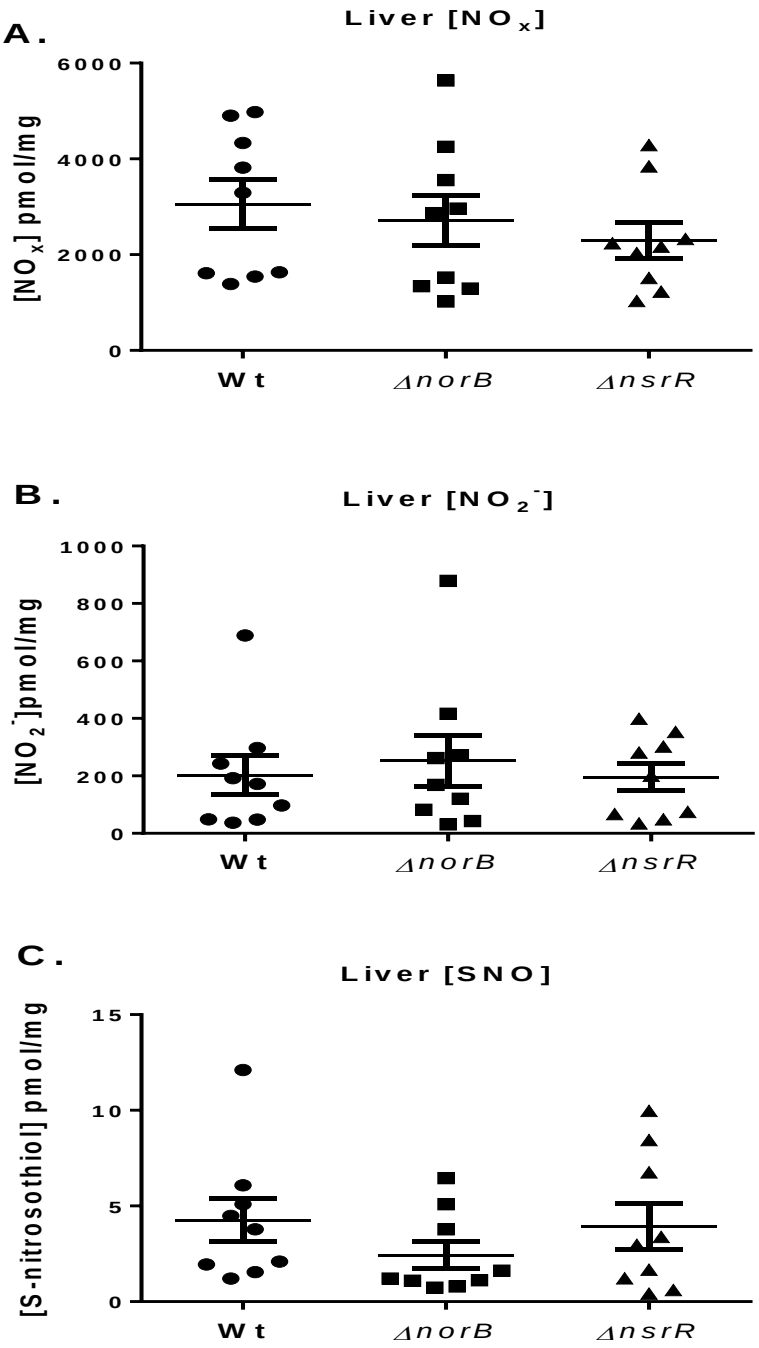

Figure 3.11 Measurement of Liver NO_x (A), NO_2^- (B), SNO (C) in mice infected with 10^7 bacteria suspended in PBS + 8 mg hTf for 8 hours.

Liver lysates were processed by a hand held rotor stator homogeniser **(Section 2.5.3).** NOx **(A)** was measured by acidified VCl_3 at 90˚C **(Section 2.6.3).** NO metabolites **(B and C)** were measured by I_3^- dependent, Ozone-based chemiluminescence with reference to a GSNO standard curve **(Section 2.6.2)**. Bars denote median. For statistical analysis One way ANOVA with Dunns post test was performed.

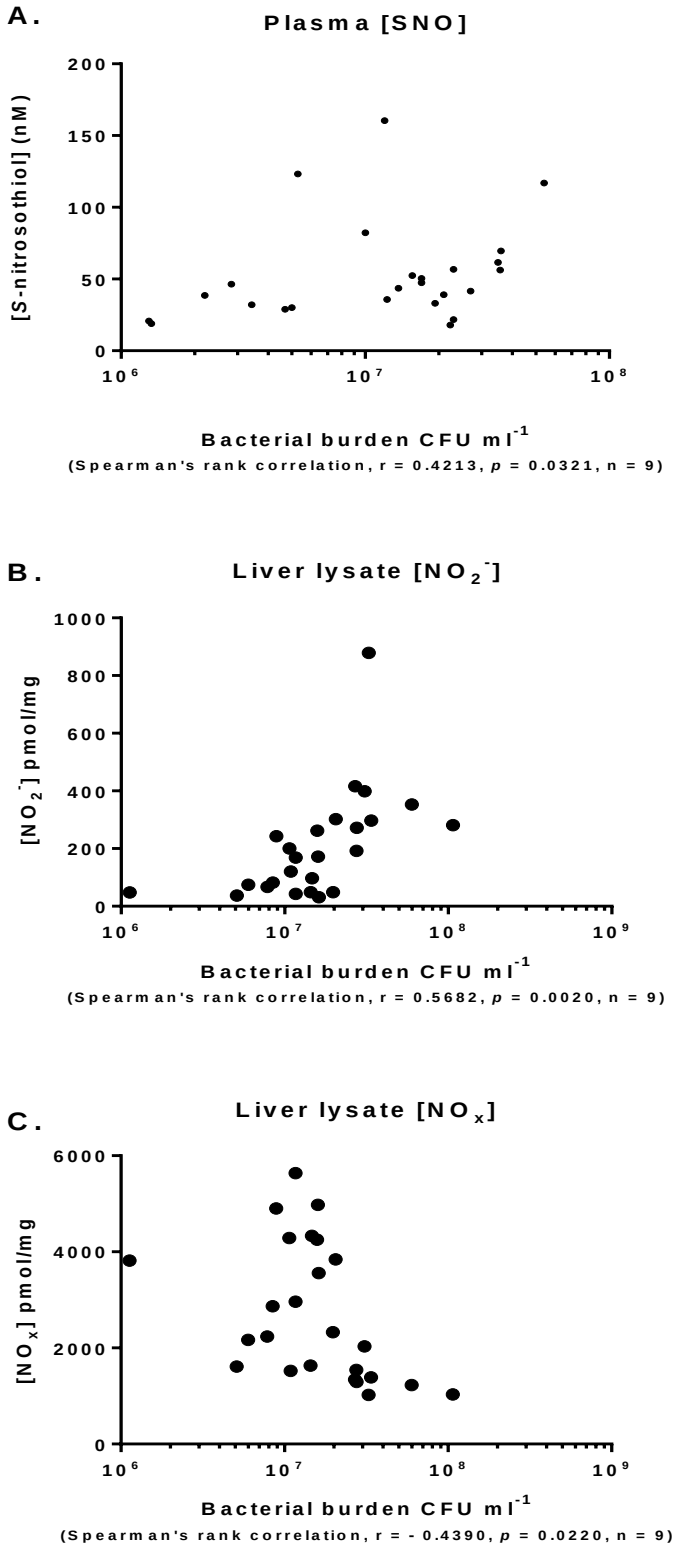

Figure 3.12 Statistically significant correlation between recovered bacterial burden and Plasma SNO A), Liver lysate NO_2^- B) and Liver lysate NO_x C) in the PBS + hTf + 10^7 bacteria/mouse supplemented sepsis model.

Spearman's rank correlation test, Graphpad prism.

3.5.3 Attempting to bolster the SNO signal from the murine model of meningococcal sepsis with LPS

Section Summary:

- ***Inclusion of LPS along with human holo transferrin increases the sepsis severity***
- ***In the presence of LPS and human holo transferrin, bacterial infection still does not result in a differential profile of NO metabolites with regards to NO denitrification machinery in whole blood and liver***

3.5.3.1 Rationale and methods

LPS treatment induces the production of SNO-albumin and SNO-Hb in rat model of sepsis within 5 hour of stimulation (Jourd'heuil *et al,* 2000). It was found to be essential for the increase in endogenously produced SNO from murine J774.2 cell lines by the activation of iNOS (Laver *et al,* 2010). In an LPS induced septic model of rat high levels of SNO from RBCs is generated in an iNOS dependent manner (Crawford *et al,* 2004). These observations indicate the role of LPS as an inducer for NO generation by iNOS activity. High iNOS is also necessary to relieve *nsrR* mediated repression of *norB.* In the presence of high concentrations of NO (> 1 µM) *nsrR* repressor comes off the NO denitrification operon to increase NO detoxification by *norB* **(Section 1.12- 1.14)** (Rock *et al,* 2007). At 8 hour time point the amount of iNOS in our model could have been insufficient to relieve *nsrR* mediated repression of *norB* **(Section 3.5.2).** Therefore, it was decided to infect the mouse with bacterial bolus containing both LPS and hTf to induce NO mediated processes.

Initial observation from our group has shown that infection of mice with LPS at concentration of 2.5 x 10^4 EU/g increases the detectable levels of SNO, which was also confirmed by biotin switch technique (Harrison, L., PhD thesis). So mice were infected intraperitoneally with bolus containing 25000 EU/g LPS, 8 mg hTf and 10^6 bacteria/mouse suspended in PBS. To keep the suffering of the animal to minimal level, a 10 fold lower bacterial dosage was used as LPS itself triggers bacteraemia. Alongside the Wt strain, two isogenic mutant strains for meningococcal denitrification pathway, Δ*aniA* and Δ*norB* were included to investigate the role of these two denitrification genes in the regulation of NO adduct production. Another condition heat killed wild type (HkWt) bacteria was also included to act as a metabolically inert strain incapable of involving *aniA* and *norB* in NO denitrification. Progression of infection was followed according to the severity scoring for sepsis **(Section 2.5.2).** Mice were terminally

anaesthetised using an intraperitoneal injection of sodium pentobarbitone (5 units/mouse). Mid-place anaesthesia was confirmed by loss of the pedal withdrawal reflex. Blood was collected by exsanguination and whole liver was excised. Plasma and haemoglobin were separated for analysis from whole blood using SNO compatible lysis buffer and stabilising solution. Whole liver was treated with 0.25% bile salt to remove external bacteria and homogenised using a hand held rotor-stator homogeniser in SNO compatible lysis buffer **(Section 2.2.2 and Figure 3.3)**. After appropriate preparation, NO metabolites in samples were measured by I_3^- dependent chemiluminescence **(Section 2.6.2).** Plasma NO_x was measured by acidified VCl_3 **(Section 2.6.3).**

3.5.3.2 Results

As can be seen from **Figure 3.13**, the infection could be prolonged up to 6 hour time point according to the severity scoring. Interestingly infection with LPS + HolohTf and Hk Wt registered the same substantial severity as other conditions.

There was no statistically significant difference in input viable count of the conditions; Wt 3.47 x 10^8 cfu/ml (IQR= 2.83 x 10^8 – 4.87 x 10^8), Δ*norB*, 4.43 x 10^8 cfu/ml (IQR= 2.27 x 10^8 – 7.57 x 10^8) and Δ*aniA*, 5.33 x 10^8 cfu/ml (IQR = 4.23 x 10^8 – 5.67 x 10^8) **(Figure 3.14 A).** Despite using a lower bacterial inocula, relatively high number of bacteria was recovered from whole blood; Wt, 4.43 x 10^8 cfu/ml (IQR= 7.87 x 10^6 – 6.9 x 10^8), Δ*norB*, 3.28 x 10^8 cfu/ml (IQR= 1.41 x 10^8 – 5.74 x 10^8) and Δ*aniA*, 4.63 x 10^8cfu/ml (IQR= 3.97 x 10^8 – 5.2 x 10^8) **(Figure 3.14 B).** Although lower than the number of bacterial output from whole blood, recovery of bacterial load from liver lysates were also substantial; Wt, 1.38 x 10^7 cfu/ml (IQR = 9.80 x 10^6 – 2.11 x 10^7), Δ*norB*, 1.54 x 10^7 (IQR= 1.32 x 10^7 – 2.0 x 10^7) and Δ*aniA*, 1.08 x 10^7 cfu/ml (IQR = 8.26 x 10^6 – 1.33 x 10^7) **(Figure 3.14 C) .**

There was no significant difference in the amount of plasma NO_x, NO_2^-, SNO, SNO-Hb and liver SNO and NO_2^- measured across the different strains studied **(Table 3.3, Figure 3.15 and Figure 3.16).**

Table 3.3 **Summary of NO metabolites measured from mice infected with 10^6 bacteria/mouse in presence of LPS + 8 mg hTf for 6 hours. (Values are given as median, with interquartile range (IQR) in parentheses)**

NO metabolites	**LPS + HolohTf**	**Wt**	**Δ*norB***	**Δ*aniA***	**HkWt (Heat killed Wt)**
Plasma NO_x	318.4 µM (122.5 - 754.5)	163.7 µM (137.1 – 284.3)	280.5 µM (162.3 – 402.2)	166.2 µM (117.9 – 568.5)	156.7 µM (89.30 – 510.3)
Plasma NO_2^-	3.77 x 10^3 nM (2.18 x10^3 – 5.70 x 10^3)	2.95 x 10^3 nM (2.05 x 10^3 – 5.22 x 10^3)	3.33 x 10^3 nM (2.62 x 10^3 – 5.02 x 10^3)	2.86 x 10^3 nM (1.87 x 10^3 – 4.80 x 10^3)	3.05 x 10^3 nM (2.22 x 10^3 – 5.54 x 10^3)
Plasma SNO	87.65 nM (80.05 – 138.2)	120.9 nM (99.38 – 153.0)	73.55 nM (49.34 – 144.3)	85.85 nM (52.59 – 212.4)	83.15 nM (74.43 – 125.4)
SNO-Hb	3.12 x 10^{-3} % SNO per heme (1.91 x 10^{-3} % – 5.73 x 10^{-3} %)	3.419 x 10^{-3} % SNO per heme (1.61 x 10^{-3} % – 4.49 x 10^{-3} %)	3.66 x 10^{-3} % SNO per heme (2.42 x 10^{-3} % – 5.82 x 10^{-3} %)	3.14 x 10^{-3} % SNO per heme (1.34 x 10^{-3} % – 7.14 x 10^{-3} %)	2.67 x 10^{-3} % SNO per heme (1.97 x 10^{-3} % – 4.19 x 10^{-3} %)
Liver SNO	2.36 pmol/mg (1.65 – 3.21)	2.17 pmol/mg (1.78 – 4.00)	3.69 pmol/mg (1.5- 3.75)	2.92 pmol/mg (1.71 – 4.14)	2.11 pmol/mg (1.26 – 2.95)
Liver NO_2^-	25.90 pmol/mg (22.50 – 32.00)	32.00 pmol/mg (31.70 – 34.50)	38.10 pmol/mg (20.00 – 49.80)	27.00 pmol/mg (22.50 – 49.60)	25.20 pmol/mg (15.60 – 26.90)

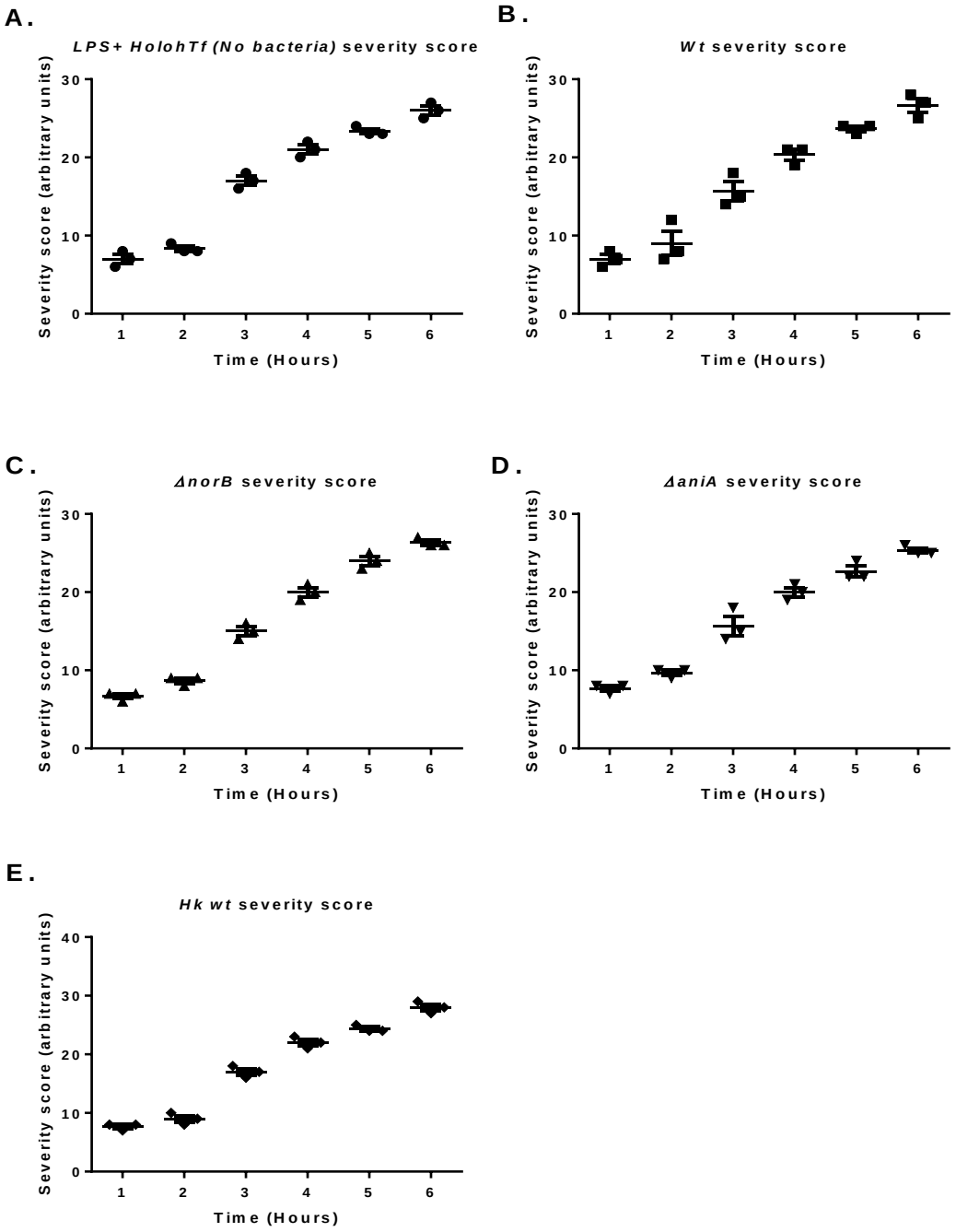

Figure 3.13 Confirmation of meningococcal sepsis by severity scoring in 7-10 weeks old female C57BI6 mice infected with 10^6 bacteria/mouse suspended in PBS + 25000 EU/g LPS + 8 mg hTf for 6 hours A) LPS + Htf, B) Wt, C) Δ*norB*, D) Δ*aniA* and E) HkWt (Heat killed Wt)

Following intraperitoneal injection mice were monitored for severity every hour according to the sepsis severity scoring guideline **(Section 2.5.2).** Total score 9-18 = moderate, 19- 24 = substantial (monitored every 30 minutes), 25-30= substantial (mice had to be culled). Bars denote median.

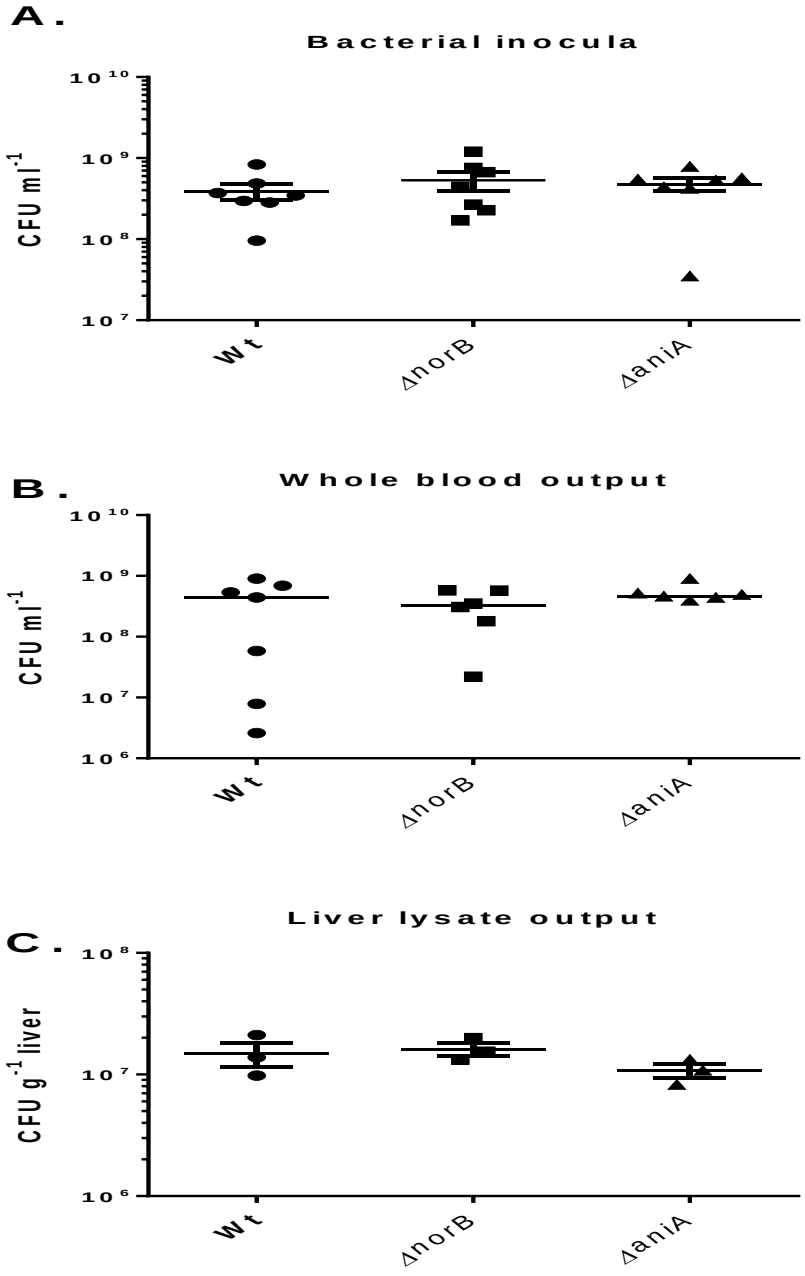

Figure 3.14 Viable bacteria recovered from inocula (A), whole blood output (B), and liver lysates output (C) in murine model infected with bolus injection of PBS + 25000 EU/g LPS + 8 mg human holo transferrin + 10^6 bacteria/mouse for 6 hours.

Samples were serially diluted and triplicate of 10 µl aliquots of each dilution were separately spotted CBA plates, left in a microbiological safety cabinet for 10 minutes to allow them to air-dry. Following overnight incubation at 37˚C, 5% CO_2, the mean number of colonies for each dilution were counted and corrected for the dilution factor and volume. Thus the mean of countable dilutions were averaged to estimate the number of bacteria present in the original suspension. Viable counts of bacteria recovered from mice liver lysates infected with *Neisseria*. Liver lysate viable counts were normalised to CFU/g of excised liver (wet weight). Bars denote median. For statistical analysis, one way ANOVA with Dunn's post test was used.

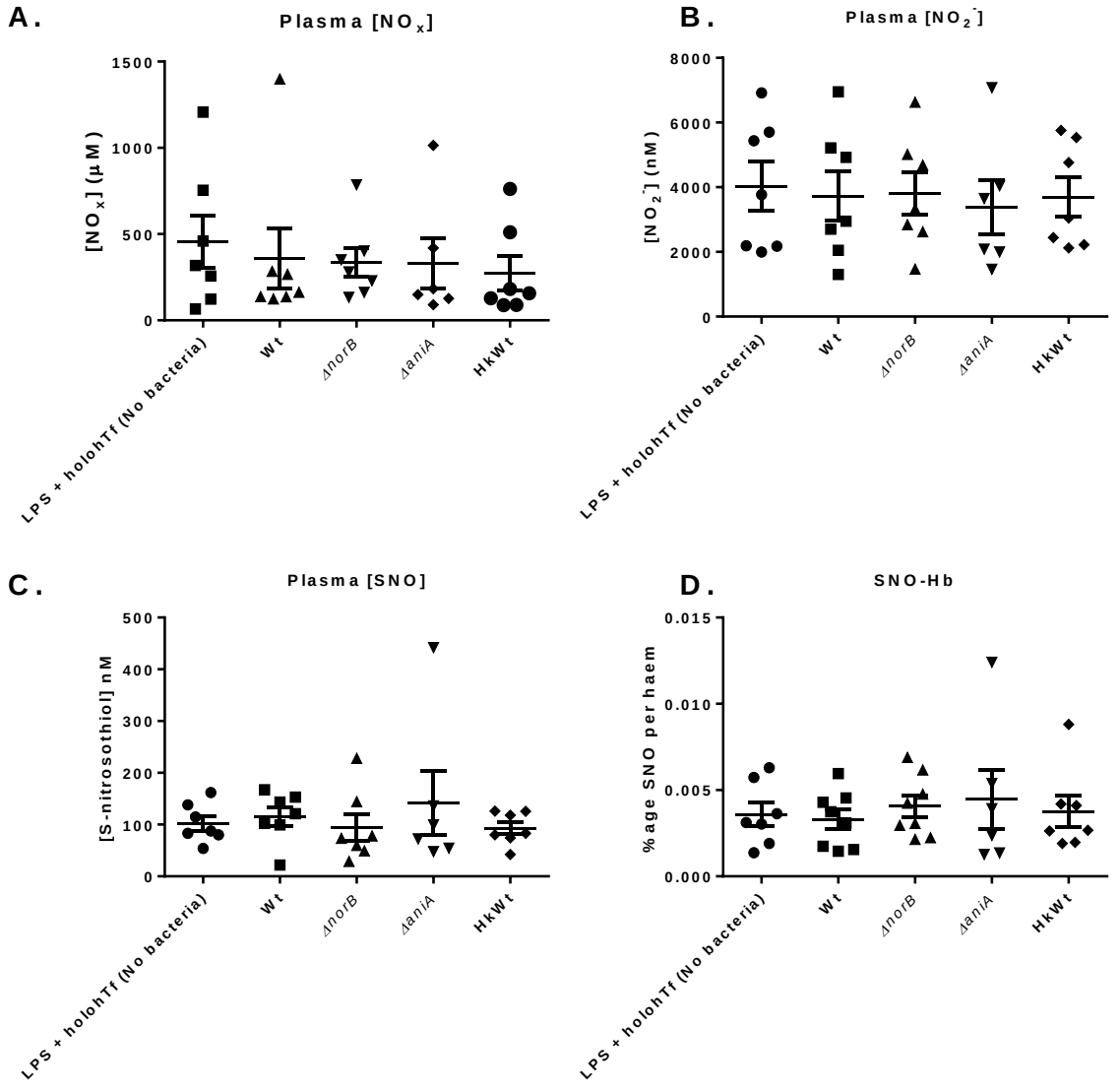

Figure 3.15 Measurement of plasma NOx (A), NO_2^- (B), SNO (C) and SNO-Hb (D) in mice infected with PBS + 25000 EU/g LPS + 8 mg hTf + 10^6 bacteria for 6 hours.

NO metabolites were measured after bolus injection of PBS + 25000 EU/g LPS+ wild type/*ΔnorB/*Δ*aniA/HkWt (Heat killed Wt) N. meningitidis* (10^7 bacteria/mouse) into 7-10 weeks old female C57BI6 mice. NO_x **(A)** was measured by acidified VCl_3 at 90˚C **(Section 2.6.3).** NO_2^- **(B)**, SNO **(C)** were measured by I_3^- dependent, Ozone-based chemiluminescence with reference to a GSNO standard curve **(Section 2.6.2)**. SNO-Hb **(D)** was normalised to heme% **(Section 2.5.6- 2.5.7)**. HkWt refers to heat inactivated bolus of Wt MC58. Bars denote median. For statistical analysis, one way ANOVA with Dunns test was performed.

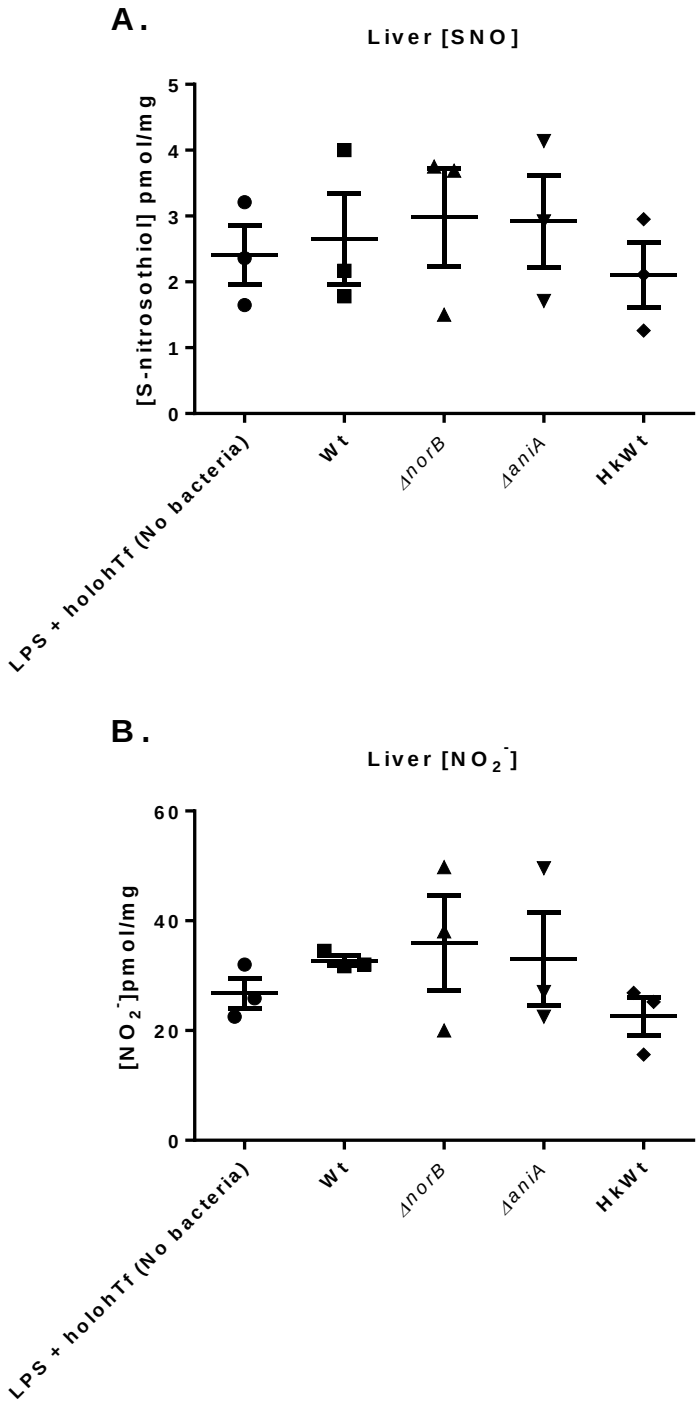

Figure 3.16 Measurement of Liver SNO (A) and NO_2^- (B) in mice infected with 10^6 bacteria suspended in PBS + 8 mg hTf + 25000 EU/g LPS for 6 hours.

Liver lysates were processed by a hand held rotor stator homogeniser **(Section 2.5.3).** NO metabolites **(A and B)** were measured by I_3^- dependent, Ozone-based chemiluminescence with reference to a GSNO standard curve **(Section 2.6.2)**. Bars denote median. For statistical analysis one way ANOVA with Dunns post test was performed. HkWt – Heat killed wild type.

3.6 Discussion

This chapter reports the establishment of a murine model of early fulminant meningococcal sepsis, in which we were able to reproducibly detect increased levels of NO metabolites such as SNO, NO_2^- and NO_x. Although *N. meningitidis* is an exclusively human pathogen, the ubiquity of *S*-nitrosylation in biology, and the higher overall NO output from murine cells in response to immunological agonists made development of a murine model of meningococcal sepsis worthwhile. We intended to use the model to test whether meningococcal NO detoxification impacts upon the concentration of NO metabolites at a systemic level during acute, fulminant infection, as we had previously demonstrated *in vitro* on the J774.2 murine macrophage cell line (Laver *et al,* 2010). This investigation was essential as it is only the animal models that provide the opportunity to investigate the regulation of a certain phenotype at the whole organism level by combining factors such as the innate, humoral and cellular immune defence machinery etc.

The role of bacterial denitrification in the regulation of NO metabolites was investigated in three variations of our murine model of meningococcal sepsis. In the initial model **(Figure 3.4-3.7)**, a high bacterial inoculum (10^9 bacteria/mouse) in PBS was used to induce sepsis. Severe septicaemia was apparent at the 6 hour time point **(Figure 3.4),** at which point our severity limits for the experiment were equalled or exceeded and the mice were euthanized. In the second model, mice were infected intraperitoneally (i/p) with 10^7 bacteria/mouse in PBS, supplemented with 8 mg human holoTf for 8 hours **(Figure 3.8 -3.12).** Inclusion of human holo transferrin was found to be optimal for inducing sepsis with a lower dosage of bacteria (10^7 bacteria/mouse) which was not capable of inducing sepsis in absence of human holoTf (data not shown). This supports the previous observation that the rapid clearance of *N. meningitidis* is prevented in transgenic mice expressing human transferrin (Zarantonelli *et al,* 2007). Inability of meningococcal transferrin to bind to murine transferrin is circumvented by the presence of human holoTf, thus providing the bacteria with access to the iron required for normal growth and metabolism. In the final model, LPS was used along with human holoTf to infect mice **(Figure 3.13 – 3.16)** with the aim of rapidly inducing iNOS expression and increasing the production of NO within the infection time frame. However, as LPS administration induces strong proinflammatory immune responses (Michie *et al*, 1988; Remick *et al,* 1990) and causes sepsis syndrome (Waage *et al,* 1987); the infection could only be continued for 6 hour before equalling or exceeding the severity limits of the study, despite using a lower bacterial dose (10^6 bacteria/mouse). In fact, the progression of sepsis severity

was the same for mice injected with only LPS and human holoTf as it was for similarly treated but simultaneously-infected mice **(Figure 3.13).**

It is noteworthy that none of the denitrification gene mutant-infected mice showed any difference in sepsis severity when compared with Wt-infected mice **(Figure 3.4, 3.8 and 3.13).** This demonstrates that lack of NO denitrification had no qualitative impact on the severity of the disease. However, the severity of infection in all three models confirmed the features of overwhelming sepsis which is one of the common aspects of invasive meningococcal disease (Pace & Pollard, 2012).

Statistically significant increases in plasma SNO, SNO-Hb **(Figure 3.6 C and D)** and liver SNO **(Figure 3.7 B)** were observed in response to bacterial infection compared to PBS control. Statistically non significant similar increase in plasma NO_2^-, NO_x and liver NO_2^- was noticed **(Table 3.1).** This is the first study to report an abundance of SNOs in the plasma and liver of early acutely septic mice infected with *N. meningitidis*. This could be due to an increase in iNOS activity and increased exposure to meningococcal LOS (Titheradge, 1999) following infection with high bacterial load (10^9 bacteria/mouse). However, there was not any statistically significant difference among the measured SNO, NO_2^- and NO_x with regards to the bacterial NO metabolism in any of our experimental models **(Figure 3.4-3.7, Figure 3.8 – 3.12 and Figure 3.13 – 3.16).**

A number of reasons could account for not seeing a difference in the production of NO metabolites by bacterial denitrification *in vivo*. Firstly, it could be due to the insufficient expression of iNOS at a given time point *in vivo*. An *in vitro* study from our group showed that iNOS expression is induced after 18 hours following the stimulation of J774.2 macrophages with LPS/IFNɣ (Laver *et al,* 2010). Similar maximal iNOS induction time was reported with RAW macrophages (Chiou *et al,* 2000). However, we could not prolong the sepsis beyond the 6 hour **(Figure 3.13)** and 8 hour **(Figure 3.8)** time points given the severity of the disease. Spatiotemporal activation of iNOS has also important ramification for *norB* activity which is switched off by the *nsrR* repressor at low NO concentration (< 1µM) (Rock *et al*, 2007). It is not clear whether and when iNOS was expressed to a level high enough for NO to trigger NorB production in an *in vivo* murine model. The similar numbers of bacteria found from the whole blood and liver lysates of wt and Δ*norB* infected mice **(Figure 3.5, 3.9 and 3.14)** further intensifies this suspicion given that the lack of *norB* results in decreased survival of the

organism in the presence of NO in human macrophages and nasopharyngeal mucosa (Stevanin *et al*, 2005).

Secondly, as meningococcal sepsis is a severe condition, we could perform certain protocols and use limited number of mice for this study. While studying sepsis in an animal model, it is essential to strike a balance between experimental objective and animal suffering. Thirdly, SNO degrading enzymes from host could be more potent in regulating the concentration of SNOs *in vivo* compared to the bacterial NO detoxification. Enzyme such as GSNO reductase (GSNOR) is conserved across species (Liu *et al*, 2001) and important for SNO homeostasis due to their capability to degrade SNO enzymatically. GSNOR has maximal activity in murine liver and is directly involved in protection of tissue during endotoxemia (Liu *et al*, 2004).

Finally, SNO depletion by bacteria does not take place or could naturally be a localised cell specific phenomenon *in vivo*. Hepatic SNO is pivotal for regeneration of damaged part of liver during endotoxin induced injury (Cox *et al*, 2014). Previously, we have shown that NO detoxification mechanism of *N. meningitidis* depletes the formation of SNO at cellular level in J774.2 cell line (Laver *et al*, 2010). In a recent work, total SNO protein from J774.2 cells infected with *N. meningitidis* were extracted using SNO-RAC technique. Proteomic analysis revealed the differential regulation of a number of SNO proteins in relation to the bacterial NO detoxification machinery (Dr Jay Laver, personal communication). In an animal model, liver could have been perfused with blood containing bacteria. Then transient NO detoxification by bacteria could possibly damage parts of liver by depleting localised SNO, which perhaps was undetectable at the tissue/whole animal level. Taken together the observation from this study it is plausible that SNO depletion by NO detoxification of *N. meningitidis* could perhaps be happening at the cellular level but not at the tissue or whole animal level.

As the only natural habitat for *N. meningitidis* is human nasopharynx, it is impossible to establish an ideal murine model for studying meningococcal sepsis. Infection with live and multiplying bacteria in tissue and blood mimics the model of human sepsis more closely than the model which involves the administration of endotoxin such as LPS. Of the three models studied here, infection of mice with 10^7 bacteria/mouse represents the most physiologically relevant model of early fulminant meningococcal sepsis **(Figure 3.8 -3.12)** due to inclusion of hTf. Although septic model with 10^6 bacteria/mouse contained hTf **(Figure 3.13- 3.16),** inclusion of LPS could mask or interfere with the effect generated in response to bacterial infection since LPS can trigger high and rapid proinflammatory cytokine response which is

several orders of magnitude higher than what is found in human septic condition (Buras *et al*, 2005).

A number of interesting and novel correlations were found between bacterial burden and NO metabolites in the murine model supplemented with hTf along with 10^7 bacteria/mouse for 8 hours **(Figure 3.8 - 3.12).** We observed significant, positive correlations between the number of bacteria cultured from plasma (in CFU/ml) and the concentration of circulating SNO, and between the number of bacteria cultured from liver lysates and the concentration of NO_2^- in these lysates **(Figure 3.12).** We also observed a significant, negative correlation between the bacterial burden of liver lysates and the total concentration of NO derivatives (NO_x) in these samples **(Figure 3.12).** These data indicate a dose-dependent systemic increase in nitric oxide synthase activity in response to meningococcal infection, which makes good biological sense: insofar as a larger stimulation leads to a larger response. In liver, where meningococci circulating in the bloodstream could conceivably aggregate in the microvasculature, the increased bacterial burden result in an overall decrease in the total amount of NO-derived species in hepatocytes, but is not associated with expression of the nitric oxide reductase. One possible explanation of these relationships is that inflammation in response to infecting meningococci resulted in hepatic ischaemia, consistent with observations of endotoxin-induced acute liver injury (Matuschak *et al*, 2001). In such a low-oxygen environment, the oxidation of NO would be precluded. This would locally increase the half-life of NO and allow diversion of NO *per se* along other metabolic routes. Most likely, NO would first come into contact with the bloodstream, with rapid formation of Hb-Fe(II)-NO and transport of hepatically-synthesised NO away from the tissue. In addition, the low oxygen tension would activate the SNO synthase function of a subset of haemoglobin molecules, which produce S-nitrosylated haemoglobin (SNO-Hb) at Cys93 of the haemoglobin beta chain as they undergo allosteric conversion from the 'T' to the 'R' state (Allen & Piantadosi, 2006; Stamler *et al*, 1997a)**.** As red blood cells harbouring SNO-Hb migrate into areas of increased oxygenation, there may be transfer of SNO groups to serum proteins by transnitrosylation; enriching the circulating pool of SNO-proteins in plasma. This could be clinically important as SNOs can play cytoprotective role in myocardial ischemic injury after endotoxemia (Lima *et al*, 2009).

In summary, *N. meningitidis* reproducibly produces severe sepsis in mice following intra-peritoneal injection and supplementation with human holo-transferrin. Meningococcal infection results in the increased abundance of NO metabolites in plasma and liver which is a novel finding. However, no differences were found in NO adducts within blood and liver in

relation to the bacterial NO detoxification machinery. There is a possibility that SNO depletion, if it occurs, is happening exclusively at a cellular level as we have shown previously (Laver *et al,* 2010) and is inapparent at the tissue/whole animal level, or that the experimental methodology utilised is unable to detect the effect.

4 Chapter 4: Creation and characterisation of a set of denitrification gene mutants (Δ*aniA*/Δ*norB*, Δ*nsrR*/Δ*norB*, Δ*aniA*/Δ*norB*/Δ*nsrR*)

4.1 Introduction

Regulation of *aniA* and *norB* is complex and involves multiple factors such as the oxygen-sensing transcription factor FNR, the transcriptional repressor AsrR, the ferric uptake regulator Fur, the two-component signalling system NarQ/NarP and the NO-sensitive repressor protein, NsrR **(Figure 1.8).**

In response to varying concentrations of NO, NsrR tightly regulates the operon containing the *aniA* and *norB* genes, which act to supplement meningococcal respiration under microaerobic conditions. Although the meningococcal *nsrR* regulon has been characterised (Heurlier *et al*, 2008; Rock *et al*, 2007), there is little known about its impact on the cellular pathology of meningococcal sepsis. To date, our group has used isogenic single mutants of *aniA, norB* and *nsrR* to investigate the different aspects of meningococcal pathogenesis both *in vitro* (Laver *et al*, 2010; Stevanin *et al*, 2007; Stevanin *et al*, 2005; Tunbridge *et al*, 2006) and *in vivo* (Harrison, L., PhD thesis, Chapter 6 and current thesis, Chapter 3). As the half life of NO in biological systems is very short, the major resevoir of nitrogen oxides in cell or tissue at any given time is NO_2^- or NO_3^-. In human tisssue, oxygenation of NO leads to production of NO_2^-. Facultative denitrifiers in the mouth and pharynx can also convert NO_3^- into NO_2^- (Lundberg *et al*, 2004). Creation of a mutant unable to metabolise both NO_2^- and NO could be an important experimental tool to study physiological conditions such as meningococcal sepsis, which is often characterised by high concentrations of circulating NO metabolites (Baines *et al*, 1999). Therefore, it was decided to create mutants where multiple genes of denitrification pathway were inactivated.

4.2 Results

4.2.1 Creation of Δ*aniA*/Δ*norB*/Δ*nsrR* (Δ*Triple)* mutant

4.2.1.1 Rationale and methods

Firstly, a triple mutant *(*Δ*aniA/*Δ*norB/*Δ*nsrR)* was created to investigate the role of bacterial denitrification genes in the absence of *nsrR*, the negative regulator of the genes involved in meningococcal partial denitrification. The triple mutant was generated through insertional inactivation of each of the three genes with three different antibiotic resistance cassettes. A kanamycin-resistance cassette in the middle of the *norB* gene was cloned into plasmid pGEM-3zf. The Kanamycin-disrupted *norB* cassette was then PCR-amplified and transformed into the existing strain Δ*nsrR/*Δ*aniA* (a kind gift from the Moir group, University of York), in which the *nsrR* gene was inactivated by an omega insertion cassette conferring resistance to tetracycline, and the *aniA* gene was inactivated by the omega cassette, conferring resistance to spectinomycin (Heurlier *et al*, 2008). The resulting strain *(*Δ*aniA/*Δ*norB/*Δ*nsrR)* was selected on spectinomycin/kanamycin/tetracycline (SKT)-containing plates.

Assembly of a construct suitable for the insertional inactivation of the *norB* gene with a kanamycin resistance-conferring cassette was to be achieved using Isothermal Assembly (ISA). The method is also known as 'Gibson Assembly' and requires all the participating components to have overlapping DNA sequences **(Figure 4.1)**. All four fragments in this reaction had overlapping adaptor sequences (see below). ISA mastermix contains a 5′ exonuclease, a thermostable DNA polymerase and a thermostable DNA ligase **(Section 2.11.4).** The 5′ exonuclease in the ISA mix 'chews up' the fragments in the reaction from the 5′ end and generates single stranded 3′ complementary overhangs **(Figure 4.1 C).** The key to the success of ISA is the fact that the exonuclease is thermo-labile and degrades after only 15 minutes when incubated at 50°C. Thermo-lability of the exonuclease ensures only a small portion of the DNA is degraded, and the molecule remains ostensibly double-stranded DNA. Following 5′ exonuclease activity, the paired ends of each of the DNA molecules to be ligated anneal to one another through complementary base-pairing, hence the requirement for identical overlapping sequences between fragments. A high fidelity DNA polymerase from the ISA mix then fills in gaps within each annealed fragment. Finally, a DNA ligase present in ISA mix covalently joins seals the nicks in assembled DNA. For a schematic overview of the isothermal assembly process, see **Figure 4.1.**

To generate a kanamycin-disrupted *norB* cassette in plasmid pGEM-3Zf, two parts of the *norB* gene sequence were chosen **(Figure 4.1 A)**. The *norB* gene (NMB1622) is 2.256 Kbp in length. The first part (524 bp) was chosen by avoiding the first 406 bp of the *norB* coding sequence. The forward primer (termed as *norB F1-FWD*) contained 30 bp sequence homologous to the pGEM-3zf before the HincII restriction site plus 20 bp from the beginning of first part of the chosen *norB* sequence. The reverse primer (*norB F1-REV*) contained 30 bp adapter sequence which was homologous to the reverse complement of the start of the Kanamycin resistance cassette from pJMK30 plus 20 bp of the reverse complement of the first part of the *norB* gene. The second part was selected by choosing the last 522 bp of *norB*. The forward primer (*norB F2-FWD*) contained a 30 bp sequence homologous to the last 30 bp of pJMK30 plus 20 bp from the start of the chosen 522 bp *norB* sequence. The reverse primer (*norB F2-REV*) contained sequence homologous to the last 30 bp of pGEM-3zf after the HincII restriction site plus 20 bp from the reverse complement of last part of *norB*. The middle section of the *norB* coding sequence was not considered for primer design, ensuring that mutants generated using the final construct could not revert to wild type expression of *norB* through excision of the kanamycin-resistance cassette. Fragments *norB F1* and *norB F2* were extended using the primer pair *norB F1-FWD/norB F1-REV* and the primer pair *norB F2-FWD/norB F2-REV*. The products were PCR amplified using My Taq Polymerase protocol **(Figure 4.2) (Section 2.11.15.2).** The products of these separate PCR reactions were ISA compatible.

The kanamycin resistance cassette (hereafter, KAN) was PCR amplified using the primer pair: *Kan-FWD/Kan-REV* using pJMK30 as template **(Figure 4.2).** PCR utilised the high fidelity Accuzyme DNA Polymerase (Bioline, UK) **(Section 2.11.15.3)**

pGEM-3zf plasmid was restriction digested with HincII restriction enzyme **(Section 2.11.9) (Figure 4.3).** All the generated PCR and restriction digest products were PCR purified using commercially available PCR Purification kit **(Section 2.11.7)** and DNA was quantified by spectrophotometry using a NanoDrop instrument **(Section 2.11.5).** The 260/280 ratio reading was recorded. A ratio between 1.8 and 2.0 was normally considered to be acceptable for DNA purity.

Each PCR fragment (F1', F2'and KAN) was added along with HincII digested plasmid (VECTOR) at equimolar concentrations between 10-100 ng within the reaction. The total volume of the VECTOR plus PCR fragments did not exceed 5 µl or 0.5 pmol DNA. The volume of the mixture was then made up to 10 µl with dH_2O, and this was further mixed with

10 µl of 2 x ISA mastermix **(Section 2.11.4).** The mixture was incubated overnight at 50°C in a thermocycler, and 1/10th volume of the ISA mixture was transformed into highly competent DH5α *E. coli* **(Section 2.11.2).** The resulting transformants, putatively containing the desired plasmid: pGEM-3zf :: *ΔnorB*: Kan^{R}, were screened on kanamycin-containing LB Agar plates **(Section 2.4.4).** Plasmid DNA was extracted from positive colonies using commercial plasmid extraction kit **(Section 2.11.8).** Identification of positive clones (i.e. those colonies carrying the desired plasmid), was confirmed by diagnostic PCR with a combination of different primers for the integration of the right fragment **(Figure 4.4).** The resulting plasmid was named: pGEM-3zf NK **(Colony 2, Figure 4.4).** This plasmid was used as a template to amplify the *ΔnorB*: Kan^{R} cassette (approximately 2.558 kbp) with *norB F1-FWD*/*norB F2-REV* primers **(Section 2.11.3)** using Accuzyme DNA polymerase **(Figure 4.5) (Section 2.11.15.3).** Multiple PCR reactions were combined and purified **(Section 2.11.7).** 2 µg of this purified product was transformed into Δ*nsrR*/Δ*aniA*, using the broth culture transformation protocol **(Section 2.11.12).** After transformation, the colonies were screened on SKT-containing GC Agar plates **(Section 2.4.2).** Positive colonies were screened by colony PCR **(Section 2.11.15.1).** At least 6 positive colonies from two independent transformation events were combined to account for potential phase and antigenic variation of individual colonies. These were plated on new antibiotic containing GC agar plates. The resulting strain was termed as Δ*Triple (*Δ*aniA/*Δ*norB/*Δ*nsrR)* and stored at -80ºC in glycerol solution for future usage.

4.2.1.2 Results

For confirming the inactivation of *aniA*, *norB* and *nsrR* in the newly created Δ*aniA*/Δ*norB*/Δ*nsrR* (Δ*Triple)*, the three gene containing regions were PCR amplified. Primers were designed as such that they were capable of amplifying the whole gene or the gene containing region **(Section 2.11.3).** Genomic DNA (GD) was extracted from the relevant strains for PCR confirmation **(Section 2.11.6).** PCR products were separated on 1% agarose gel **(Figure 4.6).**

For confirmation of *aniA* inactivation, GD from Wt, Δ*aniA* and Δ*Triple* were PCR amplified by *aniA_RUH1_FWD* and *aniA_RUH1_REV* primers (amplifies 1.3 Kb of the *aniA* region) **(Section 2.11.3).** In Lane 1, an intense band of approximately 1.3 Kb was evident from Wt GD PCR amplification. Similar band was not seen in Lanes 2-3 with Δ*aniA* and Δ*Triple* GD templates. Instead, a band of approximately 3.2 Kb length was apparent.

Products from Lanes 4-6 were PCR amplified by *norB_RUH2_FWD* and *norB_RUH2_REV* primers (amplifies 2.0 Kb of the *norB* gene) **(Section 2.11.3).** As can be seen from **Figure 4.6**, an obvious band of 2.0 Kb was present in Lane 4 with Wt PCR amplification. In Lanes 5-6, a band of approximately 2.6 Kb in size was present with Δ*norB* and Δ*Triple* GD PCR products.

For confirming *nsrR* inactivation, GD from Wt, Δ*nsrR* and Δ*Triple* were PCR amplified by *nsrR_RUH3_FWD* and *nsrR_RUH3_REV* primers (amplifies 1.4 Kb region of the *nsrR*) **(Section 2.11.3).** In Lane 7, an intense band of 1.4 Kb was present with Wt PCR amplification. Similar band was not seen with Δ*nsrR* and Δ*Triple* amplification products in Lanes 8-9. Instead a band of approximately 4.0 Kb length was apparent.

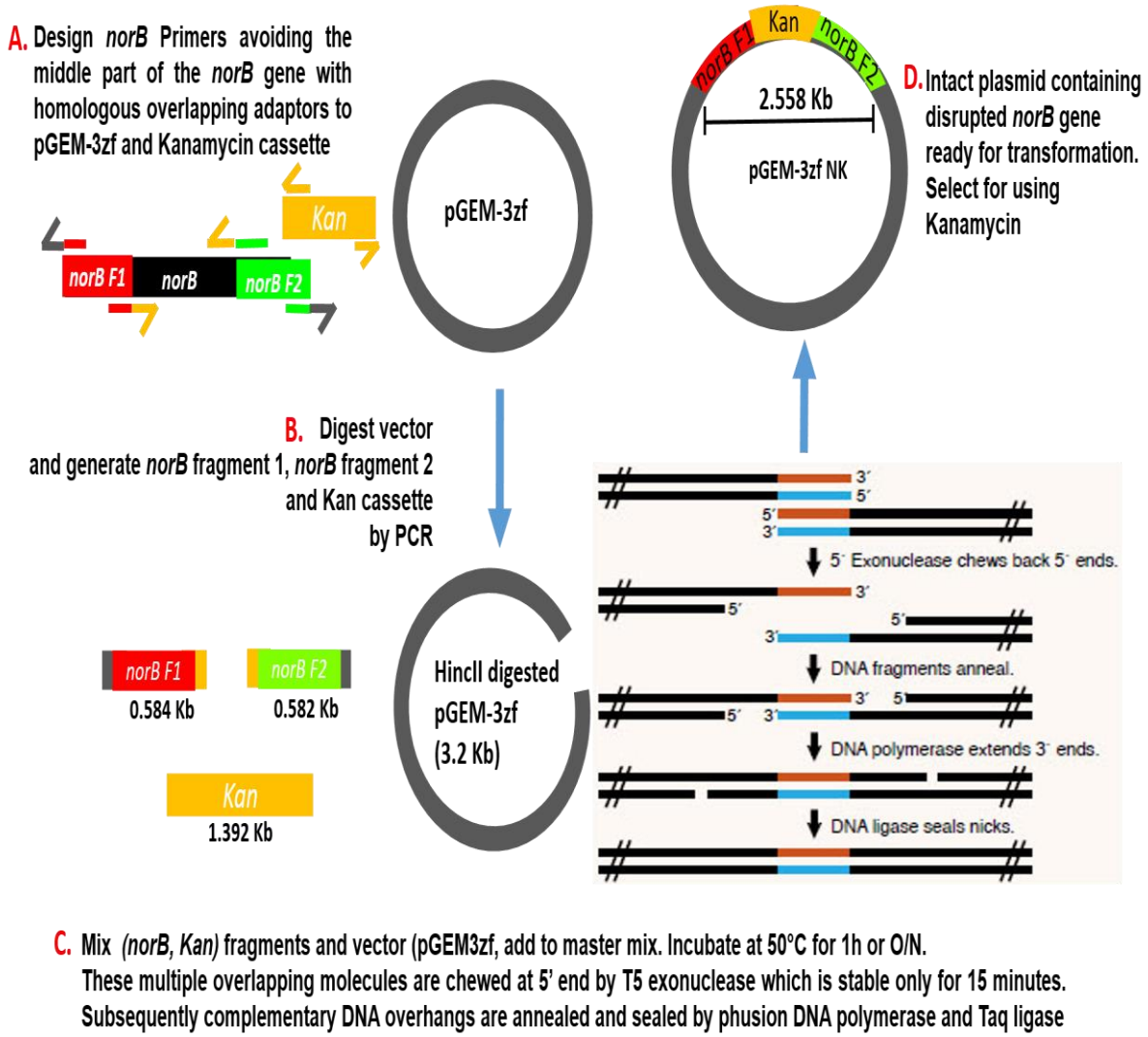

Figure 4.1 Overview of Isothermal Assembly Cloning (ISA) method for generating Kanamycin resistant *norB* cassette in pGEM-3zf plasmid.

A) Two ends of the *norB* gene (avoiding the middle part) were chosen to design primers with homologous overlapping sequence of plasmid vector, pGEM-3zf and kanamycin cassette. **B)** The products were generated by PCR amplification (*norB F1*, *norB F2*, Kan) and vector was restriction digested with HincII. **C)** All components were mixed with a cocktail containing 5′ exonuclease, DNA polymerase and Taq ligase at 50°C **(Section 2.11.4).** 5′ exonuclease chews the 5′ end of the overlapping fragments and is only stable for 15 minutes. After that DNA polymerase and Taq ligase act to anneal the fragments and seal the nicks. Therefore, *norB F1*- Kan- *norB F2* cassette containing plasmid (pGEM-3zf NK) was generated from one step isothermal reaction at 50ºC. The resulting plasmid was selected on kanamycin containing plates (Figure C adapted from Gibson assembly commercial manual).

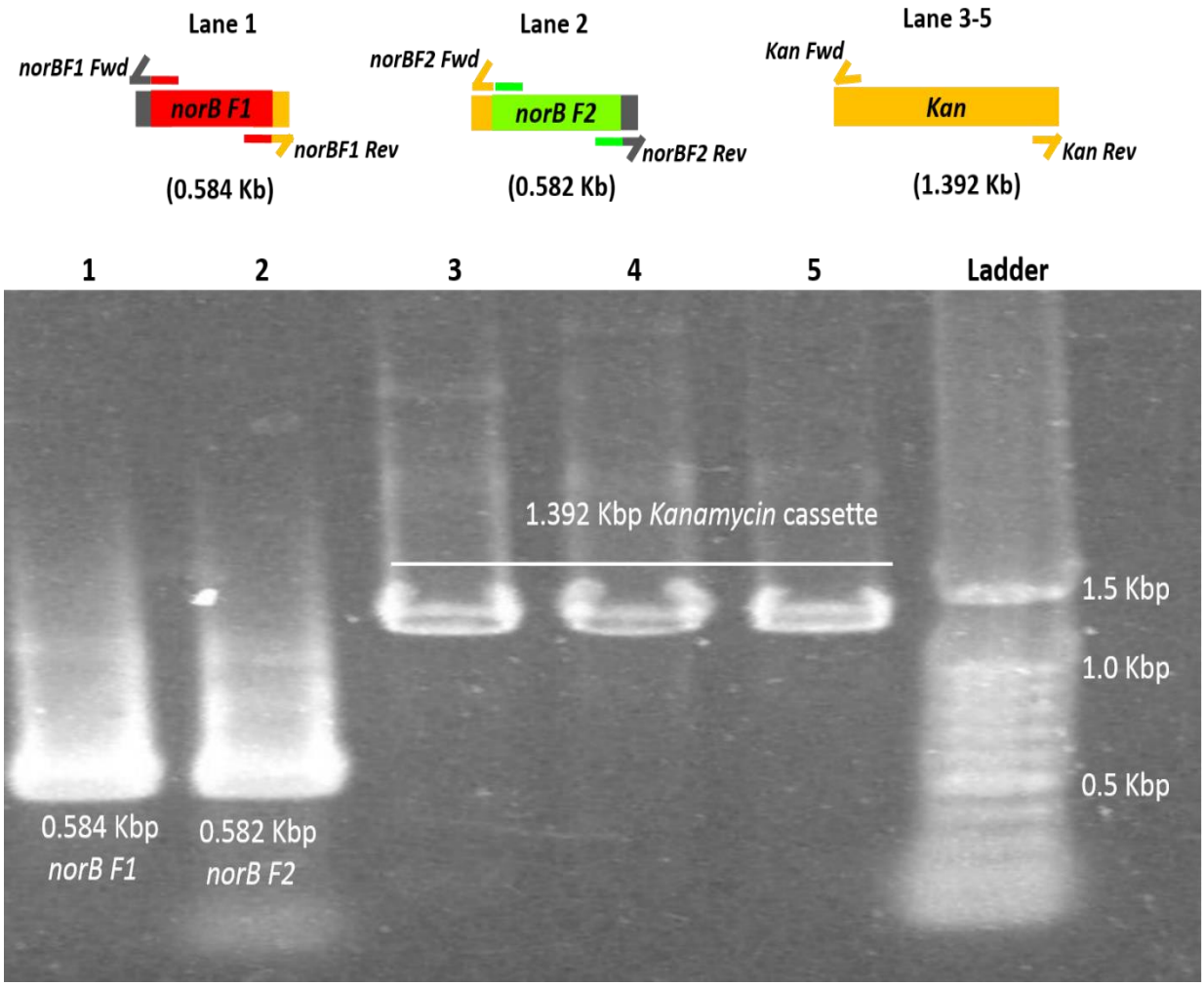

Figure 4.2 PCR amplification of *norBF1, norBF2* fragments and Kanamycin cassette.

The products were PCR amplified by My Taq Polymerase **(Section 2.11.15.2)** and were separated by running on 1% Agarose gel **(Section 2.11.14).** Product from Lane 1 was amplified using *norBF1 Fwd/norBF1 Rev* primers and from Lane 2 by *norBF2 Fwd/norBF2 Rev* primers respectively **(Section 2.11.3)**. Lane 1 represents the expected 0.584 Kbp *norBF1* and Lane 2 represents the expexted 0.582 Kbp *norBF2*. Lanes 3-5 represents the expected approximately 1.392 Kb long Kanamycin cassettes which were PCR amplified by *Kan Fwd/Kan Rev* primers using Acuzyme polymerase **(Section 2.11.15.3)** on pJMK30 template **(Table 2.2).** Promega 100 bp DNA ladder was used. Image was taken by BioRad Gel Imager.

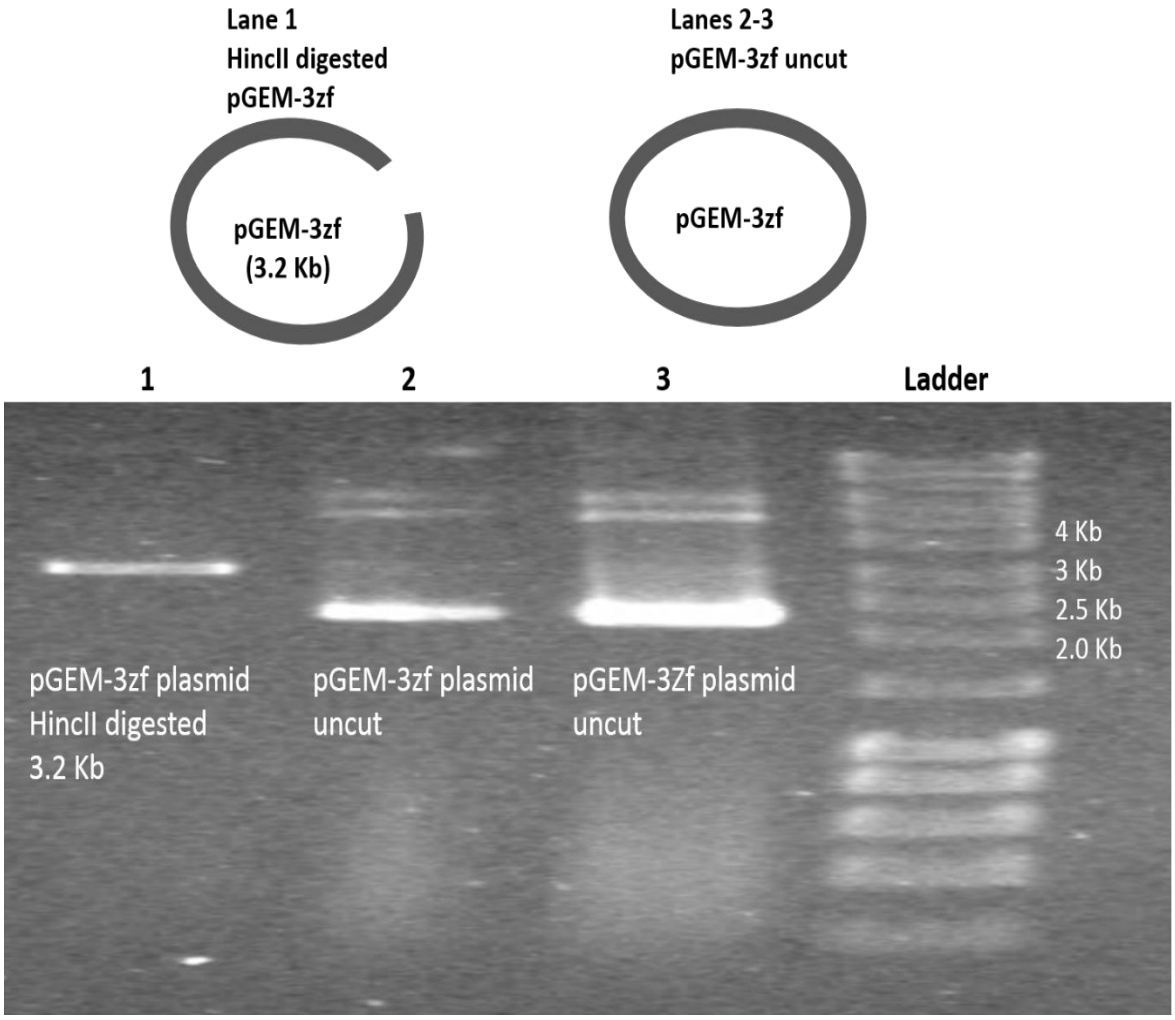

Figure 4.3 Confirmation of HincII Digestion of pGEM-3zf plasmid.

Lane 1 from the 1% agarose gel **(Section 2.11.14)** represents the HincII digested **(Section 2.11.9)** pGEM-3zf plasmid with the expected 3.2 Kb band. Lane 2 and 3 represent pGEM-3Zf uncut plasmid with the expected multiple bands. 1 Kb hyperladder from Bioline, UK was used. Image taken by BioRad gel imager.

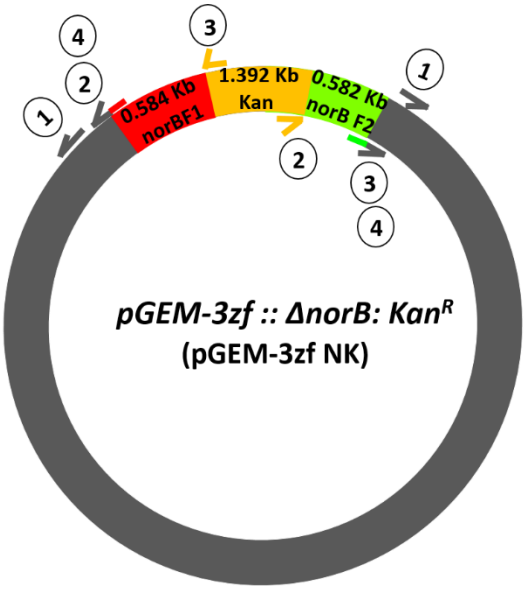

PCR primer combination	PCR primer name	Expected amplification product size
1	*M13 Fwd and Rev*	2.558 Kb
2	*F1 Fwd and Kan Rev*	1.976 Kb
3	*F2 Rev and Kan Fwd*	1.974 Kb
4	*F1 Fwd and F2 Rev*	2.558 Kb

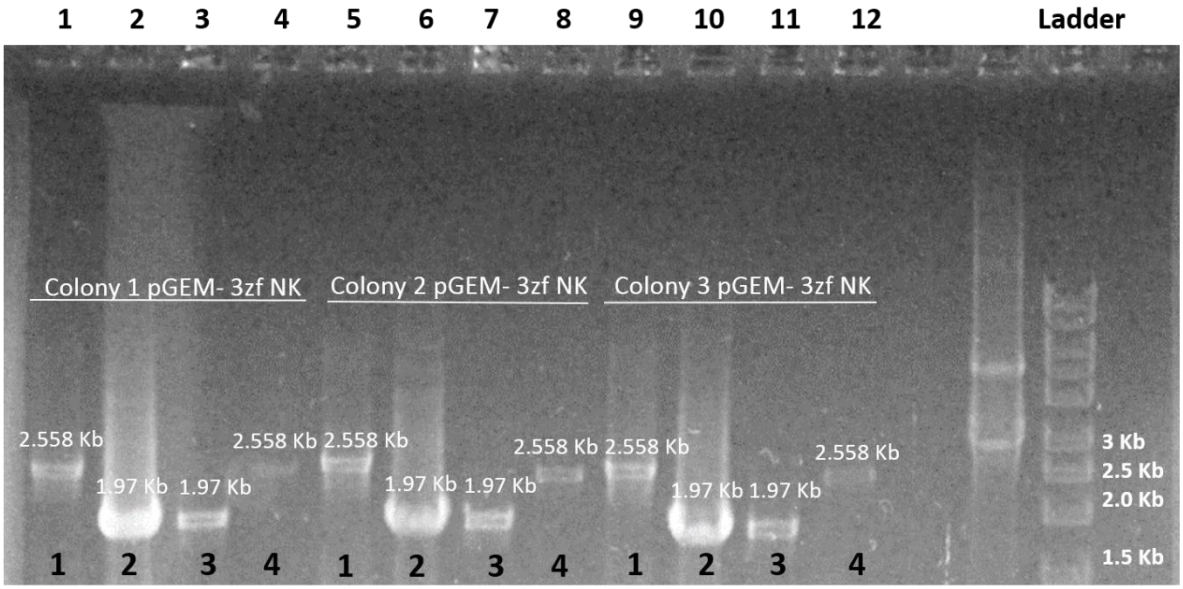

Figure 4.4 Diagnostic PCR screening for selecting positive clones of the pGEM–3zf NK plasmid after transformation of isocloning ligation mix into the DH5α competent cells.

After isocloning, the ligation mix was transformed **(Section 2.11.2)** and selected on Kanamycin containing LB Agar plates **(Section 2.4.4).** Following plasmid extraction by Qiagen kit **(Section 2.11.8)**, the three positive clones (Colony 1, Colony 2 and Colony 3) were screened for the presence of right fragment insertion using a combination of primers mentioned in the cartoon above the image of the 1% agarose gel **(Section 2.11.14).** The panel at the bottom of the agarose gel (numbers in black) represents the primer combinations. All the colonies produced expected PCR products. Colony 2 was chosen for subsequent cloning application. Image taken by BioRad gel imager.

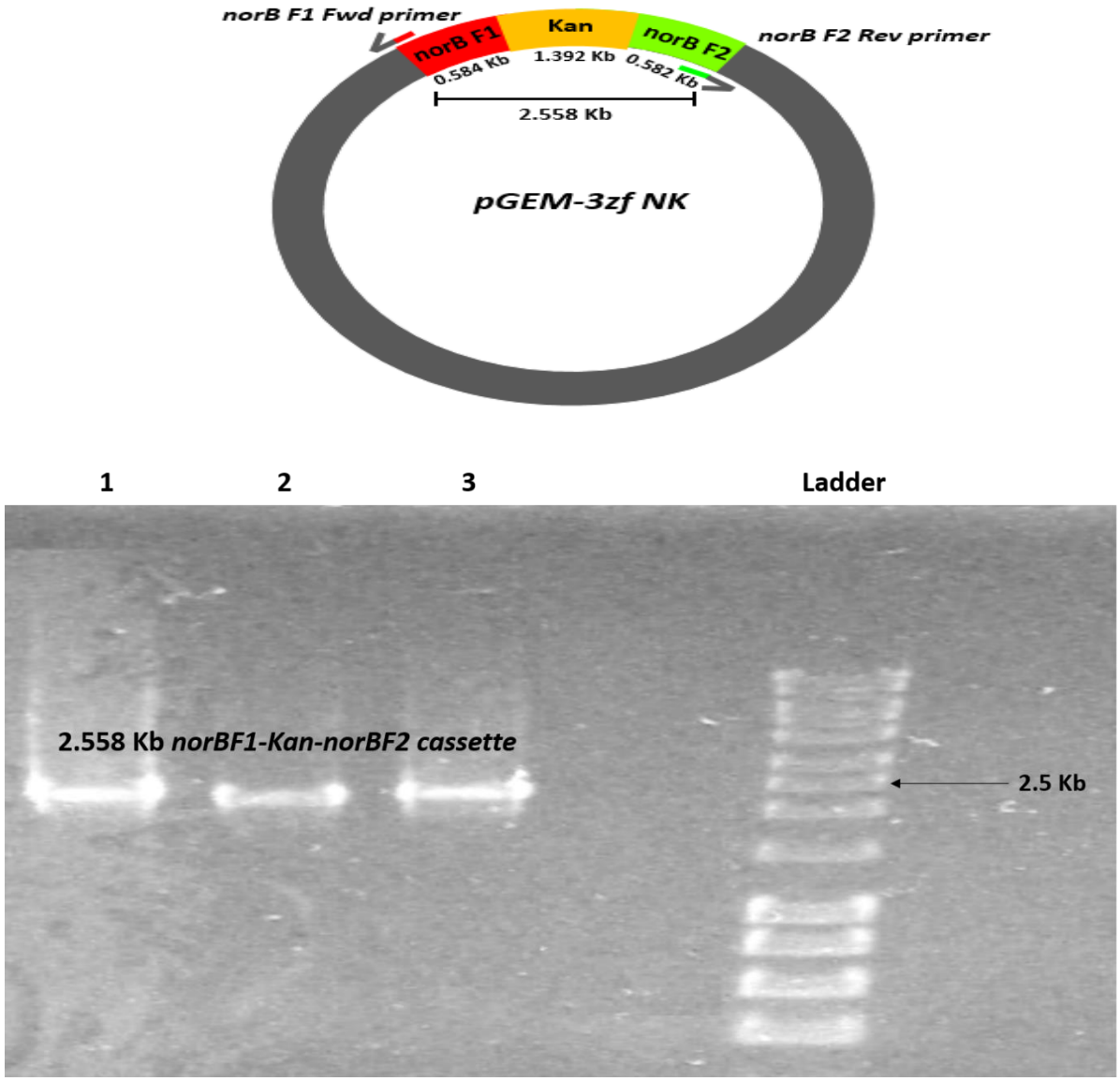

Figure 4.5 PCR amplification of *norBF1-Kan-norBF2* cassette from pGEM–3zf NK plasmid.

The 1% agarose gel **(Section 2.11.14)** represents the approximately 2.558 Kb long *norBF1-Kan-norBF2* cassette (see the cartoon above) amplified using the newly cloned pGEM-3zf NK plasmid as template **(Figure 4.4)**. The primer pair used is mentioned in the cartoon above the gel. Accuzyme polymerase **(Section 2.11.15.3)** was used for PCR amplification. Image taken by BioRad gel imager

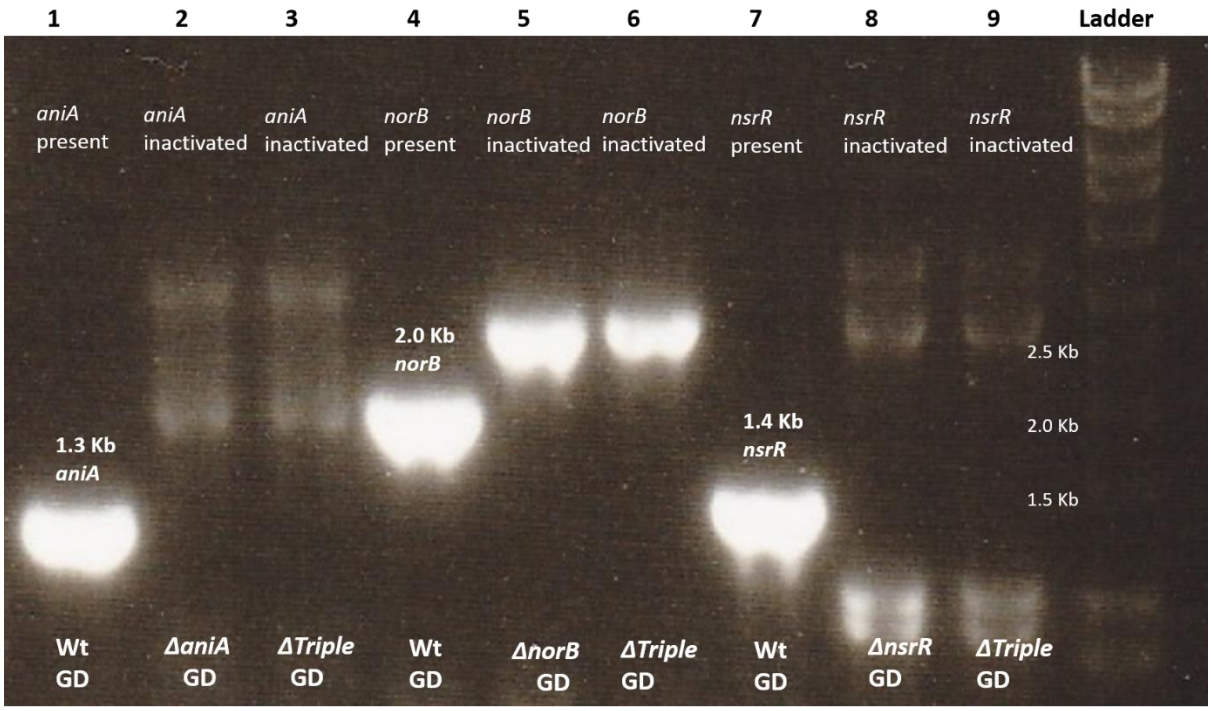

Figure 4.6 PCR confirmation of Δ*aniA/*Δ*norB/*Δ*nsrR (*Δ*Triple)* mutant creation.

Genomic DNA (GD) were extracted from the overnight grown cultures of Wt MC58*,* Δ*aniA,* Δ*norB,* Δ*nsrR* and Δ*aniA/*Δ*norB/*Δ*nsrR (*Δ*Triple)* **(Section 2.11.6)**. Primers for *aniA* (*aniA_RUH1_FWD* and *aniA_RUH1_REV*) and *norB* (*norB_RUH2_FWD* and *norB_RUH2_REV*) were designed covering the whole gene. *nsrR* amplification primers (*nsrR_RUH3_FWD* and *nsrR_RUH3_REV*) were chosen carefully for amplifying extended sequences around the gene. PCR was run using My Taq^{TM} Red Mix polymerase **(Section 2.11.15.2).** PCR products were separated on 1% agarose gel containing ethidium bromide with reference to a DNA hyperladder I (1 Kb ladder, bioline). Products from Lane 1-3, Lane 4-6, Lane 7-9 were PCR amplified by *aniA, norB* and *nsrR* primers respectively. The lane annotation panel below the gel represents the templates used for respective PCR amplification. Lane 1 showed the expected (1.3 Kb) *aniA* PCR product from Wt MC58. The same primer pair could not produce similar size product from Δ*aniA* and Δ*aniA/*Δ*norB/*Δ*nsrR* GD. Similarly *norB* and *nsrR* primer pairs were able to amplify (2.0 Kb) *norB* and (1.4 Kb) *nsrR* from Wt GD. Same primers did not produce similar size bands when PCR reaction were run with the GD from other mutants.In lanes 2-3, the approximate 3.3 Kb band represented the 2.0 Kb spectinomycin cassette flanked by disrupted *aniA* sequence ; in lanes 5-6, the approximate 2.6 Kb band represents the 1.4 Kb kanamycin cassette flanked by disrupted *norB* sequence; in lanes 8-9, the approximate 4.0 Kb band represents the 2.5 Kb tetracycline cassette flanked by disrupted *nsrR* region. Image taken by Biorad gel imager.

4.2.2 Creation of Δ*aniA/*Δ*norB* and Δ*nsrR/*Δ*norB* double mutants

4.2.2.1 Rationale and methods

It was decided to exploit the newly generated pGEM-3zf NK plasmid **(Figure 4.4)** to generate two double mutants, Δ*aniA/*Δ*norB* and Δ*nsrR/*Δ*norB*. This was to enable us to have a comprehensive set of NO denitrification gene mutants, which could be used to answer important research questions in the pathogenesis of meningococcal sepsis. The 2.5 Kb long *norB F1*- Kan- *norB F2* cassette **(Figure 4.5)** was PCR amplified using the Acuzyme polymerase **(Section 2.11.15.3).** PCR product was purified **(Section 2.11.7)** and bulked up to have at least 2 µg of product. Subsequently the cassette was transformed into Δ*aniA* (Spectinomycin) in the presence of $MgCl_2$ **(Section 2.11.12)** and the positive colonies were selected on Spectinomycin/Kanamycin contaning plates to have the resulting Δ*aniA/*Δ*norB* colonies. At least six positive colonies from two independent transformation events were combined and streaked on a fresh antibiotic containing plate to counteract phase and antigentic variation. A similar method was used to generate Δ*nsrR/*Δ*norB* strain except the *norB F1*- Kan-*norB F2* cassette was transformed into Δ*nsrR* (Tetracycline) strain and subsequent colonies were screened on Tetracycline/Kanamycin containing plates.

4.2.2.2 Results

For confirming gene inacitvation of Δ*aniA/*Δ*norB,* GD **(Section 2.11.6)** from Wt, Δ*aniA,* Δ*norB,* Δ*aniA/*Δ*norB* and colony PCR templates from colonies of freshly grown Δ*aniA/*Δ*norB* plate were PCR amplified by *aniA* primers (*aniA_RUH1_FWD, aniA_RUH1_REV*) (amplifies 1.3 Kb of the *aniA* region) and *norB* primers (*norB_RUH2_FWD* and *norB_RUH2_REV*) (amplifies 2.0 Kb of the *norB* gene) **(Section 2.11.3).** All PCR reactions were carried out by My Taq^{TM} Red Mix polymerase **(Section 2.11.15.2).**

As can be seen from **Figure 4.7,** a band of 1.3 Kb length was present in Lane 1 where Wt GD was used as a template for PCR amplification with *aniA* primers. Similar size band was not seen in Lanes 2-5. With *norB* primers, a 2.0 Kb product was evident with Wt GD amplification in Lane 6. Approximately 2.6 Kb bands were observed with Δ*aniA* and Δ*aniA/*Δ*norB* genomic DNA extracted PCR products in Lanes 7-8. However, similar size band was not seen in Lanes 9-10 with PCR amplification from colony PCR templates of Δ*aniA/*Δ*norB*.

To verify inactivation of *norB* and *nsrR* in Δ*nsrR/*Δ*norB,* PCR amplification was carried out on GD extracted from Wt, Δ*norB,* Δ*nsrR*, Δ*nsrR/*Δ*norB.* For *norB* amplification (*norB_RUH2_FWD* and *norB_RUH2_REV*) primers (amplifies 2.0 Kb of the *norB* gene) and *nsrR* amplification (*nsrR_RUH3_FWD* and *nsrR_RUH3_REV)* primers (amplifies 1.4 Kb of the *nsrR* gene) were used **(Section 2.11.3).**

Figure 4.8 shows that a 1.4 Kb band was amplified with *nsrR* primers from the Wt GD template. In Lanes 2-3, this band was not seen with the PCR products from Δ*nsrR* and Δ*nsrR/*Δ*norB* GD templates. A band of approximately 4.0 Kb length was apparent from Lanes 2-3.

With *norB* primers, a 2.0 Kb band was seen with Wt GD amplification. A band of approximately 2.6 Kb was apparent with Δ*norB* and Δ*nsrR/*Δ*norB* GD PCR products (Lanes 5-6).

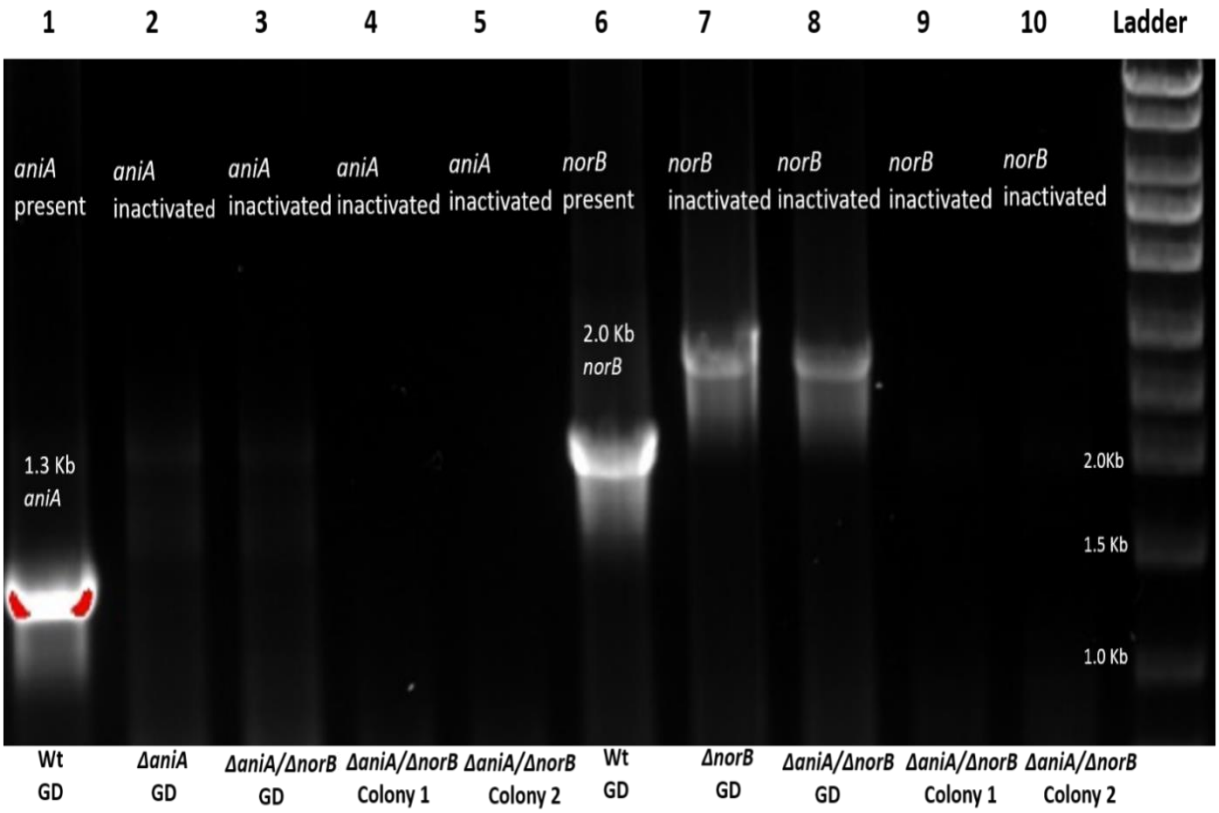

Figure 4.7 PCR confirmation of Δ*aniA/*Δ*norB* mutant creation.

The *norB F1- Kan- norB F2* cassette (2.5Kb) **(Figure 4.5)** generated from isocloning method was transformed into Δ*aniA (*Spectinomycin) and selected on Spectinomycin/Kanamycin containing plates **(Section 2.4.2).** Then the overnight grown positive colonies were used to extract genomic DNA (GD) **(Section 2.11.6)**. GD from Δ*aniA,* Δ*norB* and Δ*aniA/*Δ*norB* were used for confirmation of mutation by PCR. Alongside the GDs, positive colonies from putative strains were processed by colony PCR **(Section 2.11.15.1).** The lane annotation panel below the gel represents the templates used for respective PCR amplification. Primer pairs specific for *aniA* and *norB* were used to amplify these genes from Wt and mutant strains using My Taq^{TM} red mix polymerase **(Section 2.11.15.2).** Primers for *aniA* (*aniA_RUH1_FWD* and *aniA_RUH1_REV*) and *norB* (*norB_RUH2_FWD* and *norB_RUH2_REV*) were designed covering the whole gene. PCR products were separated on gel depending on their size. Lanes 1-5 were amplified by *aniA* primers and Lane 6-10 were amplified by *norB* primers. In both the conditions only Wt GD template produced the desired sized product (1.3 Kb *aniA* and 2.0 Kb *norB*) following PCR. In lanes 7-8, the approximate 2.6 Kb band represents the 1.4 Kb kanamycin cassette flanked by disrupted *norB* sequence; Gel was imaged by BioRad gel imager.

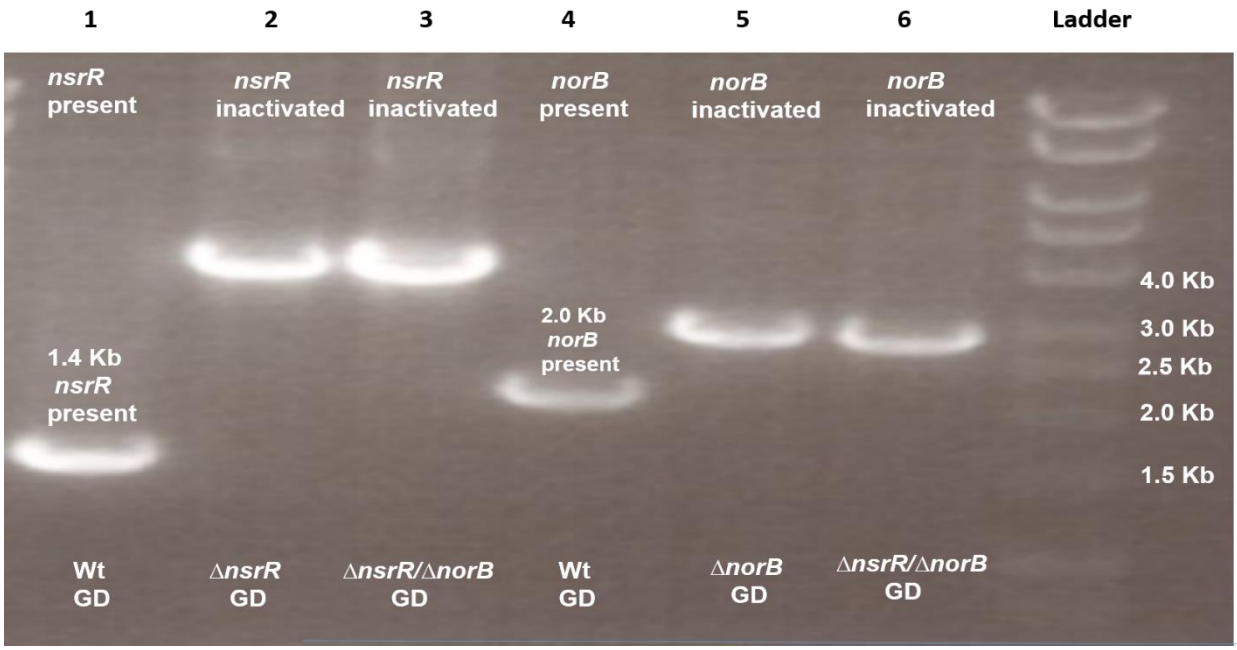

Figure 4.8 PCR confirmation of Δ*nsrR/*Δ*norB* mutant creation.

The *norB F1-* Kan- *norB F2* cassette (2.5Kb) **(Figure 4.5)** was transformed into Δ*nsrR (*Tetracycline) and selected on Tetracycline/Kanamycin containing plates to generate Δ*nsrR/*Δ*norB* mutant. Then the overnight grown positive colonies were used to extract genomic DNA (GD) **(Section 2.11.6).** GD extracted from Δ*nsrR,* Δ*norB* and Δ*nsrR/*Δ*norB* were used for confirmation of mutation by PCR. The lane annotation panel below the gel represents the templates used for respective PCR amplification. Primer pairs specific for *nsrR* and *norB* were used to amplify these genes from Wt and mutants using My Taq^{TM} red mix **(Section 2.11.15.2).** PCR products were separated on 1% agarose gel **(Section 2.11.14)** depending on their size. Lane 1-3 were amplified by *nsrR* primers (*nsrR_RUH3_FWD* and *nsrR_RUH3_REV*) and Lane 4 – 6 were amplified by *norB* primers (*norB_RUH2_FWD* and *norB_RUH2_REV*). In both the conditions only Wt GD produced the desired sized products (1.4 Kb *nsrR* region and 2.0 Kb *norB*) following PCR. In lanes 2-3, the approximate 4.0 Kb band represents the 2.5 Kb tetracycline cassette flanked by disrupted *nsrR* region; In lanes 5-6, the approximate 2.6 Kb band represents the 1.4 Kb kanamycin cassette flanked by disrupted *norB* sequence. Gel was imaged by BioRad gel imager.

4.2.3 Investigation of polar effect of gene deletion of *norB* in the newly created Δ*aniA/*Δ*norB/*Δ*nsrR*

4.2.3.1 Rationale and methods

Gene inactivation often creates a conundrum in assigning an observed phenotype to the inactivated gene. This could be often to the fact that the observed phenotype could be an outcome of cumulative effect of the primary gene inactivation and polar effect of alteration in expression of the downstream gene brought about by primary upstream gene inactivation (Link *et al*, 1997). *NorB* is encoded by NMB1622. In the same direction as NMB1622, NMB1621 which codes for a glutathione peroxidase (GpxA) is expressed **(Figure 4.9 A).** GpxA is important for protecting the organism from oxidative stress. It detoxifies peroxidases such as H_2O_2 and converts it to stable alcohol using cellular glutathione as reducing agent. *N. meningitidis* lacking GpxA is more sensitive to oxidative damage caused by H_2O_2 (Moore & Sparling, 1996). Therefore, it was essential to establish that the newly created Δ*aniA/*Δ*norB/*Δ*nsrR* strain did not have any an altered activity of downstream GpxA due to inactivation of the *norB*.

Wt, Δ*norB* and Δ*aniA/*Δ*norB/*Δ*nsrR* strains were grown overnight on GC agar plates containing appropriate antibiotics **(Section 2.4.2).** Three single colonies from each condition were inoculated into 5 ml MHB media and grown overnight with shaking. Cells from all the cultures were lysed using a sonicator. Supernatant was collected by centrifuging the cells at 10000 g for 15 minutes at 4°C and processed for the GpxA determination assay. GpxA activity was determined using a commercially available glutathione peroxidase assay kit **(Section 2.10.2).** The kit comes with cumene hydroperoxide, glutathione (GSH), NADPH and glutathione reductase (GR). Gpx reduces cumene hydroperoxide and oxidises GSH to GSSG **(Reaction 1).** Supplied glutathione reductase (GR) from the kit reduces GSSG back to GSH by consuming NADPH **(Reaction 2).** The decrease in NADPH is detected at 340 nm and is directly proportional to Gpx activity. Therefore, the kit measures glutathione peroxidase activity indirectly.

$$R\text{-}OOH + 2\ GSH \xrightarrow{Gpx} R\text{-}OH + GSSG + H_2O \quad \ldots\ldots(1)$$

$$GSSG + NADPH + H^+ \xrightarrow{GR} 2GSH + NADP^+ \quad \ldots\ldots(2)$$

4.2.3.2 Results

As evident from **Figure 4.9 B**, from the overnight growth culture of Wt, high amounts of Gpx activity was detected (319 ± 51.65 mg/ml of protein). The amount of Gpx activity detected from Δ*aniA/*Δ*norB/*Δ*nsrR* was 391.6 ± 77.39 mg/ml of protein. Low Gpx activity was detected from Δ*norB* (160 ± 52.10 mg/ml of protein). However this was not statistically significant from the other conditions where Gpx activity was quantified from the overnight grown cultures of Δ*norB* and Δ*aniA/*Δ*norB/*Δ*nsrR* ($p = 0.06$).

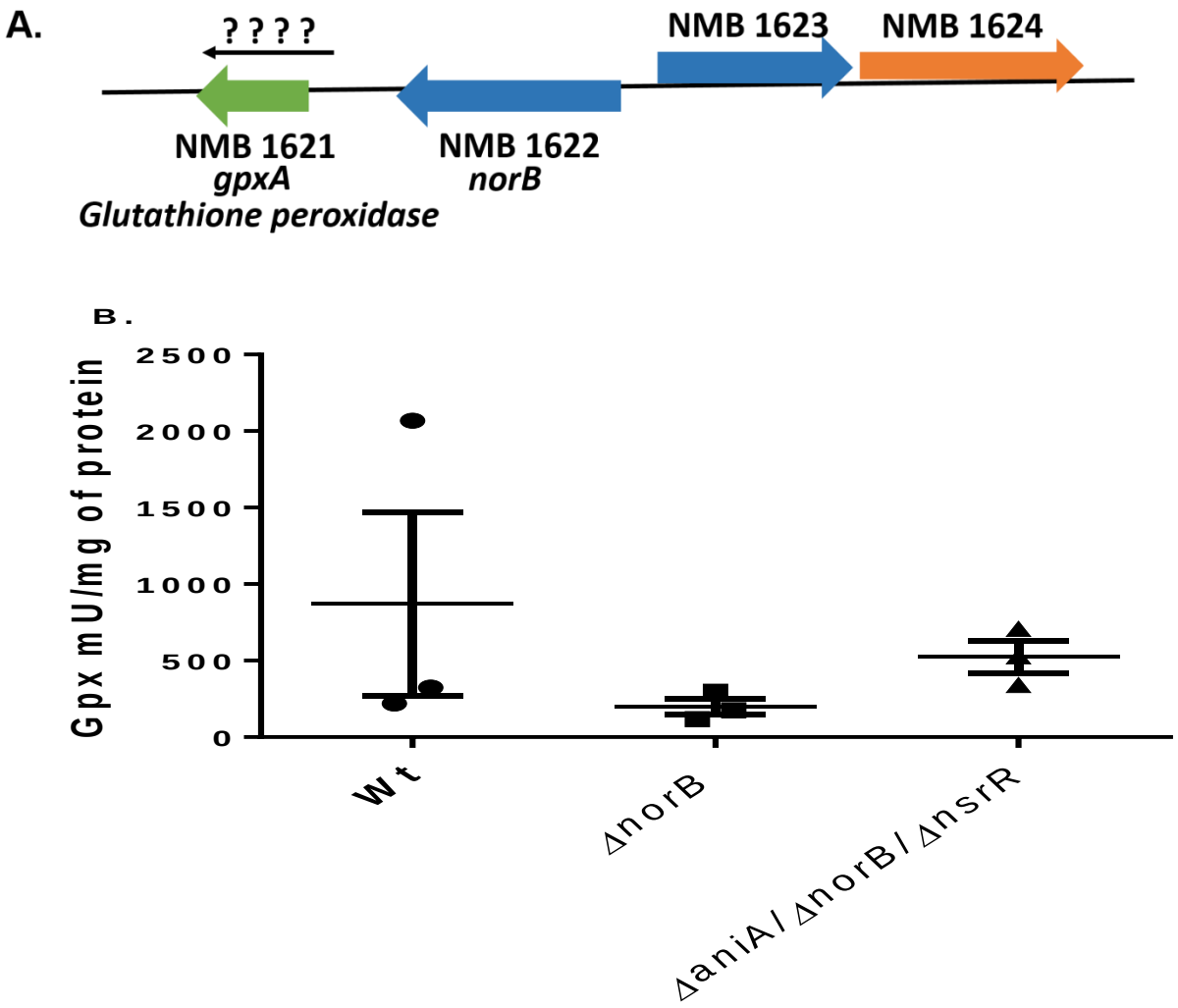

Figure 4.9 Investigation of polar effect of *norB* inactivation in Δ*aniA/*Δ*norB/*Δ*nsrR* on downstream GpxA activity.

A) *gpxA* and *norB* are coded by NMB1621 and NMB1622 respectively. Expression of both genes is unidirectional. So, effect of *norB* inactivation on GpxA activity had to be examined. B) Comparative GpxA activity measurement of *norB* deleted strains Δ*norB and* Δ*aniA/*Δ*norB/*Δ*nsrR.* All the selected strains were streaked onto GC agar plate containing vitox supplement overnight. Three single colonies were used to inoculate 5 ml MHB. Bacterial cells grown overnight were lysed by sonication and supernatant was collected after centrifugation. Supernatant was used to measure glutathione peroxidase (GpxA) activity using a commercial kit (Abcam) **(Section 2.10.2).** NAPDH consumption during enzymatic reaction was a direct indicator of GpxA activity. n = 3, Bars denote mean ± SEM, One way ANOVA with Tukey's multiple comparison test.

4.2.4 Growth characteristics of strains in aerobic condition

4.2.4.1 Rationale and methods

To examine the growth characteristics of the newly generated mutants in aerobic conditions, a comparative batch culture growth curve was performed with all the available strains (Wt, Δ*aniA,* Δ*norB,* Δ*nsrR,* Δ*aniA/*Δ*norB*, Δ*nsrR/*Δ*norB,* Δ*nsrR/*Δ*aniA,* Δ*aniA/*Δ*norB/*Δ*nsrR*) for 24 hours. Five colonies from each condition was inoculated in 25 ml Mueller Hinton Broth in 50 ml tubes and cultures were grown aerobically. At t = 0 timepoint, 1 ml of culture was removed from each tube for absorbance reading and 30 µl of each sample was used for viable count. The same procedure was repeated at 2, 4, 8, 12 and 24 hour time point. Samples were serially diluted and triplicate of 10 µl aliquots of each dilution were separately spotted on CBA plates, left in a microbiological safety cabinet for 10 minutes to allow them to air-dry. Following overnight incubation at 37°C, 5% CO_2, the mean number of colonies for each dilution were counted and corrected for the dilution factor and volume.

4.2.4.2 Results

As can be seen from **Figure 4.10 A**, the absorbance at OD_{600nm} was not statistically significant from one another at any of the time points investigated (p = 0.8543). The growth of all the strain increased with progression of time. Rapid increase in absorbance was noticed after 2 hour.

Figure 4.10 B shows the viable counts from all the strains at different timepoints. At any given timepoint there was no significant difference in viable bacteria recovered from the strains present (p = 0.2991). Comparative area under curve analysis of all the strains also did not reveal any difference over time in viable bacterial growth (p = 0.3025, One way ANOVA with Tukey's multiple comparison test).

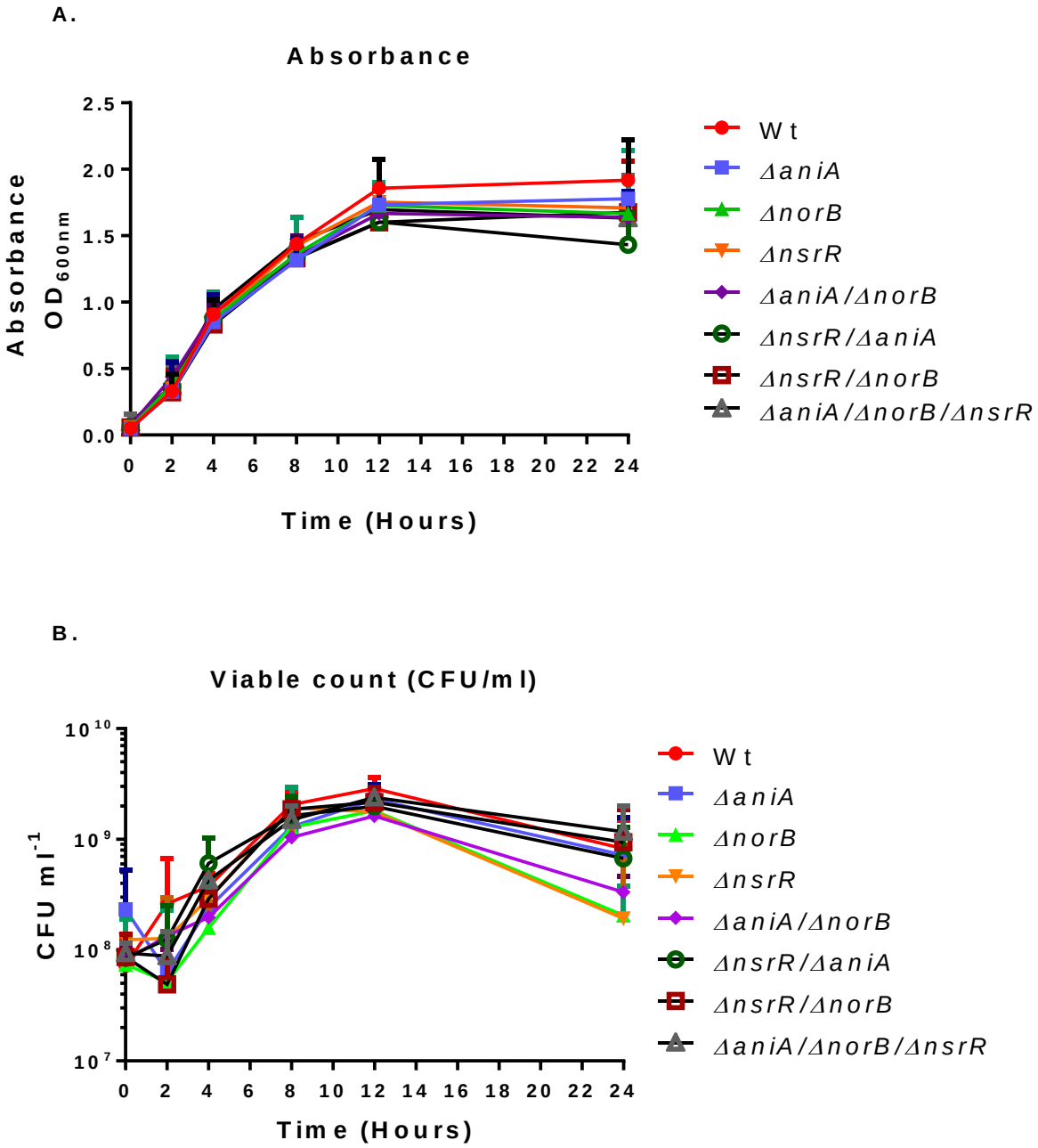

Figure 4.10 Growth curve of the newly constructed mutant strains under normal aerobic condition.

Five single colonies from each strain were incoculated in 50 ml tube containing MHB and grown with shaking at 37°C, 5% CO_2. The sample was collected every hour for **A)** Absorbance and **B)** Viable Counts (expressed in cfu/ml) readings. n = 3, Bars denote mean ± SEM. Two way ANOVA with Tukey's multiple comparison test.

4.2.5 Characterisation of metabolism of the mutant strains in presence of $NaNO_2$

4.2.5.1 Rationale and methods

To test the functional inactivation of the newly generated Δ*aniA/*Δ*norB*, Δ*nsrR/*Δ*norB* and Δ*aniA/*Δ*norB/*Δ*nsrR* strains, a batch culture growth curve was performed in Mueller Hinton Broth (MHB) supplemented with 5 mM $NaNO_2$ in microaerobic condition. This condition has been used for examining meningococcal denitrification (Anjum *et al,* 2002) (Rock & Moir, 2005). This experiment enabled us to investigate the comparative NO_2^- depletion over time in presence of different denitrification gene mutants compared to the Wt MC58. For comparative analysis Wt and Δ*nsrR/*Δ*aniA* (a kind gift from Dr James Moir, our collaborator, University of York) strains were also included. In 25 ml tubes, the cultures were normalised to OD_{600nm} = 0.05 in 25 ml MHB with 5 mM $NaNO_2$ supplementation. The cultures were grown for 24 hours without agitation. Static condition ensured limited oxygen diffusion in the media. In a separate tube, 25 ml MHB with 5 mM $NaNO_2$ was incubated without any bacteria. This condition served as positive control. Viable counts were performed at 0, 2, 4, 8, 12 and 24 hour time points by dilutional plating. A volume of 1 ml of culture from each condition was collected for absorbance reading. At the specified time points, 1 ml of each sample was transferred to sterile 1.5 ml microcentrifuge tube. The samples were centrifuged at 13000 rpm for 5 minutes and supernatants were collected. Bacteria free supernatants were used to measure nitrite (NO_2^-) by Griess Assay **(Section 2.10.1).** In this calorimetric assay nitrite is converted to diazonium salt following the reaction with acidified sulphanilamide. This salt reacts with NED solution to generate an azo dye, which is spectrophotometrically quantified on the basis of absorbance at 540 nm.

4.2.5.2 Results

As can be seen from **Figure 4.11 A,** there was no significant difference in the amount of NO_2^- detected in the presence of different bacterial strains at 0, 2, and 4 hour time points. At 8, 12 and 24 hour time points NO_2^- depletion by Wt was significantly higher compared to all other mutant strains. Area under curve analysis using the viable count data showed that growth of Wt and Δ*nsrR/*Δ*aniA* are significantly higher than that of Δ*nsrR/*Δ*norB* (***p*<0.01, One way ANOVA with Tukey's multiple comparison) **(Figure 4.11 B).** The absorbance detected with Wt infected media at 12 and 24 hour time points were significantly higher compared to other strains **(Figure 4.11 C)** ($p < 0.05$). Compared to Δ*nsrR/*Δ*norB*, absorbance readings from other strains were significantly higher at 12 and 24 hour time points ($p < 0.01$). Importantly, there

was no significant difference in the amount of NO_2^- detected from Δ*aniA/*Δ*norB*, Δ*aniA/*Δ*norB/*Δ*nsrR* infected media in comparison with the positive control media (with 5 mM $NaNO_2$ supplementation only) at any of the time points studied **(Figure 4.11 A).** In the first replicate, Wt MC58 started depleting NO_2^- at the 8 hour timepoint **(Figure 4.12 A)** whereas in the second **(Figure 4.12 B)** and third replicate NO_2^- **(Figure 4.12 C)** depletion started after 12 hour. However, in the final replicate NO_2^- depletion was apparent at the 24 hour timepoint **(Figure 4.12 D).** In all four replicates NO_2^- depletion coincided with an increase in absorbance.

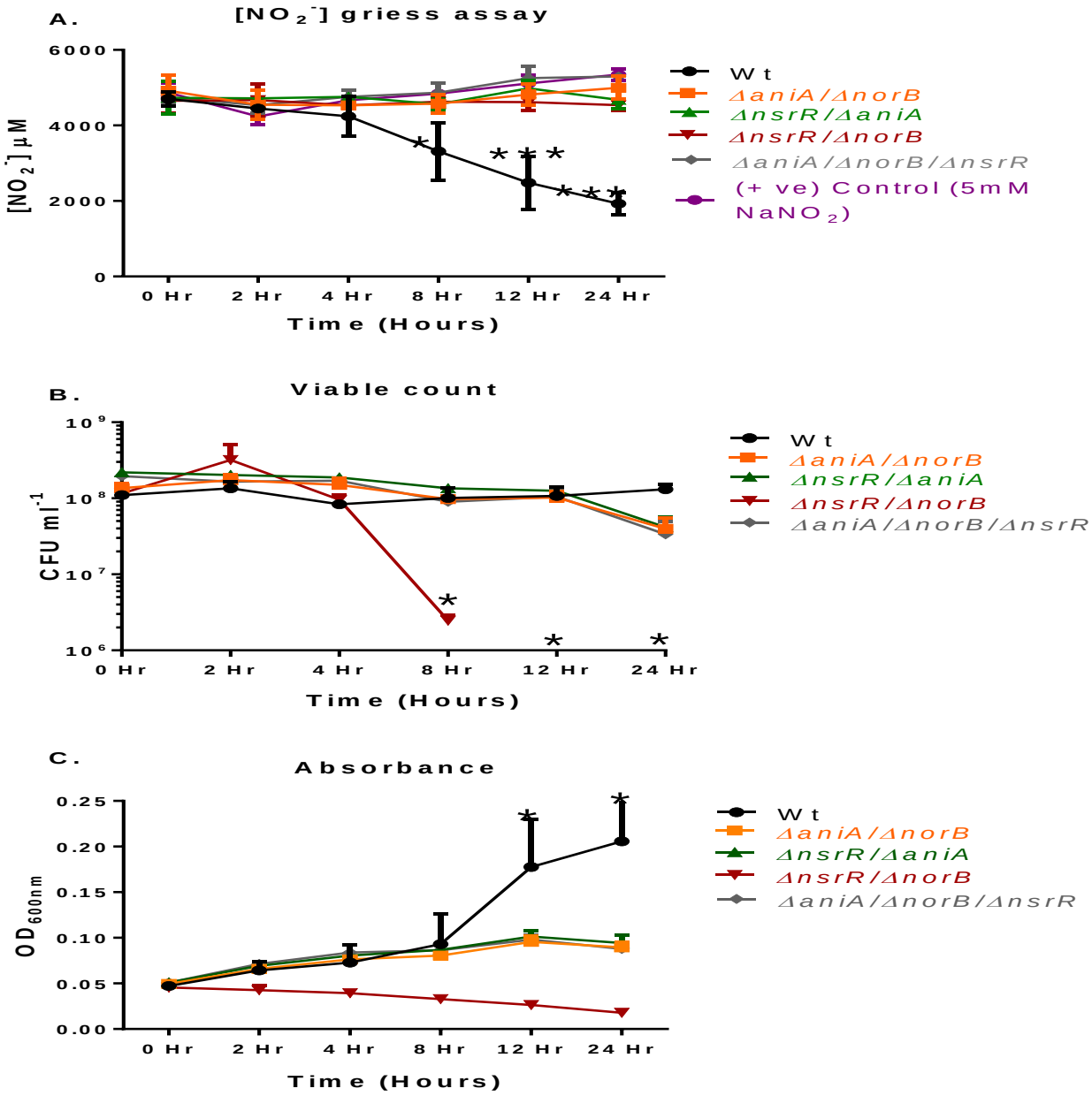

Figure 4.11 Characterisation of the functional inactivation of the newly generated mutant strains in the presence of 5 mM $NaNO_2$.

Wt, Δ*aniA/*Δ*norB,* Δ*nsrR/*Δ*norB,* Δ*nsrR/*Δ*aniA,* Δ*aniA/*Δ*norB/*Δ*nsrR* were grown in the 25 ml MHB containing 5 mM $NaNO_2$ in 50 ml tubes without agitation. Media was collected at 0, 2, 4, 8, 12 and 24 hour timepoints to take viable count readings. 1 ml of sample from each condition was stored for later **A)** [NO_2^-] measurement by Griess Assay **(Section 2.10.1) B)** 30 µl of sample from each timepoint was serially diluted and plated on CBA plate for measuring viable count (cfu/ml) next day, **C)** 1 ml of sample was used for measuring absorbance OD_{600nm}. Bars denote means ± SEM. n = 4, *p<0.05, ***p<0.0001, Two way ANOVA with Tukey's multiple comparison test. Apart from Δ*nsrR/*Δ*aniA* (A kind gift from Moir group, York), other mutant strains (Δ*aniA/*Δ*norB,* Δ*nsrR/*Δ*norB,* Δ*aniA/*Δ*norB/*Δ*nsrR)* were generated by the author.

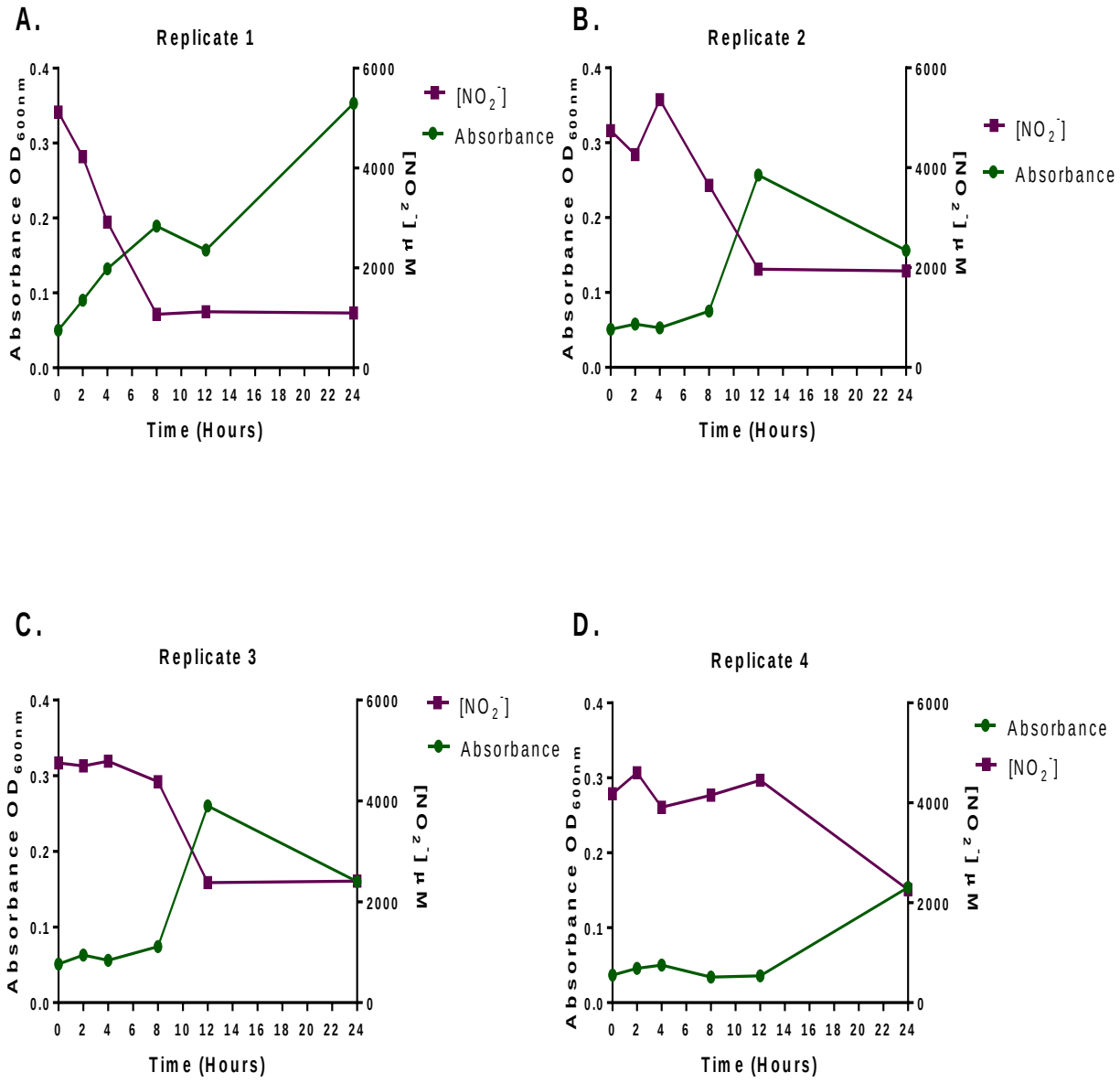

Figure 4.12 Transition from oxidative respiration to denitrification in four identical cultures of *N. meningitidis* Wt MC58.

All the cultures were incubated in 25 ml MHB with an initial OD_{600nm} of 0.05 in the presence of 5 mM $NaNO_2$ under microaerobic condition at 37°C, 5% CO_2. Media was collected at 0, 2, 4, 8, 12 and 24 hour timepoints. 1 ml of sample from each condition was stored for later [NO_2^-] measurement by Griess Assay **(Section 2.10.1)** and another 1 ml was used for measuring absorbance at OD_{600nm}.

4.2.6 Characterisation of metabolism by mutant strains in the presence of an NO donor, Spermine NONOate

4.2.6.1 Rationale and methods

A second batch culture growth curve in the presence of an NO donor, 50 µM Spermine NONOate (further referred as SperNO) was performed to metabolically characterise the newly created mutant strains. This was done to check the functional inactivation of *norB*. NO from media inoculated with different strains will be measured as NO_2^-, one of the stable break down products of NO. SperNO spontaneously dissociates to donate 1.5 molecules of NO per molecule. Therefore, the bacteria had high NO supplementation in the media from the onset of the growth curve. Wt, Δ*aniA/*Δ*norB*, Δ*nsrR/*Δ*aniA* and Δ*aniA/*Δ*norB/*Δ*nsrR* were grown in Mueller Hinton Broth in the presence of 50 µM SperNO for 24 hours. All the strains were normalised to an OD_{600nm} ~ 0.03 in 50 tubes containing 25 ml MHB supplemented with freshly prepared 50 µM SperNO. Cultures were agitated at 320 rev/minute for 24 hours. In parallel, as a positive control, media containing 50 µM SperNO without any bacteria was added to the growth conditions. Samples were collected at 0, 2, 4, 6, 8, 12 and 24 hour time points. From each condition 1 ml culture was used for measuring bacterial viable counts by dilutional plating. Another 1 ml of culture was centrifuged at 13000 rpm for 5 minutes and bacteria free supernatant was stored at -80°C. NO_2^- was measured by Griess assay. NO_2^- is detected after formation of an azo dye following the reaction with acidified sulphanilamide and NED solution **(Section 2.10.1).** Due to lack of an NO electrode, we could not directly measure NO present in these samples.

4.2.6.2 Results

There was rapid depletion of NO (detected in the form of NO_2^- by Griess assay) **(Figure 4.13 A)** from 2 hour and later time points with the Δ*nsrR/*Δ*aniA* infected media compared to other strains. This statistically significant decrease in NO_2^- was evident at all the time points studied. However, at the 6 hour time point the number of viable bacteria recovered from Δ*nsrR/*Δ*aniA* media was significantly higher than the recovery from media infected with other strains **(Figure 4.13 B)**. Interestingly, there was no significant difference between NO_2^- **(Figure 4.13 A)** output from Δ*nsrR/*Δ*aniA* and Wt infected media at 8, 12 and 24 hour time points. This observation was not influenced by the number of bacteria as there was no significant difference in viable bacteria recovered from Wt and Δ*nsrR/*Δ*aniA* stimulated media at these time points **(Figure 4.13 B and Figure 4.13 C).**

At 8, 12 and 24 hour time points, the amount of detected NO_2^- **(Figure 4.13 A)** from the Wt infected media was significantly lower than the media stimulated with Δ*aniA/*Δ*norB*, Δ*aniA/*Δ*norB/*Δ*nsrR* strains and positive control (50 µM SperNO).

It was noteworthy that at none of the time points studied there was any significant difference in the measured NO_2^- **(Figure 4.13 A)** from the Δ*aniA/*Δ*norB*, Δ*aniA/*Δ*norB/*Δ*nsrR* infected media in comparison to that of positive control (50 µM SperNO supplementation in the media).

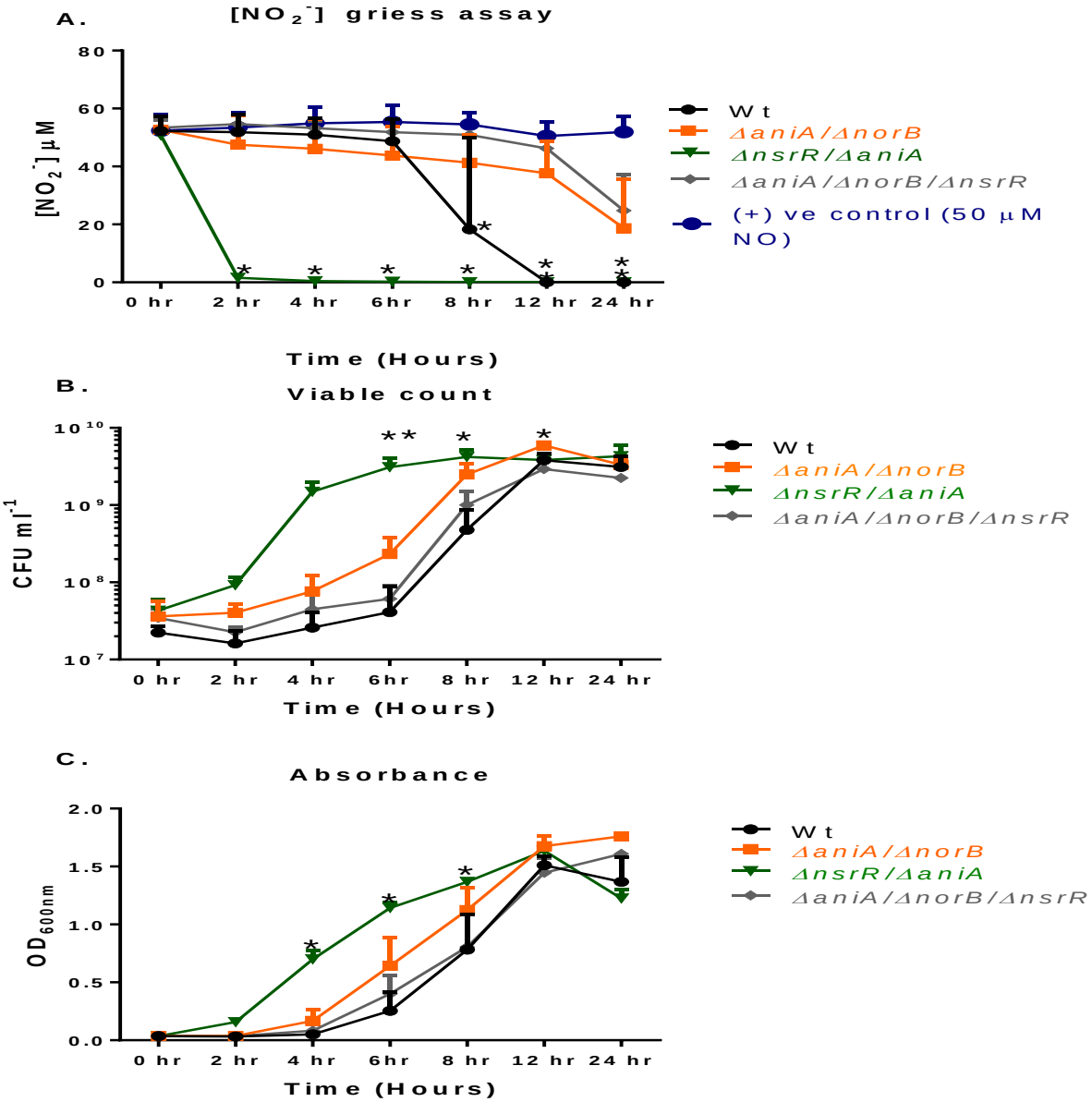

Figure 4.13 Characterisation of the functional inactivation of the newly generated mutant strains in the presence of 50 µM SpermineNONOate.

Wt, Δ*aniA/*Δ*norB, *Δ*nsrR/*Δ*aniA, *Δ*aniA/*Δ*norB/*Δ*nsrR* were grown in 25 ml MHB containing 50 ml tubes in the presence of 50 µM SpermineNONOate at 37°C, 5% CO_2. Media was collected at 0, 2, 4, 6, 8, 12 and 24 hour timepoints to take viable count readings. Supernatant from 1 ml of sample from each condition was stored for later **A)** [NO_2^-] measurement by Griess assay **(Section 2.10.1) B)** 30 µl of sample from each timepoint was plated on CBA plate for measuring viable count next day **C)** 1 ml of sample was taken at each timepoint to measure absorbance at OD_{600nm}. Positive control, 50 µM SperNO. Bars denote means ± SEM. n = 3, **p*<0.05, ***p*<0.01, Two way ANOVA with Tukey's multiple comparison test. Apart from Δ*nsrR/*Δ*aniA* (A kind gift from Moir group, York), other mutant strains (Δ*aniA/*Δ*norB, *Δ*aniA/*Δ*norB/*Δ*nsrR)* were generated by the author.

4.3 Discussion

This chapter reports the first creation and characterisation of Δ*aniA/*Δ*norB* and Δ*aniA/*Δ*norB/*Δ*nsrR* mutants for studying the roles of multiple genes of the denitrification pathway of *N. meningitidis* in pathogenesis. ISA **(Figure 4.1)** was used to generate the Kanamycin containing *norB* cassette which was transformed into Δ*nsrR/*Δ*aniA* to get the final Δ*aniA/*Δ*norB/*Δ*nsrR* mutant. The ISA cloning offers several advantages over traditional cloning by restriction digest. Firstly, it allows the user to join multiple fragments (up to 5) in a single reaction without having to use multiple restriction enzymes. Secondly, the fragments to be cloned are just added to the ISA mix which can be simply prepared and stored in aliquots for long term use **(Section 2.11.4).** So, the process is simple and reliable. In addition, it is less error prone as a viable plasmid is only generated if all the participating fragments are ligated. Therefore, it eases the painstaking step of screening a positive clone submerged in a lawn of often false positive colonies. However, it is to be noted that the success of ISA cloning is largely dependent on designing the right set of primers with overlapping end regions of participating components **(Figure 4.1 A).** Therefore, care has to be taken for choosing optimal primer for the subsequent PCR reaction condition.

PCR amplification confirmed the inactivation of *aniA, norB* and *nsrR* in the Δ*Triple* (Δ*aniA/*Δ*norB/*Δ*nsrR*) strain **(Figure 4.6).** Primer pairs were designed to amplify 1.3 Kb, 2.0 Kb and 1.4 Kb products from *aniA, norB and nsrR* regions respectively. Expected products were seen with Wt GD amplification. Similar sized bands were not seen with Δ*Triple* PCR indicating the inactivation of *aniA, norB* and *nsrR*. In lanes 2-3, the approximate 3.2 Kb band represents the 2.0 Kb spectinomycin cassette flanked by disrupted *aniA* sequence ; in lanes 5-6, the approximate 2.6 Kb band represents the 1.4 Kb kanamycin cassette flanked by disrupted *norB* sequence; in lanes 8-9, the approximate 4.0 Kb band represents the 2.5 Kb tetracycline cassette flanked by disrupted *nsrR* region. PCR reaction by *nsrR* primers produced an unexpected 1 Kb band with Wt, Δ*nsrR* and Δ*Triple* GD (Lanes 8 -10, **Figure 4.6**). This could be due to non-specific binding of primers to elsewhere in the genome. These non-specific products apparent on the gel could have been gel extracted and sequenced after cloning into a suitable plasmid vector to identify the region of genome that has been amplified. However, it was deemed not be essential as later metabolic characterisation confirmed the functional inactivation of the genes **(Section 4.2.5 and Section 4.2.6).** Confirmatory PCR for gene inactivation in Δ*aniA/*Δ*norB* and Δ*nsrR/*Δ*norB* were performed by the same sets of *aniA, norB* and *nsrR* primers. Inactivation of the genes was confirmed by the similar evident bands **(Figure**

4.7 and Figure 4.8) where the expected products were found with the Wt GD template but not with the mutant GD templates.

Downstream polar effects of the *norB* deletion were examined by measuring GpxA (NMB 1621) activity **(Figure 4.9).** In the newly created strain Δ*aniA/*Δ*norB/*Δ*nsrR* where *norB* was inactivated there was no defect in GpxA activity compared to Wt and Δ*norB*. However, it is to be noted that one of the three replicates for Wt GpxA activity showed a large variation in output compared to the other two replicates. Therefore, the inclusion of this replicate rendered the *p* value to a small amount ($p = 0.06$) which was close to being statistically significant. Therefore, more replicates have to be performed to establish that *norB* deletion did not cause any polar effect in Δ*aniA/*Δ*norB/*Δ*nsrR*.

Isogenic single mutants *(*Δ*aniA,* Δ*norB,* Δ*nsrR*) were grown alongside the newly generated strains *(*Δ*aniA/*Δ*norB,* Δ*nsrR/*Δ*norB* and Δ*aniA/*Δ*norB/*Δ*nsrR)* in an aerobic growth condition **(Figure 4.10).** No difference was seen in the measured absorbance and viable count across the strains.

Batch culture growth curves were performed to test the functional inactivation genes in Δ*aniA/*Δ*norB*, Δ*nsrR/*Δ*norB* and Δ*aniA/*Δ*norB/*Δ*nsrR* strains in the presence of 5 mM $NaNO_2$ and 50 µM SperNO **(Figure 4.11 and Figure 4.13).**

Observations with the Wt strain from batch culture growth curve in the presence of 5 mM $NaNO_2$ was concomitant with the respiration by denitrification **(Figure 4.11 and Figure 4.12)**. Initially, there could have been a small amount of NO produced by minimal activity of AniA mediated by FNR in the presence of oxygen. This could have been detoxified by constitutively expressed cytochrome c′. When all the available oxygen was utilised, the bacteria switched from aerobic growth to denitrification. This caused increased *aniA* activity by association of FNR with its promoter. As NO produced by *aniA* reached ~ 1 µM concentration threshold, *nsrR* mediated repression of *aniA* and *norB* were relieved and expression of these genes were increased. Thus, Wt strain was able to produce enough *norB* to detoxify high amounts of NO produced by *aniA* and grow rapidly in oxygen depleted condition **(Figure 4.11).** It has been demonstrated that *N. meningitidis* prefers denitrification over oxygen respiration in the presence of high amounts of intermediate NO accumulation as such in presence of 5 mM $NaNO_2$ (Rock *et al*, 2005). However, in microaerobic condition, as the concentrations of NO becomes exceedingly high (> 1 µM) it reduces the expression of *aniA.* This could be due to inactivation of FNR by dinitrosyl-iron-cysteine complex which is formed when NO binds to

the [4Fe - 4S]$^{2+}$ cluster of FNR (Cruz-Ramos *et al,* 2002). Subsequently FNR dissociates from the *aniA* promoter resulting in diminished NO_2^- reduction as FNR binding is mandatory for *aniA* expression (Lissenden *et al,* 2000). However, expression of other denitrification genes such as *norB, dnrN* remain highly activated to counteract toxicity by accumulation of excessive NO. Therefore, *N. meningitidis* tightly regulates AniA activity by dual functions of NsrR and FNR in response to varying concentrations of NO to prevent toxicity induced by NO accumulation and also to support growth by denitrification in parallel.

Media extracted from the newly created strains, Δ*aniA/*Δ*norB* and Δ*aniA/*Δ*norB/*Δ*nsrR* had the similar amount of NO_2^- **(Figure 4.11 A)** as found with the positive control at any monitored time point. The viable counts of these strains also remained steady over the course of 24 hour growth curve. However, the growth was significantly lower than the Wt at 8, 12 and 24 hour time points **(Figure 4.11 C).** This was due to the fact that when the oxygen in the media was consumed by the organism, the mutants could not switch to denitrification due lack of functional *aniA*. If both the strains had the functional denitrification genes *aniA* and *norB,* high levels of NO produced by the activity of *aniA* would have been detoxified by *norB* and their growth pattern would have been similar to that of wild type. In contrast, Δ*nsrR/*Δ*norB* was not able to deplete NO_2^- to level of Wt despite the presence of a functional *aniA* and an inactivated *nsrR* at 8, 12 and 24 hour time points **(Figure 4.11 A).** This was due to the rapid reduction of viable cells from Δ*nsrR/*Δ*norB* at these time points **(Figure 4.11 B and Figure 4.11 C).** An isogenic single Δ*norB* grows poorly compared to Wt in the presence of 5 mM NO_2^- (Anjum *et al,* 2002). For Δ*nsrR/*Δ*norB*, activity of a functional *aniA* resulted in overproduction of NO in absence of *nsrR,* which could not be detoxified due the inactivated *norB*. Accumulated NO if not detoxified can damage mitochondrial respiration by forming iron-NO complex with iron group from cytochrome oxidase (Brown, 2001). NO can reversibly inhibit cyctochrome c oxidase, the terminal enzyme of mitochondrial respiratory chain, leading to the inhibition of cellular respiration (Cleeter *et al,* 1994). The only oxidase of the meningococcal respiratory chain, cytochrome cbb_3 type oxidase is also inhibited by NO (Rock *et al,* 2005). Therefore, in the presence of 5 mM NO_2^-, Δ*nsrR/*Δ*norB* did not grow from 8 hour time point due to toxicity exerted by *aniA* activity derived NO.

It is noteworthy that in all four growth curves performed in presence of 5 mM $NaNO_2$ without agitation, Wt MC58 made a successful transition from oxidative respiration to denitrification **(Figure 4.12).** This was evidenced by the increase in growth (absorbance) coinciding with the depletion of NO_2^- **(Figure 4.12 A, B, C, D)** and thereby confirming the AniA activity.

However, there have been several studies that reported mutations in *aniA* sequence in isolates of *N. meningitidis* which is conserved across other *Neisseria spp* (Barth *et al,* 2009; Ku *et al,* 2009; Stefanelli *et al,* 2008). In other *Neisseria spp.*, AniA can receive electrons from cytochrome C_5 and via a second route via the CcoP domain of cytochrome cbb_3. However, AniA of *N. meningitidis* only receives electrons from cytochrome C_5 **(Figure 1.7)** as the second route of electron transfer from cbb_3 oxidase to *aniA* is non functional due to a single nucleotide polymorphism in the *ccoP* domain of cbb_3 which is a meningococci specific adaptation (Aspholm *et al,* 2010). This indicates that there could be an evolutionary pressure on *N. meningitidis* to remove *aniA.* Another study reported that transition from oxidation to denitrification is unstable and inconsistent in meningococci. AniA activity was observed in four out of six identical microaerobic cultures of *N. meningitidis* (Moir, 2011). According to the data presented in this chapter the denitrification occurred at different times in four identical cultures **(Figure 4.12 A, B, C and D).** This observation further verified that transition from oxidation to denitrification is sophisticated and variable. Variable transient accumulation of NO by *aniA* activity could account for the variable transition from aerobic growth to denitrification (Rock *et al,* 2005).

SperNO donates NO rapidly into the media. NO_2^- was detected as the breakdown product of NO **(Figure 4.13 A),** Δ*nsrR/*Δ*aniA* began NO_2^- depletion early at 2 hour and similar trend continued until 24 hour **(Figure 4.13 A).** This observation was not unexpected given that *norB* from Δ*nsrR/*Δ*aniA* can start metabolising NO early in the absence of *nsrR*. There was a significant increase in growth of this strain at 6 hour time point which could be due to rapid removal of NO mediated toxicity by functional *norB* **(Figure 4.13 B).** NO_2^- depletion by Wt was significantly higher compared to Δ*aniA/*Δ*norB* and Δ*aniA/*Δ*norB/*Δ*nsrR* at 8, 12 and 24 hour timepoints. However, amount of NO detected in form of NO_2^- from Δ*aniA/*Δ*norB* and Δ*aniA/*Δ*norB/*Δ*nsrR* was not significantly different compared to the media with only 50 µM SperNO supplementation **(Figure 4.13 A).**

Taken together all the observations from two batch culture growth curves, we provide evidence for functional inactivation of the *aniA, norB* and *nsrR* genes in the mutant strains, Δ*aniA/*Δ*norB,* Δ*nsrR/*Δ*norB* and Δ*aniA/*Δ*norB/*Δ*nsrR*. *nsrR* is an NO sensitive negative regulator of meningococcal denitrification genes (Rock *et al,* 2005). Unlike *E. coli nsrR*, where it regulates as many as 40 genes (Filenko *et al,* 2007), *nsrR* of *N. meningitidis* regulates a compact set of five genes. Alongside AniA and NorB, it represses the activity of DnrN, a putative protein for repairing iron-sulfur cluster in nitrosative damage and NirV, a putative

nitrite reductase assembly protein (Heurlier *et al*, 2008). It was noteworthy in none of the growth curves analysed **(Figure 4.11 and Figure 4.13),** there was any statistically significant difference in the NO_2^- and viable count output between Δ*aniA/*Δ*norB* and Δ*aniA/*Δ*norB/*Δ*nsrR*. This observation indicates that in batch culture growth conditions supplemented with NO or NO_2^-, inactivation of *nsrR* does not differentially regulate the NO metabolic output in the presence of DnrN and NirV.

5 Chapter 5: Effect of meningococcal NO metabolism on the regulation of barrier function and innate immune response in human primary bronchial airway epithelial cells

5.1 Introduction

As an exclusive coloniser of the human nasopharynx, *N. meningitidis* has to withstand high concentrations of NO present in that environment (Busch *et al,* 2000). It can use its denitrification pathway to supplement its growth under oxygen limited condition (Rock & Moir, 2005). Previously our group has shown that the NO detoxification pathway of *N. meningitidis* helps the bacteria to survive inside human MDMs and nasopharyngeal mucosa (Stevanin *et al,* 2005). The organism is an accidental pathogen and in unknown circumstances, known to be influenced by the particular meningococcal strain, environmental factors and human genetic predispositions to disease, can go on to become a deadly pathogen**.** To cause pathology, bacteria have to cross the nasopharyngeal barrier and enter into systemic circulation via the bloodstream. In order to gain access to the bloodstream following acquisition at the nasopharynx, meningococci have to interact with the nasopharyngeal epithelial barrier. This layer consists of polarised and differentiated columnar epithelial cells, which are joined by tight junctions controlling the entry of pathogens and other noxious substances. Although various types of cells such as mucus secreting goblet cells are present, the majority of the cells at this layer are ciliated forming a brush border (Chevillard *et al,* 1993). Differentiated, human primary bronchial airway epithelial cells, cultured at the air-liquid interphase (HPEC-ALI) constitutes a closely representative model of this barrier, as they consist of columnar and polarised epithelial cells with tight junctions and also contain mucus producing goblet cells. Although the cell line is developed following bronchoscopy from human bronchial epithelium, it is an ideal model for studying the biology of meningococcal interaction since the respiratory tract is covered by a differentiated columnar epithelium from the posterior nostrils down to bronchioles. Furthermore, NO is an important mediator of inflammation (Neri *et al,* 2010) and barrier function of airway epithelium (Olson *et al,* 2009). Multiple studies have demonstrated that increased NO detected from airway epithelium, in the form of its oxidation and reactive products, NO_2^-, NO_3^- correlate positively with the high level of airway inflammation (Fitzpatrick *et al,* 2009; Kharitonov & Barnes, 2006; Sittipunt *et al,* 2001).

Our group has previously established that meningococcal NO detoxification differentially regulates the cytokine TNFα release from human MDMs (Stevanin *et al,* 2007). To date there is no information on the interaction of *N. meningitidis* with HPEC-ALI. An ability to alter the barrier function and immune response by bacterial NO metabolism could modulate the interaction of meningococci with the epithelium and facilitate the colonisation and invasion process. Therefore, it was decided to use the newly generated and characterised Δ*aniA/*Δ*norB* and Δ*aniA/*Δ*norB/*Δ*nsrR* strains (Chapter 4) to infect the HPEC-ALIs to test the hypothesis that the meningococcal NO metabolism affects the barrier function and the immune response of the HPEC-ALIs. This study will also shed light on the role of genes (*dnrN* and *nirV*) (Section 1.13.3) other than the meningococcal denitrification pathway (*aniA* and *norB*) regulated by *nsrR* on the barrier function and cytokine profile of the HPEC-ALIs.

5.2 Differentiated, human primary bronchial airway epithelial cell at air-liquid interface (HPEC-ALI)

The epithelial surface of the airway is continuously exposed to inhaled noxious particles such as dust and microbes. Secretions made from the airway act as the first line of defence against the foreign particles. In this way, the epithelial barrier functions to protect the internal milieu of the lung from the external environment. HPEC-ALI culture represents a physiologically relevant model for studying the interaction of bacteria with the epithelial cell. Although once perceived as only a physical barrier, the epithelium plays a pivotal role in the maintenance of airway homeostasis. Now it is well established that the barrier function of HPEC-ALI can be split into three types: chemical, immunological and physical (Swindle *et al,* 2009). Epithelial cells can be cultured at the air-liquid interface (ALI), using defined media that helps to develop the differentiated phenotype. This cell model is typified by a pseudostratified and polarised phenotype, and contains ciliated and goblet cells with high transepithelial resistance (TER) **(Section 5.2.1)**. Goblet cells produce mucus secreting mucin for the clearance of dust particles and microbes. In addition, neuro-endocrine and clara cells are also present. Details on how the HPEC-ALI cells were cultured and maintained are described in Chapter 2 **(Section 2.9)** and **Figure 5.1** is a cartoon representing the tight junction complex of the differentiated HPEC-ALI.

5.2.1 HPEC-ALI as physical barrier

Epithelial cells make adhesive contact with adjacent cells and form sheets. This characteristic gives rise to a 'cobblestone' pattern (Boublil *et al*, 2013). Tight junctions (TJ) and adherent junctions (AJ) make up the 'apical junction complex' located closed to the airway lumen **(Figure 5.1).** TJs are pivotal for maintaining the function of epithelium as a selectively permeable barrier. They control the passage of ions and solutes via the paracellular pathway and define epithelial cell polarity by separating apical and basolateral compartment (Sawada *et al*, 2003). Transmembrane proteins such as claudins (Krause *et al*, 2008) and occludins (Furuse *et al*, 1993) make up TJs. These proteins are linked to the actin filament network by zona occludens (ZO) proteins such as ZO-1, ZO-2 and ZO-3 (Fanning & Anderson, 2009; Fanning *et al*,1998; Fanning *et al*,2012). Secreted mucus from epithelium is a part of the chemical barrier function and plays a crucial role in protecting the epithelium from toxic agents and pathogens. Mucus is highly proteinaceous and is comprised mainly of mucins. Mucins (MUC2, MUC5AC, MUC5B, MUC6) are large and highly charged proteins responsible for forming the mucus layer (Loxham *et al*, 2014). This layer protects the epithelium against a range of particles of different morphologies and sizes. **NO is an important molecule in the maintenance of epithelial barrier function (Bove *et al,* 2007; Rose *et al,* 2002).** Using both an endotoxemic murine model and Calu-3 human respiratory epithelial cell line, it was demonstrated that increased iNOS activity is responsible for altered tight junction protein expression (Han *et al*, 2004). **TER is an indirect marker of tight junction formation and barrier function integrity (Pedemonte, 1995).** The first use of TER to check cellular integrity of a cell monolayer was reported by von Bonsdorff and colleagues in 1985 (von Bonsdorff *et al*, 1985). During TER measurement, ohmic resistance of the barrier forming layer is determined using an EVOM Voltohmmeter (World precision instruments) with chopstick electrodes **(Section 2.10.3).** It is used as an indicator of barrier function permeability and a marker of disruption of the epithelial layer. **In order to examine whether the NO detoxification machinery of the meningococcus is able to modulate the physical barrier functions of the epithelium, similar to the way in which the same process acts remotely to modulate the host cell burden of *S*-nitrosothiol in iNOS-expressing macrophage cells (Laver *et al,* 2010), TER measurement of *Neisseria*–infected, differentiated, human primary bronchial airway epithelial cell at the air-liquid interphase (HPEC-ALI) was performed using a voltohmmeter.**

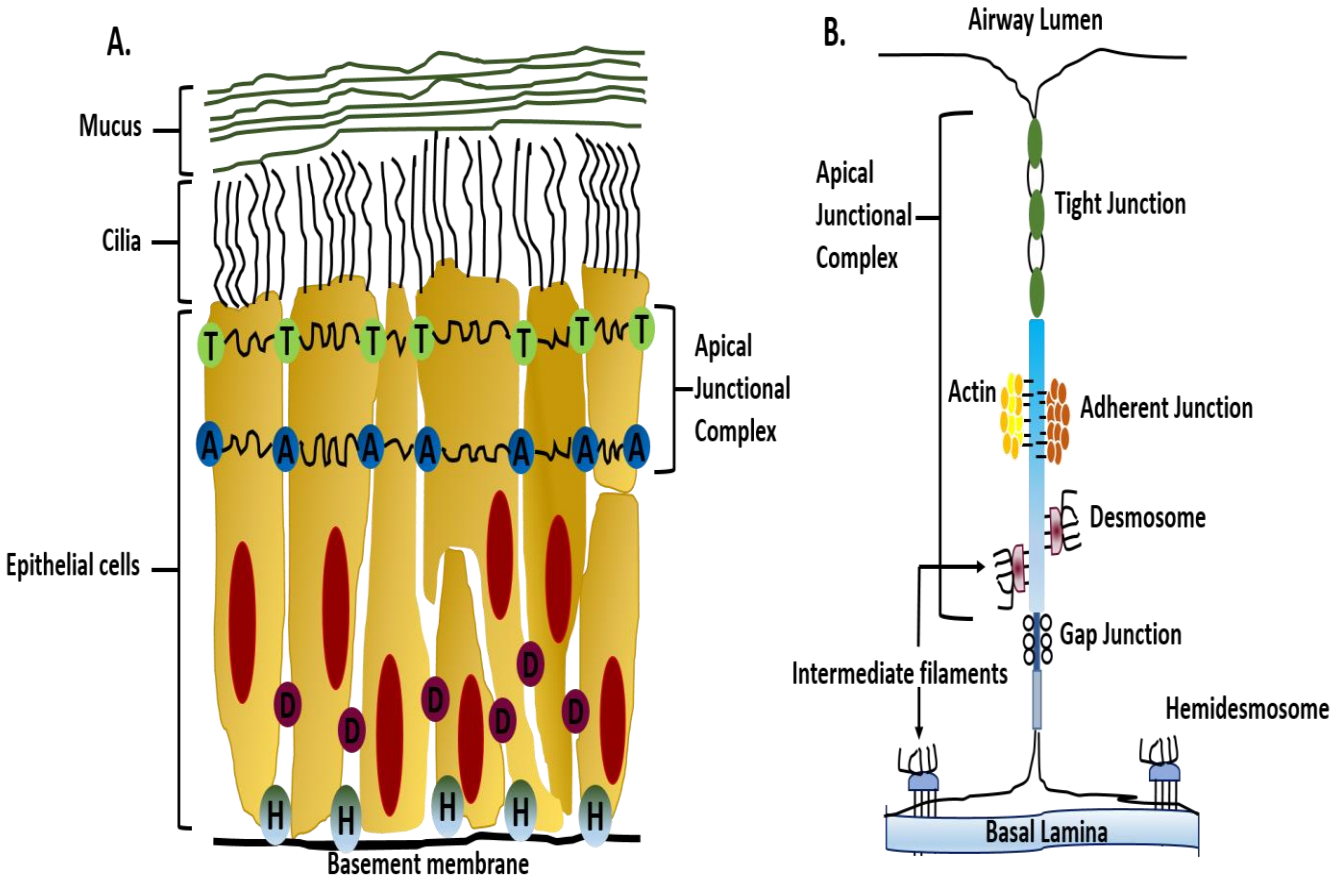

Figure 5.1 Differentiated bronchial airway epithelial cells with tight junction complex.

The primary epithelium acts as a selective barrier against the invading pathogen. This action is achieved by the activity of adhesion molecules such as tight junction (T) and adherent junction (A) present in the apical junction complex and lateral desmosomes (D), basolateral hemidesmosomes (H) anchoring cells to the basal membrane. Detail structure of the junctional complex is depicted in Figure B.

5.2.2 HPEC-ALI as chemical barrier

NO produced from epithelium is the part of the chemical barrier. All three types of NOS (eNOS, iNOS and nNOS) have been detected in human airway epithelium (Sherman *et al,* 1999). NO plays a pivotal role in lungs and has been linked with inflammatory lung disease such as asthma where high levels of exhaled NO are found (Barnes & Liew, 1995; Kharitonov *et al,* 1994). iNOS is continuously expressed in human lungs *in vivo* both at the mRNA and protein levels (Kobzik *et al,* 1993). Although basal levels of NO are detected from differentiated human airway epithelium, iNOS expression is upregulated following exposure to TNFα and IL1β. Both these factors are likely to be encountered in the aftermath of meningococcal infection. NO in airway epithelium has been implicated in the modulation of numerous functions such as epithelial ion transport (Hardiman *et al,* 2004; Helms *et al,* 2005), ciliary beat frequency (Li *et al,* 2000), antimicrobial and antiviral host defence (Darling & Evans, 2003; Zheng *et al,* 2003) and mucus secretion (Branka *et al,* 1997). **All these observations make NO a marker and modulator of the infection and inflammation of the airway epithelium.**

5.2.3 HPEC-ALI as an immunological barrier

Although most inhaled substances are cleared without an inflammatory response, the airway epithelium plays an important role in the immune defence against infection. Different PRR (pattern recognition receptor) present in the epithelium recognise pathogen associated molecular patterns (PAMP). Activation of toll-like receptors results in the activation of multiple pro-inflammatory cytokines and chemokines. Chemokine IL-8 is an important player of the immune regulation of the epithelium. A study demonstrated that NO increases IL-8 expression in lung epithelial cells (Sparkman & Boggaram, 2004). Increased IL-8 has been detected from the serum and CSF of the patients with meningococcal disease (Halstensen *et al,* 1993). A positive correlation between increased IL-8 release and meningococcal infection has been reported from the patients with fulminant meningococcal sepsis (Møller *et al,* 2005). TNFα cytokine is a marker of airway inflammation and it can also regulate TJ permeability (Steed *et al,* 2010). NO can activate Tumor Necrosis Factor-α-Converting Enzyme (TACE) by nitrosation which releases membrane bound cytokines such as TNFα (Zhang *et al,* 2000). Endogenous TNFα induces NO release from the murine retinal epithelial cell (Goureau *et al,* 1997). Although our group has established that NO denitrification of *N. meningitidis* differentially regulates the production of TNFα from human MDMs (Stevanin *et al,* 2007), there is no information on the role of meningococcal denitrification machinery on cytokine

release from the HPEC-ALIs. **Therefore, IL-8 and TNFα were measured following infection with the newly created Δ*aniA*/Δ*norB* and Δ*aniA*/Δ*norB*/Δ*nsrR* (Chapter 4) strains in this study to test the hypothesis that NO metabolism can differentially modulate the cytokine (TNFα) and chemokine (IL-8) release from the HPEC-ALIs.**

5.3 Results

5.3.1 Infection of HPEC-ALI with *N. meningitidis* results in a decreased TER and increased cytokine release but meningococcal NO metabolism does not differentially regulate the TER and cytokine release

5.3.1.1 Rationale and methods

N. meningitidis has to penetrate the nasopharyngeal or microvascular epithelium to enter the bloodstream. Differentiated HPEC-ALI mimics the human nasopharyngeal epithelial cells by having similar mucociliary and polarised properties **(Section 5.2).** Since NO is an important mediator of barrier function and modulator of the immune response in airway epithelium **(Section 5.2.1, 5.2.2 and 5.2.3),** it was decided to examine the effect of meningococcal NO metabolism on the TER and cytokine release of HPEC-ALIs.

HPECs were obtained from the healthy volunteers by epithelial brushing **(Section 2.9.4.1).** The cells were seeded onto collagen coated transwell **(Section 2.9.4.3).** Each transwell containing plate was incubated overnight (at 37°C, 5% CO_2) to allow the formation of a confluent monolayer. After reaching confluence, apical media was removed to take the cells to the air-liquid interphase (ALI) **(Section 2.9.4.4).** Media from the basal compartment was removed and replaced with ALI media **(Section 2.9.3.6)** which contained high concentration of retinoic acid and growth factor containing BEGM media. Retinoic acid and other growth factors promoted the differentiation of the HPEC-ALI. The TER reading was checked after 7, 14 and 21 days to confirm the differentiation state **(Section 2.9.4.7)**. After roughly 21 days the cells were observed by microscopy for the presence of cobblestone type phenotype. In addition, TER reading was checked to examine if it fell within the range of 1.0 Ω - 3.0 Ω, which is a marker of differentiated HPEC. Ciliated cells were observed by microscopy after 18-21 days. These characteristics confirmed the differentiated state of the HPEC-ALI **(Figure 2.1).** Penicillin/streptavidin antibiotics in the ALI media were normally used for the maintenance of ALI cultures to avoid contamination **(Section 2.9.4.6)** but were removed on the day before the experiment to avoid interference with bacterial growth during infection. Cells from one transwell were trypsinised and the cell number was counted using a hemocytometer **(Section 2.9.4.8).** The cell count was used to calculate the amount of bacterial cells required for each Multiplicity of Infection (MOI). Approximately 0.2 - 0.7 x 10^6 cells were found from one transwell and this count was used to determine the required multiplicity of infection (MOI). TER reading was taken using an EVOM voltohmmeter prior to infection. After washing in IMS

and HBSS solutions, the dried electrodes were positioned at 90° angle to the base of the plate, with the longest electrode on the outside (basal) and shortest electrode on the inside (apical) side of the transwell insert and TER reading was noted **(Section 2.10.3)**. Wild type *Neisseria meningitidis* strain MC58 and the Δ*aniA/*Δ*norB* and Δ*aniA/*Δ*norB/*Δ*nsrR* mutant derivatives thereof were grown up in MHB to mid log phase. Bacteria were pelleted, washed and then resuspended into 100 µl HBSS at the appropriate MOI (1 to 100). Infected HBSS was added to the apical compartment. To minimise disruption to the air-liquid interface, and to roughly simulate *in vivo* conditions (whereby potentially colonising meningococci are introduced to the epithelium via respiratory fomites), it was decided to keep the period of infection to a minimum (1 hour). In addition, preliminary experiments showed that the presence of infection bolus in apical compartment longer than 1 hour significantly reduces the viability of the HPEC-ALIs (data not shown). After 1 hour, the infected HBSS was carefully aspirated from the apical compartment. The HPEC-ALIs were then incubated at 37°C, 5% CO_2 for a further 24 hour. After 24 hour, 100 µl of HBSS was added to the apical compartment of each well and incubated for 15 minutes to extract apical secretions. Subsequently TER was measured by EVOM Voltohmmeter **(Section 2.10.3).** Bacterial viability on the apical surface was determined by tenfold serial dilution and plating on Columbia Blood agar, retrospectively adjusting for dilution factor and volume of the apical supernatant. The remainder of the apical and basolateral secretions were collected in microcentrifuge tubes and supernatants were stored in the freezer after centrifugation. The supernatants were later used to measure the concentrations of IL-8 and TNFα by ELISA **(Section 2.8.1)**. IL-8 released from both the basal and apical compartments were measured, however detectable levels of TNFα were only measurable in the supernatant derived from the basal compartment (data not shown). A generic overview of the experimental procedures in presented in **Figure 5.2**.

5.3.1.2 Results

As can be seen from **Figure 5.3 A**, bacterial infection with MOI 1-100 lowers TER readings of HPECs compared to control. However, only infection with MOI 100 of Wt (0.35 Ω ± 0.08), Δ*aniA/*Δ*norB* (0.31 Ω ± 0.07) and Δ*aniA/*Δ*norB/*Δ*nsrR* (0.41 Ω ± 0.12) were found to be statistically significant compared to control TER (1) ($p< 0.05$). Importantly, a negative correlation between bacterial load and TER (Spearman correlation test. $p = 0.01$) was found **(Figure 5.3 B)**. Mutant bacteria with disrupted denitrification pathways, Δ*aniA/*Δ*norB* and Δ*aniA/*Δ*norB/*Δ*nsrR*, did not differentially modulate the TER response.

TNFα from the apical compartment was below the limits of detection (data not shown). There was an increase in TNFα output from the basolateral compartment when cells were infected at MOI 100 of Wt MC58 (131.7 pmol/µl ± 27.29), Δ*aniA/*Δ*norB* (181.2 pmol/µl ± 53.53) and Δ*aniA/*Δ*norB/*Δ*nsrR* (138.1 pmol/µl ± 33.88), as compared to control (13.88 pmol/µl ± 5.78) (**Figure 5.4 A**). However, the increase was only significant in the case of Δ*aniA/*Δ*norB* ($p < 0.05$). A positive correlation between bacterial load and TNFα (Spearman correlation test, $p = 0.01$) was also found **(Figure 5.4 B).**

Figure 5.5 shows that infection of cells at MOI 100 led to a significant increase in the concentration of IL-8 in the apical compartment, Wt (6.81×10^4 pmol/µl ± 2.34×10^4), Δ*aniA/*Δ*norB/*Δ*nsrR* (6.49×10^4 pmol/µl ± 1.43×10^4), as compared to the uninfected control (3.68×10^3 pmol/µl ± 704.3) ($p < 0.05$). A similar pattern was noticed in the basolateral compartment (**Figure 5.6**). Compared to the control (3.86×10^3 pmol/µl ± 1.21×10^3), infection of epithelial cells at an MOI 100 of Wt (6.93×10^4 pmol/µl ± 1.85×10^4), Δ*aniA/*Δ*norB* (7.65×10^4 pmol/µl ± 3.52×10^4) and Δ*aniA/*Δ*norB/*Δ*nsrR* (7.66×10^4 pmol/µl ± 3.23×10^4), significantly increased basal IL-8 release from HPECs-ALI ($p < 0.05$).

However, neither of the cytokines examined was differentially altered by the newly created strains Δ*aniA/*Δ*norB* and Δ*aniA/*Δ*norB/*Δ*nsrR* compared to Wt infection.

As can be seen from Tables 5.1 and 5.2, there was no significant difference in the number of viable bacteria used to inoculate the epithelial cells (**Table 5.1**) **(Figure 5.7 A),** or in the output supernatant collected after the infection period (**Table 5.2**) **(Figure 5.7 B).** Interestingly, the number of output viable bacteria recovered for MOI 1-100 infections were not significantly different, indicating our bacterial population had in each case grown up to the highest levels sustainable by the HPEC-ALI model.

Table 5.1 Input viable count

Strain	Cfu/ml
Wt	1.45×10^8 cfu/ml ± 2.78×10^7
Δ*aniA*/Δ*norB*	1.64×10^8 cfu/ml ± 4.28×10^7
Δ*aniA*/Δ*norB*/Δ*nsrR*	1.66×10^8 cfu/ml ± 5.26×10^7

Table 5.2 Output viable count

Strain	MOI	Cfu/ml
Wt	1	4.83×10^6 cfu/ml ± 3.27×10^6
	10	2.67×10^6 cfu/ml ± 2.20×10^6
	100	3.38×10^6 cfu/ml ± 2.74×10^6
Δ*aniA*/Δ*norB*	1	1.22×10^7 cfu/ml ± 4.00×10^6
	10	1.37×10^7 cfu/ml ± 8.85×10^6
	100	2.08×10^7 cfu/ml ± 6.07×10^6
Δ*aniA*/Δ*norB*/Δ*nsrR*	1	2.28×10^6 cfu/ml ± 1.34×10^6
	10	3.88×10^6 cfu/ml ± 1.42×10^6
	100	1.88×10^7 cfu/ml ± 6.64×10^6

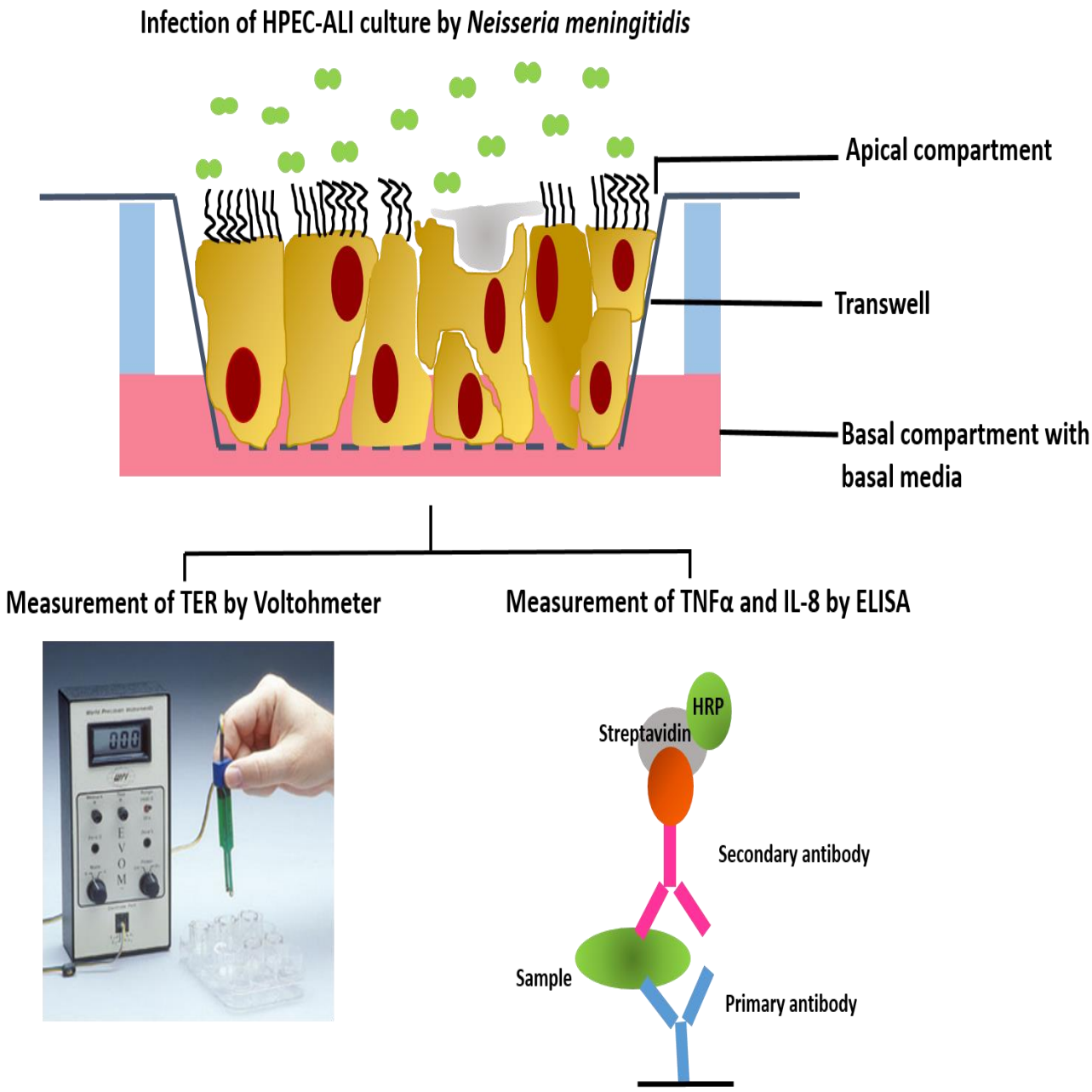

Figure 5.2 Methods for measuring TER, TNFα and IL-8 after infecting the HPEC-ALI culture with denitrification mutants of *N. meningitidis.*

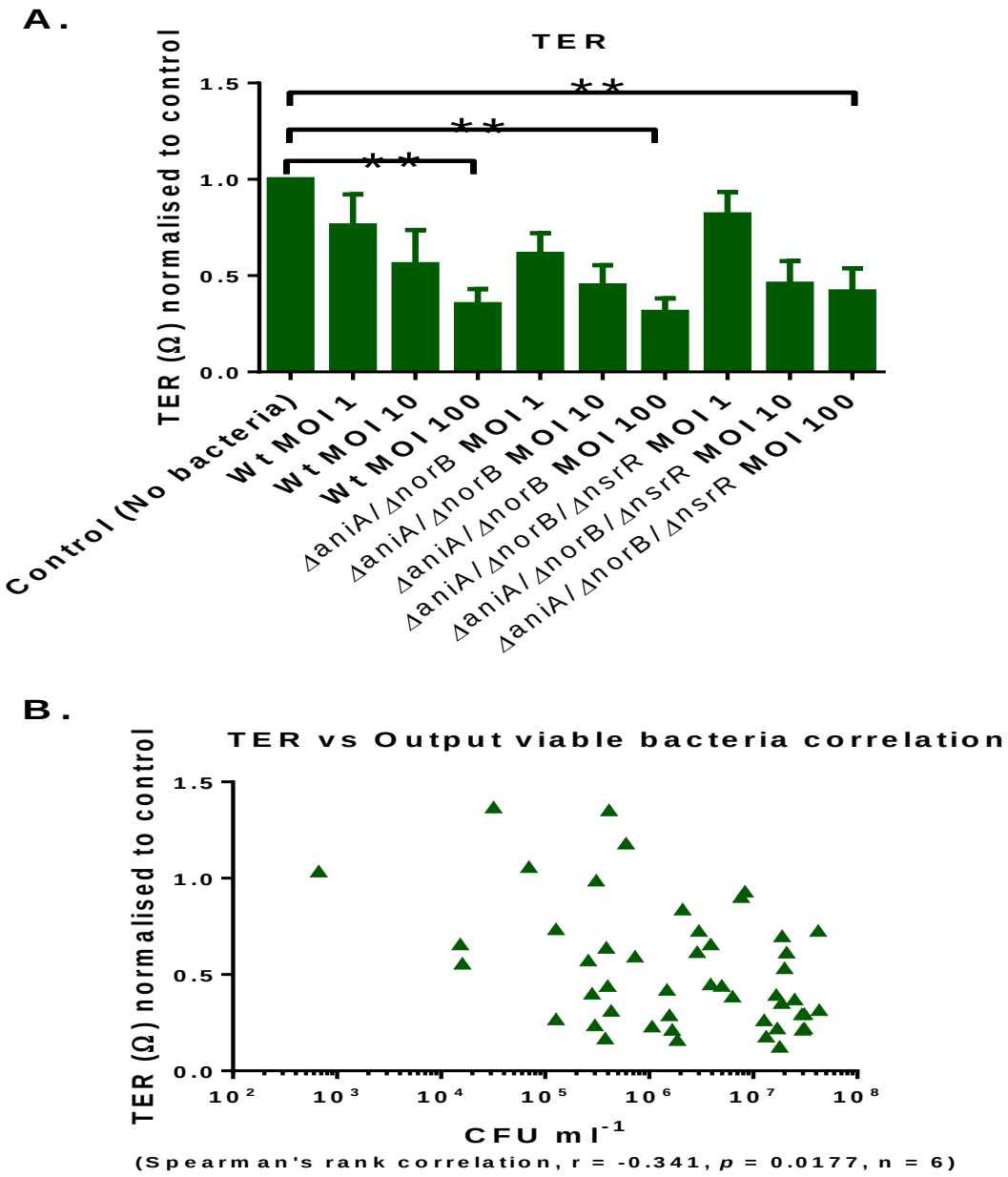

Figure 5.3 Measurement of A) TER and B) Correlation graph for TER vs Output viable count of the differentiated HPEC-ALI infected with Wt, Δ*aniA*/Δ*norB*, Δ*aniA*/Δ*norB*/Δ*nsrR* (MOI 1-100).

Bacteria grown up to logarithmic phase were used to infect the HPEC-ALIs for 1 hour suspended in 100 µl HBSS after measuring the **A) TER (Section 2.10.3).** Then after removing the bacteria, plate was incubated for 24 hours at air-liquid interphase. Following day 100 µl HBSS was added to the transwells and incubated for 15 minutes. Then TER was measured by Voltohmmeter. TER reading before and after the experiments were used to calculate the final TER and normalised to the control (No bacteria) condition. Data represents mean ± SEM * p< 0.05, One way ANOVA with Dunn's multiple comparison test, n= 6. **B) Statistically significant negative correlation between recovered output bacterial burden and TER reading.** Spearman's rank correlation test, graphpad prism.

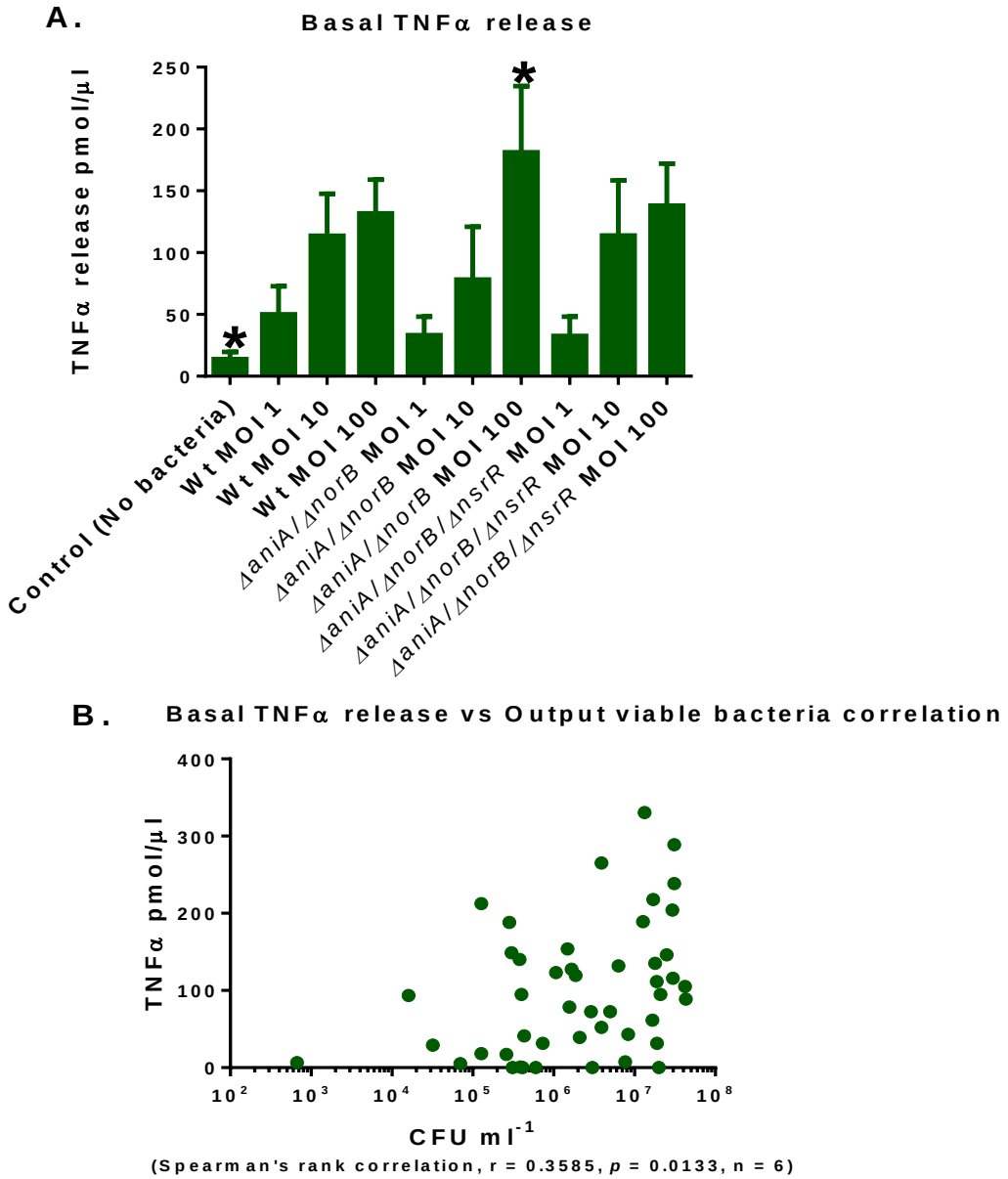

Figure 5.4 Measurement of A) TNFα and B) Correlation graph for TNFα vs Output viable count of the differentiated HPEC-ALI infected with Wt, Δ*aniA/*Δ*norB,* Δ*aniA/*Δ*norB/*Δ*nsrR* (MOI 1-100).

Bacteria grown up to logarithmic phase were used to infect HPECs for 1 hour suspended in 100 µl HBSS after measuring the TER **(Section 2.10.3).** Then after removing the bacteria, plate was incubated for 24 hours at air-liquid interphase. Following day 100 µl HBSS was added to the transwells and incubated for 15 minutes. Basal supernatant was collected and TNFα was measured by ELISA in duplicates **(Section 2.8.1).** Data represents mean ± SEM * $p< 0.05$, One way ANOVA with Tukey's multiple comparison test, n= 6. **B) Statistically significant positive correlation between recovered output bacterial burden and basal TNFα release.** Spearman's rank correlation test, graphpad prism.

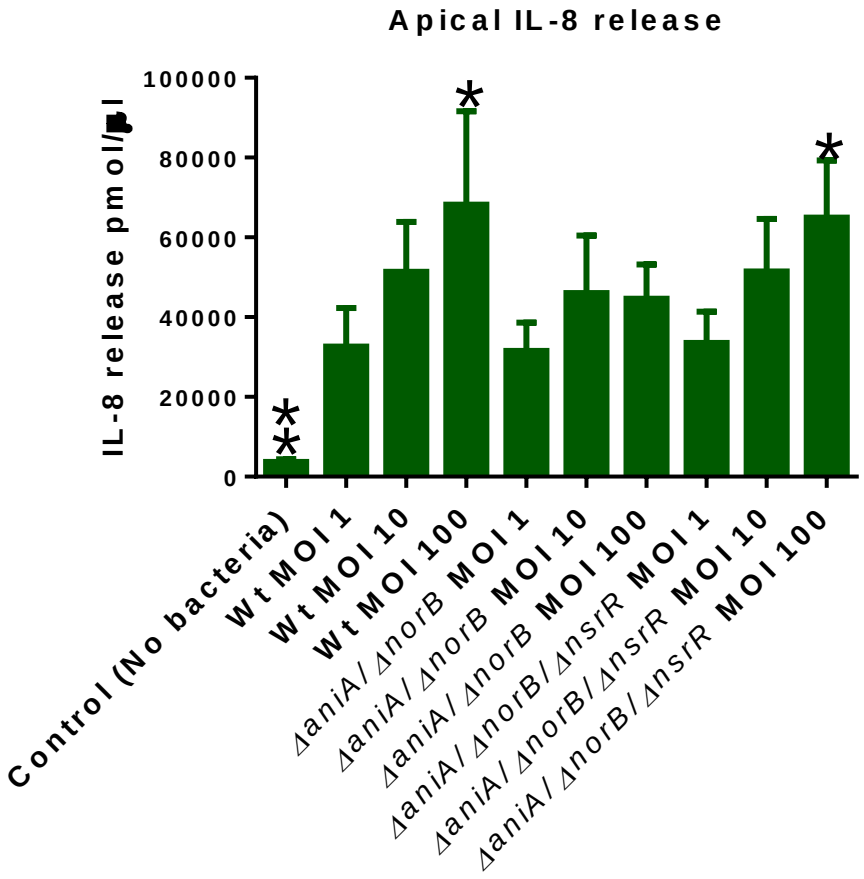

Figure 5.5 Measurement of IL-8 release from the apical compartment of the differentiated HPEC-ALIs infected with Wt, Δ*aniA/*Δ*norB*, Δ*aniA/*Δ*norB/*Δ*nsrR* (MOI 1-100).

Cells were infected for an hour with logarithmic phase bacteria (Wt**,** Δ*aniA/*Δ*norB,* Δ*aniA/*Δ*norB/*Δ*nsrR)* suspended in 100 µl HBSS. After removing bacteria, HPECs were incubated further at air-liquid interphase for 24 hours. After 24 hour 100 µl HBSS was added to the apical compartment and supernatant was collected after centrifugation. IL-8 concentration was determined by ELISA in duplicates **(Section 2.8.1).** Data represents mean ± SEM. **p*<0.05, One way ANOVA with Tukey's multiple comparison test. n = 6.

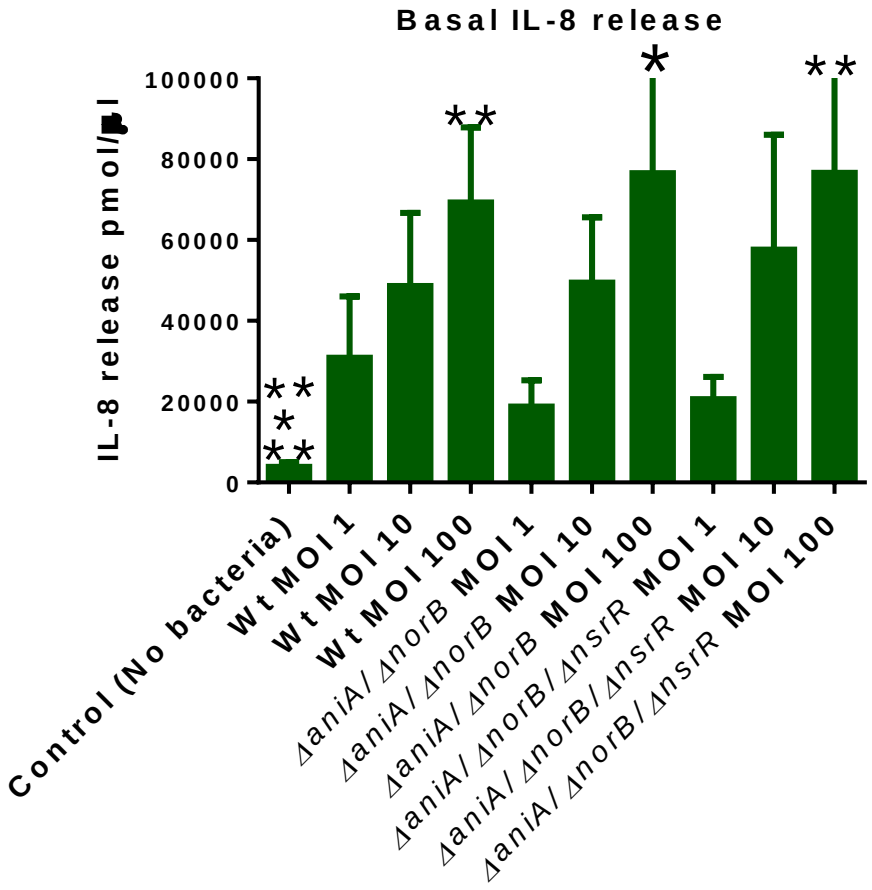

Figure 5.6 Measurement of IL-8 release from the basolateral compartment of the differentiated HPEC-ALIs infected with Wt, Δ*aniA*/Δ*norB*, Δ*aniA*/Δ*norB*/Δ*nsrR* (MOI 1-100).

Cells were infected for an hour with logarithmic phase bacteria (Wt**,** Δ*aniA*/Δ*norB,* Δ*aniA*/Δ*norB*/Δ*nsrR)* suspended in 100 µl HBSS. After removing bacteria, HPECs were incubated further at air-liquid interphase for 24 hours. After 24 hour 100 µl HBSS was added to the apical compartment and supernatant was collected after centrifugation. Basolateral supernatant was also collected from basal compartment after centrifugation. Basal IL-8 concentration was determined by ELISA in duplicates **(Section 2.8.1).** Data represents mean ± SEM. *p<0.05, **p<0.01, Kruskal Wallis test, n = 6.

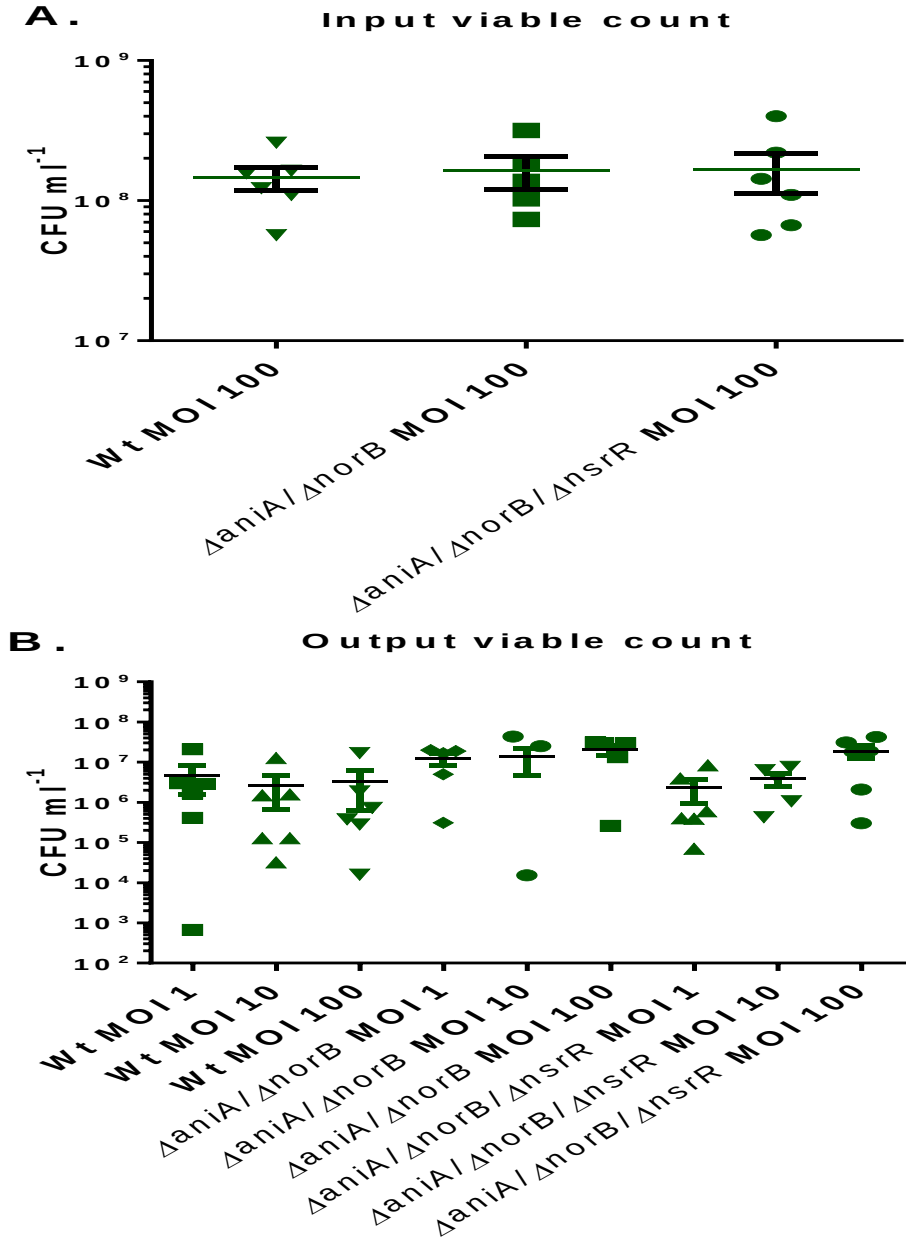

Figure 5.7 A) Input and B) Output viable count from the differentiated HPEC-ALI infected with Wt, Δ*aniA/*Δ*norB*, Δ*aniA/*Δ*norB/*Δ*nsrR* at MOI 1-100.

A) Bacteria were grown up to logarithmic phase. Appropriate number of bacterial pellet was resuspended in HBSS to give MOI 1- 100 and was used to infect the HPEC-ALIs. Triplicates of 10 µl aliquots of each dilution were separately spotted on Columbia blood agar plates. Following overnight incubation at 37°C, 5% CO_2, the mean number of colonies for each dilution were counted and corrected for the dilution factor and volume. **B)** After 24 hour 100 µl HBSS was added to the apical compartment and an aliquot of this was used to determine the number of viable bacteria post incubation. Data represents mean ± SEM. Kruskal Wallis test, n =6

5.3.2 Induction of HPEC-ALI with a slow releasing NO donor SNAP (S-Nitroso-N-acetyl-DL-Penicillamine) does not affect the TER and cytokine profile of HPEC-ALI in relation to meningococcal NO denitrification pathway

5.3.2.1 Rationale and methods

Infection of epithelial cells with the newly created meningococcal denitrification mutants did not differentially modulate the TER and cytokine release from HPEC-ALIs in the presence of *de novo* synthesised NO (**Section 5.3.1**). Although human airway inflammation is reported to be an NO rich environment (Bove & van der Vliet, 2006), it is conceivable that the lack of any measurable impact of the meningococcal partial denitrification pathway on the epithelial barrier parameters was due to an insufficiency in the overall levels of NO in each well. Given the chemistry of NO, including its high partition coefficient and freely diffusible nature, it is likely that the NO concentration present in the airway is much higher than a small number of infected epithelial cells can generate *de novo*. Concentrations of NO in exhaled breath represent the accumulated synthesis of NO from thousands of epithelial cells, in addition to iNOS-mediated responses by cellular mediators of innate immunity such as macrophages. It is plausible therefore, given their location on the respiratory surface; that the aggregative, 'cloud' effect of NO generation results in exposure of HPEC-ALI cells *in situ* to much higher concentrations of NO than they are able to generate themselves *in vitro*. The NO insufficiency in this model might in turn mean that the critical threshold concentration of NO required to de-repress NsrR-regulated promoters in *N. meningitidis* is not reached, with the result that the genetic differences between the strains used in this study do not translate into phenotypic differences. To ensure that the partial denitrification pathway of our strains is being de-repressed by NO, it was decided to supplement the HPEC-ALI model with media containing a slow releasing NO donor, SNAP. This was done for two main reasons. Firstly, SNAP is a slow releasing NO donor which has a half-life of 5 hour in aqueous solution (Ignarro *et al,* 1981). So the bacterial strains and HPEC-ALIs will be exposed to NO over a longer period of time for relieving the *nsrR* mediated repression of the meningococcal denitrification. Secondly, a concentration of 500 µM SNAP differentially regulates the chemokine and cytokine profile of human MDMs (Stevanin *et al,* 2007) and lowers the IL-8 release of the human bronchial epithelial (HBEC) cells (Neri *et al,* 2010). However, there is no information on the effects of SNAP and meningococcal denitrification machinery on HPEC-ALI. The HPEC-ALIs were infected with MOI 100 of Wt, Δ*aniA*/Δ*norB* and Δ*aniA*/Δ*norB*/Δ*nsrR* in the presence of 500

µM SNAP in the basal compartment. The rest of the experimental procedures were carried out as mentioned in **Section 5.3.1.1.**

5.3.2.2 Results

Figure 5.8 demonstrates that infection with meningococcal infection significantly reduced the TER (Wt MOI 100, 0.55 Ω ± 0.04; Δ*aniA/*Δ*norB* MOI 100, 0.66 Ω ± 0.01 ; Δ*aniA/*Δ*norB/*Δ*nsrR* MOI 100, 0.66 Ω ± 0.14) of HPEC-ALIs compared to control (1 Ω) ($p < 0.05$). However, meningococcal denitrification pathway did not differentially regulate the TER response of HPEC-ALI.

There was a statistically non-significant increase in TNFα release with bacterial infection (Wt MOI 100, 239.5 pmol/µl ± 103.3; Δ*aniA/*Δ*norB* MOI 100, 99.22 pmol/µl ± 77.34; Δ*aniA/*Δ*norB/*Δ*nsrR* MOI 100, 109.6 pmol/µl ± 82.32) compared to control (32.31 pmol/µl ± 29.52) and 500 µM SNAP (84.58 pmol/µl ± 73.80) ($p = 0.46$) **(Figure 5.9)**

Similar non-significant increase was noticed for apical IL-8 secretion with meningococcal infection (Wt MOI 100, 6.99×10^4 pmol/µl ± 7.01×10^3, Δ*aniA/*Δ*norB* MOI 100, 7.35×10^4 pmol/µl ± 9.03×10^3; Δ*aniA/*Δ*norB/*Δ*nsrR* MOI 100, 8.18×10^4 pmol/µl ± 1.64×10^4) compared to control (3.21×10^4 pmol/µl ± 3.0×10^4) and 500 µM SNAP (3.6×10^4 pmol/µl ± 2.35×10^4) ($p = 0.29$) **(Figure 5.10)** and also from basal IL-8 secretion (Wt MOI 100, 6.74×10^4 pmol/µl ± 2.31×10^4; Δ*aniA/*Δ*norB* MOI 100, 5.72×10^4 pmol/µl ± 2.95×10^4; Δ*aniA/*Δ*norB/*Δ*nsrR* MOI 100, 6.98×10^4 pmol/µl ± 2.01×10^4) compared to control (3.75×10^4 pmol/µl ± 2.4×10^4) and 500 µM SNAP (3.66×10^4 pmol/µl ± 2.43×10^4) ($p = 0.79$) **(Figure 5.11).** But meningococcal denitrification machinery did not significantly alter the release of IL-8 from neither apical nor the basal compartment.

It was important to note that there was no statistically significant difference in input viable count of any of the strains (Wt MOI 100, 1.58×10^8 cfu/ml ± 3.21×10^7; Δ*aniA/*Δ*norB* MOI 100, 1.75×10^8 ± 3.94×10^7; Δ*aniA/*Δ*norB/*Δ*nsrR* MOI 100, 1.9×10^8 cfu/ml ± 3.79×10^7) ($p = 0.83$) **(Figure 5.12 A).** Non-significant difference was also observed in output viable count after infection (Wt MOI 100, 3.80×10^6 cfu/ml ± 3.75×10^6; Δ*aniA/*Δ*norB* MOI 100, 3.07×10^7 ± 2.96×10^7; Δ*aniA/*Δ*norB/*Δ*nsrR* MOI 100, 5.24×10^6 cfu/ml ± 5.23×10^6) ($p = 0.51$) **(Figure 5.12 B).**

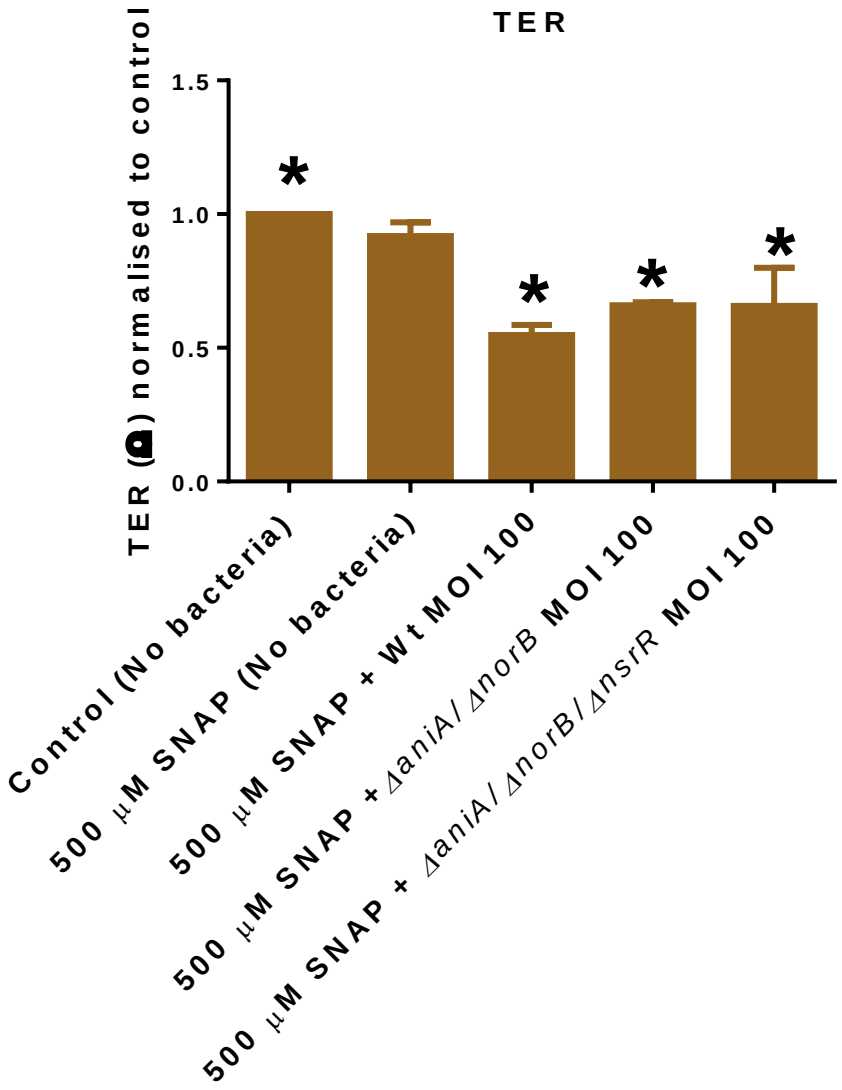

Figure 5.8 Measurement of TER of the differentiated HPEC-ALI infected with Wt, Δ*aniA/*Δ*norB,* Δ*aniA/*Δ*norB/*Δ*nsrR* (MOI 100) in the presence of 500 µM SNAP.

Bacteria grown up to logarithmic phase were used to infect HPECs for an hour suspended in 100 µl HBSS containing 500 µM SNAP after measuring TER **(Section 2.10.3)**. In addition, 500 µM SNAP was also added to the basal compartment. Then after removing the HBSS after 1 hour, HPEC-ALIs were incubated further for 24 hours. Following day 100 µl HBSS was added to the transwells and incubated for 15 minutes. Then TER was measured by Voltohmmeter. TER reading before and after the experiments were used to calculate the final TER and normalised to the control (No bacteria) condition. Data represents mean ± SEM * $p < 0.05$, One way ANOVA with Tukey's multiple comparison test, n= 3.

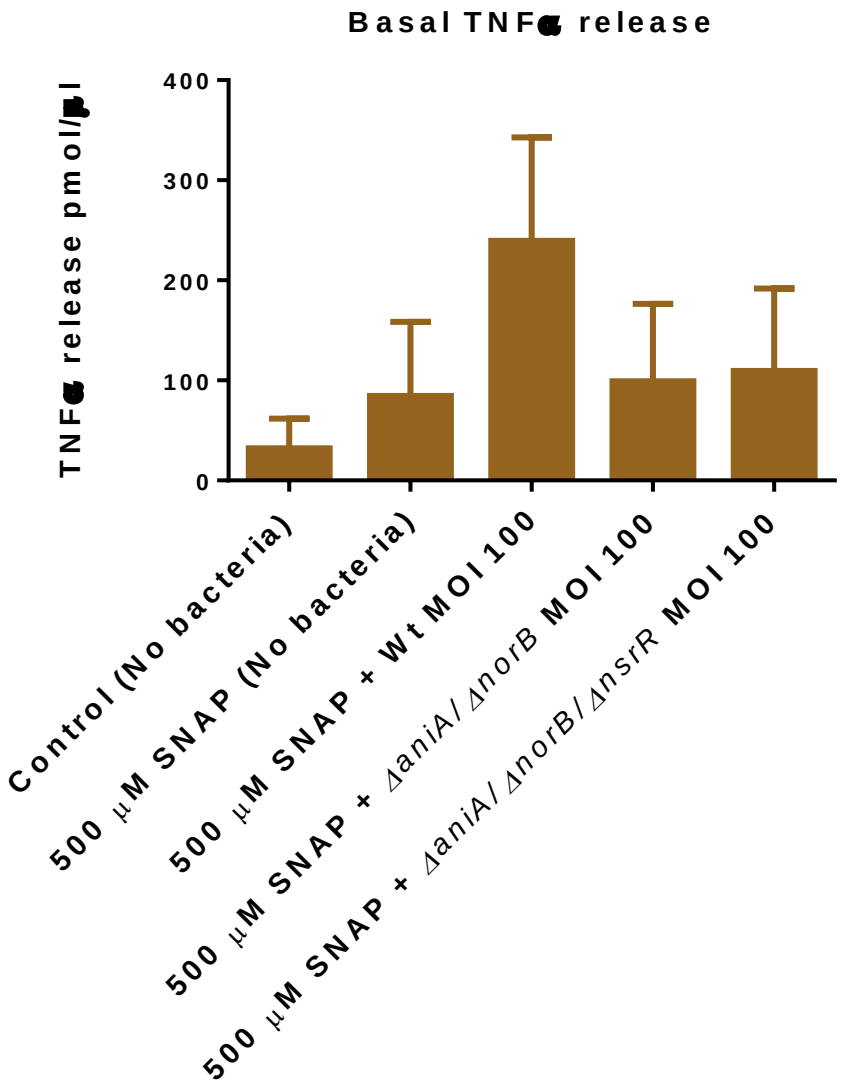

Figure 5.9 Measurement of TNFα of the differentiated HPEC-ALIs infected with Wt, Δ*aniA/*Δ*norB,* Δ*aniA/*Δ*norB/*Δ*nsrR* (MOI 100) in the presence of 500 µM SNAP.

Bacteria grown up to logarithmic phase were used to infect HPECs for an hour suspended in 100 µl HBSS containing 500 µM SNAP after measuring TER **(Section 2.10.3)**. In addition, 500 µM SNAP was also added to the basal compartment. Then after removing the HBSS after 1 hour, HPEC-ALIs were incubated further for 24 hours. Following day 100 µl HBSS was added to the transwells and incubated for 15 minutes. Basal supernatant was collected and TNFα was measured by ELISA in duplicates **(Section 2.8.1).** Data represents mean ± SEM One way ANOVA with Tukey's multiple comparison test, n= 3.

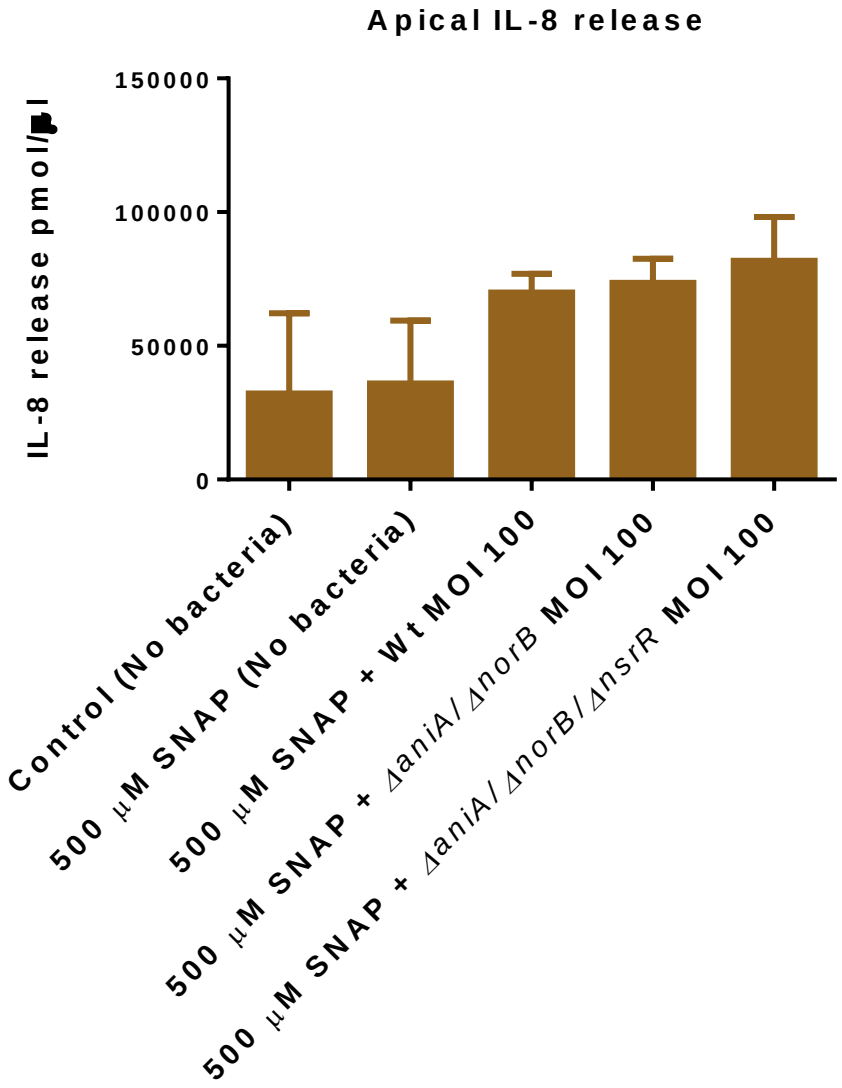

Figure 5.10 Measurement of IL-8 release from apical supernatants of the differentiated HPEC-ALIs infected with Wt, Δ*aniA/*Δ*norB*, Δ*aniA/*Δ*norB/*Δ*nsrR* (MOI 100) in the presence of 500 µM SNAP.

Cells were infected for an hour with logarithmic phase bacteria (Wt**,** Δ*aniA/*Δ*norB,* Δ*aniA/*Δ*norB/*Δ*nsrR*) suspended in 100 µl HBSS containing 500 µM SNAP. In addition, 500 µM SNAP was also added to the basal compartment. After removing bacteria after 1 hour, HPEC-ALIs were incubated further for 24 hours. 100 µl HBSS was added to the apical compartment and supernatant was collected after centrifugation. IL-8 concentration was determined by ELISA in duplicates **(Section 2.8.1).** Data represents mean ± SEM. One way ANOVA with Tukey's multiple comparison test, n = 3.

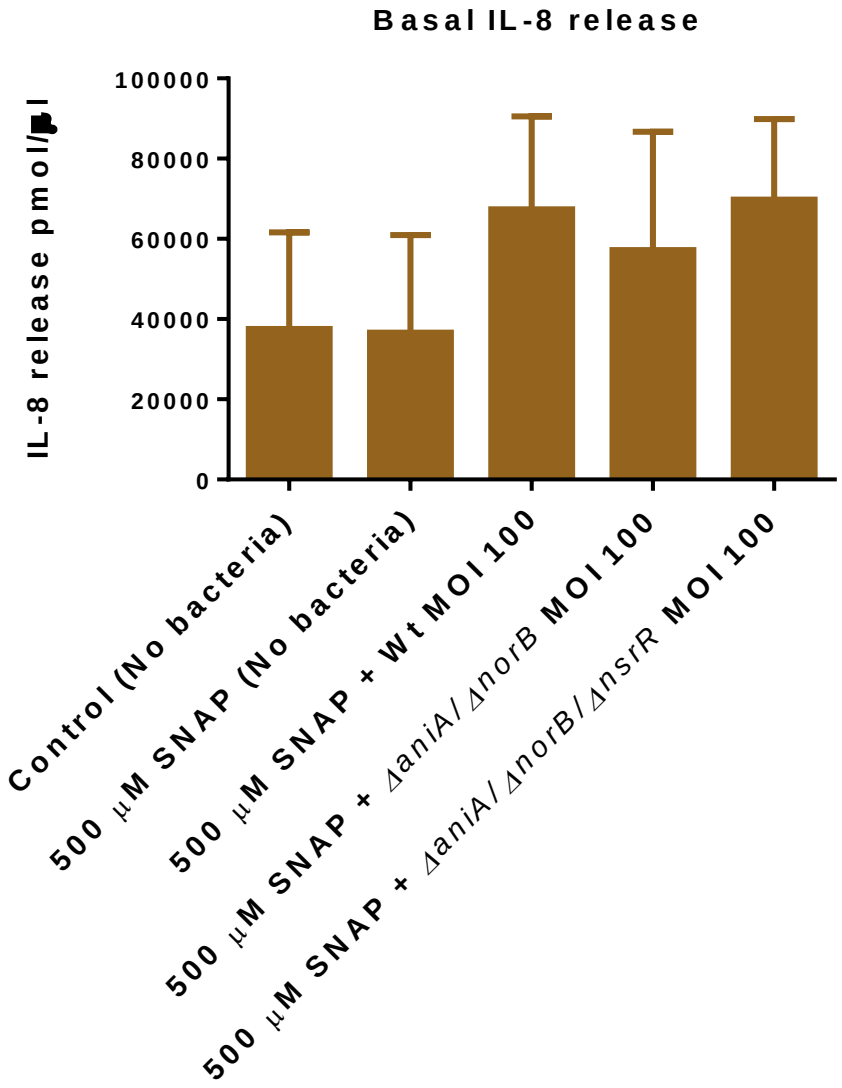

Figure 5.11 Measurement of IL-8 release from basal supernatants of the differentiated HPEC-ALIs infected with Wt, Δ*aniA/*Δ*norB*, Δ*aniA/*Δ*norB/*Δ*nsrR* (MOI 100) in the presence of 500 µM SNAP.

Cells were infected for an hour with logarithmic phase bacteria (Wt**,** Δ*aniA/*Δ*norB,* Δ*aniA/*Δ*norB/*Δ*nsrR*) suspended in 100 µl HBSS containing 500 µM SNAP. In addition, 500 µM SNAP was also added to the basal compartment. After removing bacteria after 1 hour, HPEC-ALIs were incubated further for 24 hours. 100 µl HBSS was added to the apical compartment and supernatant was collected after centrifugation. Basolateral supernatant was also collected from basal compartment after centrifugation. IL-8 concentration was determined by ELISA in duplicates **(Section 2.8.1).** Data represents mean ± SEM. One way ANOVA with Tukey's multiple comparison test, n = 3.

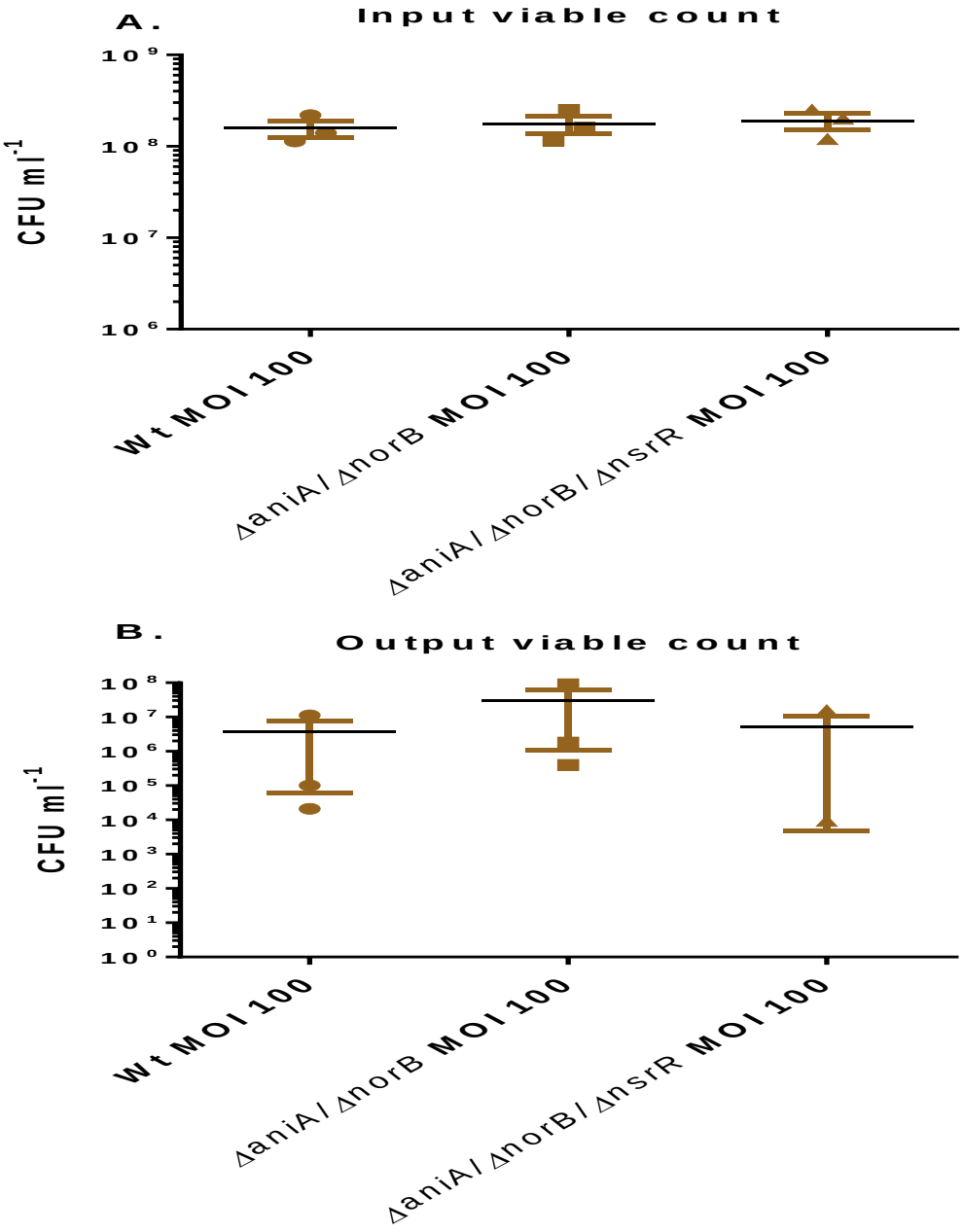

Figure 5.12 A) Input and B) Output viable count from the differentiated HPEC-ALI infected with Wt, Δ*aniA*/Δ*norB*, Δ*aniA*/Δ*norB*/Δ*nsrR* at MOI 100 in the presence of 500 µM SNAP.

A) Bacteria were grown up to logarithmic phase. Appropriate number of bacterial pellet was resuspended in HBSS to give MOI 1 - 100. Triplicate of 10 µl aliquots of each dilution were separately spotted on Columbia blood agar plates. Following overnight incubation at 37˚C, 5% CO_2, the mean number of colonies for each dilution were counted and corrected for the dilution factor and volume. **B)** After 24 hour, 100 µl HBSS was added to the apical compartment and an aliquot of this was used to determine the number of viable bacteria post incubation. Data represents mean ± SEM. One way ANOVA with Tukey's multiple comparison test, n = 3.

5.4 Discussion

There have been numerous studies on the interaction of *N. meningitidis* with epithelial cell lines. Unlike other studies where immortalised epithelial cells such as T84 (colonic epithelial cell) (Pujol *et al,* 1997) (Merz *et al,* 1996) or Calu-3 (human bronchial epithelial cell) (Sutherland *et al,* 2010) have been used for studying the interaction of meningococci with epithelial cells, the HPEC-ALI used in this study constitutes a closer representation of the *in vivo,* nasopharyngeal environment. This chapter reports the first investigation of the effect of the meningococcal partial denitrification pathway on the barrier function and immune response of HPEC-ALI. However, despite our best efforts to mimic the *in vivo* environment of these cells, including supplementation of the system with NO donor compounds, our investigation shows that meningococcal denitrification machinery does not modulate the barrier function and immunological profile of HPEC-ALIs.

There have been contradictory findings on the route meningococci take to traverse the epithelium. Using a bilayer model consisting of endometrial and epithelial-endothelial cells, it was demonstrated that meningococci use both para and transcellular routes for the traversal of epithelium (Birkness *et al,* 1995). In contrast, the meningococcus crosses the brain microvascular endothelium using a paracellular route, as evidenced by the depletion of junction proteins (Coureuil *et al,* 2009). Another study using T84, a human polarised colonic epithelial cell, demonstrated that meningococci can cross the epithelial monolayer without altering the tight junctions (Merz *et al,* 1996). More investigations have demonstrated that the meningococcus traverses the T84 human polarised colonic epithelial cell and the Calu-3 respiratory epithelial using a transcellular route, without disrupting the TER (Pujol *et al,* 1997; Sutherland *et al,* 2010). In contrast to studies with these immortalised and non-contextual cell lines, where TER is unperturbed by meningococcal infection; the current study reports a decrease in TER of a primary HPEC monolayer. This dose-dependent phenomenon shows a positive correlation between bacterial load and a decrease in TER (**Figure 5.3 B)**. Infection with any of our bacterial strains at MOI 100 significantly reduced the TER in all conditions **(Figure 5.3 and 5.8).** A reduction in TER following bacterial infection has been reported for other bacterial species. Infection with enteropathogenic *E.coli* also causes a significant reduction in TER of Caco-2 and MDCK epithelial cells without disrupting the tight junction protein (Canil *et al,* 1993). Progressive decreases in TER with modification of tight junction structures was noticed with *Salmonella typhimurium* infection of MDCK epithelium (Jepson *et al,* 1995). Infection of T84 with *Campylobacter jejuni* significantly reduces TER and disrupts

the tight junction complex (Wine *et al,* 2008). Tight junction function could be altered due to the infection with a high number of bacteria present at the entry site. There could have been an increased availability of TNFα, LPS and IFNɣ in the epithelium due to the meningococcal infection. Indeed, an abundance of TNFα, LPS and IFNɣ has been shown to be responsible for a reduction in TER from rat retinal pigment epithelium (Zech *et al,* 1998).

NO has both stimulatory and inhibitory effects on IL-8 release. In response to incubation with NO donors such as 1 mM SNP and 500 µM SNAP for 24 hours, the IL-8 output from human bronchial epithelial cell was shown to be reduced (Neri *et al,* 2010). The reduction was diminished by preincubating the cells with NOS inhibitor L-NAME. In contrast, the level of IL-8 release from human MDMs is increased in the presence of 500 µM SNAP (Stevanin *et al,* 2007). However, this alteration in IL-8 release was not seen in the case of HPEC-ALIs where 500 µM SNAP was present compared to control infection with only HBSS media (**Figure 5.10 and 5.11**).

Increased IL-8 **(Figure 5.5, 5.6, 5.10 and 5.11)** and TNFα **(Figure 5.4 A and 5.9)** release were observed with meningococcal infection (at MOI 100) of HPEC-ALIs compared to the uninfected control cells. This is not unexpected given that TNFα and IL-8 are pro-inflammatory signalling molecules, released in response to bacterial infection. This is in keeping with the observation where bacterial infection caused by *Salmonella* and *Listeria monocytogenes* result in an increased IL-8 release from intestinal and cervical epithelial cell (Eckmann *et al,* 1993). A positive correlation between increased IL-8 release from plasma and meningococcal LPS has been reported for the patients with fulminant meningococcal septicaemia (Møller *et al,* 2005). However, it is noteworthy that during the infection of HPEC-ALI with meningococcal strains at MOI 100, the TNFα release **(Figure 5.4 A and 5.9)** was lower than the IL-8 release **(Figure 5.5, 5.6, 5.10 and 5.11)** in all conditions. This is in agreement with the previous finding where increased IL-8 release but undetectable levels of TNFα release was found after infection of epithelial cells with *Helicobacter pylori* (Huang *et al,* 1995). This would make sense as a decreased TNFα response would help the meningococci to survive better in the epithelium as it is likely to induce a weak proinflammatory response against the bacteria. High meningococcal viable count output **(Figure 5.7 A, B and 5.12 A, B)** from HPEC-ALI points to this possibility.

Multiple explanations could account for meningococcal NO metabolism not differentially altering the barrier function and immune response of the HPEC-ALIs. Firstly, since HEPC-ALI is a primary cell line cultured from different volunteers, there is most probably a much higher degree of interdonor variation in the development of the immune response to bacterial infection. In the event that modulation of the barrier functions and immunological chemistry of these cells by the partial denitrification pathway is nuanced or extremely subtle, we might lose our signal amongst the experimental 'noise'. This could of course be counteracted with further repetition of the experiment, but the culture of HPEC-ALIs is both extremely time consuming and expensive. Our initial findings suggest there may be limited gains in carrying out this work. Secondly, low levels of TNFα **(Figure 5.4 A and 5.9)** release following meningococcal infection points to the possibility of a reduced NO activity as it has been suggested that TNFα acts as an inducer of NOS expression from endothelial and epithelial cells (Donnelly & Barnes, 2002; Robbins *et al,* 1997; Yan *et al,* 1997) . Another study demonstrated that NO can activate the TNF-converting enzyme (TACE) responsible for releasing the membrane bound TNFα (Zhang *et al,* 2000). Thirdly, NOS bioactivity during airway inflammation following infection of HPEC-ALI with meningococci could have been reduced by the increased arginase activity **(Figure 5.3 – 5.7).** Arginase is the magnesium containing final enzyme of the urea cycle that converts L-arginine to urea (Christianson, 2005). Availability of L-arginine is one of the key factors that determine the NO activity in cellular environment given that L-arginine is a substrate for NOS activity **(Section 1.9)**. Two distinct types of mammalian arginases, arginase I and arginase II are detected in the human airway epithelium (Wu & Morris, 1998). Dramatic induction of arginase I and II have been observed during the airway inflammatory condition such as asthma (Meurs *et al,* 2003; Zimmermann *et al,* 2003). Increased arginase activity would reduce the available arginine to a suboptimal level for any NO related activity. Therefore, it might have inhibited the NOS expression and limit NO production required for observing any meningococcal NO metabolism mediated impact on barrier function or immune response of the HPEC-ALI **(Figure 5.3 – 5.7).** To circumvent this possibility an exogenous NO donor was added for the later experiment. However, any alteration in immune response and barrier function was still unapparent **(Figure 5.8 – 5.12).** Therefore it could be possible that meningococcal NO metabolism does not differentially regulate the TER and cytokine release of the HPEC-ALIs.

6 Chapter 6: Effect of meningococcal denitrification on biofilm formation *in vitro*

6.1 Introduction

As an obligate commensal, *N. meningitidis* has to withstand the immune response mediated by the innate and adaptive immune defence mechanism of the nasopharynx. This indicates the adaptation of a special lifestyle to resist clearance by the immune system. Indeed, IgA antibody in saliva and increased serum bactericidal antibody response have been detected from the meningococcal carriage population (Caugant *et al*, 2007). Formation of biofilm could be one of the strategies employed by the meningococci to maintain the carriage stage and avoid immune mediated killing in nasopharynx. Although there is no definitive evidence to date for meningococcal biofilm formation *in vivo*, histological studies on carrier population have reported the presence of microcolonies on tonsillar tissue indicating the presence of a biofilm type phenotype in the carriage state (Neil & Apicella, 2009). There is evidence for meningococcal biofilm formation *in vitro* from multiple studies (Lappann *et al*, 2006; Neil *et al*, 2009; Yi *et al*, 2004). **Since the nasopharynx is an oxygen poor environment and rich in NO (Andersson *et al*, 2002; Lundberg & Weitzberg, 1999), an ability to denitrify could confer an additional survival advantage to the *N. meningitidis* to form biofilm and maintain colonisation. Therefore, it was decided to examine if meningococcal denitrification pathway has an impact on biofilm formation *in vitro* by using the newly created and characterised Δ*aniA*/Δ*norB* strain (Chapter 4).**

6.2 Bacterial biofilm formation and NO

Presence of biofilm like structure dates back to the early record in fossil found from the hydrothermal environment. Bacterial microcolonies have been identified from 3.3 - 3.4 billion year old South African Korngberg formation and 3.2 billion year old hydrothermal rocks of Australia in the deep sea (Rasmussen, 2000; Westall *et al*, 2001). A biofilm is a group of microorganisms attached to a surface by forming extracellular polymeric substance (EPS) which facilitates the attachment and matrix formation (Donlan, 2001). Organisms in biofilm population have distinct growth rate and gene expression, metabolic and proteomic profile compared to the single species in planktonic form. In the model organism for biofilm study *Pseudomonas aeruginosa*, biofilm formation can be divided into five stages; 1) weak attachment to the surface, 2) transcriptional changes and tight binding to the surface for environmental adaptation, 3) bacterial aggregation and microcolony formation, 4) mature

biofilm development and 5) detachment of biofilm from the surface to move to a separate location (Hall-Stoodley *et al,* 2004). Formation of biofilm offers the organism protection from numerous environmental stress such as acid exposure (Welin-Neilands & Svensäter, 2007), metal toxicity (Teitzel & Parsek, 2003), phagocytosis (Leid *et al,* 2002), antibiotics (Stewart & Costerton, 2001), antimicrobial (Mah & O'Toole, 2001) agents and immune response (Domenech *et al,* 2013).

Studies have demonstrated that non capsulated *N. meningitidis* can form biofilm *in vitro* both on plastic tubing (Yi *et al,* 2004) and continuous flow chambers (Lappann *et al,* 2006). However, encapsulated meningococci can also form biofilm as evidenced by a study performed on SV-40 transformed human bronchial epithelial (HBE) cell (Neil *et al,* 2009).

NO have both positive and negative impacts on bacterial biofilm formation. The effect is dependent on multiple factors such as the concentration of NO present in the biofilm environment. *Pseudomonas aeruginosa* is a pathogen in cystic fibrosis (Davies, 2002) and its pathogenicity has been linked to the ability to form biofilm (Costerton *et al,* 1999). In *Pseudomonas aeruginosa*, high concentrations (µM level) of NO induce biofilm formation whereas sublethal concentrations (~25 to 500 nM) cause the sessile bacterial population to disperse (Barraud *et al,* 2006). In contrast, high concentrations (~125 -1000 µM) of NO reduce biofilm formation by *Staphylococcus aureus* but low concentrations (0.9 – 2 µM) of NO increase biofilm biomass (Jardeleza *et al,* 2011). One of the mechanisms by which NO forms biofilm is by controlling the level of c-di-GMP molecule which is an inducer for biofilm formation (Plate & Marletta, 2012).

It is well established that the closely related pathogenic species, *Neisseria gonorrhoeae*, forms biofilm both *in vitro* and *in vivo* (Greiner *et al,* 2005*;* Steichen *et al,* 2008). There have been several studies that confirmed a link between denitrification pathway and biofilm formation by *N. gonorrhoeae* (Falsetta *et al,* 2009; Falsetta *et al,* 2010). These studies demonstrated the importance of *aniA* and *norB* in gonococcal biofilm formation. However, there has not been any study investigating the effect of meningococcal denitrification pathway on biofilm formation *in vitro*. Therefore it was decided to examine if meningococcal NO denitrification has an impact on biofilm formation *in vitro.*

6.3 Results

6.3.1 The absence of denitrification pathway affects meningococcal biofilm formation *in vitro*

6.3.1.1 Rationale and methods

As a coloniser of nasopharynx, meningococci are likely to compete with other commensal species for the available nutrients. Initial experiments in our laboratory condition showed that a 50% strength growth media (MHB and TSB) induces meningococcal biofilm formation *in vitro* (Data not shown) in microaerobic condition. A range of concentrations of TSB media has been titrated and successfully used for inducing biofilm formation of *Pseudomonas, Streptococcus* and *N. lactamica* (personal communication with Sara Hughes, NHS Southampton). In the closely related species *N. gonorrhoeae*, it has been demonstrated both *aniA* and *norB* are important for biofilm formation (Falsetta *et al,* 2009; Falsetta *et al,* 2010). A comparative proteomic analysis revealed that the glyceraldehyde-3-phosphate dehydrogenase, one of the enzymes of oxygen independent glycolytic pathway is upregulated in biofilm layer compared to the planktonic cells of *N. meningitidis* (van Alen *et al,* 2010). To examine the impact of meningococcal denitrification genes, biofilm formation was induced by nutrient starving and a comparative biofilm formation analysis was performed between Wt and the newly created Δ*aniA/*Δ*norB* **(Chapter 4)** strain in microaerobic condition.

Biofilm was quantified by Crystal Violet (CV) staining. CV staining has been repeatedly used to study the static biofilm from a number of bacterial species for years (Favre-Bonté *et al,* 2003; Merritt *et al,* 2005) including *N. meningitidis* (Lappann *et al,* 2006; Yi *et al,* 2004). In the aqueous solution CV dissociates into CV^+ and OH^- ions. The CV^+ component can penetrate the bacterial cell wall and stain the bacteria purple by interacting with the negatively charged component of bacteria. The intensity of this purple dye is quantified using a spectrophotometer (Jenway 7315). This reading provides an estimation of the biomass in biofilm.

Ten colonies of *N. meningitidis* strain (Wt and Δ*aniA/*Δ*norB*) were grown in the presence of 50 µM SpermineNONOate containing MHB and were normalised to an $OD_{600nm} = 0.5$. Multiple colonies were chosen to account for the phase variable properties of *N. meningitidis*. The cells were resuspended in fresh 2 ml of full strength MHB media, after discarding the old media following centrifugation. Bacterial cultures were seeded onto 6 well polystyrene plates (Biolite, Thermo). The plates had an electrostatic surface treatment on the polystyrene to promote attachment. To induce biofilm formation by nutrient starving, 2 ml of reduced strength MHB broth (50% MHB+ 50% PBS) which we termed as 'starvation media' was added to the 2 ml of

bacteria containing full strength media. This gave a total media strength of 75%. Another set of duplicate wells were used for growing biofilm for 48 hours in parallel. On this plate, 2 ml of media from the biofilm seeding plate was removed after 24 hours and replaced with 2 ml of fresh starvation media. Therefore, the plates for 48 hour biofilm formation which started with a 75% media strength had a media strength of 62.5% after 24 hours. Special care was taken to keep the working hood sterile while setting up the biofilm plates. All the media and PBS was filter sterilised through a 0.22 µm Millex^{R} filter using syringe. Each bacterial strain was seeded in duplicates; one well was used for crystal violet staining whereas the other well was used for counting the number of viable bacteria in biofilm layer. The plates were incubated at 37°C, 5% CO_2. After 24 hour the media above the biofilm was removed and centrifuged to pellet the planktonic bacteria. The pellet was resuspended in PBS and the number of viable bacteria was counted by dilutional plating. After removing the planktonic bacteria containing media, the biofilm was washed twice with 4 ml sterile PBS. Pipetting had to be carried out gently from one particular corner of the well so that the biofilm was not dislodged. Following the wash step 2 ml of 0.1% crystal violet solution was added to the biofilm and left for 20 minutes at room temperature. The CV was removed and washed twice with 2 ml PBS by very gentle pipetting. Then 1.2 ml of 100% ethanol was applied on top of the biofilm to elute the crystal violet. After 20 minutes CV containing ethanol from biofilm containing wells was removed to fresh 1.5 ml tubes and centrifuged for 5 minutes at 13000 rpm. The supernatant from each tube was transferred to cuvette and absorbance was measured at 600_{nm} using a spectrophotometer (Jenway 7315). Another well from the duplicate well was used to count the number of viable bacteria present in the biofilm layer. All the media from this well was removed and biofilm was washed twice with PBS. All the residual PBS was removed and 1 ml of fresh PBS was applied to the well. The cells in the biofilm were scraped into PBS using a cell scraper and the cell containing PBS was transferred to a fresh 1.5 ml microcentrifuge tube. The tubes were centrifuged at 13000 rpm for 5 minutes to pellet the bacteria present in biofilm. The PBS was removed and bacteria was resuspended in 1 ml fresh PBS. Using 30 µl of this mix, viable count was performed with a dilutional counting method.

6.3.1.2 Results

CV staining data shows that Δ*aniA/*Δ*norB* (OD_{600nm} 0.07 ± 0.01) showed a significantly reduced biofilm forming ability compared to Wt MC58 (OD_{600nm} 0.44 ± 0.06) after 24 hours ($p < 0.01$) **(Figure 6.1 A)**. There was no significant difference in the input inocula of the strains (Wt, 4.99 x 10^8 cfu/ml ± 1.03 x 10^8, Δ*aniA/*Δ*norB,* 3.17 x 10^8 cfu/ml ± 6.2 x 10^7) ($p = 0.24$)

(Figure 6.1 B). After 24 hours the viable biofilm biomass from Wt (4.21×10^8 cfu/ml ± 1.97×10^8) was significantly higher than that of Δ*aniA/*Δ*norB* (2.09×10^6 cfu/ml ± 1.27×10^6) ($p < 0.05$) **(Figure 6.1 C).** However there was no statistically significant difference in the number of viable planktonic bacteria between Wt (4.0×10^8 cfu/ml ± 2.63×10^8) and Δ*aniA/*Δ*norB* (4.63×10^8 cfu/ml ± 1.47×10^8) ($p = 0.47$) **(Figure 6.1 D).** Viable planktonic bacteria and viable biofilm biomass were combined to get the total viable biomass. There was no statistically significant difference in the total viable biomass in any of the conditions studied after 24 hours (Wt, 8.21×10^8 cfu/ml ± 2.4×10^8 and Δ*aniA/*Δ*norB,* 4.65×10^8 cfu/ml ± 1.48×10^8) ($p = 0.39$) **(Figure 6.1 E).**

As can be seen from **Figure 6.2 A,** Wt MC58 (OD_{600nm}, 0.40 ± 0.09) showed significantly higher biofilm forming ability compared to Δ*aniA/*Δ*norB* (OD_{600nm}, 0.08 ± 0.008) after 48 hours ($p < 0.05$). The viable biofilm biomass recovered from Wt (2.47×10^7 cfu/ml ± 1.17×10^7) was significantly higher than Δ*aniA/*Δ*norB* (9.35×10^4 cfu/ml ± 6.62×10^4) ($p < 0.01$) **(Figure 6.2 C).** There was no statistically significant difference across the strains in viable planktonic biomass recovery (Wt, 3.14×10^7 cfu/ml ± 2.77×10^7, Δ*aniA/*Δ*norB,* 3.34×10^7 cfu/ml ± 2.69×10^7) ($p = 0.47$) **(Figure 6.2 D).** Similarly, there was no statistically significant difference in the total viable biomass recovered from any of the conditions (Wt, 5.61×10^7 cfu/ml ± 3.18×10^7 and Δ*aniA/*Δ*norB,* 3.35×10^7 cfu/ml ± 2.7×10^7) ($p = 0.39$) **(Figure 6.2 E).**

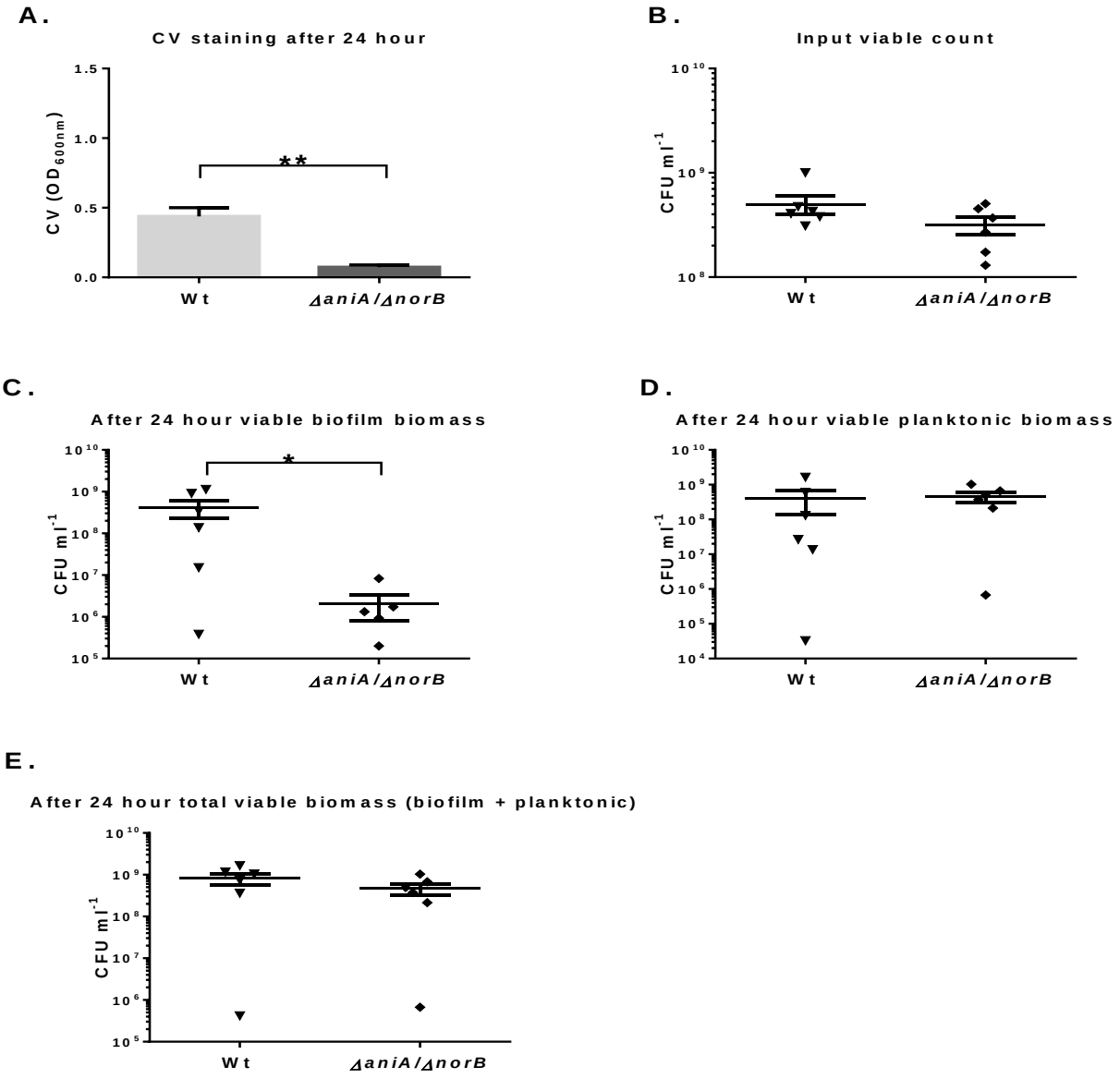

Figure 6.1 Role of meningococcal denitrification on biofilm formation *in vitro* (24 hour)

Wt MC58, Δ*aniA*/Δ*norB* strains were grown in Mueller-hinton broth (MHB) in the presence of 50 µM SpermineNONOate and normalised to an OD_{600nm} = 0.5 in the full strength media. The old media was discarded after centrifugation and cells were resuspended in fresh media. Bacteria were seeded onto 6 well plates (Biolite, Thermo) in 4 ml of reduced strength MHB broth (50% MHB+ 50% PBS) and incubated at 37°C, 5% CO_2. 30 µl of this culture was serially diluted and plated on CBA plates for input viable count **(B),** Each condition was performed in 4 wells (2 for 24 hour and 2 for 48 hour). After 24 hour, 2 of the wells were processed for CV (Crystal Violet) staining **A)**, viable biomass in biofilm **C)** and viable count from the planktonic media above biofilm **D)** were determined after cell scrapping. Total viable biomass in well was calculated by combining viable biofilm and planktonic biomass **E)**, *p< 0.05, ** p < 0.01, Mann-Whitney test, n = 6. Data represents mean ± SEM.

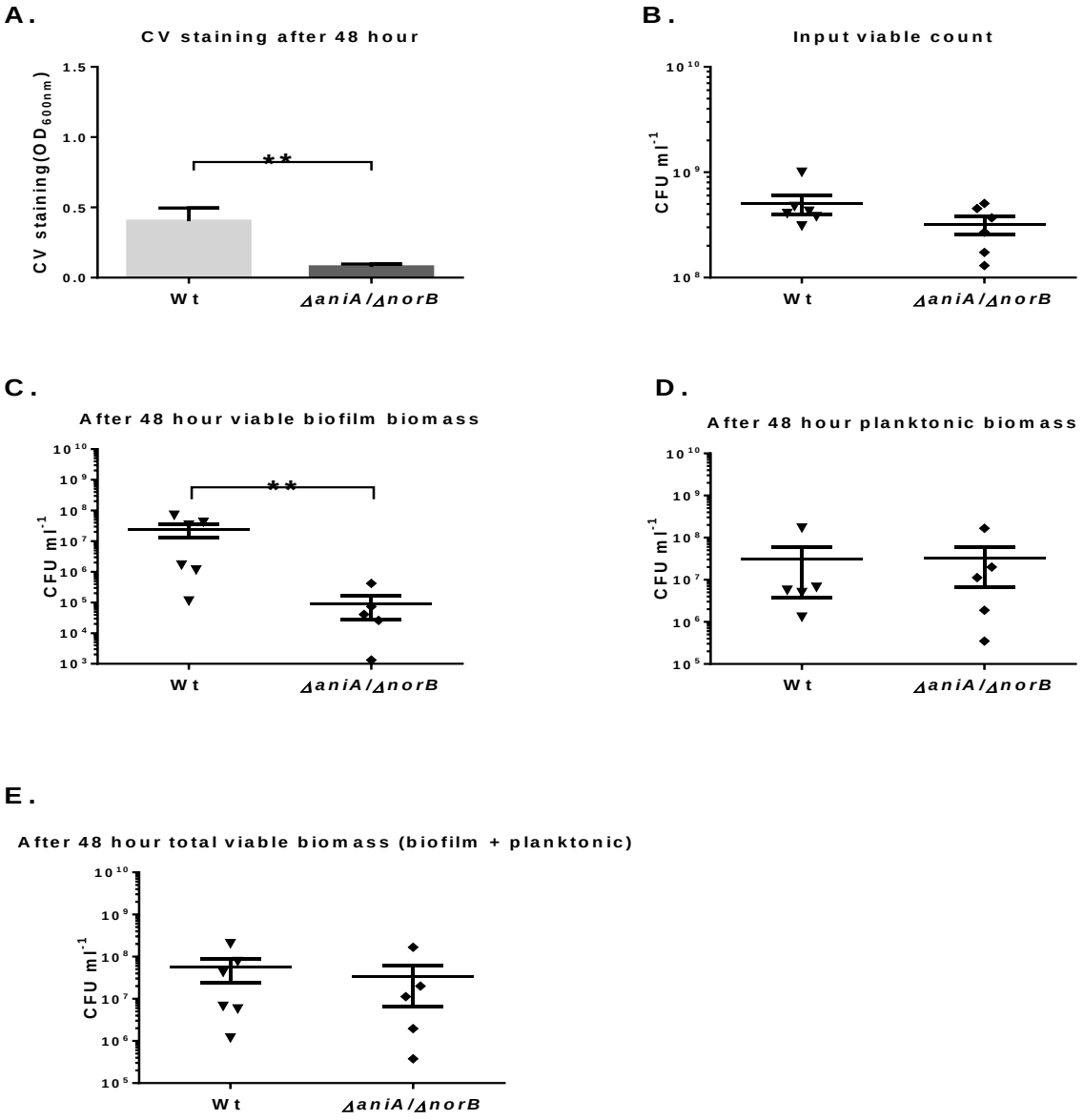

Figure 6.2 Role of meningococcal denitrification on biofilm formation *in vitro* (48 hour).

Wt MC58, Δ*aniA/*Δ*norB* strains were grown in Mueller-hinton broth (MHB) in the presence of 50 µM SpermineNONOate and normalised to an OD_{600nm} = 0.5 in full strength media. The old media was discarded and cells were resuspended in fresh media after centrifugation. Bacteria were seeded onto 6 well plates (Biolite, Thermo) in 4 ml of reduced strength MHB broth (50% MHB+ 50% PBS) and incubated at 37°C, 5% CO_2. 30 µl of this culture was serially diluted and plated on CBA plates for input viable count **(B).** Each condition was performed in 4 wells (2 for 24 hour and 2 for 48 hour). After 48 hour, 2 of the wells were processed for CV staining **A)** viable biomass in biofilm **C)** and viable count from the planktonic media above biofilm **D)** were determined after cell scrapping. Total viable biomass in well was calculated by combining viable biofilm and planktonic biomass **E).** $^{**}p < 0.01$ Mann-Whitney test, n = 6. Data represents mean ± SEM.

6.3.2 Reverse complementation of Δ*aniA* under the control of an IPTG inducible promoter

6.3.2.1 Rationale and methods

In *N. gonorrhoeae* both *aniA* and *norB* have been found to be upregulated in biofilms (Falsetta *et al,* 2009). Although a significant difference in biofilm formation was found with Δ*aniA/*Δ*norB* compared to the Wt strain **(Section 6.3.1)**, the individual role of *aniA* and *norB* was not conclusive from the observation. Since biofilm represents a high population of bacteria, there would be less availability of oxygen for aerobic respiration due to competition. The biofilm formation was induced by nutrient starvation in microaerobic (static) condition in our laboratory **(Figure 6.1 - 6.2).** Therefore, an ability to switch from oxidative to microaerobic respiration would have been pivotal in enabling the meningococci to form biofilm. Meningococci initiate the alternative respiratory pathway of denitrification by using the nitrite reductase (*aniA*) in oxygen limited conditions **(explained in Section 1.14).** Using *gfp* transcriptional fusion it has been demonstrated that *aniA* is expressed predominantly in the substratum of the gonococcal biofilm (Falsetta *et al,* 2010). Proteomic analysis also showed an upregulation of AniA in gonococcal biofilm (Phillips *et al,* 2012). To test the hypothesis that *aniA* plays a similar role in the meningococcal biofilm formation *in vitro*, it was decided to construct a reverse complemented strain of Δ*aniA (*referred as Δ*aniA*/*aniA*$^{IPTG+}$ here after) which would enable us to perform similar biofilm experiment as mentioned before **(Section 6.3.1)** in the presence of Wt, Δ*aniA* and Δ*aniA*/*aniA*$^{IPTG+}$ strains.

For reverse complementing *aniA* under the control of an IPTG inducible promoter, the pGCC4 plasmid was selected (Mehr *et al,* 2000; Mehr & Seifert, 1998). It has been successfully used for reverse complementing genes in *N. meningitidis* (Hung *et al,* 2013*;* Kumar *et al,* 2011). The plasmid enables to insert meningococcal gene under the transcriptional control of lac regulatory elements between *aspC* and *lctP* region by using the restriction enzymes from the multiple cloning sites **(Figure 6.3)**. Avoiding a native promoter and regulatory region, 1.173 Kb coding sequence of *aniA* (NMB1623) was PCR amplified from the Wt MC58 genomic DNA. To achieve this primers (*Ampli_aniA_Comp_Forward*, with PacI restriction site and *Ampli_aniA_Comp_Reverse,* with FseI restriction site, **Table 2.6**) were used following the Q5 polymerase protocol **(Section 2.11.15.5)**. The selected PacI and FseI enzymes do not have any overlapping cut sites within the coding region of *aniA*. Following PCR purification **(Section 2.11.7),** the product was digested along with the pGCC4 vector plasmid using PacI and FseI restriction digest enzymes (NEB) **(Section 2.11.9).** After digestion the pGCC4 was treated with

Antarctic phosphatase (NEB) **(Section 2.11.11)** which acts to minimise the re-circularisation of vector plasmid. The phosphatase treatment catalyses the removal of 5′ phosphate termini from the DNA and thereby minimising the possibility of vector recircularisation by ligase during the ligation step. After heat-inactivation of the enzymes, the double digested PCR fragment and pGCC4 were ligated using the NEB's ligation kit **(Section 2.11.10).** The ligation product was transformed into the DH5α competent cells **(Section 2.11.2)** and the positive plasmids were selected on kanamycin and erythromycin containing LB agar plates **(Section 2.4.4)**. Integration of *aniA* into pGCC4 was confirmed by sequencing **(Sequencing Primers 1 and 2, Table 2.6 and see the attached CD-ROM for sequencing data)** and diagnostic PCR **(Figure 6.4).** The resulting plasmid which was chosen for subsequent cloning application was termed as pGCC4:: $aniA^{IPTG3+}$, Kan^R, Ery^R. Then approximately an 8.1 Kb fragment from this plasmid was PCR amplified along with the *aniA* gene cloned between *aspC* and *lctP* using the phusion polymerase protocol **(Figure 6.5) (Section 2.11.15.4).** This fragment was transformed into the Δ*aniA* strain using the broth culture transformation protocol **(Section 2.11.12)** and selected on spectinomycin/erythromycin containing plates **(Section 2.4.2).** Then after GD extraction **(Section 2.11.6),** integration of the correct sequence was tested by sequencing primers **(Table 2.6)** (See the attached CD-ROM for sequencing data). After sequencing confirmation the positive colonies were combined. The resulting strain was termed as Δ*aniA/aniA*$^{IPTG+}$ and stored in 60% glycerol containing solution at - 80°C for future usage.

6.3.2.2 Results

For confirming restoration of *aniA*, GD were extracted from Wt, Δ*aniA* and Δ*aniA/aniA*$^{IPTG+}$. Primers (*aniA_Fwd_start* and *aniA_Rev_end*) **(Table 2.6)** were designed as such that they amplified the 1.173 Kb *aniA* coding sequence region from Wt GD **(Figure 6.6) (Section 2.11.3).** A similar band was apparent with GD extracted from Δ*aniA/aniA*$^{IPTG+}$ but not from the GD extracted from Δ*aniA*.

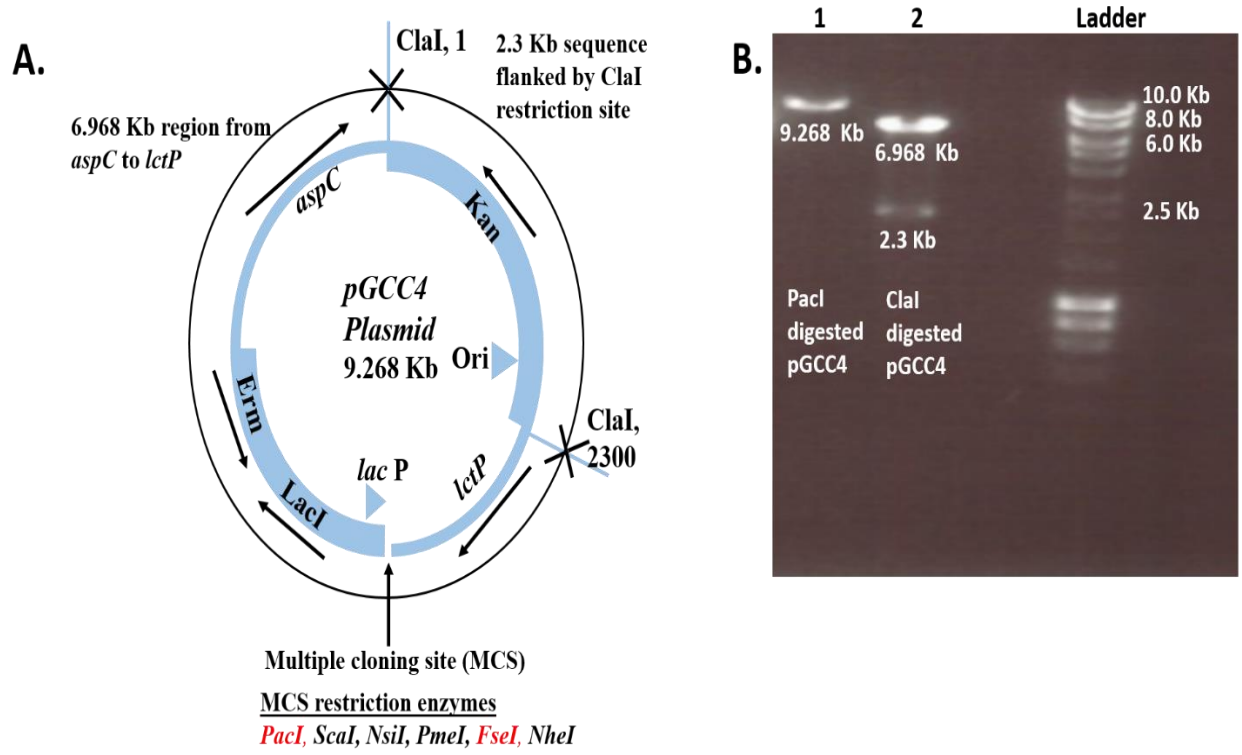

Figure 6.3 Testing of pGCC4 plasmid for reverse complementing Δ*aniA* under the control of an IPTG inducible promoter.

A) A functional copy of the gene to be complemented is ectopically inserted at an unlinked chromosomal locus between the *lctP* (L-lactate permease) and *aspC* (Aspartate aminotransferase) genes of *Neisseria* genome under the control of IPTG inducible lac regulatory elements (*lac P* and *LacI*), linked to an Erm (Erythromycin) resistant cassette. Multiple cloning site is located after the lacP which harbours multiple restriction enzymes for cloning. For reverse complementing *aniA* under the control of an IPTG inducible promoter (lacP), PacI and FseI enzymes were chosen (highlighted in red) as the *aniA* gene does have any cut site for these enzymes (Figure adapted from Addgene website) **B)** After receiving the pGCC4 plasmid from our collaborator (Prof Chris Tang, Oxford), it was tested by restriction digest. PacI, ClaI digested **(Section 2.11.9)** pGCC4 were run on the 1% agarose gel **(Section 2.11.14)** to test the plasmid. PacI is an enzyme from the MCS (A) which linearises pGCC4 and produces a band length of 9.268 Kb (Lane 1, Figure B). As can be seen from Figure A, approximately 2.3 Kb sequence of pGCC4 is flanked by ClaI restriction site. Therefore, ClaI digestion of pGCC4 yields two bands which are of approximately 6.968 Kb and 2.3 Kb length (Lane 2, Figure B)

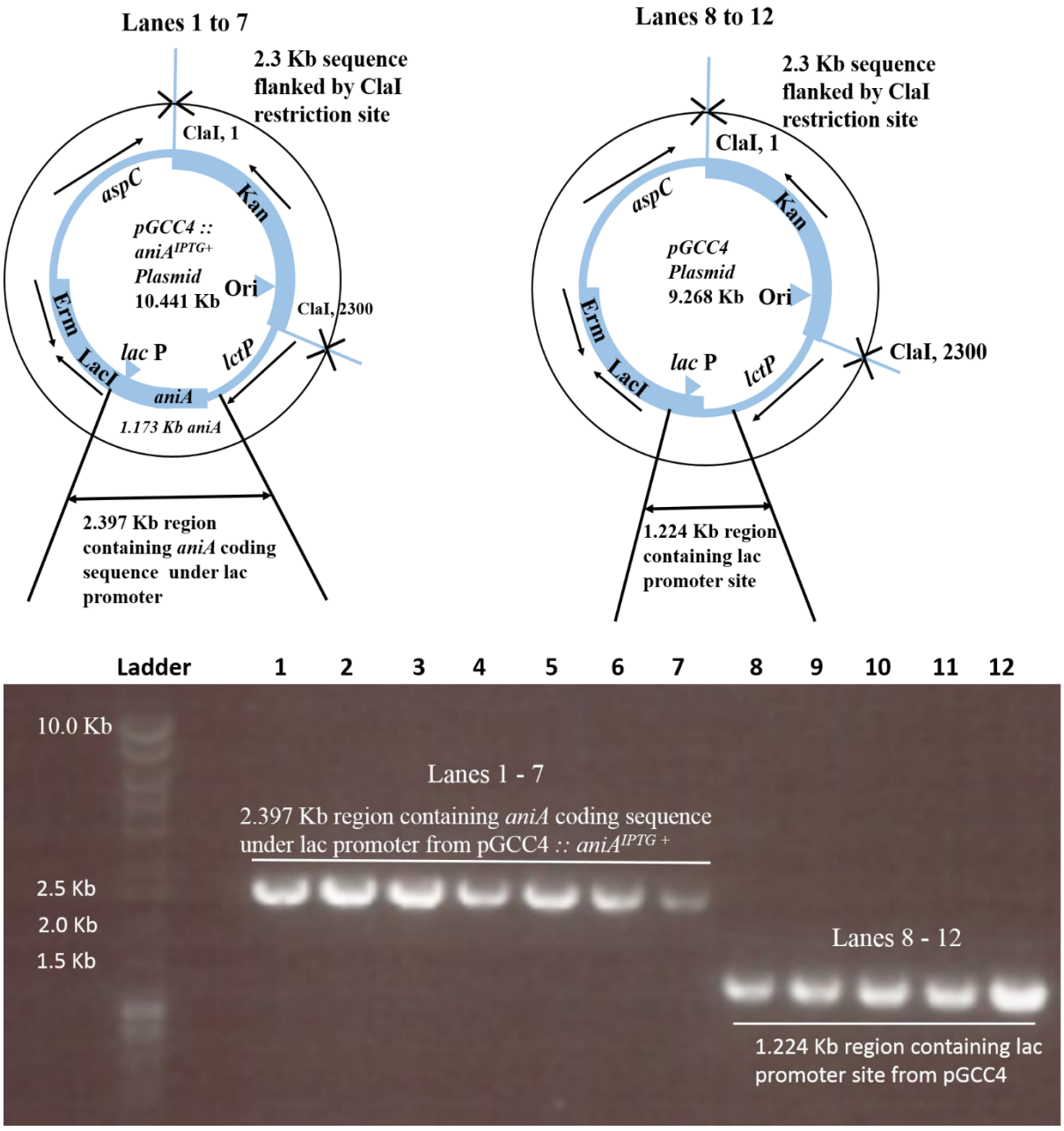

Figure 6.4 Diagnostic PCR for the selection of pGCC4::*aniA*$^{IPTG+}$ plasmid containing *aniA* coding region under the control of lac promoter

Integration of *aniA* into pGCC4 was confirmed by designing primers (*pGCC4_diagnostic_Fwd* and *pGCC4_diagnostic_Rev*) **(Section 2.11.3)** which amplified 2.397 Kb region containing *aniA* coding sequence under lac promoter using pGCC4::*aniA*$^{+}$, Kan^{R}, Ery^{R} plasmids as template **(Lanes 1-7)**. NEB phusion protocol was used **(2.11.15.4).** Similar PCR amplification was performed using pGCC4 as a template **(Lanes 8-12).** Details of the amplified products are mentioned in the cartoon above the gel. Colony number 3 **(Lane 3)** was selected as later cloning application after sequencing confirmation and was named as pGCC4 :: *aniA*$^{IPTG3+}$, Kan^{R}, Ery^{R}.

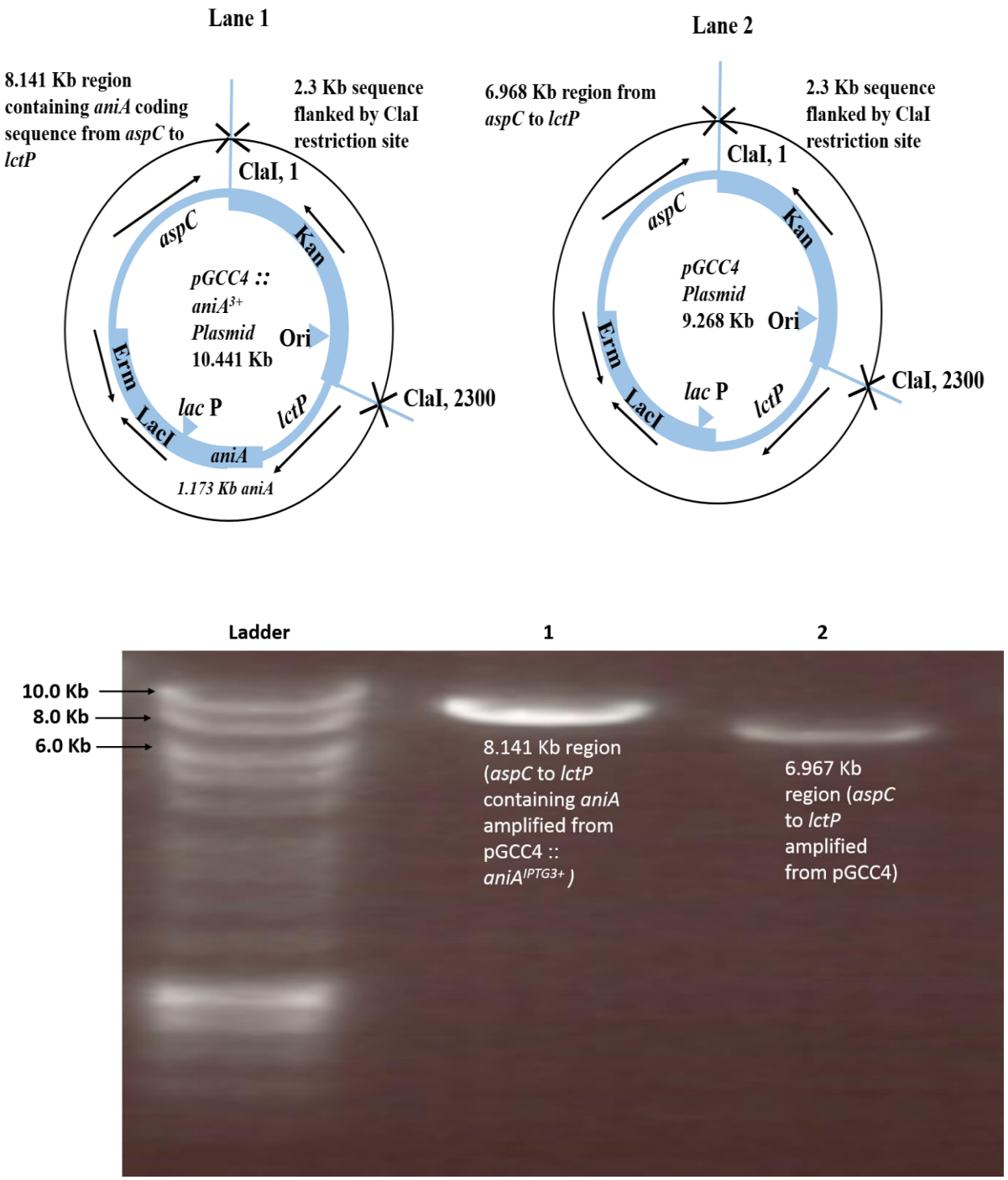

Figure 6.5 Amplification of *aspC* to *lctP* region along with *aniA* coding sequence under lac promoter from pGCC4::*aniA*$^{IPTG3+}$ for transforming into Δ*aniA*.

Integration of *aniA* into pGCC4::*aniA*$^{IPTG3+}$ was confirmed by designing primers (*Ampli-pGCC4Forward* and *Ampli-pGCC4Reverse)* **(Section 2.11.3)** which amplified the entire region from *aspC* to *lctP* using pGCC4::*aniA*$^{IPTG3+}$, Kan^{R}, Ery^{R} plasmid as template (Lane 1). Similar PCR amplification was performed using pGCC4 as a template (Lane 2). Details of the amplified products are mentioned in the cartoon above the gel. The correct size of band (8.141 Kb) was found with the PCR reaction using pGCC4::*aniA*$^{IPTG3+}$, Kan^{R}, Ery^{R} as template. The product was transformed into Δ*aniA* for generating Δ*aniA/aniA*$^{IPTG+}$ strain.

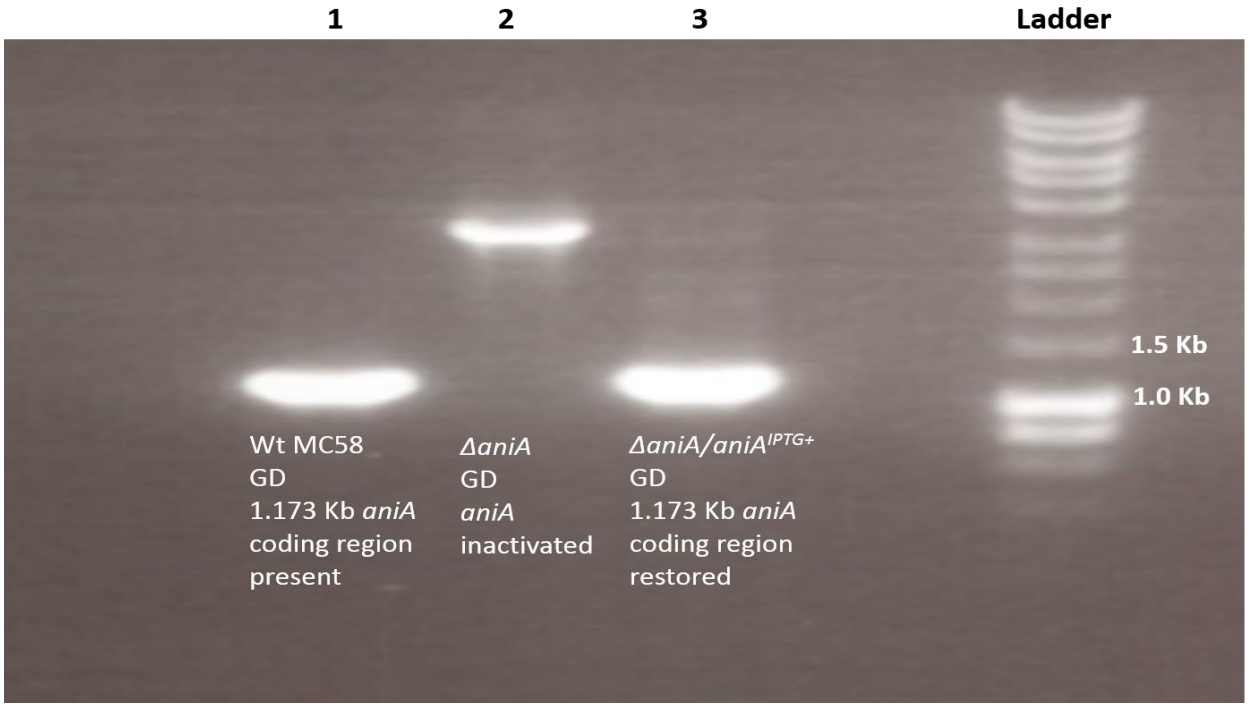

Figure 6.6 PCR confirmation of *aniA* restoration in Δ*aniA/aniA*$^{IPTG+}$

Genomic DNA (GD) **(Section 2.11.6)** was extracted from the Δ*aniA/aniA*$^{IPTG+}$ in which *aniA* was cloned after the IPTG inducible promoter. In parallel, GD was extracted from Wt, Δ*aniA*. PCR was performed using the Q5 polymerase **(Section 2.11.15.5)** and the PCR products were run in 1% agarose gel **(Section 2.11.14)** to separate the products according to their size. The primers (*Ampli_aniA_Comp_Forward* and *Ampli_aniA_Comp_Reverse*) covering *aniA* coding region in chromosome showed a 1.173 Kb band from the Wt GD (Lane 1). Same size band was absent in Δ*aniA* GD (Lane 2) but present in Δ*aniA*/*aniA*$^{IPTG+}$ GD (Lane 3). The approximately 3.2 Kb band with Δ*aniA* GD amplification product (Lane 2) represents the 2.0 Kb spectinomycin cassette flanked by disrupted *aniA* sequence.

6.3.3 *aniA* activity is not restored in the newly created IPTG inducible Δ*aniA/aniA*$^{IPTG+}$ strain

6.3.3.1 Rationale and methods

The newly generated Δ*aniA/aniA*$^{IPTG+}$ **(Section 6.3.2)** had to be characterised for the restoration of *aniA* activity. To achieve this Δ*aniA/aniA*$^{IPTG+}$ was grown alongside the Wt MC58 and Δ*aniA* in batch culture growth curve performed in MHB supplemented with 5 mM $NaNO_2$ in microaerobic condition. This condition has been used for examining meningococcal denitrification (Anjum *et al*, 2002; Rock *et al*, 2005). This experiment enabled us to investigate the comparative NO_2^- depletion over time. In 25 ml tubes, the cultures were normalised to OD_{600nm} = 0.05 in 25 ml MHB with 5 mM $NaNO_2$ and where appropriate with 1 mM IPTG (Sigma-Aldrich, UK) supplementation. The cultures were grown for 24 hours without agitation at 37°C, 5% CO_2. Static condition ensured limited oxygen diffusion in the media. In a separate tube, 25 ml MHB with 5 mM $NaNO_2$ was incubated without any bacteria. This condition served as positive control. Similar batch culture growth curves were also performed in the presence of 1 mM IPTG in aerobic condition at 320 rev/minute. This was done to examine if agitation can induce *aniA* activity triggered by IPTG. Viable counts were performed at 0, 4, 8, 12 and 24 hour time points by dilutional plating. At the specified time points, 1 ml of each sample was transferred to sterile 1.5 ml microcentrifuge tube. The samples were centrifuged at 13000 rpm for 5 minutes and supernatants were collected. Bacteria free supernatants were used to measure nitrite (NO_2^-) by Griess Assay **(Section 2.10.1).**

6.3.3.2 Results

As can be seen from **Figure 6.7 A**, there was a statistically significant difference in NO_2^- reduction by the Wt strain in the presence of IPTG at 12, 24 hour and at 8, 12 and 24 hour without IPTG compared to all other strains including Δ*aniA/aniA*$^{IPTG+}$ ($p < 0.05$). There was no difference in viable count output **(Figure 6.7 B).** In the case of aerobic batch culture growth curve in the presence of IPTG, there was no significant difference in the NO_2^-, viable count readings from any of the strains including Δ*aniA/aniA*$^{IPTG+}$ **(Figure 6.8).**

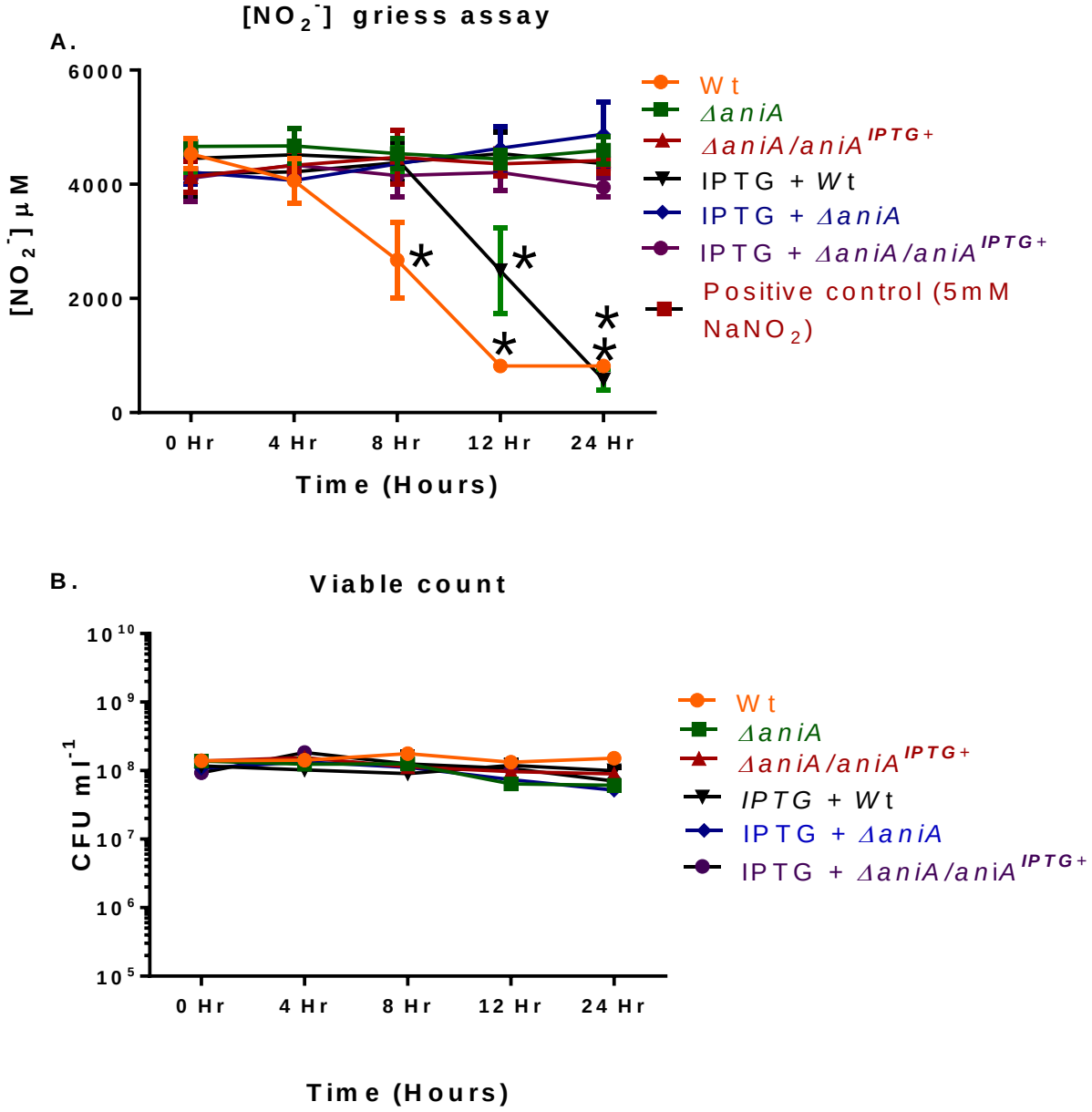

Figure 6.7 Functional characterisation of the newly generated IPTG inducible Δ*aniA/aniA*$^{IPTG+}$ in the presence of $NaNO_2$ in microaerobic condition.

Wt, Δ*aniA,* Δ*aniA/aniA*$^{IPTG+}$ were grown in 25 ml MHB containing 5 mM $NaNO_2$ in 50 ml tubes with or without 1 mM IPTG. Cultures were grown at 37°C, 5% CO_2 and media were collected at 0, 4, 8, 12 and 24 hour timepoints to take viable count readings. 1 ml of sample from each condition was stored for later **A)** [NO_2^-] measurement by Griess Assay **(Section 2.10.1), B)** 30 µl of sample from each timepoint was serially diluted and plated on CBA plate for measuring viable count (cfu/ml) next day. Bars denote means ± SEM. n = 4, Two way ANOVA with Tukey's multiple comparison test.

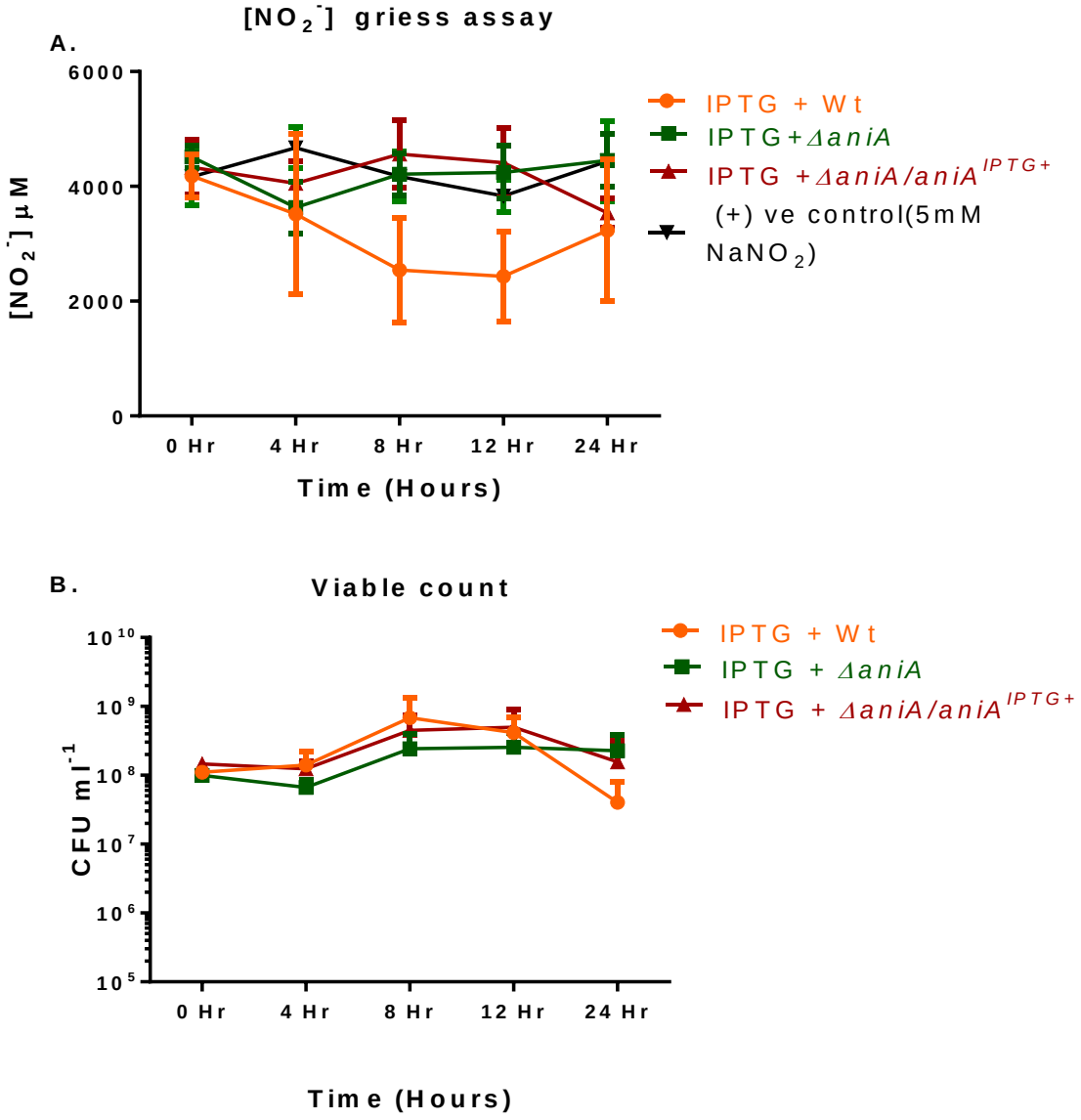

Figure 6.8 Functional characterisation of the newly generated IPTG inducible Δ*aniA/aniA*$^{IPTG+}$ in the presence of $NaNO_2$ in aerobic condition.

Wt, Δ*aniA*, Δ*aniA/aniA*$^{IPTG+}$ were grown in 25 ml MHB containing 5 mM $NaNO_2$ and 1 mM IPTG in 50 ml tubes with agitation at 320 rev/minutes. The cultures were incubated at 37°C, 5% CO_2. Media were collected at 0, 4, 8, 12 and 24 hour timepoints to take viable count readings. A volume of 1 ml of sample from each condition was stored for later **A)** [NO_2^-] measurement by Griess Assay **(Section 2.10.1)**, **B)** 30 µl of sample from each timepoint was serially diluted and plated on CBA plate for measuring viable count (cfu/ml) next day. Bars denote means ± SEM. n = 3, Two way ANOVA with Tukey's multiple comparison test.

6.3.4 Reverse complementation of *aniA* under the control of its endogenous promoter

6.3.4.1 Rationale and methods

In the newly created Δ*aniA/aniA*$^{IPTG+}$, 1.173 Kb *aniA* coding sequence starting from 'ATG' start codon to 'TAA' stop codon was cloned without the upstream regulatory elements. The regulation of *aniA* is a complex process and is dependent on the co-ordination of multiple factors such as FNR (Edwards *et al*, 2010; Rock *et al*, 2005), NsrR (Heurlier *et al*, 2008; Rock *et al*, 2007), FUR (Delany *et al*, 2004) and NarQ/NarP (Rock *et al*, 2005) which all have binding sites upstream of *aniA* coding region **(for details see Section 1.13- 1.14).** Therefore, the absence of regulatory region in the upstream of *aniA* could have been one of the reasons *aniA* activity was not restored in Δ*aniA/aniA*$^{IPTG+}$ **(Section 6.3.2, 6.3.3).** So, it was decided to reverse complement *aniA* along with the upstream essential regulatory sequences. Alongside the promoter binding sites, the selected region contained the binding sites for the regulatory proteins such FNR, NarP, NsrR, FUR **(Figure 6.10)**. For reverse complementing *aniA* under its endogenous promoter, pGCC5 plasmid (Addgene) was used **(Figure 6.9).** It enables to complement the desired gene under the control of its endogenous promoter at an unlinked chromosomal locus between *aspC* and *lctP* region linked to a chloramphenicol resistant cassette **(Figure 6.9).** It has been used to successfully reverse complement mutant strain of *N. gonorrhoeae* (Stohl *et al*, 2005).

The selected Forward primer (*AniA_compl_RUH8_FWD)* and reverse primer (*AniA_compl_RUH8_REV)* contained AatII and NsiI restriction enzyme sites respectively and were designed to PCR amplify *aniA* coding sequence along with its 300 bp upstream endogenous regulatory elements (1.6 Kb) **(Figure 6.10).** Approximately 1.6 Kb long PCR product was bulked up, PCR purified **(Section 2.11.7)** and verified by running on 1% Agarose gel. PCR purified *aniA* along with its upstream regulatory region (using Phusion polymerase) **(Section 2.11.15.4)** and vector plasmid pGCC5 were double digested first with NsiI (with low salt buffer) and then sequentially with AatII (high salt buffer) **(Section 2.11.9).** After heat inactivating the enzymes, restriction digest products were run on 1% Agarose gel for confirmation **(Section 2.11.14).** Subsequently, ligation was performed at vector to insert ratios of 1:1, 1:3 and 1:5 using NEB's T4 DNA ligase **(Section 2.11.10).** Following day products from ligation was transformed into DH5α competent cells **(Section 2.11.2).** The resulting colonies were selected on Kanamycin containing plates. Plasmid DNA was extracted from the selected positive colonies **(Section 2.11.8)** and positive colonies were verified by diagnostic PCR **(Figure 6.11).** The selected *pGCC5::aniA*$^{2+}$ was verified by the sequencing primers

(*Comp_check_RUH19_aniA1* and *Comp_check_RUH20_aniA2)* **(See the attached CD ROM for sequencing data)**. A primer pair was designed for pGCC5 as such that forward primer (*Comp1_check_RUH14_lctP/aspC_FWD)* was complementary to the beginning of *lctP* and reverse primer (*Comp1_check_RUH14_lctP/aspC_REV)* was complementary to the end of *aspC***.** These primer pairs were used to PCR amplify *aniA* along with its native promoter from the newly created pGCC5::*aniA*$^{2+}$ using NEB's phusion polymerase **(Figure 6.12) (Section 2.11.15.4).** PCR product was bulked up and purified **(Section 2.11.7).** After qualitative and quantitative assessment of PCR product by NanoDrop **(Section 2.11.5),** PCR product was transformed into the Δ*aniA* by spot transformation **(Section 2.11.13).** Resulting colonies were selected on spectinomycin/chloramphenicol containing plates **(Section 2.4.2).** Positive colonies were selected by colony PCR **(Section 2.11.15.1)** using *AniA_compl_RUH8_FWD* and *AniA_compl_RUH8_REV* primers which amplified the *aniA* containing 1.6 Kb region **(Figure 6.13).** The confirmed Δ*aniA/aniA*$^{+}$ was stored in 60% glycerol containing solution in -80°C for future usage.

6.3.4.2 Results

GD were extracted from Wt, Δ*aniA* and Δ*aniA/aniA*$^{+}$ strains **(Section 2.11.6).** PCR amplication was carried out with *AniA_compl_RUH8_FWD* and *AniA_compl_RUH8_REV* primers using My Taq^{TM} Red Mix polymerase **(Section 2.11.15.2).** Primers amplified the 1.6 Kb *aniA* region along with its endogenous promoter. With Wt and Δ*aniA/aniA*$^{+}$ PCR products, approximately a 1.6 Kb band representing the *aniA* region along with its upstream regulatory elements was evident **(Figure 6.14).** However, the similar band was not seen with Δ*aniA* GD PCR. An approximately 3.6 Kb long band was seen with both the Δ*aniA* and Δ*aniA/aniA*$^{+}$ GD amplification products (Lanes 2-3).

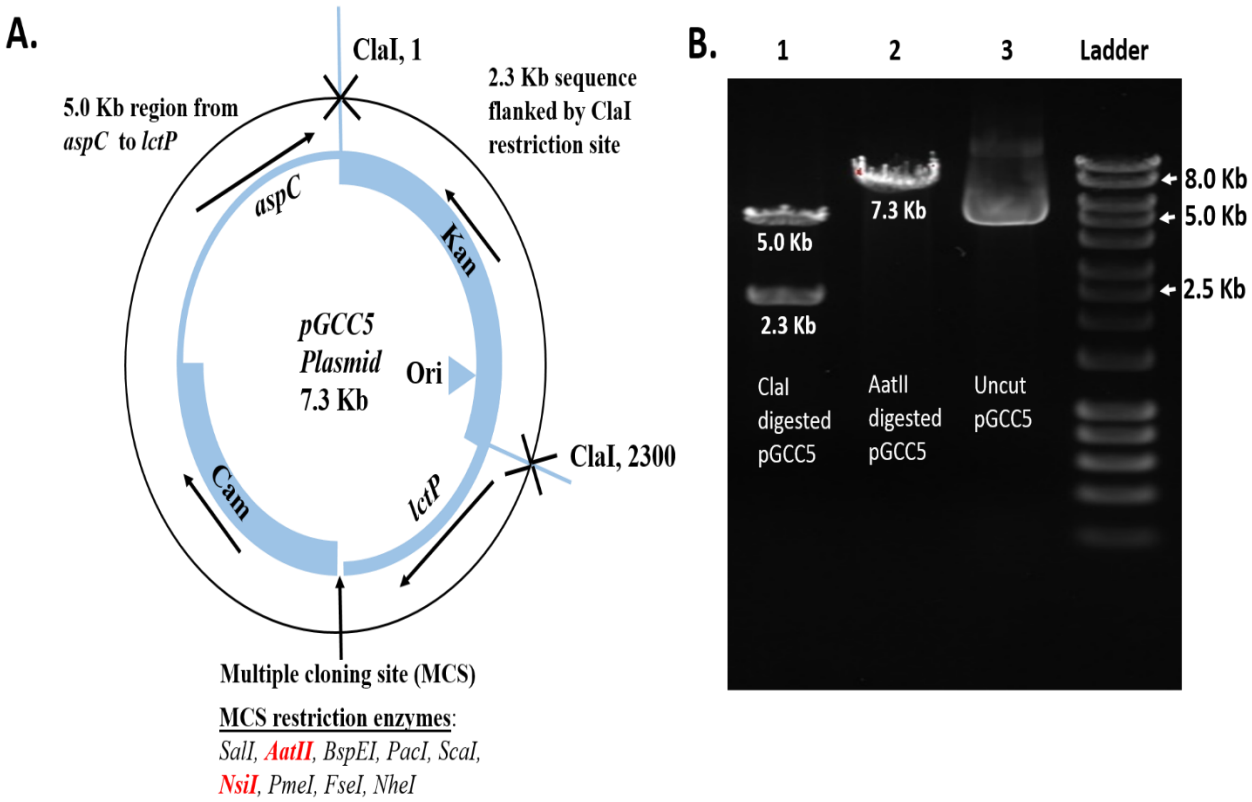

Figure 6.9 Testing of pGCC5 plasmid for complementing Δ*aniA* under the control of its endogenous promoter.

A) pGCC5 is used to complement mutation under the control of its endogenous promoter. A functional copy of the gene to be complemented is ectopically inserted at an unlinked chromosomal locus between the *lctP* and *aspC* genes under the control of its endogenous promoter and linked to a Cam (Chloramphenicol) resistance cassette. (Figure adapted from Addgene website) Multiple cloning site harbours multiple restriction enzymes for cloning. For *aniA* complementation under its endogenous promoter along with the regulatory sequences, AatII and NsiI enzymes were chosen (highlighted in red) **B)** After receiving the plasmid from Addgene, restriction digest reactions were performed to test the plasmid. ClaI, AatII digested **(Section 2.11.9)** pGCC5 were run on the 1% agarose gel **(Section 2.11.14)**. As can be seen from Figure A, approximately 2.3 Kb sequence is flanked by ClaI. Therefore, ClaI digestion of pGCC5 yields two bands which are of 5.0 Kb and 2.3 Kb length (Lane 1, Figure B). AatII is an enzyme from the MCS which linearises pGCC5 and produces a band length of approximately 7.3 Kb (Lane 2, Figure B), Lane 3 represents the uncut pGCC5. Image captured by Biorad gel imager

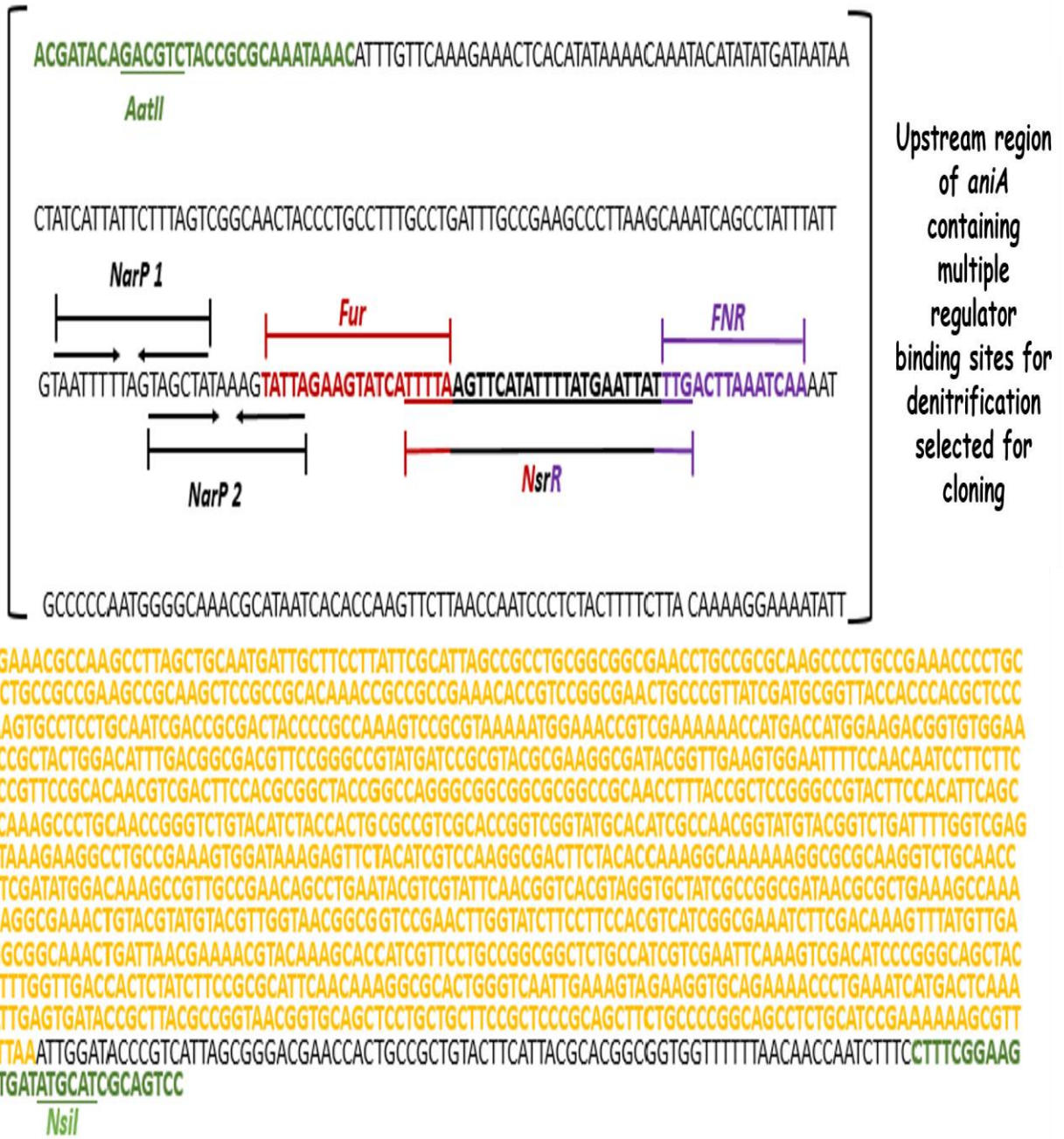

Figure 6.10 Sequence selected for reverse complementation of *aniA* along with its endogenous promoter and upstream regulatory protein (FNR, NsrR, FUR, NarP) binding sites.

The cartoon represents the selected 300 basepair upstream region of *aniA* coding regions (in the bracket) plus 100 bp downstream region of the *aniA* gene. *aniA* coding region is highlighted in yellow. All the four regulators directly or indirectly affect the *aniA* activity and therefore are important for denitrification (for details on these regulators the readers are referred to **(Section 1.12 - 1.14).** The sequences highlighted in green represents the selected regions for primer design with the selected restriction enzymes (*AatII* and *NsiI*) from the MCS of pGCC5 **(Figure 6.9)** which do not have any overlapping cut sites within the *aniA* region.

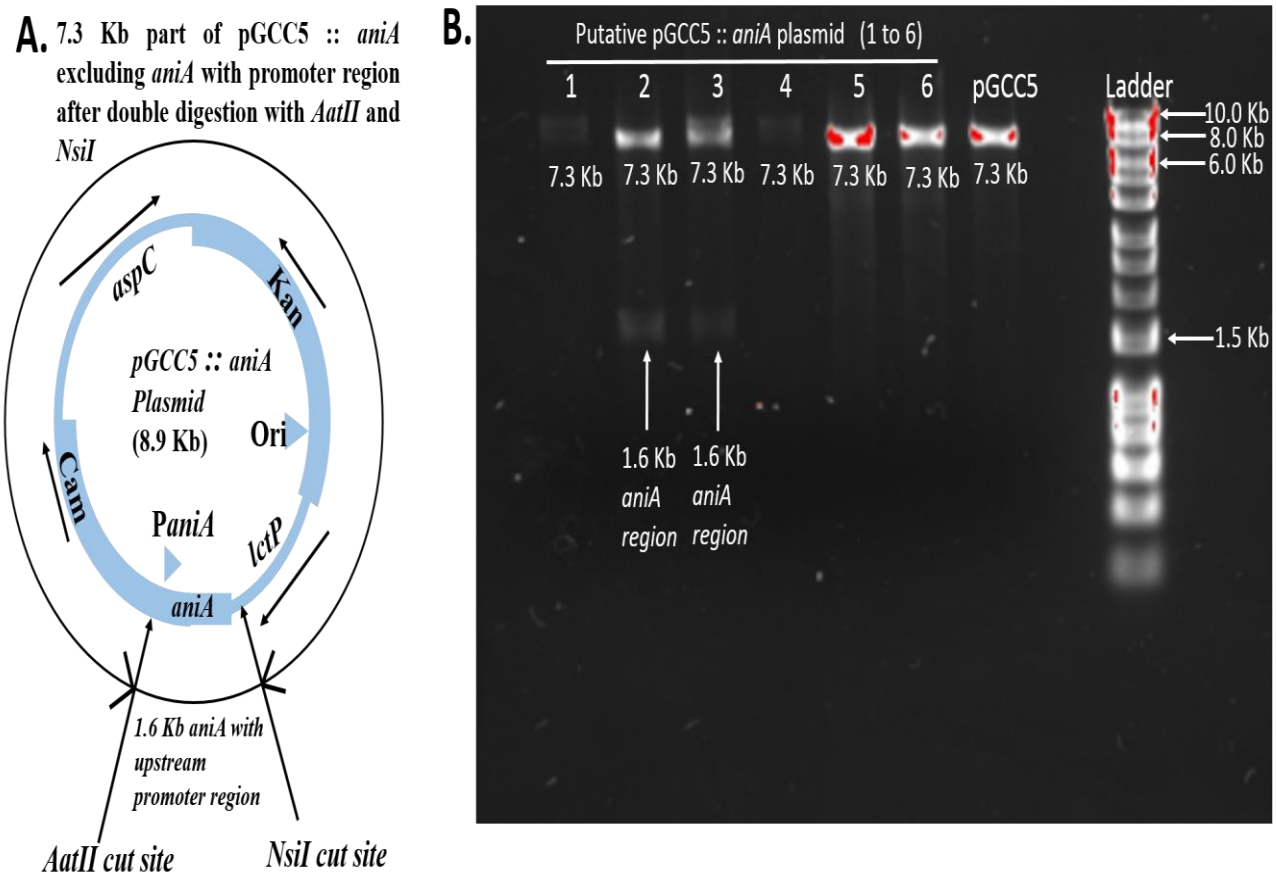

Figure 6.11 Diagnostic restriction digest for selecting positive pGCC5::*aniA* plasmid.

After cloning *aniA* with upstream endogenous promoter region into AatII and NsiI restriction sites of pGCC5 plasmid (as shown in Figure A), positive clones were selected on Kanamycin containing plates. After plasmid extraction selected colonies were double digested **(Section 2.11.9)** with NsiI and AatII restriction enzymes. Digested product was run on 1% agarose gel **(Section 2.11.14)** to separate the products according to their size. As can be seen from the Figure B, *pGCC5::aniA (2)* and *pGCC5::aniA (3)* plasmids contained the expected 1.6 Kb *aniA* region and 7.3 Kb part of the remaining pGCC5 plasmid (Figure A). *pGCC5::aniA (2)* was selected for subsequent cloning application after sequencing confirmation (See the attached CD ROM for sequencing data) and termed as pGCC5::*aniA*$^{2+}$. Image captured by Biorad gel imager.

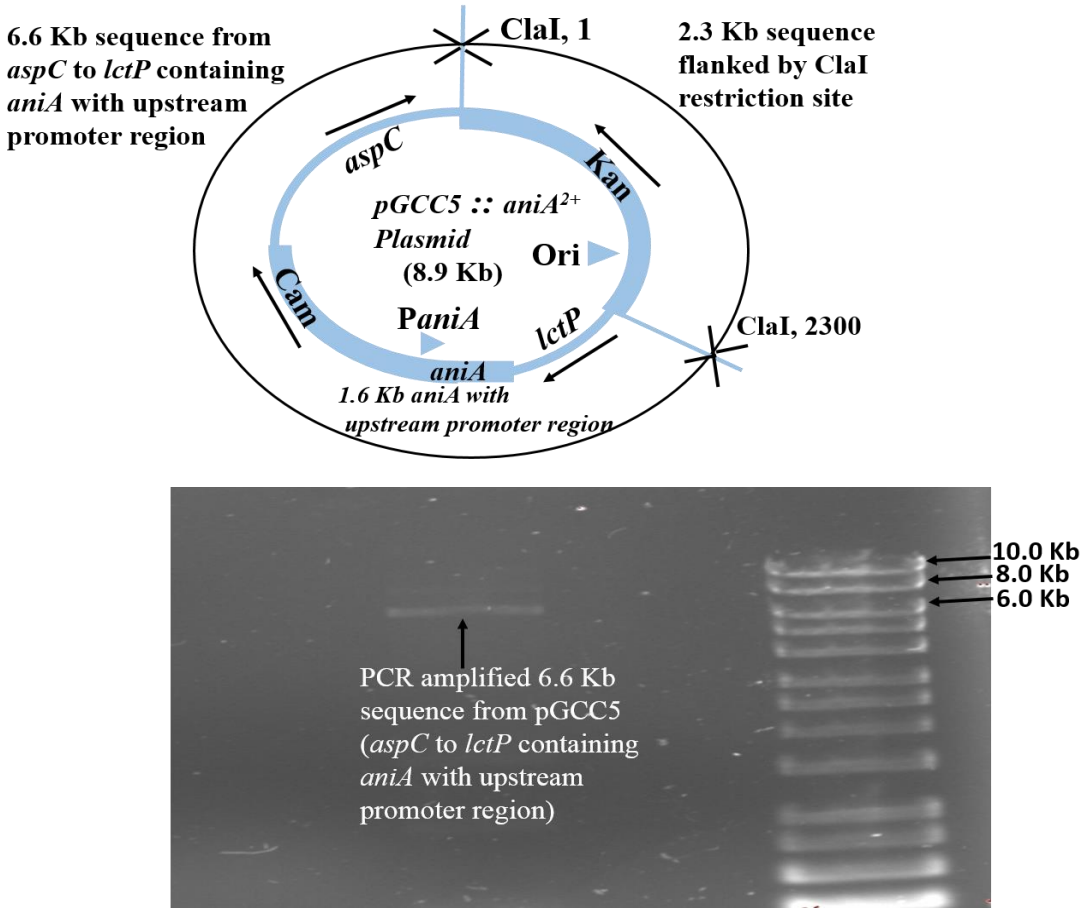

Figure 6.12 Amplification of *aspC* to *lctP* region containing *aniA* with its upstream promoter region using pGCC5 :: *aniA*$^{2+}$ as template for transforming into Δ*aniA*.

Integration of *aniA* into *pGCC5*:: *aniA*$^{2+}$ was confirmed by designing primers (*Ampli-pGCC4 Forward* and *Ampli-pGCC4Reverse)* **(Section 2.11.3)** which amplified the entire region from *aspC* to *lctP* containing *aniA* with upstream promoter region using *pGCC5 :: aniA*$^{2+}$, Kan^{R}, Cam^{R} plasmid as template. Details of the amplified products are mentioned in the cartoon above the gel. The correct size of band (6.6 Kb) was found with the PCR reaction using *pGCC5* :: *aniA*$^{2+}$, Kan^{R}, Cam^{R} as template. NEB's phusion polymerase was used for PCR **(Section 2.11.15.3).** After gel confirmation the 6.6 Kb fragment was transformed into the Δ*aniA* strain. Image captured by Biorad gel imager.

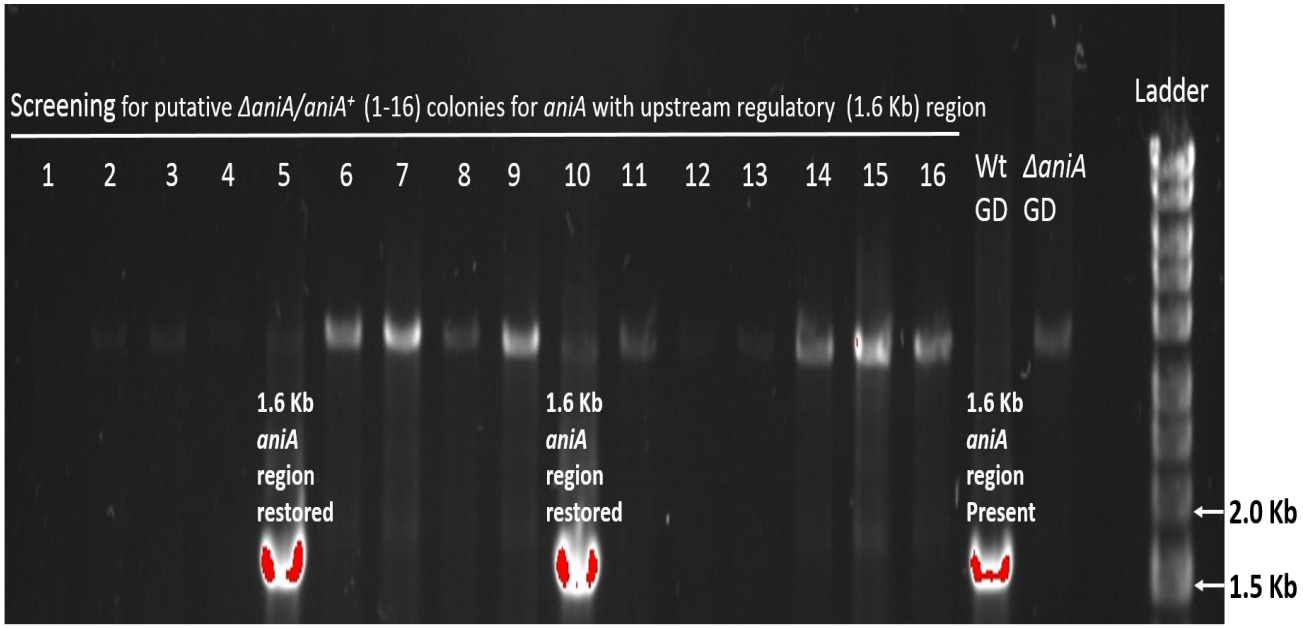

Figure 6.13 Confirmation of positive colonies from the reverse complemented Δ*aniA/aniA*$^+$ under its native promoter by colony PCR.

Colony PCR **(Section 2.11.15.1)** was performed on the putative Δ*aniA/aniA*$^+$ colonies selected on Spectinomycin/Chloramphenicol containing plates using My Taq polymerase **(Section 2.11.15.2)**. *AniA_compl_RUH8_FWD* and *AniA_compl_RUH8_REV* primers **(Section 2.11.3)** were used to amplify 1.6 Kb sequence containing *aniA* along with its 300 bp upstream regulatory region. PCR products were run on 1% agarose gel **(Section 2.11.14)**. Colony 5 and Colony 10 contained the expected 1.6 Kb band similar to the Wt MC58 GD and were used for subsequent characterisation. Image captured by Biorad gel imager.

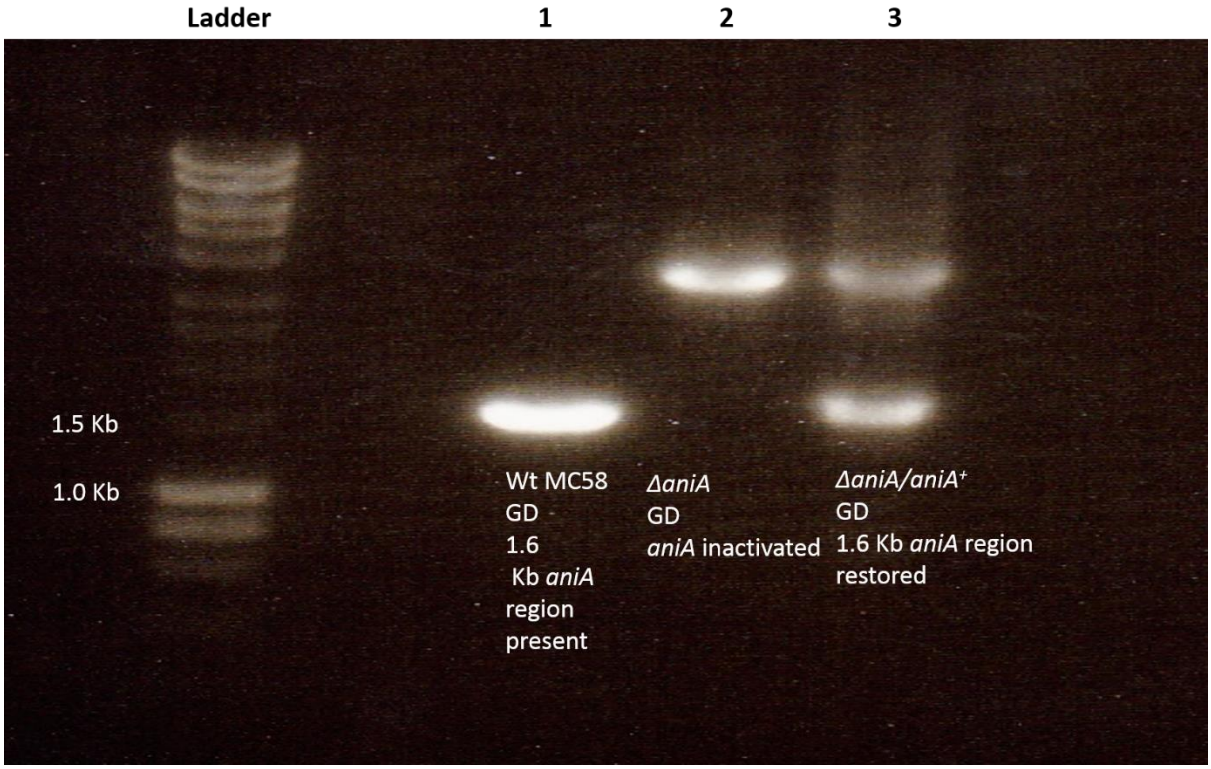

Figure 6.14 PCR confirmation of the reverse complementation of Δ*aniA/aniA*$^+$ under its endogenous promoter region.

Genomic DNA (GD) **(Section 2.11.6)** was isolated from Wt, Δ*aniA* and Δ*aniA/aniA*$^+$ colonies. PCR was performed using My Taq polymerase (Bioline) **(Section 2.11.15.2)** with *AniA_compl_RUH8_FWD* and *AniA_compl_RUH8_REV* primers and the PCR products were run in 1% agarose gel **(Section 2.11.14)** to separate the products according to their size. The primers covering *aniA* along with its endogenous promoter in chromosome showed a 1.6 Kb band from the Wt GD (Lane 1). Same size band was absent in Δ*aniA* (Lane 2) but present in Δ*aniA*/*aniA*$^+$ (Lane 3). Lanes 2 and 3 represent a band of approximately 3.6 Kb in size from PCR products with Δ*aniA* and Δ*aniA/aniA*$^+$ GD templates. This represents 2.0 Kb spectinomycin cassette flanked by disrupted *aniA* region. Therefore, PCR product with Δ*aniA/aniA*$^+$ GD showed two bands; one representing the newly integrated *aniA* along with its upstream regulatory elements (1.6 Kb) and the other band representing spectinomycin cassette flanked by disrupted *aniA* region (3.6 Kb). These observations confirmed the successful integration of *aniA* along with its upstream promoter region into Δ*aniA*/*aniA*$^+$. Image taken by BioRad gel imager.

6.3.5 *aniA* activity is restored in the Δ*aniA/aniA*$^+$ strain where *aniA* was complemented along with its endogenous promoter and upstream regulatory elements

6.3.5.1 Rationale and methods

The newly created Δ*aniA/aniA*$^+$ had to be characterised for the restoration of NO_2^- metabolism. To test the functional restoration of *aniA* in the newly generated Δ*aniA/aniA*$^+$, a batch culture growth curve was performed in MHB supplemented with 5 mM $NaNO_2$. The newly created Δ*aniA/aniA*$^+$ was grown alongside the Wt and Δ*aniA* strains for comparison. The cultures were grown for 24 hours with mild agitation at 90 rev/minute. In 50 ml tubes, the cultures were normalised to OD_{600nm} = 0.05 in 25 ml MHB with 5 mM $NaNO_2$ supplementation before incubating the cultures at 37°C, 5% CO_2 incubator. In a separate tube, 25 ml MHB with 5 mM $NaNO_2$ was incubated without any bacteria. This condition served as positive control. Viable counts were performed at 0, 2, 4, 8, 12 and 24 hour time points by dilutional plating. At the specified time points, 1 ml of each sample was transferred to sterile 1.5 ml microcentrifuge tube. The samples were centrifuged at 13000 rpm for 5 minutes and supernatants were collected. Bacteria free supernatants were used to measure nitrite (NO_2^-) by Griess Assay **(Section 2.10.1).**

6.3.5.2 Results

Figure 6.15 demonstrates that there was a statistically significant reduction in NO_2^- with the Δ*aniA/aniA*$^+$ containing media compared to Wt and Δ*aniA* at 12 and 24 hour timepoints ($p < 0.05$). The bacterial viable count for Δ*aniA/aniA*$^+$ was statistically significantly higher at 12 and 24 hour timepoints compared to the Wt and Δ*aniA* ($p < 0.05$). In four identical replicates of Δ*aniA/aniA*$^+$, the first three replicates **(1, 2 and 3)** demonstrated an obvious transition from oxidative respiration to denitrification but for the last replicate the transition was not apparent. **(Figure 6.16)**

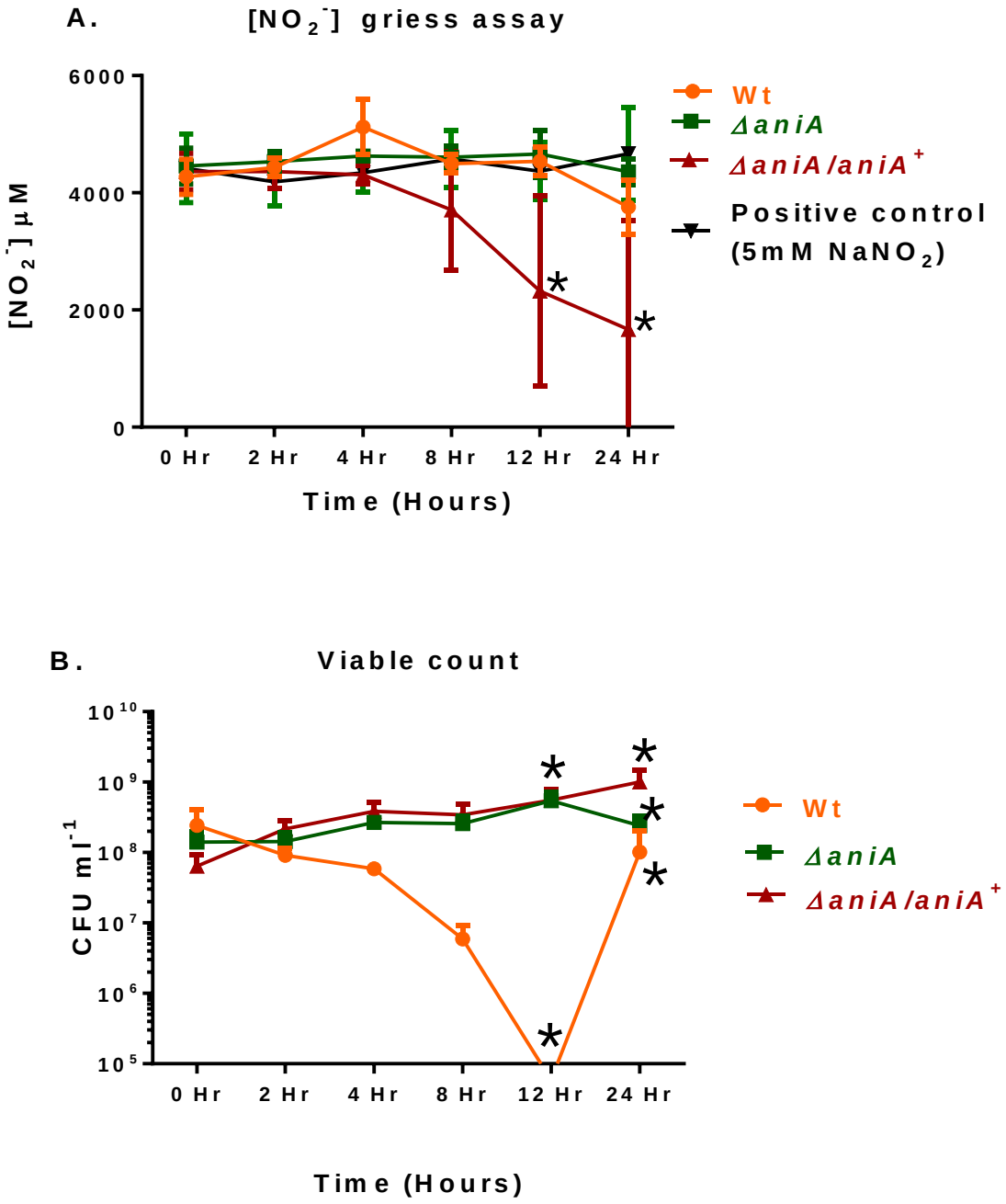

Figure 6.15 Functional characterisation of the newly generated complemented strain Δ*aniA/aniA*$^+$ in the presence of 5 mM $NaNO_2$ in microaerobic condition.

Wt, Δ*aniA*, Δ*aniA/aniA*$^+$ were grown in 25 ml MHB containing 5 mM $NaNO_2$ in 50 ml tubes at 90 rev/minute agitation. The cultures were incubated at 37°C, 5% CO_2. Media were collected at 0, 2, 4, 8, 12 and 24 hour timepoints to take viable count readings. 1 ml of sample from each condition was stored for later **A)** [NO_2^-] was measured by Griess Assay **(Section 2.10.1), B)** 30 µl of sample from each timepoint was serially diluted and plated on CBA plate for measuring viable count (cfu/ml) next day. Bars denote means ± SEM. n = 4, *p<0.05, Two way ANOVA with Tukey's multiple comparison test.

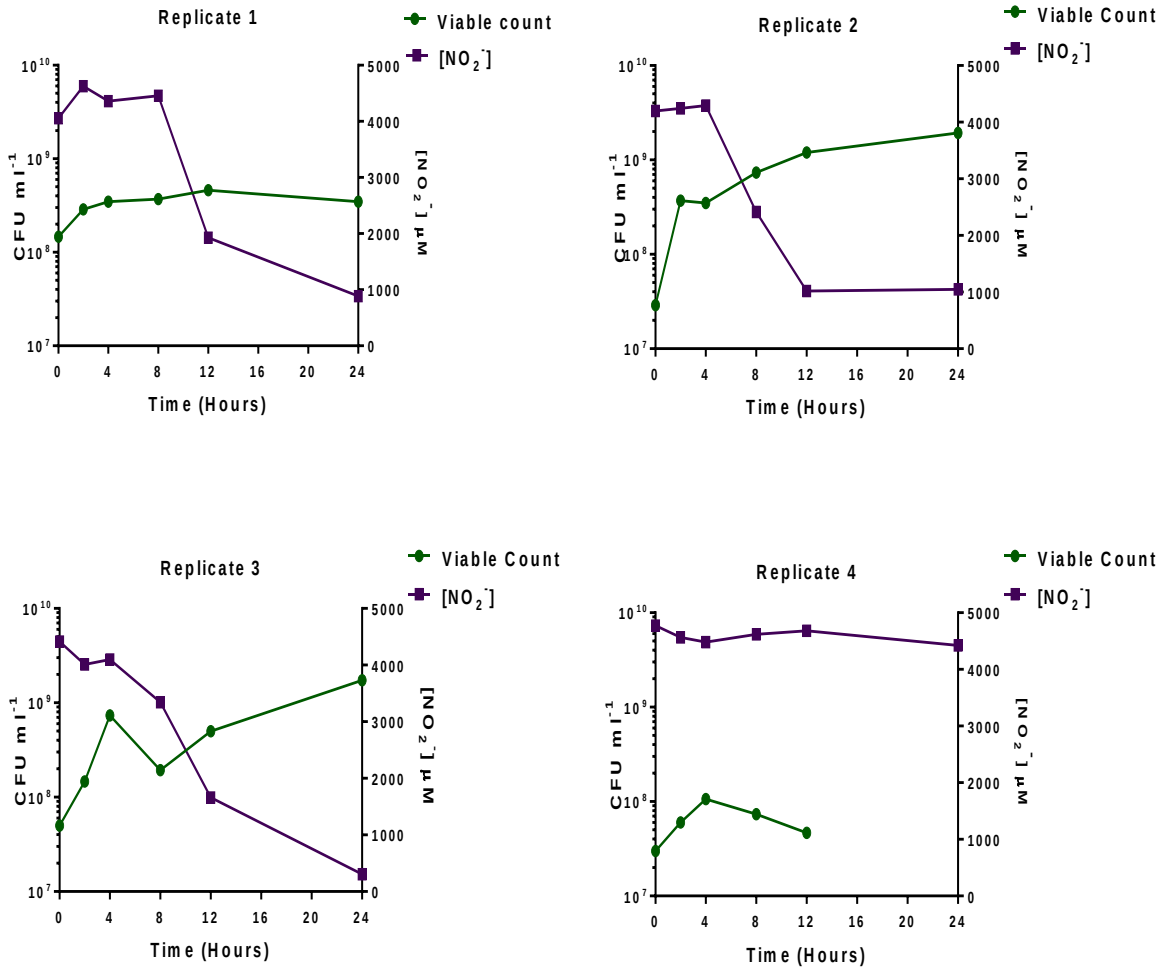

Figure 6.16 Transition from oxidative respiration to denitrification in the three out of four identical cultures of Δ*aniA/aniA*$^+$.

All the cultures were incubated in 25 ml MHB with an initial OD_{600nm} of 0.05 in the presence of 5 mM $NaNO_2$ with mild agitation at 90 rev/minute. Media were collected at 0, 2, 4, 8, 12 and 24 hour timepoints. 1 ml of sample from each condition was stored for later [NO_2^-] measurement by Griess Assay **(Section 2.10.1)** and another 1 ml was used for doing viable count using dilutional plating.

6.4 Discussion

This chapter presents preliminary data that the meningococcal denitrification pathway has a role in differential biofilm formation *in vitro* **(Figure 6.1 - 6.2).** Given that presence of exopolysaccharides (EPS) is feature of a true biofilm structure (Hall-Stoodley *et al*, 2004), microscopic analysis has to be performed after staining the biofilm to confirm this. Congo red staining helps to detect the β-glucan component of EPS (Yi *et al*, 2004). Interestingly, meningococci formed biofilm with 50 µM SpermineNONOate supplementation in starvation media in static condition. SpermineNONOate is a rapid acting NO donor which was added to induce removal of the *nsrR* mediated repression of the meningococcal denitrification pathway (Heurlier *et al*, 2008; Rock *et al*, 2007). Some of the NO released by SpermineNO would have been converted to NO_2^- over time. This would have induced the expression of denitrification genes in a starved media as the competition amongst the bacteria to exploit the scarce alternative energy resources would have been intense.

For testing the role of *aniA* in biofilm formation, a reverse complemented strain (Δ*aniA/aniA*$^+$) was generated and successfully characterised. This is the first study reporting successful reverse complementation of Δ*aniA/aniA*$^+$ strain **(Figure 6.14, 6.15 and 6.16).** However, essential experiments for investigating the role of *aniA* in differential biofilm formation using the newly characterised Δ*aniA/aniA*$^+$ alongside the Δ*aniA* and Wt strains as presented in **Section 6.3.1** could not be performed due to the time constraints on the project.

As can be seen from **Figure 6.6**, a 1.173 Kb *aniA* was apparent for Δ*aniA/aniA*$^{IPTG+}$ strain and Wt but not from the Δ*aniA* as expected. The 1.173 Kb sequence represents the coding sequence of *aniA*. However, the functional characterisation growth curves **(Figure 6.7 – 6.8)** showed that *aniA* activity was not restored in the Δ*aniA/aniA*$^{IPTG+}$ when induced by the addition of 1 mM IPTG in the growth media.

Figure 6.14 showed that Δ*aniA/aniA*$^+$ where *aniA* was reverse complemented along with its upstream regulatory protein (NarP, Fur, NsrR and FNR) binding sites and the endogenous promoter **(Figure 6.10),** it showed the expected 1.6 Kb band after PCR which was also evident with the Wt GD amplification PCR product. In addition, another band was apparent with Δ*aniA* and Δ*aniA/aniA*$^+$ GD PCR amplification products **(Figure 6.14).** This 3.6 Kb band represented the 2.0 Kb spectinomycin cassette flanked by disrupted *aniA* regions. Therefore the two bands (3.6 Kb and 1.6 Kb) with Δ*aniA/aniA*$^+$ GD PCR template confirmed the presence of disrupted version of *aniA* (3.6 Kb band) as well as a complemented version of *aniA* along with its

endogenous upstream regulatory elements (1.6 Kb) at a different locus. The functional characterisation growth curve **(Figure 6.15)** also provided evidence for the *aniA* activity restoration in Δ*aniA/aniA*$^+$ as shown by a significant decrease in NO_2^- **(Figure 6.15 A)** but a significant increase in viable count **(Figure 6.15 B)** at 8 and 12 hour timepoints compared to Wt and Δ*aniA* conditions. This implies that along with the environmental cues such as the absence of oxygen and presence of NO_2^-, *aniA* activity is regulated by a complex set of regulatory proteins which have binding sites to the upstream of *aniA* coding region **(Figure 6.10).**

It is noteworthy that three out of four replicates performed in the presence of 5 mM $NaNO_2$, Δ*ania/aniA*$^+$ made a successful transition from oxidative respiration to denitrification **(Figure 6.16).** This was evidenced by the increase in growth (viable count) coinciding with the depletion of NO_2^- **(Figure 6.16 A, B, C)** and thereby confirming the restored AniA activity in the newly created Δ*aniA/aniA*$^+$. However, NO_2^- depletion was not apparent in the fourth replicate **(Figure 6.16 D).** It could have been due to an unexpected reduction in the number of viable bacteria recovered with Δ*aniA/aniA*$^+$ at 24 hour timepoint. Unlike other microaerobic growth curves performed in this project **(Chapter 4, Figure 4.11 and Chapter 6, Figure 6.7),** obvious transition from aerobic to microaerobic growth was not apparent with the Wt MC 58 strain in the Δ*aniA/aniA*$^+$ characterisation growth curve **(Figure 6.15).** Transition from aerobic to microaerobic respiration was apparent only in one out of four identical batch culture growth curves of Wt MC58 (separate graph for Wt replicates data not shown)**.** This is not surprising given that there have been several studies reporting the presence of polymorphisms in *aniA* activity in the isolates of *N. meningitidis* which is conserved across other *Neisseria spp (*Barth *et al,* 2009*;* Ku *et al,* 2009*;* Stefanelli *et al,* 2008). Another study reported that transition from oxidation to denitrification is unstable and inconsistent in meningococci. AniA activity was observed in four out of six identical microaerobic cultures of *N. meningitidis* (Moir, 2011). In other *Neisseria spp.,* AniA can receive electrons from both cytochrome C_5 and via the CcoP domain of cytochrome cbb_3 oxidase. However, AniA of *N. meningitidis* only receives electrons from the cytochrome C_5 as one of the CcoP domain of cytochrome cbb_3 oxidase is non functional due to a single nucleotide polymorphism which is a meningococci specific adaptation (Aspholm *et al,* 2010). This indicates that there could be an evolutionary pressure on *N. meningitidis* to remove *aniA.* Variable transient accumulation of NO by *aniA* activity could account for the variable transition from aerobic growth to denitrification (Rock *et al,* 2005). A significant reduction in the viable count from Wt MC58 strain in the presence of 5

mM $NaNO_2$ **(Figure 6.15 B)** indicates that there would have been an unexpected NO mediated cytotoxicity in the culture.

It is to be noted that there is limited clinical evidence to date for biofilm formation by *N. meningitidis in vivo*. In the biopsies takes from patients with purpura fulminas, a feature of meningococcal sepsis, virulence factors such as capsule, pili and porA were found to be expressed in microcolonies (Harrison *et al,* 2002). Histological studies from rat tissue have demonstrated that meningococci can proliferate in microcolony like structures in these brain capillaries when the blood flow is temporarily low (Mairey *et al,* 2006). This observation would imply that it is possible for meningococcal biofilm to exist in the bloodstream of septic patients. Although biofilm is generally considered to be a feature of chronic infection, these observations indicate that meningococcal biofilm formation could occur during a symptomatic infection. During another study where tonsils were removed from the carriers of *N. meningitidis,* microcolonies were found below the epithelial surface (Sim *et al,* 2000). Given that microcolonies form the basic unit of bacterial biofilm (Costerton *et al,* 1995), the tonsillar meningococcal aggregate could resemble the actual biofilm structure. Evidence for biofilm formation exists in the nasopharynx, the natural niche for the meningococci (Coticchia *et al,* 2007). However, microcolonies found from none of the studies mentioned above were followed up with high resolution imaging for determining the presence of a biofilm matrix, which would have confirmed the presence of a mature biofilm. Therefore a comprehensive study on the tissues excised during adenoidectomy, tonsillectomy and subsequent experimental characterisation of tissue section for the presence of mature meningococcal biofilm would be useful. Since the nasopharynx is an oxygen poor and NO rich environment (Lundberg & Weitzberg, 1999), the meningococcal denitrification pathway would play a vital role in establishing the mature biofilm. The data presented in this chapter indicated that an inability to denitrify results in impaired biofilm formation *in vitro* **(Figure 6.1 - 6.2).** Since *aniA* is essential for switching to denitrification from oxidative respiration, the generation and characterisation of Δ*aniA/aniA*$^+$ **(Section 6.5- 6.6)** will be pivotal in investigating the hypothesis that *aniA* is essential for meningococcal biofilm formation *in vitro* in future.

7 Chapter 7: General Discussion

Using the pre-existing NO metabolising gene mutants, we demonstrate that meningococcal NO metabolism does not differentially regulate the physiologically important regulatory molecules such as SNO, NO_2^-, NO_x in a murine model of early acute meningococcal sepsis **(Chapter 3)**. The newly generated strains with the deletion of multiple genes responsible for NO metabolism were created and characterised to explore the effect of multiple genes on meningococcal pathogenesis **(Chapter 4)**. Barrier function and cytokine profile of the HPEC-ALIs **(Chapter 5),** a primary epithelial cell sharing similar properties to nasopharyngeal epithelium were unperturbed by meningococcal NO metabolism. Preliminary data showed that NO metabolism could be important for meningococcal biofilm formation *in vitro* which is to be followed up in future experiments using the newly generated and characterised reverse complemented strain *(Δ$aniA/aniA^+$)* **(Chapter 6).**

Previously, our group has shown that bacterial NO detoxification reduces the concentration of host-cell S-nitrosothiol (SNO), a vital post-translational modification akin to phosphorylation, in murine macrophages *in vitro* (Laver *et al,* 2010). Proteomic analysis on the same cell line revealed that a number of SNO proteins are differentially regulated in relation to the bacterial NO detoxification machinery (Dr Jay Laver, personal communication). In the murine model of early fulminant meningococcal septicaemia, we were able to reproducibly detect NO metabolites following meningococcal infection **(Chapter 3)**. We showed that bacterial burden correlates positively with plasma SNO and hepatic NO_2^- but negatively with hepatic NO_x. This is the first study reporting an abundance of SNO molecules in an early murine model of acute sepsis. Inclusion of human holo transferrin made the model more physiologically relevant to human as meningococci can only harness iron by binding to human transferrin due to receptor compatibility of meningococcal transferrin binding proteins (Gorringe *et al*, 2005; Renauld-Mongenie *et al*, 2004). However, bacterial NO metabolism did not differentially modulate SNO and other NO metabolite profile of murine blood and liver tissue**.** Multiple reasons could account for not observing meningococcal NO metabolism mediated effect on SNO depletion *in vivo* contrary to the finding from the *in vitro* study in the murine J774.2 cell line (Laver *et al,* 2010). As explained in the discussion section of Chapter 3 **(Section 3.6),** SNO depletion by meningococcal NO metabolism could be a localised cell specific (i.e. macrophages) phenomenon which is not detectable *in vivo* at the whole tissue/animal level. Secondly, there could have been lack of meningococcal NO metabolism due to the abundance of oxygen and a lack of spatiotemporally available NO required for observing any NO mediated effect *in vivo.*

Multiple studies on human septic patients have reported decreased amount of oxygen consumption in tissues due to defective mitochondrial oxidative respiration (Adrie *et al*, 2001; Brealey *et al*, 2002; Garrabou *et al*, 2012; Yamakawa *et al*, 2013). Decreased oxygen consumption in ileum and liver has been reported in model of septic rat and mouse respectively (Carchman *et al*, 2013; King *et al*, 1999). As observed with human septic patients mitochondrial dysfunction has been attributed for decreased oxidative respiration by host tissues in septic model of rodents (Brealey *et al*, 2004; Singer, 2014). A microarray analysis performed on RNA extracted from critically ill acute septic patients at 0, 4, 8, 12, 24 and 48 hour time points revealed that the expression of genes relating to oxidative phosphorylation falls early and continues to decrease throughout the course of sepsis (Raman *et al*, 2015). As more than 90% of the available oxygen in body is used by mitochondria (Nathan & Singer, 1999) it could be possible that in our murine model of early acute meningococcal sepsis, there was an abundance of oxygen due to inability of the host cells to consume oxygen for ATP generation via oxidative respiration. Previous study has demonstrated that *norB* is essential for the survival of meningococci in nasopharyngeal mucosa and human macrophages (Stevanin *et al*, 2005). The viable bacteria recovered from Δ*norB* infection were significantly lower than that of Wt infection. This effect was diminished when the cells were treated with NOS inhibitor, N^G-Monomethyl-L-arginine (L-NMMA) implying that *norB* mediated survival is important in highly cytotoxic NO environment. In our *in vivo* murine model there was no statistically significant difference between the recovery of number of viable bacteria from Wt and Δ*norB* infected mice **(Figure 3.5, 3.9 and 3.14).** Therefore, it is possible that generated cytotoxic amounts of NO by murine tissues in response to meningococcal infection would have inhibited the oxidative respiration of the host cells by interacting with the mitochondrial enzyme complexes (Almeida *et al*, 2005; Brown, 2001; Cleeter *et al*, 1994) leading to the accumulation of unconsumed oxygen. Indeed evidence from multiple studies exist for mitochondrial dysfunction mediated by NO overproduction in both human and rodent septic models (Brealey *et al*, 2002; Brealey *et al*, 2004; Vanasco *et al*, 2012). An oxygen abundant and spatiotemporally NO deficient environment can lead to a number of important ramifications for observing any meningococcal NO metabolism mediated activity. Firstly, meningococci prefer respiration by O_2 reduction over NO_2^- reduction as O_2 has higher affinity for electron compared to NO_2^-. This is due to fact that the redox potential of O_2/H_2O (+820 mV) is higher than that of NO_2^-/NO (+348 mV) (Conrad, 1990). Furthermore, higher energy is liberated by proton translocation by the flow of electrons towards O_2 physiologically in comparison to that of NO_2^-. The translocated protons are used to generate ATP for the organism. In presence of

both O_2 and NO_2^-, reduction of O_2 is preferable due to the generation of higher energy in the form of more ATPs. Therefore, meningococci would continue aerobic respiration in the presence of high oxygen. This would have led to diminished or reduced activity of meningococcal denitrification pathway pivotal for observing any NO mediated effect in our murine model of early acute sepsis. Secondly, *in vitro* study showed that meningococcal *norB* mediated SNO depletion was not evident when the J774.2 murine macrophages were co-infected with bacterial strains in the presence of an iNOS inhibitor (1400W) (Laver *et al*, 2010). This implies that *norB* precludes SNO formation by degrading the S-nitrosylating substrate, NO required for SNO formation instead of degrading the pre-existing SNO molecules. The lack of spatiotemporally available NO would also result in the persistence of *nsrR* mediated repression of *norB* activity as high NO concentration (~1 µM) is a pre-requisite for relieving *nsrR* mediated repression of denitrification regulon (Heurlier *et al*, 2008; Rock *et al*, 2007). Therefore, an oxygen abundant and spatiotemporally NO deficient environment *in vivo* would imply that there was not enough NO for detecting the impairment of SNO formation by meningococcal *norB* activity as observed *in vitro*.

To investigate the effect of multiple meningococcal denitrification genes (*aniA* and *norB*) on the cellular pathology of meningococcal sepsis, we constructed and characterised a panel of NO metabolising gene mutants (Δ*aniA/*Δ*norB*, Δ*nsrR/*Δ*norB*, Δ*aniA/*Δ*norB/*Δ*nsrR*) using the isocloning method **(Chapter 4).** Although functional inactivation of the denitrification genes were demonstrated in the newly generated mutants *(*Δ*aniA/*Δ*norB,* Δ*nsrR/*Δ*norB,* Δ*aniA/*Δ*norB/*Δ*nsrR*) **(Chapter 4),** it will be useful to perform western blot using antibodies developed against AniA, NorB and NsrR to check for these protein production. The blots can be performed on samples extracted at different timepoints to get an estimation of these protein expression over time. It would also be interesting to examine the *aniA* coding region complemented Δ*aniA/aniA*$^{IPTG+}$ for any AniA protein production as the functional restoration was not observed in the characterisation growth curves **(Figure 6.7 - 6.8).** Similar AniA detection western blot can be performed to test the AniA production in the newly generated Δ*aniA/aniA*$^{+}$ strain where *aniA* was complemented along with the upstream regulatory elements **(Figure 6.14 - 6.16).** This would inform us about comparative AniA protein activity in all the replicates where we and other researchers observed inconsistent *aniA* activity (Barth *et al*, 2009; Moir, 2011). Pili, opa and opc are essential components of *N. meningitidis* for mediating the interaction with host cells **(Section 1.7).** Therefore, along with the wild type strain, the newly generated strains can be tested for the identical expression of these proteins.

This can be achieved by performing western blot using the monoclonal antibodies developed against these proteins (Kolb-Mäurer *et al,* 2001).

In addition, direct *norB* mediated NO metabolism was not evident from the growth curves presented in **Chapter 4 (Figure 4.11 and 4.13).** By using NO electrode it is possible to monitor the direct NO consumption by bacteria in batch culture growth curves (Heurlier *et al*, 2008; Rock *et al,* 2007). Direct detection of NO in identical batch culture growth curves **(Figure 4.11 and Figure 4.13)** will provide information on comparative NO consumption by different bacterial strains. In parallel with the growth curves in presence of a rapid acting NO donor (SpermineNONOate) **(Figure 4.13),** growth curves in presence of a slow NO releasing donor such as NOC-18 can be performed. This will help to measure the comparative NO consumption by different bacterial strains over longer period of time as NOC-18 has a half life of 20 hour (Keefer *et al,* 1996). These experiments will help not only to prove the *norB* inactivation in the newly generated strains comprehensively but also will provide a quantitative measurement of NO metabolism by different bacterial strains in batch culture growth curve. More replicates need to be performed to establish that there is no statistically significant difference in the downstream GpxA activity in Δ*norB,* Δ*aniA/*Δ*norB/*Δ*nsrR* due to polar effect caused by *norB* deletion in these strains compared to the Wt MC58 **(Figure 4.9).** Other newly generated *norB* deleted strains (Δ*aniA/*Δ*norB* and Δ*nsrR/*Δ*norB*) can also be included in the comparative GpxA assay for investigating the polar effect of *norB* deletion in these strains.

We demonstrated that bacterial burden inversely correlates with the barrier function (TER) but positively with the cytokine profile (IL-8, TNFα) of HPEC-ALI, a cell line having similar features to nasopharyngeal epithelial cell. However, meningococcal denitrification did not have any differential role in the regulation of barrier function and cytokine profile of the HPEC-ALIs in the experimental system we used **(Chapter 5).** There could have been a lack of NO activity in the HPEC-ALI system. Measurement of NO_x by chemiluminescence from the apical and basal supernatants of the HPEC-ALIs shows basal level of NO_x production (data not shown). This is important as NO can activate the TNF-converting enzyme (TACE) responsible for releasing the membrane bound TNFα (Zhang *et al,* 2000). Low levels of TNFα **(Figure 5.4 A and 5.9)** release following meningococcal infection points to the possibility of a reduced NO activity as TNFα acts as an inducer of NOS expression from endothelial and epithelial cells (Donnelly & Barnes, 2002; Robbins *et al,* 1997; Yan *et al,* 1997). Although both Δ*aniA/*Δ*norB* and Δ*aniA/*Δ*norB/*Δ*nsrR* lack NO metabolic capability due to the absence of *norB,* deletion of *aniA* meant that any present NO_2^- in the media would not have been reduced to NO and thereby

minimising a route for maximal presence of NO in an infection model of HPEC-ALIs. To address this an isogenic Δ*norB* can be used alongside the wild type strain to investigate any effect that may show the biggest difference from the wild type under conditions where NO metabolism is important.

Preliminary data also showed when biofilm formation was induced by nutrient starvation, Δ*aniA/*Δ*norB* showed a significantly reduced biofilm forming ability compared to the Wt strain measured by the crystal violet staining **(Chapter 6).** However, microscopic analysis has to be performed to confirm the presence of exopolysaccharides (EPS) in biofilm matrix given that EPS is an essential characteristic for a true biofilm structure (Hall-Stoodley *et al,* 2004). Congo red stains the β-(1→4)-linked D-glucopyranosyl units or β-(1→3)-D-glucan component of the exopolysaccharides in biofilm (Yi *et al,* 2004). Therefore, if stained positive it would confirm the presence of a true biofilm structure in the experimental system we used. Advanced microscopic toolkits such as confocal or scanning electron microscopy have to be used to examine the biofilm structure with high resolution and magnification (Asahi *et al,* 2015; Mueller *et al,* 2006). To study the interaction of biofilm with substratum atomic force microscopy can be used. It enables to model the biofilm substratum in both qualitative and quantitative manner by providing high resolution images at atomic level (Beech *et al,* 2002). This will be particularly important for our experimental system where preliminary data **(Section 6.3.1)** indicated that biofilm formation by bacterial denitrification could be a substratum specific phenomenon.

A previous study demonstrated that deletion of *narP*, a regulator of denitrification for both *N. gonorrhoeae* (Householder *et al,* 1999) and *N. meningitidis* (Barth *et al,* 2009) results in impaired meningococcal biofilm formation (Jamet *et al,* 2013). For investigating the role of *aniA* in the differential regulation of biofilm formation, a reverse complemented strain (Δ*aniA/aniA*$^{+}$) was created and characterised. This work provides important foundation for studying the role of meningococcal denitrification on biofilm formation. The future follow up work has the potential to shed light on the process of meningococcal colonisation as biofilm formation could be one of the strategies adopted by meningococci to survive and thrive in an NO rich environment such as nasopharynx (Lundberg *et al,* 1995; Lundberg & Weitzberg, 1999).

A number of studies (Lappann *et al,* 2006; Yi *et al,* 2004) have demonstrated that non-capsulated meningococcal strains cannot form biofilm which is contradictory to the finding

from another study where capsulated meningococci formed biofilm (Neil *et al*, 2009). Although the strains used in this project had capsular background, the presence of capsulated meningococci in biofilm has to be verified experimentally given that the expression of capsular genes is subject to regulation by phase variation through slipped strand mispairing and reversible insertion of mobile elements (Hammerschmidt *et al,* 1996a; Hammerschmidt *et al,* 1996b). Furthermore, the expression of capsule can be switched off/on at a high rate (Swartley *et al,* 1997). Capsule is an essential component of meningococcal adaptation machinery to resist complement mediated killing (Jarvis & Vedros, 1987) and for intracellular survival (Spinosa *et al,* 2007). Therefore, the investigation if capsulated meningococci can form biofilm is important given that the capsulated population would be better suited to evade host-immune clearance and cross the epithelial/endothelial cells (Nikulin *et al,* 2006; Spinosa *et al,* 2007). For verifying the presence of capsule in biofilm, the bacterial lysates from different experimental strains can be tested by PCR for the expression of *siaD* (polysialyltransferase), a gene responsible for coding the sialic acid component of meningococcal capsule or *ctrA*, an exclusive component of the meningococcal capsule biosynthesis locus (Bennett *et al,* 2004; Taha *et al,* 2005). In addition, ELISA can also be performed on the bacterial lysates for identifying capsule measured as immunoglobulins using specific antibodies directed against serogroup B capsule (Jordens *et al,* 2004; Williams *et al,* 2003).

Biofilm data presented in **Section 6.3.1** were performed in a 50% nutrient content starvation media that was altered just at specific timepoints (before the experiment and after 24 hour). However a flowsystem can be used to control the influx of nutrients into the media to determine the formation of biofilm at different nutrient compositions (Apicella *et al*, 2012). It will also enable us to continually supply NO into the system at a controlled manner which would mimic the physiological condition more closely. It will facilitate the investigation of the role of NO on biofilm formation over time. The newly constructed and characterised Δ*aniA/aniA*$^{+}$ could not be used to perform similar experiment as described in **Section 6.3.1** due to the time constraints on the project. Therefore, Δ*aniA/aniA*$^{+}$ will be used along with the Wt and Δ*aniA* in future to test the hypothesis that *aniA* is necessary for meningococcal biofilm formation *in vitro*. In parallel, Δ*norB/norB*$^{+}$ has to be constructed for performing similar experiments to examine the role of *norB* in differential biofilm formation. This future work has the potential to shed light on the contribution of meningococcal denitrification pathway on biofilm formation, a process which can be exploited by the meningococci to colonise and avoid innate immune mediated killing in the nasopharynx.

8 Chapter 8: References

Adrie C, Bachelet M, Vayssier-Taussat M, Russo-Marie F, Bouchaert I, Adib-Conquy M, Cavaillon JM, Pinsky MR, Dhainaut JF, Polla BS (2001) Mitochondrial membrane potential and apoptosis peripheral blood monocytes in severe human sepsis. *Am J Respir Crit Care Med* **164:** 389-395

Al-Tawfiq JA, Clark TA, Memish ZA (2010) Meningococcal disease: the organism, clinical presentation, and worldwide epidemiology. *J Travel Med* **17:** 3-8

Ala'aldeen DA, Oldfield NJ, Bidmos FA, Abouseada NM, Ahmed NW, Turner DP, Neal KR, Bayliss CD (2011) Carriage of meningococci by university students, United Kingdom. *Emerg Infect Dis* **17:** 1762-1763

Allen BW, Piantadosi CA (2006) How do red blood cells cause hypoxic vasodilation? The SNO-hemoglobin paradigm. *Am J Physiol Heart Circ Physiol* **291:** H1507-H1512

Almeida A, Cidad P, Delgado-Esteban M, Fernandez E, Garcia-Nogales P, Bolanos JP (2005) Inhibition of mitochondrial respiration by nitric oxide: its role in glucose metabolism and neuroprotection. *J Neurosci Res* **79:** 166-171

Andersson JA, Cervin A, Lindberg S, Uddman R, Cardell LO (2002) The paranasal sinuses as reservoirs for nitric oxide. *Acta Otolaryngol* **122:** 861-865

Anjum MF, Stevanin TM, Read RC, Moir JW (2002) Nitric oxide metabolism in *Neisseria meningitidis*. *J Bacteriol* **184:** 2987-2993

Apicella MA, Shao J, Neil RB (2012) Methods for studying *Neisseria meningitidis* biofilms. *Methods Mol Biol* **799:** 169-184

Arnold WP, Mittal CK, Katsuki S, Murad F (1977) Nitric oxide activates guanylate cyclase and increases guanosine 3′:5′-cyclic monophosphate levels in various tissue preparations. *Proc Natl Acad Sci USA* **74:** 3203-3207

Artenstein MS, Gold R, Zimmerly JG, Wyle FA, Schneider H, Harkins C (1970) Prevention of meningococcal disease by group C polysaccharide vaccine. *New Eng J Med* **282:** 417-420

Asahi Y, Miura J, Tsuda T, Kuwabata S, Tsunashima K, Noiri Y, Sakata T, Ebisu S, Hayashi M (2015) Simple observation of *Streptococcus* mutans biofilm by scanning electron microscopy using ionic liquids. *AMB Express* **5:** 6

Aspholm M, Aas FE, Harrison OB, Quinn D, Vik Å, Viburiene R, Tønjum T, Moir J, Maiden MCJ, Koomey M (2010) Structural alterations in a component of cytochrome c oxidase and molecular evolution of pathogenic *Neisseria* in humans. *PLoS Pathog* **6:** e1001055

Bai X, Findlow J, Borrow R (2011) Recombinant protein meningococcal serogroup B vaccine combined with outer membrane vesicles. *Expert Opin Biol Ther* **11:** 969-985

Baines PB, Stanford S, Bishop-Bailey D, Sills JA, Thomson AP, Mitchell JA, Fear SC, Hart CA, Petros AJ (1999) Nitric oxide production in meningococcal disease is directly related to disease severity. *Crit Care Med* **27:** 1187-1190

Baraff LJ, Lee SI, Schriger DL (1993) Outcomes of bacterial meningitis in children: a meta-analysis. *Pediatr Infect Dis J* **12:** 389-394

Barnes PJ, Liew FY (1995) Nitric oxide and asthmatic inflammation. *Immunol Today* **16:** 128-130

Barraud N, Hassett DJ, Hwang SH, Rice SA, Kjelleberg S, Webb JS (2006) Involvement of nitric oxide in biofilm dispersal of *Pseudomonas aeruginosa*. *J Bacteriol* **188:** 7344-7353

Bartberger MD, Mannion JD, Powell SC, Stamler JS, Houk KN, Toone EJ (2001) S-N dissociation energies of S-nitrosothiols: on the origins of nitrosothiol decomposition rates. *J Am Chem Soc* **123:** 8868-8869

Barth KR, Isabella VM, Clark VL (2009) Biochemical and genomic analysis of the denitrification pathway within the genus *Neisseria*. *Microbiology* **155:** 4093-4103

Bartolini E, Frigimelica E, Giovinazzi S, Galli G, Shaik Y, Genco C, Welsch JA, Granoff DM, Grandi G, Grifantini R (2006) Role of FNR and FNR-regulated, sugar fermentation genes in *Neisseria meningitidis* infection. *Mol Microbiol* **60:** 963-972

Bauer FJ, Rudel T, Stein M, Meyer TF (1999) Mutagenesis of the *Neisseria gonorrhoeae* porin reduces invasion in epithelial cells and enhances phagocyte responsiveness. *Mol Microbiol* **31:** 903-913

Beaumont HJ, Lens SI, Reijnders WN, Westerhoff HV, van Spanning RJ (2004) Expression of nitrite reductase in *Nitrosomonas europaea* involves NsrR, a novel nitrite-sensitive transcription repressor. *Mol Microbiol* **54:** 148-158

Beech IB, Smith JR, Steele AA, Penegar I, Campbell SA (2002) The use of atomic force microscopy for studying interactions of bacterial biofilms with surfaces. *Colloids and Surfaces B: Biointerfaces* **23:** 231-247

Benhar M, Forrester MT, Stamler JS (2009) Protein denitrosylation: enzymatic mechanisms and cellular functions. *Nat Rev Mol Cell Biol* **10:** 721-732

Bennett DE, Mulhall RM, Cafferkey MT (2004) PCR-based assay for detection of *Neisseria meningitidis* capsular serogroups 29E, X, and Z. *J Clin Microbiol* **42:** 1764-1765

Beno DW, Devine LF, Larson GL (1968) Identification of *Neisseria meningitidis* carbohydrate fermentation patterns in Mueller-Hinton broth. *J Bacteriol* **96:** 563

Bentley SD, Vernikos GS, Snyder LAS, Churcher C, Arrowsmith C, Chillingworth T, Cronin A, Davis PH, Holroyd NE, Jagels K, Maddison M, Moule S, Rabbinowitsch E, Sharp S, Unwin L, Whitehead S, Quail MA, Achtman M, Barrell B, Saunders NJ, Parkhill J (2007) Meningococcal genetic variation mechanisms viewed through comparative analysis of serogroup C strain FAM18. *PLoS Genet* **3:** 230-240

Berks BC, Ferguson SJ, Moir JW, Richardson DJ (1995) Enzymes and associated electron transport systems that catalyse the respiratory reduction of nitrogen oxides and oxyanions. *Biochim Biophys Acta* **1232:** 97-173

Bevanger L, Bergh K, Gisnas G, Caugant DA, Froholm LO (1998) Identification of nasopharyngeal carriage of an outbreak strain of *Neisseria meningitidis* by pulsed-field gel electrophoresis versus phenotypic methods. *J Med Microbiol* **47:** 993-998

Bhattacharjee AK, Jennings HJ, Kenny CP, Martin A, Smith IC (1975) Structural determination of the sialic acid polysaccharide antigens of *Neisseria meningitidis* serogroups B and C with carbon 13 nuclear magnetic resonance. *J Biol Chem* **250:** 1926-1932

Binet MRB, Cruz-Ramos H, Laver J, Hughes MN, Poole RK (2002) Nitric oxide releases intracellular zinc from prokaryotic metallothionein in *Escherichia coli*. *FEMS Microbiol Lett* **213:** 121-126

Birkness KA, Swisher BL, White EH, Long EG, Ewing EP, Jr., Quinn FD (1995) A tissue culture bilayer model to study the passage of *Neisseria meningitidis*. *Infect Immun* **63:** 402-409

Bodenmiller DM, Spiro S (2006) The yjeB (*nsrR*) gene of *Escherichia coli* encodes a nitric oxide-sensitive transcriptional regulator. *J Bacteriol* **188:** 874-881

Bogdan C (2001) Nitric oxide and the immune response. *Nat Immunol* **2:** 907-916

Bone RC, Balk RA, Cerra FB, Dellinger RP, Fein AM, Knaus WA, Schein RM, Sibbald WJ (1992) Definitions for sepsis and organ failure and guidelines for the use of innovative therapies in sepsis. the accp/sccm consensus conference committee. american college of chest physicians/society of critical care medicine. *Chest* **101:** 1644-1655

Boon EM, Huang SH, Marletta MA (2005) A molecular basis for NO selectivity in soluble guanylate cyclase. *Nat Chem Biol* **1:** 53-59

Booy R, Habibi P, Nadel S, de Munter C, Britto J, Morrison A, Levin M (2001) Reduction in case fatality rate from meningococcal disease associated with improved healthcare delivery. *Arch Dis Child* **85:** 386-390

Boublil L, Assemat E, Borot MC, Boland S, Martinon L, Sciare J, Baeza-Squiban A (2013) Development of a repeated exposure protocol of human bronchial epithelium in vitro to study the long-term effects of atmospheric particles. *Toxicol In Vitro* **27:** 533-542

Boulanger MJ, Murphy ME (2002) Crystal structure of the soluble domain of the major anaerobically induced outer membrane protein (AniA) from pathogenic *Neisseria:* a new class of copper-containing nitrite reductases. *J Mol Biol* **315:** 1111-1127

Bove PF, van der Vliet A (2006) Nitric oxide and reactive nitrogen species in airway epithelial signaling and inflammation. *Free Radic Biol Med* **41:** 515-527

Bove PF, Wesley UV, Greul AK, Hristova M, Dostmann WR, van der Vliet A (2007) Nitric oxide promotes airway epithelial wound repair through enhanced activation of MMP-9. *Am J Respir Cell Mol Biol* **36:** 138-146

Brandtzaeg P, Ovsteboo R, Kierulf P (1992) Compartmentalization of lipopolysaccharide production correlates with clinical presentation in meningococcal disease. *J Infect Dis* **166:** 650-652

Brandtzaeg P, van Deuren M (2012) Classification and pathogenesis of meningococcal infections. *Methods Mol Biol* **799:** 21-35

Branham SE (1953) Serological relationships among meningococci. *Bacteriol Rev* **17:** 175-188

Branka JE, Vallette G, Jarry A, Laboisse CL (1997) Stimulation of mucin exocytosis from human epithelial cells by nitric oxide: evidence for a cGMP-dependent and a cGMP-independent pathway. *Biochem J* **323:** 521-524

Brealey D, Brand M, Hargreaves I, Heales S, Land J, Smolenski R, Davies NA, Cooper CE, Singer M (2002) Association between mitochondrial dysfunction and severity and outcome of septic shock. *Lancet* **360:** 219-223

Brealey D, Karyampudi S, Jacques TS, Novelli M, Stidwill R, Taylor V, Smolenski RT, Singer M (2004) Mitochondrial dysfunction in a long-term rodent model of sepsis and organ failure. *Am J Physiol Regul Integr Comp Physiol* **286:** R491-R497

Bristow WM, Peenen PFDV, Volk R (1965) Epidemic meningitis in naval recruits. *Am J Public Health Nations Health* **55:** 1039-1045

Brook I (2003) Effects of antimicrobial therapy on the microbial flora of the adenoids. *J Antimicrob Chemother* **51:** 1331-1337

Brown GC (2001) Regulation of mitochondrial respiration by nitric oxide inhibition of cytochrome c oxidase. *Biochim Biophys Acta* **1504:** 46-57

Brown GC, Cooper CE (1994) Nanomolar concentrations of nitric oxide reversibly inhibit synaptosomal respiration by competing with oxygen at cytochrome oxidase. *FEBS Lett* **356:** 295-298

Buerk DG (2007) Nitric oxide regulation of microvascular oxygen. *Antioxid Redox Signal* **9:** 829-843

Buras JA, Holzmann B, Sitkovsky M (2005) Animal models of sepsis: setting the stage. *Nat Rev Drug Discov* **4:** 854-865

Burgner D, Rockett K, Kwiatkowski D (1999) Nitric oxide and infectious diseases. *Arch Dis Child* **81:** 185-188

Busch T, Kuhlen R, Knorr M, Kelly K, Lewandowski K, Rossaint R, Falke KJ, Gerlach H (2000) Nasal, pulmonary and autoinhaled nitric oxide at rest and during moderate exercise. *Intensive Care Med* **26:** 391-399

Callaghan MJ, Jolley KA, Maiden MCJ (2006) Opacity-associated adhesin repertoire in hyperinvasive *Neisseria meningitidis*. *Infect Immun* **74:** 5085-5094

Canil C, Rosenshine I, Ruschkowski S, Donnenberg MS, Kaper JB, Finlay BB (1993) Enteropathogenic *Escherichia coli* decreases the transepithelial electrical resistance of polarized epithelial monolayers. *Infect Immun* **61:** 2755-2762

Capecchi B, Adu-Bobie J, Di Marcello F, Ciucchi L, Masignani V, Taddei A, Rappuoli R, Pizza M, Arico B (2005) *Neisseria meningitidis* NadA is a new invasin which promotes bacterial adhesion to and penetration into human epithelial cells. *Mol Microbiol* **55:** 687-698

Carchman EH, Whelan S, Loughran P, Mollen K, Stratamirovic S, Shiva S, Rosengart MR, Zuckerbraun BS (2013) Experimental sepsis-induced mitochondrial biogenesis is dependent on autophagy, TLR4, and TLR9 signaling in liver. *FASEB J* **27:** 4703-4711

Cardinale JA, Clark VL (2000) Expression of AniA, the major anaerobically induced outer membrane protein of *Neisseria gonorrhoeae*, provides protection against killing by normal human sera. *Infect Immun* **68:** 4368-4369

Cartwright K, Noah N, Peltola H (2001) Meningococcal disease in Europe: epidemiology, mortality, and prevention with conjugate vaccines. Report of a European advisory board meeting Vienna, Austria, 6-8 October, 2000. *Vaccine* **19:** 4347-4356

Caugant DA, Hoiby EA, Magnus P, Scheel O, Hoel T, Bjune G, Wedege E, Eng J, Froholm LO (1994) Asymptomatic carriage of *Neisseria meningitidis* in a randomly sampled population. *J Clin Microbiol* **32:** 323-330

Caugant DA, Maiden MCJ (2009) Meningococcal carriage and disease—Population biology and evolution. *Vaccine* **27:** B64-B70

Caugant DA, Tzanakaki G, Kriz P (2007) Lessons from meningococcal carriage studies. *FEMS Microbiol Rev* **31:** 52-63

Chamot-Rooke J, Mikaty G, Malosse C, Soyer M, Dumont A, Gault J, Imhaus AF, Martin P, Trellet M, Clary G, Chafey P, Camoin L, Nilges M, Nassif X, Dumenil G (2011) Posttranslational modification of pili upon cell contact triggers *N. meningitidis* dissemination. *Science* **331:** 778-782

Chevillard M, Hinnrasky J, Pierrot D, Zahm JM, Klossek JM, Puchelle E (1993) Differentiation of human surface upper airway epithelial cells in primary culture on a floating collagen gel. *Epithelial Cell Biol* **2:** 17-25

Chiou WF, Chen CF, Lin JJ (2000) Mechanisms of suppression of inducible nitric oxide synthase (iNOS) expression in RAW 264.7 cells by andrographolide. *Br J Pharmacol* **129:** 1553-1560

Christensen H, May M, Bowen L, Hickman M, Trotter CL (2010) Meningococcal carriage by age: a systematic review and meta-analysis. *Lancet Infect Dis* **10:** 853-861

Christianson DW (2005) Arginase: structure, mechanism, and physiological role in male and female sexual arousal. *Acc Chem Res* **38:** 191-201

Clark VL, Campbell LA, Palermo DA, Evans TM, Klimpel KW (1987) Induction and repression of outer membrane proteins by anaerobic growth of *Neisseria gonorrhoeae*. *Infect Immun* **55:** 1359-1364

Cleeter MWJ, Cooper JM, Darley-Usmar VM, Moncada S, Schapira AHV (1994) Reversible inhibition of cytochrome c oxidase, the terminal enzyme of the mitochondrial respiratory chain, by nitric oxide: Implications for neurodegenerative diseases. *FEBS Lett* **345:** 50-54

Comanducci M, Bambini S, Brunelli B, Adu-Bobie J, Arico B, Capecchi B, Giuliani MM, Masignani V, Santini L, Savino S, Granoff DM, Caugant DA, Pizza M, Rappuoli R, Mora M (2002) NadA, a novel vaccine candidate of *Neisseria meningitidis*. *J Exp Med* **195:** 1445-1454

Comanducci M, Bambini S, Caugant DA, Mora M, Brunelli B, Capecchi B, Ciucchi L, Rappuoli R, Pizza M (2004) NadA diversity and carriage in *Neisseria meningitidis*. *Infect Immun* **72:** 4217-4223

Conrad R (1990) Flux of NOx between soil and atmosphere: importance and soil microbial metabolism. In *Denitrification in Soil and Sediment*, Revsbech N, Sørensen J (eds), Vol. 56, pp 105-128.

Costerton JW, Lewandowski Z, Caldwell DE, Korber DR, Lappin-Scott HM (1995) Microbial biofilms. *Annu Rev Microbiol* **49:** 711-745

Costerton JW, Stewart PS, Greenberg EP (1999) Bacterial biofilms: a common cause of persistent infections. *Science* **284:** 1318-1322

Coticchia J, Zuliani G, Coleman C, et al. (2007) Biofilm surface area in the pediatric nasopharynx: Chronic rhinosinusitis vs obstructive sleep apnea. *Arch Otolaryngol Head Neck Surg* **133:** 110-114

Coureuil M, Mikaty G, Miller F, Lécuyer H, Bernard C, Bourdoulous S, Duménil G, Mège R-M, Weksler BB, Romero IA, Couraud P-O, Nassif X (2009) Meningococcal type IV pili recruit the polarity complex to cross the brain endothelium. *Science* **325:** 83-87

Cox AG, Saunders DC, Kelsey PB, Jr., Conway AA, Tesmenitsky Y, Marchini JF, Brown KK, Stamler JS, Colagiovanni DB, Rosenthal GJ, Croce KJ, North TE, Goessling W (2014) S-nitrosothiol signaling regulates liver development and improves outcome following toxic liver injury. *Cell Rep* **6:** 56-69

Crane BR, Arvai AS, Gachhui R, Wu C, Ghosh DK, Getzoff ED, Stuehr DJ, Tainer JA (1997) The structure of nitric oxide synthase oxygenase domain and inhibitor complexes. *Science* **278:** 425-431

Crawford JH, Chacko BK, Pruitt HM, Piknova B, Hogg N, Patel RP (2004) Transduction of NO-bioactivity by the red blood cell in sepsis: novel mechanisms of vasodilation during acute inflammatory disease. *Blood* **104:** 1375-1382

Cross R, Aish J, Paston SJ, Poole RK, Moir JW (2000) Cytochrome c' from *Rhodobacter capsulatus* confers increased resistance to nitric oxide. *J Bacteriol* **182:** 1442-1447

Cross R, Lloyd D, Poole RK, Moir JW (2001) Enzymatic removal of nitric oxide catalyzed by cytochrome c' in *Rhodobacter capsulatus*. *J Bacteriol* **183:** 3050-3054

Cruz-Ramos H, Crack J, Wu G, Hughes MN, Scott C, Thomson AJ, Green J, Poole RK (2002) NO sensing by FNR: regulation of the *Escherichia coli* NO-detoxifying flavohaemoglobin, Hmp. *EMBO J* **21:** 3235-3244

Culotta E, Koshland D (1992) NO news is good news. *Science* **258:** 1862-1865

Danielson L, Mann, E. (1806) Letter to medical and agricultural registrar. *Boston, MA*

Dankert J (2004) *Neisseria*. IN Cohen, J.P., W. (Ed.). *Infectious Diseases, 2nd ed New York Mosby:* **2173**

Darling KE, Evans TJ (2003) Effects of nitric oxide on *Pseudomonas aeruginosa* infection of epithelial cells from a human respiratory cell line derived from a patient with cystic fibrosis. *Infect Immun* **71:** 2341-2349

Darton T, Guiver M, Naylor S, Jack DL, Kaczmarski EB, Borrow R, Read RC (2009) Severity of meningococcal disease associated with genomic bacterial load. *Clin Infect Dis* **48:** 587-594

Davidsen T, Tonjum T (2006) Meningococcal genome dynamics. *Nat Rev Micro* **4:** 11-22

Davies JC (2002) *Pseudomonas aeruginosa* in cystic fibrosis: pathogenesis and persistence. *Paediatr Respir Rev* **3:** 128-134

De Groote MA, Fang FC (1995) NO inhibitions: antimicrobial properties of nitric oxide. *Clin Infect Dis* **21** S162-S165

Deasy AM, Guccione E, Dale AP, Andrews N, Evans CM, Bennett JS, Bratcher HB, Maiden MCJ, Gorringe AR, Read RC (2015) Nasal inoculation of the commensal *Neisseria lactamica* inhibits carriage of *Neisseria meningitidis* by young adults: a controlled human infection study. *Clin Infect Dis* **60:** 1512 - 1520

Deeudom M, Koomey M, Moir JW (2008) Roles of c-type cytochromes in respiration in *Neisseria meningitidis*. *Microbiology* **154:** 2857-2864

Dehio C, Gray-Owen SD, Meyer TF (1998) The role of *Neisserial* Opa proteins in interactions with host cells. *Trends Microbiol* **6:** 489-495

Delany I, Rappuoli R, Scarlato V (2004) Fur functions as an activator and as a repressor of putative virulence genes in *Neisseria meningitidis*. *Mol Microbiol* **52:** 1081-1090

Desvaux M, Parham NJ, Henderson IR (2004) The autotransporter secretion system. *Res Microbiol* **155:** 53-60

Domenech M, Ramos-Sevillano E, García E, Moscoso M, Yuste J (2013) Biofilm formation avoids complement immunity and phagocytosis of *Streptococcus pneumoniae*. *Infect Immun* **81:** 2606-2615

Donlan RM (2001) Biofilm formation: a clinically relevant microbiological process. *Clin Infect Dis* **33:** 1387-1392

Donnelly LE, Barnes PJ (2002) Expression and regulation of inducible nitric oxide synthase from human primary airway epithelial cells. *Am J Respir Cell Mol Biol* **26:** 144-151

Donovan C, Blewitt J (2009) An overview of meningitis and meningococcal septicaemia. *Emerg Nurse* **17:** 30-36

Dopter C (1909) Etude de quelques germes isoles du rhino-pharynx, voisans du meningocoque (parameningocoques). *C R Roc Biol (Paris)* **74**

Eckmann L, Kagnoff MF, Fierer J (1993) Epithelial cells secrete the chemokine interleukin-8 in response to bacterial entry. *Infect Immun* **61:** 4569-4574

Edwards J, Cole LJ, Green JB, Thomson MJ, Wood AJ, Whittingham JL, Moir JWB (2010) Binding to DNA protects *Neisseria meningitidis* fumarate and nitrate reductase regulator (FNR) from oxygen. *J Biol Chem* **285:** 1105-1112

Edwards J, Quinn D, Rowbottom K-A, Whittingham Jean L, Thomson Melanie J, Moir James WB (2012) *Neisseria meningitidis* and *Neisseria gonorrhoeae* are differently adapted in the regulation of denitrification: single nucleotide polymorphisms that enable species-specific tuning of the aerobic–anaerobic switch. *Biochem J* **445:** 69-79

Evans CM, Pratt CB, Matheson M, Vaughan TE, Findlow J, Borrow R, Gorringe AR, Read RC (2011) Nasopharyngeal colonization by *Neisseria lactamica* and induction of protective immunity against *Neisseria meningitidis*. *Clin Infect Dis* **52:** 70-77

Exley RM, Shaw J, Mowe E, Sun Y-h, West NP, Williamson M, Botto M, Smith H, Tang CM (2005) Available carbon source influences the resistance of *Neisseria meningitidis* against complement. *J Exp Med* **201:** 1637-1645

Falsetta ML, Bair TB, Ku SC, Vanden Hoven RN, Steichen CT, McEwan AG, Jennings MP, Apicella MA (2009) Transcriptional profiling identifies the metabolic phenotype of gonococcal biofilms. *Infect Immun* **77:** 3522-3532

Falsetta ML, McEwan AG, Jennings MP, Apicella MA (2010) Anaerobic metabolism occurs in the substratum of gonococcal biofilms and may be sustained in part by nitric oxide. *Infect Immun* **78:** 2320-2328

Fang FC (1997) Perspectives series: host/pathogen interactions. Mechanisms of nitric oxide-related antimicrobial activity. *J Clin Invest* **99:** 2818-2825

Fanning AS, Anderson JM (2009) Zonula occludens-1 and -2 are cytosolic scaffolds that regulate the assembly of cellular junctions. *Ann N Y Acad Sci* **1165:** 113-120

Fanning AS, Jameson BJ, Jesaitis LA, Anderson JM (1998) The tight junction protein ZO-1 establishes a link between the transmembrane protein occludin and the actin cytoskeleton. *J Biol Chem* **273:** 29745-29753

Fanning AS, Van Itallie CM, Anderson JM (2012) Zonula occludens-1 and -2 regulate apical cell structure and the zonula adherens cytoskeleton in polarized epithelia. *Mol Biol Cell* **23:** 577-590

Faust SN, Levin M, Harrison OB, Goldin RD, Lockhart MS, Kondaveeti S, Laszik Z, Esmon CT, Heyderman RS (2001) Dysfunction of endothelial protein C activation in severe meningococcal sepsis. *N Engl J Med* **345:** 408-416

Favre-Bonté S, Köhler T, Van Delden C (2003) Biofilm formation by *Pseudomonas aeruginosa*: role of the C4-HSL cell-to-cell signal and inhibition by azithromycin. *J Antimicrob Chemother* **52:** 598-604

Filenko N, Spiro S, Browning DF, Squire D, Overton TW, Cole J, Constantinidou C (2007) The NsrR regulon of *Escherichia coli* K-12 includes genes encoding the hybrid cluster protein and the periplasmic, respiratory nitrite reductase. *J Bacteriol* **189:** 4410-4417

Finne J, Bitter-Suermann D, Goridis C, Finne U (1987) An IgG monoclonal antibody to group B meningococci cross-reacts with developmentally regulated polysialic acid units of glycoproteins in neural and extraneural tissues. *J Immunol* **138:** 4402-4407

Fitzpatrick AM, Brown LA, Holguin F, Teague WG (2009) Levels of nitric oxide oxidation products are increased in the epithelial lining fluid of children with persistent asthma. *J Allergy Clin Immunol* **124:** 990-996

Flexner S (1913) The results of the serum treatment in thirteen hundred cases of epidemic meningitis. *J Exp Med* **17:** 553-576

Fontijn A, Sabadell AJ, Ronco RJ (1970) Homogeneous chemiluminescent measurement of nitric oxide with ozone. Implications for continuous selective monitoring of gaseous air pollutants. *Anal Chem* **42:** 575-579

Foster MW, Hess DT, Stamler JS (2009) Protein S-nitrosylation in health and disease: a current perspective. *Trends Mol Med* **15:** 391-404

Foster MW, McMahon TJ, Stamler JS (2003) S-nitrosylation in health and disease. *Trends Mol Med* **9:** 160-168

Frasch CE, Wendell DZ, J.T. P (1985) Serotype antigens of *Neisseria meningitidis* and a proposed scheme for designation of serotypes. *Rev Infect Dis* **7:** 504-510

Friebe A, Koesling D (2003) Regulation of nitric oxide-sensitive guanylyl cyclase. *Circ Res* **93:** 96-105

Furchgott RF, Zawadzki JV (1980) The obligatory role of endothelial cells in the relaxation of arterial smooth muscle by acetylcholine. *Nature* **288:** 373-376

Furuse M, Hirase T, Itoh M, Nagafuchi A, Yonemura S, Tsukita S (1993) Occludin: a novel integral membrane protein localizing at tight junctions. *J Cell Biol* **123:** 1777-1788

Garrabou G, Moren C, Lopez S, Tobias E, Cardellach F, Miro O, Casademont J (2012) The effects of sepsis on mitochondria. *J Infect Dis* **205:** 392-400

Gaston BM, Carver J, Doctor A, Palmer LA (2003) S-nitrosylation signaling in cell biology. *Mol Interv* **3:** 253-263

Gilberthorpe NJ, Lee ME, Stevanin TM, Read RC, Poole RK (2007) NsrR: a key regulator circumventing *Salmonella enterica* serovar *typhimurium* oxidative and nitrosative stress *in vitro* and in IFN-gamma-stimulated J774.2 macrophages. *Microbiology* **153:** 1756-1771

Gladwin MT, Wang X, Reiter CD, Yang BK, Vivas EX, Bonaventura C, Schechter AN (2002) S-Nitrosohemoglobin is unstable in the reductive erythrocyte environment and lacks O_2/NO^- linked allosteric function. *J Biol Chem* **277:** 27818-27828

Gomez-Jimenez J, Salgado A, Mourelle M, Martin MC, Segura RM, Peracaula R, Moncada S (1995) L-arginine: nitric oxide pathway in endotoxemia and human septic shock. *Crit Care Med* **23:** 253-258

Gorimar TS (1985) Total nitrogen determination by chemiluminescence. IN VAN DYKE, K. (Ed). *Bioluminescence and chemiluminescence: Instruments and Applications* **Boca Raton, FL, CRC press**

Gorringe AR, Reddin KM, Funnell SG, Johansson L, Rytkonen A, Jonsson AB (2005) Experimental disease models for the assessment of meningococcal vaccines. *Vaccine* **23:** 2214-2217

Goureau O, Amiot F, Dautry F, Courtois Y (1997) Control of nitric oxide production by endogenous TNF-alpha in mouse retinal pigmented epithelial and Muller glial cells. *Biochem Biophys Res Commun* **240:** 132-135

Greenwood BM, Blakebrough IS, Bradley AK, Wali S, Whittle HC (1984) Meningococcal disease and season in sub-Saharan Africa. *Lancet* **1:** 1339-1342

Greiner LL, Edwards JL, Shao J, Rabinak C, Entz D, Apicella MA (2005) Biofilm formation by *Neisseria gonorrhoeae*. *Infect Immun* **73:** 1964-1970

Griess P (1879) Bemerkungen zu der Abhandlung der HH. Weselsky und Benedikt „Ueber einige Azoverbindungen"□. *Berichte der deutschen chemischen Gesellschaft* **12:** 426-428

Hadi HA, Wooldridge KG, Robinson K, Ala'Aldeen DA (2001) Identification and characterization of App: an immunogenic autotransporter protein of *Neisseria meningitidis*. *Mol Microbiol* **41:** 611-623

Hall-Stoodley L, Costerton JW, Stoodley P (2004) Bacterial biofilms: from the Natural environment to infectious diseases. *Nat Rev Micro* **2:** 95-108

Halstensen A, Ceska M, Brandtzaeg P, Redl H, Naess A, Waage A (1993) Interleukin-8 in serum and cerebrospinal fluid from patients with meningococcal disease. *J Infect Dis* **167:** 471-475

Hammerschmidt S, Hilse R, van Putten JP, Gerardy-Schahn R, Unkmeir A, Frosch M (1996a) Modulation of cell surface sialic acid expression in *Neisseria meningitidis* via a transposable genetic element. *EMBO J* **15:** 192-198

Hammerschmidt S, Muller A, Sillmann H, Muhlenhoff M, Borrow R, Fox A, van Putten J, Zollinger WD, Gerardy-Schahn R, Frosch M (1996b) Capsule phase variation in *Neisseria meningitidis* serogroup B by slipped-strand mispairing in the polysialyltransferase gene *(siaD)*: correlation with bacterial invasion and the outbreak of meningococcal disease. *Mol Microbiol* **20:** 1211-1220

Han X, Fink MP, Uchiyama T, Yang R, Delude RL (2004) Increased iNOS activity is essential for pulmonary epithelial tight junction dysfunction in endotoxemic mice. *Am J Physiol Lung Cell Mol Physiol* **286:** L259-L267

Hardiman KM, McNicholas-Bevensee CM, Fortenberry J, Myles CT, Malik B, Eaton DC, Matalon S (2004) Regulation of amiloride-sensitive Na^+ transport by basal nitric oxide. *Am J Respir Cell Mol Biol* **30:** 720-728

Harrison OB, Robertson BD, Faust SN, Jepson MA, Goldin RD, Levin M, Heyderman RS (2002) Analysis of pathogen-host cell interactions in purpura fulminans: expression of capsule, type IV pili, and PorA by *Neisseria meningitidis in vivo*. *Infect Immun* **70:** 5193-5201

Hart CA, Cuevas LE (1997) Meningococcal disease in Africa. *Ann Trop Med Parasitol* **91:** 777-785

Helms MN, Yu L, Malik B, Kleinhenz DJ, Hart CM, Eaton DC (2005) Role of SGK1 in nitric oxide inhibition of ENaC in Na^+ transporting epithelia. *Am J Physiol Cell Physiol* **289:** C717-726

Henson SE, Nichols TC, Holers VM, Karp DR (1999) The ectoenzyme gamma-glutamyl transpeptidase regulates antiproliferative effects of S-nitrosoglutathione on human T and B lymphocytes. *J Immunol* **163:** 1845-1852

Heurlier K, Thomson MJ, Aziz N, Moir JW (2008) The nitric oxide (NO)-sensing repressor NsrR of *Neisseria meningitidis* has a compact regulon of genes involved in NO synthesis and detoxification. *J Bacteriol* **190:** 2488-2495

Heyderman RS, Klein NJ, Shennan GI, Levin M (1992) Reduction of the anticoagulant activity of glycosaminoglycans on the surface of the vascular endothelium by endotoxin and neutrophils: evaluation by an amidolytic assay. *Thromb Res* **67:** 677-685

Hoehn GT, Clark VL (1990) Distribution of a protein antigenically related to the major anaerobically induced gonococcal outer membrane protein among other *Neisseria* species. *Infect Immun* **58:** 3929-3933

Hoehn GT, Clark VL (1992a) Isolation and nucleotide sequence of the gene (*aniA*) encoding the major anaerobically induced outer membrane protein of *Neisseria gonorrhoeae*. *Infect Immun* **60:** 4695-4703

Hoehn GT, Clark VL (1992b) The major anaerobically induced outer membrane protein of *Neisseria gonorrhoeae*, Pan 1, is a lipoprotein. *Infect Immun* **60:** 4704-4708

Hogg N (2000) Biological chemistry and clinical potential of S-nitrosothiols. *Free Radic Biol Med* **28:** 1478-1486

Hogg N (2002) The biochemistry and physiology of S-nitrosothiols. *Annu Rev Pharmacol Toxicol* **42:** 585-600

Hollenberg SM, Broussard M, Osman J, Parrillo JE (2000) Increased microvascular reactivity and improved mortality in septic mice lacking inducible nitric oxide synthase. *Circ Res* **86:** 774-778

Hom GJ, Grant SK, Wolfe G, Bach TJ, MacIntyre DE, Hutchinson NI (1995) Lipopolysaccharide-induced hypotension and vascular hyporeactivity in the rat: tissue analysis of nitric oxide synthase mRNA and protein expression in the presence and absence of dexamethasone, NG-monomethyl-L-arginine or indomethacin. *J Pharmacol Exp Ther* **272:** 452-459

Householder TC, Belli WA, Lissenden S, Cole JA, Clark VL (1999) cis- and trans-acting elements involved in regulation of *aniA*, the gene encoding the major anaerobically induced outer membrane protein in *Neisseria gonorrhoeae*. *J Bacteriol* **181:** 541-551

Householder TC, Fozo EM, Cardinale JA, Clark VL (2000) Gonococcal nitric oxide reductase is encoded by a single gene, *norB*, which is required for anaerobic growth and is induced by nitric oxide. *Infect Immun* **68:** 5241-5246

Huang J, O'Toole PW, Doig P, Trust TJ (1995) Stimulation of interleukin-8 production in epithelial cell lines by *Helicobacter pylori*. *Infect Immun* **63:** 1732-1738

Humbert P, Niroomand F, Fischer G, Mayer B, Koesling D, Hinsch KD, Gausepohl H, Frank R, Schultz G, Bohme E (1990) Purification of soluble guanylyl cyclase from bovine lung by a new immunoaffinity chromatographic method. *Eur J Biochem* **190:** 273-278

Hung MC, Heckels JE, Christodoulides M (2013) The adhesin complex protein (ACP) of *Neisseria meningitidis* is a new adhesin with vaccine potential. *MBio* **4:** pii: e00041-00013

Huston WM, Lowe EC, Butler CS, Moir JW (2005) Purification and characterization of cytochrome c' from *Neisseria meningitidis*. *Biochem Soc Trans* **33:** 187-189

Ignarro LJ (1990) Biosynthesis and metabolism of endothelium-derived nitric oxide. *Annu Rev Pharmacol Toxicol* **30:** 535-560

Ignarro LJ, Buga GM, Wood KS, Byrns RE, Chaudhuri G (1987) Endothelium-derived relaxing factor produced and released from artery and vein is nitric oxide. *Proc Natl Acad Sci U S A* **84:** 9265-9269

Ignarro LJ, Fukuto JM, Griscavage JM, Rogers NE, Byrns RE (1993) Oxidation of nitric oxide in aqueous solution to nitrite but not nitrate: comparison with enzymatically formed nitric oxide from L-arginine. *Proc Natl Acad Sci U S A* **90:** 8103-8107

Ignarro LJ, Lippton H, Edwards JC, Baricos WH, Hyman AL, Kadowitz PJ, Gruetter CA (1981) Mechanism of vascular smooth muscle relaxation by organic nitrates, nitrites, nitroprusside and nitric oxide: evidence for the involvement of S-nitrosothiols as active intermediates. *J Pharmacol Exp Ther* **218:** 739-749

Isabella V, Wright LF, Barth K, Spence JM, Grogan S, Genco CA, Clark VL (2008) cis- and trans-acting elements involved in regulation of *norB (norZ)*, the gene encoding nitric oxide reductase in *Neisseria gonorrhoeae*. *Microbiology* **154:** 226-239

Jackson LA, Schuchat A, Reeves MW, Wenger JD (1995) Serogroup C meningococcal outbreaks in the United States. An emerging threat. *JAMA* **273:** 383-389

Jamet A, Euphrasie D, Martin P, Nassif X (2013) Identification of genes involved in *Neisseria meningitidis* colonization. *Infect Immun* **81:** 3375-3381

Jardeleza C, Foreman A, Baker L, Paramasivan S, Field J, Tan LW, Wormald PJ (2011) The effects of nitric oxide on *Staphylococcus aureus* biofilm growth and its implications in chronic rhinosinusitis. *Int Forum Allergy Rhinol* **1:** 438-444

Jarvis GA, Vedros NA (1987) Sialic acid of group B Neisseria meningitidis regulates alternative complement pathway activation. *Infect Immun* **55:** 174-180

Jepson MA, Collares-Buzato CB, Clark MA, Hirst BH, Simmons NL (1995) Rapid disruption of epithelial barrier function by *Salmonella typhimurium* is associated with structural modification of intercellular junctions. *Infect Immun* **63:** 356-359

Jia L, Bonaventura C, Bonaventura J, Stamler JS (1996) S-nitrosohaemoglobin: a dynamic activity of blood involved in vascular control. *Nature* **380:** 221-226

Jolley KA, Maiden MC (2010) BIGSdb: Scalable analysis of bacterial genome variation at the population level. *BMC Bioinformatics* **11:** 595

Jordens JZ, Williams JN, Jones GR, Christodoulides M, Heckels JE (2004) Development of immunity to Serogroup B meningococci during carriage of *Neisseria meningitidis* in a cohort of university students. *Infect Immun* **72:** 6503-6510

Jourd'heuil D, Gray L, Grisham MB (2000) S-nitrosothiol formation in blood of lipopolysaccharide-treated rats. *Biochem Biophys Res Commun* **273:** 22-26

Justino MC, Almeida CC, Teixeira M, Saraiva LM (2007) *Escherichia coli* di-iron YtfE protein is necessary for the repair of stress-damaged iron-sulfur clusters. *J Biol Chem* **282:** 10352-10359

Kallstrom H, Liszewski MK, Atkinson JP, Jonsson AB (1997) Membrane cofactor protein (MCP or CD46) is a cellular pilus receptor for pathogenic *Neisseria*. *Mol Microbiol* **25:** 639-647

Keefer LK, Nims RW, Davies KM, Wink DA (1996) "NONOates" (1-substituted diazen-1-ium-1,2-diolates) as nitric oxide donors: convenient nitric oxide dosage forms. *Methods Enzymol* **268:** 281-293

Khan NA, Khan A, Savelkoul HF, Benner R (2002) Inhibition of septic shock in mice by an oligopeptide from the beta-chain of human chorionic gonadotrophin hormone. *Hum Immunol* **63:** 1-7

Kharitonov SA, Barnes PJ (2006) Exhaled biomarkers. *Chest* **130:** 1541-1546

Kharitonov SA, Yates D, Robbins RA, Logan-Sinclair R, Shinebourne EA, Barnes PJ (1994) Increased nitric oxide in exhaled air of asthmatic patients. *Lancet* **343:** 133-135

Kiefer F (1896) Zur differentialdiagnose des erregers der epidemischen cerebrospinal-meningitis und der gonorrhoe. *Berl Klin Wochenschr,* **33** 628-630

Kilbourn RG, Traber DL, Szabo C (1997) Nitric oxide and shock. *Dis Mon* **43:** 277-348

Kim HW, Greenburg AG (2002) Nitric oxide scavenging, alone or with nitric oxide synthesis inhibition, modulates vascular hyporeactivity in rats with intraperitoneal sepsis. *Shock* **17:** 423-426

King CJ, Tytgat S, Delude RL, Fink MP (1999) Ileal mucosal oxygen consumption is decreased in endotoxemic rats but is restored toward normal by treatment with aminoguanidine. *Crit Care Med* **27:** 2518-2524

Kirchner M, Heuer D, Meyer TF (2005) CD46-independent binding of *neisserial* type IV pili and the major pilus adhesin, PilC, to human epithelial cells. *Infect Immun* **73:** 3072-3082

Klein NJ, Shennan GI, Heyderman RS, Levin M (1992) Alteration in glycosaminoglycan metabolism and surface charge on human umbilical vein endothelial cells induced by cytokines, endotoxin and neutrophils. *J Cell Sci* **102** 821-832

Knapp JS, Clark VL (1984) Anaerobic growth of *Neisseria gonorrhoeae* coupled to nitrite reduction. *Infect Immun* **46:** 176-181

Knowles RG, Merrett M, Salter M, Moncada S (1990) Differential induction of brain, lung and liver nitric oxide synthase by endotoxin in the rat. *Biochem J* **270:** 833-836

Kobzik L, Bredt DS, Lowenstein CJ, Drazen J, Gaston B, Sugarbaker D, Stamler JS (1993) Nitric oxide synthase in human and rat lung: immunocytochemical and histochemical localization. *Am J Respir Cell Mol Biol* **9:** 371-377

Kolb-Mäurer A, Unkmeir A, Kämmerer U, Hübner C, Leimbach T, Stade A, Kämpgen E, Frosch M, Dietrich G (2001) Interaction of *Neisseria meningitidis* with Human Dendritic Cells. *Infect Immun* **69:** 6912-6922

Korner H, Sofia HJ, Zumft WG (2003) Phylogeny of the bacterial superfamily of Crp-Fnr transcription regulators: exploiting the metabolic spectrum by controlling alternative gene programs. *FEMS Microbiol Rev* **27:** 559-592

Krause G, Winkler L, Mueller SL, Haseloff RF, Piontek J, Blasig IE (2008) Structure and function of claudins. *Biochim Biophys Acta* **1778:** 631-645

Kroll JS, Wilks KE, Farrant JL, Langford PR (1998) Natural genetic exchange between *Haemophilus* and *Neisseria*: intergeneric transfer of chromosomal genes between major human pathogens. *Proc Natl Acad Sci U S A* **95:** 12381-12385

Ku SC, Schulz BL, Power PM, Jennings MP (2009) The pilin O-glycosylation pathway of pathogenic *Neisseria* is a general system that glycosylates AniA, an outer membrane nitrite reductase. *Biochem Biophys Res Commun* **378:** 84-89

Kumar A, Brar R, Wang P, Dee L, Skorupa G, Khadour F, Schulz R, Parrillo JE (1999) Role of nitric oxide and cGMP in human septic serum-induced depression of cardiac myocyte contractility. *Am J Physiol* **276:** R265-262R276

Kumar A, Thota V, Dee L, Olson J, Uretz E, Parrillo JE (1996) Tumor necrosis factor alpha and interleukin 1beta are responsible for *in vitro* myocardial cell depression induced by human septic shock serum. *J Exp Med* **183:** 949-958

Kumar P, Sannigrahi S, Scoullar J, Kahler CM, Tzeng Y-L (2011) Characterization of DsbD in *Neisseria meningitidis*. *Mol Microbiol* **79:** 1557-1573

Lambden PR, Guest JR (1976) Mutants of *Escherichia coli* K12 unable to use fumarate as an anaerobic electron acceptor. *J Gen Microbiol* **97:** 145-160

Lappann M, Haagensen JA, Claus H, Vogel U, Molin S (2006) Meningococcal biofilm formation: structure, development and phenotypes in a standardized continuous flow system. *Mol Microbiol* **62:** 1292-1309

Laubach VE, Shesely EG, Smithies O, Sherman PA (1995) Mice lacking inducible nitric oxide synthase are not resistant to lipopolysaccharide-induced death. *Proc Natl Acad Sci U S A* **92:** 10688-10692

Laver JR, Stevanin TM, Messenger SL, Lunn AD, Lee ME, Moir JW, Poole RK, Read RC (2010) Bacterial nitric oxide detoxification prevents host cell S-nitrosothiol formation: a novel mechanism of bacterial pathogenesis. *FASEB J* **24:** 286-295

Laver JR, Stevanin TM, Read RC (2008) Chemiluminescence quantification of NO and its derivatives in liquid samples. *Methods Enzymol* **436:** 113-127

Leid JG, Shirtliff ME, Costerton JW, Stoodley, Paul (2002) Human leukocytes adhere to, penetrate, and respond to *Staphylococcus aureus* biofilms. *Infect Immun* **70:** 6339-6345

Li D, Shirakami G, Zhan X, Johns RA (2000) Regulation of ciliary beat frequency by the nitric oxide-cyclic guanosine monophosphate signaling pathway in rat airway epithelial cells. *Am J Respir Cell Mol Biol* **23:** 175-181

Ligon BL (2005) Albert Ludwig Sigesmund Neisser: discoverer of the cause of gonorrhea. *Semin Pediatr Infect Dis* **16:** 336-341

Lima B, Lam GK, Xie L, Diesen DL, Villamizar N, Nienaber J, Messina E, Bowles D, Kontos CD, Hare JM, Stamler JS, Rockman HA (2009) Endogenous S-nitrosothiols protect against myocardial injury. *Proc Natl Acad Sci U S A* **106:** 6297-6302

Lindqvist K (1960) A *Neisseria* species associated with infectious keratoconjunctivitis of sheep--*Neisseria ovis* Nov. Spec. *J Infect Dis* **106:** 162-165

Link AJ, Phillips D, Church GM (1997) Methods for generating precise deletions and insertions in the genome of wild-type *Escherichia coli*: application to open reading frame characterization. *J Bacteriol* **179:** 6228-6237

Linz B, Schenker M, Zhu P, Achtman M (2000) Frequent interspecific genetic exchange between commensal *Neisseriae* and *Neisseria meningitidis*. *Mol Microbiol* **36:** 1049-1058

Lipton SA, Choi YB, Sucher NJ, Chen HS (1998) Neuroprotective versus neurodestructive effects of NO-related species. *Biofactors* **8:** 33-40

Lissenden S, Mohan S, Overton T, Regan T, Crooke H, Cardinale JA, Householder TC, Adams P, O'Conner CD, Clark VL, Smith H, Cole JA (2000) Identification of transcription activators that regulate gonococcal adaptation from aerobic to anaerobic or oxygen-limited growth. *Mol Microbiol* **37:** 839-855

Liu L, Hausladen A, Zeng M, Que L, Heitman J, Stamler JS (2001) A metabolic enzyme for S-nitrosothiol conserved from bacteria to humans. *Nature* **410:** 490-494

Liu L, Yan Y, Zeng M, Zhang J, Hanes MA, Ahearn G, McMahon TJ, Dickfeld T, Marshall HE, Que LG, Stamler JS (2004) Essential roles of S-nitrosothiols in vascular homeostasis and endotoxic shock. *Cell* **116:** 617-628

Liu T-Y, Gotschlich EC, Jonssen EK, Wysocki JR (1971) Studies on the meningococcal polysaccharides: I. composition and chemical properties of the group A polysaccharide *J Biol Chem* **246:** 2849-2858

Lopez-Sanchez LM, Corrales FJ, Gonzalez R, Ferrin G, Munoz-Castaneda JR, Ranchal I, Hidalgo AB, Briceno J, Lopez-Cillero P, Gomez MA, De La Mata M, Muntane J, Rodriguez-Ariza A (2008) Alteration of S-nitrosothiol homeostasis and targets for protein S-nitrosation in human hepatocytes. *Proteomics* **8:** 4709-4720

Lopez A, Lorente JA, Steingrub J, Bakker J, McLuckie A, Willatts S, Brockway M, Anzueto A, Holzapfel L, Breen D, Silverman MS, Takala J, Donaldson J, Arneson C, Grove G, Grossman S, Grover R (2004) Multiple-center, randomized, placebo-controlled, double-blind study of the nitric oxide synthase inhibitor 546C88: effect on survival in patients with septic shock. *Crit Care Med* **32:** 21-30

Loxham M, Davies DE, Blume C (2014) Epithelial function and dysfunction in asthma. *Clin Exp Allergy* **44:** 1299-1313

Lundberg JO, Farkas-Szallasi T, Weitzberg E, Rinder J, Lidholm J, Anggaard A, Hokfelt T, Lundberg JM, Alving K (1995) High nitric oxide production in human paranasal sinuses. *Nat Med* **1:** 370-373

Lundberg JO, Weitzberg E, Cole JA, Benjamin N (2004) Nitrate, bacteria and human health. *Nat Rev Micro* **2:** 593-602

Lundberg JO, Weitzberg E, Nordvall SL, Kuylenstierna R, Lundberg JM, Alving K (1994) Primarily nasal origin of exhaled nitric oxide and absence in Kartagener's syndrome. *Eur Respir J* **7:** 1501-1504

Lundberg JON, Weitzberg E (1999) Nasal nitric oxide in man. *Thorax* **54:** 947-952

MacLennan J, Kafatos G, Neal K, Andrews N, Cameron JC, Roberts R, Evans MR, Cann K, Baxter DN, Maiden MC, Stuart JM (2006) Social behavior and meningococcal carriage in British teenagers. *Emerg Infect Dis* **12:** 950-957

Mah TF, O'Toole GA (2001) Mechanisms of biofilm resistance to antimicrobial agents. *Trends Microbiol* **9:** 34-39

Maiden MC, Bygraves JA, Feil E, Morelli G, Russell JE, Urwin R, Zhang Q, Zhou J, Zurth K, Caugant DA, Feavers IM, Achtman M, Spratt BG (1998) Multilocus sequence typing: a

portable approach to the identification of clones within populations of pathogenic microorganisms. *Proc Natl Acad Sci U S A* **95:** 3140-3145

Mairey E, Genovesio A, Donnadieu E, Bernard C, Jaubert F, Pinard E, Seylaz J, Olivo-Marin J-C, Nassif X, Duménil G (2006) Cerebral microcirculation shear stress levels determine *Neisseria meningitidis* attachment sites along the blood–brain barrier. *J Exp Med* **203:** 1939-1950

Marchiafava E, Celli, A. (1884) Spra i micrococchi della meningite cerebrospinale epidemica. *Gazz degli Ospedali* **5:59**

Marley R, Feelisch M, Holt S, Moore K (2000) A chemiluminescense-based assay for S-nitrosoalbumin and other plasma S-nitrosothiols. *Free Radic Res* **32:** 1-9

Marsh N, Marsh A (2000) A Short history of nitroglycerine and nitric oxide in pharmacology and physiology. *Clin Exp Pharmacol Physiol* **27:** 313-319

Martin DR, Walker SJ, Baker MG, Lennon DR (1998) New Zealand epidemic of meningococcal disease identified by a strain with phenotype B:4:P1.4. *J Infect Dis* **177:** 497-500

Massari P, Ram S, Macleod H, Wetzler LM (2003) The role of porins in *neisserial* pathogenesis and immunity. *Trends Microbiol* **11:** 87-93

Matuschak GM, Henry KA, Johanns CA, Lechner AJ (2001) Liver-lung interactions following *Escherichia coli* bacteremic sepsis and secondary hepatic ischemia/reperfusion injury. *Am J Respir Crit Care Med* **163:** 1002-1009

McGuinness BT, Clarke IN, Lambden PR, Barlow AK, Heckels JE, Poolman JT, Jones DM (1991) Point mutation in meningococcal *porA* gene associated with increased endemic disease. *Lancet* **337:** 514-517

McInnes I, Liew F (2002) Immunomodulatory actions of nitric oxide. In *Nitric Oxide and Infection*, Fang F (ed), 10, pp 199-213. Springer US

Mehr IJ, Long CD, Serkin CD, Seifert HS (2000) A homologue of the recombination-dependent growth gene, *rdgC*, is involved in gonococcal pilin antigenic variation. *Genetics* **154:** 523-532

Mehr IJ, Seifert HS (1998) Differential roles of homologous recombination pathways in *Neisseria gonorrhoeae* pilin antigenic variation, DNA transformation and DNA repair. *Mol Microbiol* **30:** 697-710

Mellies J, Jose J, Meyer TF (1997) The *Neisseria gonorrhoeae* gene *aniA* encodes an inducible nitrite reductase. *Mol Gen Genet* **256:** 525-532

Merritt JH, Kadouri DE, O'Toole GA (2005) Growing and Analyzing Static Biofilms. In *Current Protocols in Microbiology*. John Wiley & Sons, Inc.

Merz AJ, Rifenbery DB, Arvidson CG, So M (1996) Traversal of a polarized epithelium by pathogenic *Neisseriae:* facilitation by type IV pili and maintenance of epithelial barrier function. *Mol Med* **2:** 745-754

Meurs H, Maarsingh H, Zaagsma J (2003) Arginase and asthma: novel insights into nitric oxide homeostasis and airway hyperresponsiveness. *Trends Pharmacol Sci* **24:** 450-455

Michie HR, Manogue KR, Spriggs DR, Revhaug A, O'Dwyer S, Dinarello CA, Cerami A, Wolff SM, Wilmore DW (1988) Detection of circulating tumor necrosis factor after endotoxin administration. *N Engl J Med* **318:** 1481-1486

Miles AA, Misra SS, Irwin JO (1938) The estimation of the bactericidal power of the blood. *J Hyg (Lond)* **38:** 732-749

Moir JW (2011) A snapshot of a pathogenic bacterium mid-evolution: *Neisseria meningitidis* is becoming a nitric oxide-tolerant aerobe. *Biochem Soc Trans* **39:** 1890-1894

Molesworth AM, Cuevas LE, Connor SJ, Morse AP, Thomson MC (2003) Environmental risk and meningitis epidemics in Africa. *Emerg Infect Dis* **9:** 1287-1293

Møller A-SW, Bjerre A, Brusletto B, Joø GB, Brandtzaeg P, Kierulf P (2005) Chemokine patterns in meningococcal disease. *J Infect Dis* **191:** 768-775

Moller JK (2012) Detection of *Neisseria meningitidis* in cerebrospinal fluid using a multiplex PCR and the Luminex detection technology. *Methods Mol Biol* **799:** 37-53

Moncada S, Palmer RM, Higgs EA (1988) The discovery of nitric oxide as the endogenous nitrovasodilator. *Hypertension* **12:** 365-372

Moore TD, Sparling PF (1996) Interruption of the *gpxA* gene increases the sensitivity of *Neisseria meningitidis* to paraquat. *J Bacteriol* **178:** 4301-4305

Mothershed EA, Sacchi CT, Whitney AM, Barnett GA, Ajello GW, Schmink S, Mayer LW, Phelan M, Taylor TH, Jr., Bernhardt SA, Rosenstein NE, Popovic T (2004) Use of real-time PCR to resolve slide agglutination discrepancies in serogroup identification of *Neisseria meningitidis*. *J Clin Microbiol* **42:** 320-328

Mueller LN, de Brouwer JF, Almeida JS, Stal LJ, Xavier JB (2006) Analysis of a marine phototrophic biofilm by confocal laser scanning microscopy using the new image quantification software PHLIP. *BMC Ecology* **6:** 1-15

Murad F (2004) Discovery of some of the biological effects of nitric oxide and its role in cell signaling. *Biosci Rep* **24:** 452-474

Nassif X (1999) Interactions between encapsulated *Neisseria meningitidis* and host cells. *Int Microbiol* **2:** 133-136

Nassif X, Beretti JL, Lowy J, Stenberg P, O'Gaora P, Pfeifer J, Normark S, So M (1994) Roles of pilin and PilC in adhesion of *Neisseria meningitidis* to human epithelial and endothelial cells. *Proc Natl Acad Sci U S A* **91:** 3769-3773

Nathan AT, Singer M (1999) The oxygen trail: tissue oxygenation. *Brit Med Bull* **55:** 96-108

Nathan C, Xie QW (1994) Regulation of biosynthesis of nitric oxide. *J Biol Chem* **269:** 13725-13728

Nedelec J, Boucraut J, Garnier JM, Bernard D, Rougon G (1990) Evidence for autoimmune antibodies directed against embryonic neural cell adhesion molecules (N-CAM) in patients with group B meningitis. *J Neuroimmunol* **29:** 49-56

Neil RB, Apicella MA (2009) Clinical and laboratory evidence for *Neisseria meningitidis* biofilms. *Future microbiol* **4:** 555-563

Neil RB, Shao JQ, Apicella MA (2009) Biofilm formation on human airway epithelia by encapsulated *Neisseria meningitidis* serogroup B. *Microbes Infect* **11:** 281-287

Neri T, Conti I, Cerri C, Tavanti L, Paggiaro P, Celi A (2010) Divergent effects of nitric oxide on airway epithelial cell activation. *Biol Res* **43:** 467-473

Nikulin J, Panzner U, Frosch M, Schubert-Unkmeir A (2006) Intracellular survival and replication of *Neisseria meningitidis* in human brain microvascular endothelial cells. *Int J Med Microbiol* **296:** 553-558

Ochoa JB, Udekwu AO, Billiar TR, Curran RD, Cerra FB, Simmons RL, Peitzman AB (1991) Nitrogen oxide levels in patients after trauma and during sepsis. *Ann Surg* **214:** 621-626

Olea C, Jr., Herzik MA, Jr., Kuriyan J, Marletta MA (2010) Structural insights into the molecular mechanism of H-NOX activation. *Protein Sci* **19:** 881-887

Olson N, Greul AK, Hristova M, Bove PF, Kasahara DI, van der Vliet A (2009) Nitric oxide and airway epithelial barrier function: regulation of tight junction proteins and epithelial permeability. *Arch Biochem Biophys* **484:** 205-213

Oragui EE, Nadel S, Kyd P, Levin M (2000) Increased excretion of urinary glycosaminoglycans in meningococcal septicemia and their relationship to proteinuria. *Crit Care Med* **28:** 3002-3008

Overton TW, Whitehead R, Li Y, Snyder LA, Saunders NJ, Smith H, Cole JA (2006) Coordinated regulation of the *Neisseria gonorrhoeae*-truncated denitrification pathway by the nitric oxide-sensitive repressor, NsrR, and nitrite-insensitive NarQ-NarP. *J Biol Chem* **281:** 33115-33126

Pace D, Pollard AJ (2012) Meningococcal disease: Clinical presentation and sequelae. *Vaccine* **30:** B3-B9

Pacher P, Beckman JS, Liaudet L (2007) Nitric oxide and peroxynitrite in health and disease. *Physiol Rev* **87:** 315-424

Palmer RM, Ashton DS, Moncada S (1988) Vascular endothelial cells synthesize nitric oxide from L-arginine. *Nature* **333:** 664-666

Parkhill J, Achtman M, James KD, Bentley SD, Churcher C, Klee SR, Morelli G, Basham D, Brown D, Chillingworth T, Davies RM, Davis P, Devlin K, Feltwell T, Hamlin N, Holroyd S, Jagels K, Leather S, Moule S, Mungall K, Quail MA, Rajandream MA, Rutherford KM, Simmonds M, Skelton J, Whitehead S, Spratt BG, Barrell BG (2000) Complete DNA sequence of a serogroup A strain of *Neisseria meningitidis* Z2491. *Nature* **404:** 502-506

Pathan N, Faust SN, Levin M (2003) Pathophysiology of meningococcal meningitis and septicaemia. *Arch Dis Child* **88:** 601-607

Pedemonte CH (1995) Inhibition of $Na(^{+})$ pump expression by impairment of protein glycosylation is independent of the reduced sodium entry into the cell. *J Membr Biol* **147:** 223-231

Phillips NJ, Steichen CT, Schilling B, Post DM, Niles RK, Bair TB, Falsetta ML, Apicella MA, Gibson BW (2012) Proteomic analysis of *Neisseria gonorrhoeae* biofilms shows shift to anaerobic respiration and changes in nutrient transport and outermembrane proteins. *PLoS One* **7:** 1-19

Pinner RW, Spellman PA, Stephens DS (1991) Evidence for functionally distinct pili expressed by *Neisseria meningitidis*. *Infect Immun* **59:** 3169-3175

Pitcher RS, Watmough NJ (2004) The bacterial cytochrome cbb3 oxidases. *Biochim Biophys Acta* **1655:** 388-399

Pizza M, Scarlato V, Masignani V, Giuliani MM, Arico B, Comanducci M, Jennings GT, Baldi L, Bartolini E, Capecchi B, Galeotti CL, Luzzi E, Manetti R, Marchetti E, Mora M, Nuti S, Ratti G, Santini L, Savino S, Scarselli M, Storni E, Zuo P, Broeker M, Hundt E, Knapp B, Blair E, Mason T, Tettelin H, Hood DW, Jeffries AC, Saunders NJ, Granoff DM, Venter JC, Moxon ER, Grandi G, Rappuoli R (2000) Identification of vaccine candidates against serogroup B meningococcus by whole-genome sequencing. *Science* **287:** 1816-1820

Plate L, Marletta Michael A (2012) Nitric oxide modulates bacterial biofilm formation through a multicomponent cyclic-di-GMP signaling network. *Mol Cell* **46:** 449-460

Pollard AJ (2004) Global epidemiology of meningococcal disease and vaccine efficacy. *Pediatr Infect Dis J* **23:** S274-279

Preisig O, Zufferey R, Thöny-Meyer L, Appleby CA, Hennecke H (1996) A high-affinity cbb3-type cytochrome oxidase terminates the symbiosis-specific respiratory chain of *Bradyrhizobium japonicum*. *J Bacteriol* **178:** 1532-1538

Proft T, Baker EN (2009) Pili in Gram-negative and Gram-positive bacteria — structure, assembly and their role in disease. *Cell Mol Life Sci* **66:** 613-635

Pujol C, Eugene E, de Saint Martin L, Nassif X (1997) Interaction of *Neisseria meningitidis* with a polarized monolayer of epithelial cells. *Infect Immun* **65:** 4836-4842

Quincke H (1893) Uber meningitidis serosa. *Samml Klin Vort (Leipzig),* **67:** 655-694

Rajapaksa S, Starr M (2010) Meningococcal sepsis. *Aust Fam Physician* **39:** 276-278

Raman S, Klein N, Kwan A, Hubank M, Rahman S, Rashid A, Peters MJ (2015) Oxidative phosphorylation gene expression falls at onset and throughout the development of meningococcal sepsis-induced multi-organ failure in children. *Intens Care Med* **41:** 1489-1490

Rappuoli R (2001) Reverse vaccinology, a genome-based approach to vaccine development. *Vaccine* **19:** 2688-2691

Rasmussen B (2000) Filamentous microfossils in a 3,235-million-year-old volcanogenic massive sulphide deposit. *Nature* **405:** 676-679

Read RC, Cannings C, Naylor SC, Timms JM, Maheswaran R, Borrow R, Kaczmarski EB, Duff GW (2003) Variation within genes encoding interleukin-1 and the interleukin-1 receptor antagonist influence the severity of meningococcal disease. *Ann Intern Med* **138:** 534-541

Remick DG, Strieter RM, Eskandari MK, Nguyen DT, Genord MA, Raiford CL, Kunkel SL (1990) Role of tumor necrosis factor-alpha in lipopolysaccharide-induced pathologic alterations. *Am J Pathol* **136:** 49-60

Renauld-Mongenie G, Poncet D, Mignon M, Fraysse S, Chabanel C, Danve B, Krell T, Quentin-Millet MJ (2004) Role of transferrin receptor from a *Neisseria meningitidis* tbpB isotype II strain in human transferrin binding and virulence. *Infect Immun* **72:** 3461-3470

Robbins RA, Sisson JH, Springall DR, Nelson KJ, Taylor JA, Mason NA, Polak JM, Townley RG (1997) Human lung mononuclear cells induce nitric oxide synthase in murine airway epithelial cells *in vitro:* role of TNFalpha and IL-1beta. *Am J Respir Crit Care Med* **155:** 268-273

Rock JD, Mahnane MR, Anjum MF, Shaw JG, Read RC, Moir JW (2005) The pathogen *Neisseria meningitidis* requires oxygen, but supplements growth by denitrification. Nitrite, nitric oxide and oxygen control respiratory flux at genetic and metabolic levels. *Mol Microbiol* **58:** 800-809

Rock JD, Moir JW (2005) Microaerobic denitrification in *Neisseria meningitidis*. *Biochem Soc Trans* **33:** 134-136

Rock JD, Thomson MJ, Read RC, Moir JW (2007) Regulation of denitrification genes in *Neisseria meningitidis* by nitric oxide and the repressor NsrR. *J Bacteriol* **189:** 1138-1144

Rose F, Guthmann B, Tenenbaum T, Fink L, Ghofrani A, Weissmann N, Konig P, Ermert L, Dahlem G, Haenze J, Kummer W, Seeger W, Grimminger F (2002) Apical, but not basolateral, endotoxin preincubation protects alveolar epithelial cells against hydrogen peroxide-induced loss of barrier function: the role of nitric oxide synthesis. *J Immunol* **169:** 1474-1481

Rosenstein NE, Perkins BA, Stephens DS, Popovic T, Hughes JM (2001) Meningococcal Disease. *N Eng J Med* **344:** 1378-1388

Rouphael NG, Stephens DS (2012) *Neisseria meningitidis*: biology, microbiology, and epidemiology. *Methods Mol Biol* **799:** 1-20

Samouilov A, Zweier JL (1998) Development of chemiluminescence-based methods for specific quantitation of nitrosylated thiols. *Anal Biochem* **258:** 322-330

Sawada N, Murata M, Kikuchi K, Osanai M, Tobioka H, Kojima T, Chiba H (2003) Tight junctions and human diseases. *Med Electron Microsc* **36:** 147-156

Scarselli M, Serruto D, Montanari P, Capecchi B, Adu-Bobie J, Veggi D, Rappuoli R, Pizza M, Aricò B (2006) *Neisseria meningitidis* NhhA is a multifunctional trimeric autotransporter adhesin. *Mol Microbiol* **61:** 631-644

Schapiro JM, Libby SJ, Fang FC (2003) Inhibition of bacterial DNA replication by zinc mobilization during nitrosative stress. *Proc Natl Acad Sci* **100:** 8496-8501

Schmidt HH, Hofmann H, Schindler U, Shutenko ZS, Cunningham DD, Feelisch M (1996) No .NO from NO synthase. *Proc Natl Acad Sci U S A* **93:** 14492-14497

Schneemann M, Schoedon G (2002) Species differences in macrophage NO production are important. *Nat Immunol* **3:** 102

Schoen C, Blom J, Claus H, Schramm-Glück A, Brandt P, Müller T, Goesmann A, Joseph B, Konietzny S, Kurzai O, Schmitt C, Friedrich T, Linke B, Vogel U, Frosch M (2008) Whole-genome comparison of disease and carriage strains provides insights into virulence evolution in *Neisseria meningitidis*. *Proc Natl Acad Sci* **105:** 3473-3478

Scholten RJ, Kuipers B, Valkenburg HA, Dankert J, Zollinger WD, Poolman JT (1994) Lipo-oligosaccharide immunotyping of *Neisseria meningitidis* by a whole-cell ELISA with monoclonal antibodies. *J Med Microbiol* **41:** 236-243

Schonhoff CM, Matsuoka M, Tummala H, Johnson MA, Estevez AG, Wu R, Kamaid A, Ricart KC, Hashimoto Y, Gaston B, Macdonald TL, Xu Z, Mannick JB (2006) S-nitrosothiol depletion in amyotrophic lateral sclerosis. *Proc Natl Acad Sci U S A* **103:** 2404-2409

Schultz K-D, Schultz K, Schultz G (1977) Sodium nitroprusside and other smooth muscle-relaxants increase cyclic GMP levels in rat ductus deferens. *Nature* **265:** 750-751

Schwentker FF, Gelman S, Long PH (1984) The treatment of meningococcic meningitis with sulfanilamide: Preliminary report. *JAMA* **251:** 788-790

Sehba FA, Friedrich V, Jr., Makonnen G, Bederson JB (2007) Acute cerebral vascular injury after subarachnoid hemorrhage and its prevention by administration of a nitric oxide donor. *J Neurosurg* **106:** 321-329

Sengupta R, Ryter SW, Zuckerbraun BS, Tzeng E, Billiar TR, Stoyanovsky DA (2007) Thioredoxin catalyzes the denitrosation of low-molecular mass and protein S-nitrosothiols. *Biochemistry* **46:** 8472-8483

Sennequier N, Stuehr DJ (1996) Analysis of Substrate-Induced Electronic, Catalytic, and Structural Changes in Inducible NO Synthase. *Biochemistry* **35:** 5883-5892

Serruto D, Adu-Bobie J, Scarselli M, Veggi D, Pizza M, Rappuoli R, Arico B (2003) *Neisseria meningitidis* App, a new adhesin with autocatalytic serine protease activity. *Mol Microbiol* **48:** 323-334

Serruto D, Bottomley MJ, Ram S, Giuliani MM, Rappuoli R (2012) The new multicomponent vaccine against meningococcal serogroup B, 4CMenB: immunological, functional and structural characterization of the antigens. *Vaccine* **30** B87-B97

Seth D, Stamler JS (2010) The SNO-proteome: causation and classifications. *Curr Opin Chem Biol* **15:** 129 - 136

Sharpe MA, Cooper CE (1998) Interaction of peroxynitrite with mitochondrial cytochrome oxidase. Catalytic production of nitric oxide and irreversible inhibition of enzyme activity. *J Biol Chem* **273:** 30961-30972

Sheng H, Reynolds JD, Auten RL, Demchenko IT, Piantadosi CA, Stamler JS, Warner DS (2010) Pharmacologically augmented S-Nitrosylated hemoglobin improves recovery from murine Subarachnoid Hemorrhage. *Stroke* **42:** 471 - 476

Sherman TS, Chen Z, Yuhanna IS, Lau KS, Margraf LR, Shaul PW (1999) Nitric oxide synthase isoform expression in the developing lung epithelium. *Am J Physiol* **276:** L383-390

Shi Y, Li HQ, Shen CK, Wang JH, Qin SW, Liu R, Pan J (1993) Plasma nitric oxide levels in newborn infants with sepsis. *J Pediatr* **123:** 435-438

Sim RJ, Harrison MM, Moxon ER, Tang CM (2000) Underestimation of meningococci in tonsillar tissue by nasopharyngeal swabbing. *Lancet* **356:** 1653-1654

Singer M (2014) The role of mitochondrial dysfunction in sepsis-induced multi-organ failure. *Virulence* **5:** 66-72

Sittipunt C, Steinberg KP, Ruzinski JT, Myles C, Zhu S, Goodman RB, Hudson LD, Matalon S, Martin TR (2001) Nitric oxide and nitrotyrosine in the lungs of patients with acute respiratory distress syndrome. *Am J Respir Crit Care Med* **163:** 503-510

Sjölinder H, Eriksson J, Maudsdotter L, Aro H, Jonsson A-B (2008) Meningococcal outer membrane protein NhhA is essential for colonization and disease by preventing phagocytosis and complement attack. *Infect Immun* **76:** 5412-5420

Slaterus KW (1961) Serological typing of meningococci by means of micro-precipitation. *Antonie van Leeuwenhoek* **27:** 305-315

Smith HO, Gwinn ML, Salzberg SL (1999) DNA uptake signal sequences in naturally transformable bacteria. *Res Microbiol* **150:** 603-616

Sneath PH, Barrett SJ (1996) A new species of *Neisseria* from the dental plaque of the domestic cow, *Neisseria dentiae* sp. nov. *Lett Appl Microbiol* **23:** 355-358

Soriano-Gabarro M, Wolter J, Hogea C, Vyse A (2011) Carriage of *Neisseria meningitidis* in Europe: a review of studies undertaken in the region. *Expert Rev Anti Infect Ther* **9:** 761-774

Sparkman L, Boggaram V (2004) Nitric oxide increases IL-8 gene transcription and mRNA stability to enhance IL-8 gene expression in lung epithelial cells. *Am J Physiol Lung Cell Mol Physiol* **287:** L764-773

Spinosa MR, Progida C, Tala A, Cogli L, Alifano P, Bucci C (2007) The *Neisseria meningitidis* capsule is important for intracellular survival in human cells. *Infect Immun* **75:** 3594-3603

St Geme JW, 3rd, de la Morena ML, Falkow S (1994) A *Haemophilus influenzae* IgA protease-like protein promotes intimate interaction with human epithelial cells. *Mol Microbiol* **14:** 217-233

Stamler JS (2004) S-nitrosothiols in the blood: roles, amounts, and methods of analysis. *Circ Res* **94:** 414-417

Stamler JS, Jia L, Eu JP, McMahon TJ, Demchenko IT, Bonaventura J, Gernert K, Piantadosi CA (1997a) Blood flow regulation by S-nitrosohemoglobin in the physiological oxygen gradient. *Science* **276:** 2034-2037

Stamler JS, Lamas S, Fang FC (2001) Nitrosylation. the prototypic redox-based signaling mechanism. *Cell* **106:** 675-683

Stamler JS, Toone EJ, Lipton SA, Sucher NJ (1997b) (S)NO signals: translocation, regulation, and a consensus motif. *Neuron* **18:** 691-696

Steed E, Balda MS, Matter K (2010) Dynamics and functions of tight junctions. *Trends Cell Biol* **20:** 142-149

Stefanelli P, Colotti G, Neri A, Salucci ML, Miccoli R, Di Leandro L, Ippoliti R (2008) Molecular characterization of nitrite reductase gene *(aniA)* and gene product in *Neisseria meningitidis* isolates: Is *aniA* essential for meningococcal survival? *IUBMB Life* **60:** 629-636

Steichen CT, Shao JQ, Ketterer MR, Apicella MA (2008) Gonococcal cervicitis: a role for biofilm in pathogenesis. *J Infect Dis* **198:** 1856-1861

Stephens DS, Greenwood B, Brandtzaeg P (2007) Epidemic meningitis, meningococcaemia, and *Neisseria meningitidis*. *Lancet* **369:** 2196-2210

Stepuro, II, Adamchuk RI, Piletskaya TP, Stepuro VI, Maskevich SA (2000) Ultrasound-induced formation of S-nitrosoglutathione and S-nitrosocysteine in aerobic aqueous solutions of glutathione and cysteine. *Biochemistry (Mosc)* **65:** 1385-1396

Stevanin TM, Laver JR, Poole RK, Moir JW, Read RC (2007) Metabolism of nitric oxide by *Neisseria meningitidis* modifies release of NO-regulated cytokines and chemokines by human macrophages. *Microbes Infect* **9:** 981-987

Stevanin TM, Moir JW, Read RC (2005) Nitric oxide detoxification systems enhance survival of *Neisseria meningitidis* in human macrophages and in nasopharyngeal mucosa. *Infect Immun* **73:** 3322-3329

Stewart PS, Costerton JW (2001) Antibiotic resistance of bacteria in biofilms. *Lancet* **358:** 135-138

Stewart V, Parales J, Jr. (1988) Identification and expression of genes narL and narX of the nar (nitrate reductase) locus in *Escherichia coli* K-12. *J Bacteriol* **170:** 1589-1597

Stohl EA, Criss AK, Seifert HS (2005) The transcriptome response of *Neisseria gonorrhoeae* to hydrogen peroxide reveals genes with previously uncharacterized roles in oxidative damage protection. *Mol Microbiol* **58:** 520-532

Stone JR, Marletta MA (1994) Soluble guanylate cyclase from bovine lung: activation with nitric oxide and carbon monoxide and spectral characterization of the ferrous and ferric states. *Biochemistry* **33:** 5636-5640

Stuehr DJ, Kwon NS, Nathan CF, Griffith OW, Feldman PL, Wiseman J (1991) . *J Biol Chem* **266:** 6259-6263

Sullivan TD, LaScolea LJ, Jr. (1987) *Neisseria meningitidis* bacteremia in children: quantitation of bacteremia and spontaneous clinical recovery without antibiotic therapy. *Pediatrics* **80:** 63-67

Sutherland TC, Quattroni P, Exley RM, Tang CM (2010) Transcellular passage of *Neisseria meningitidis* across a polarized respiratory epithelium. *Infect Immun* **78:** 3832-3847

Swartley JS, Marfin AA, Edupuganti S, Liu LJ, Cieslak P, Perkins B, Wenger JD, Stephens DS (1997) Capsule switching of *Neisseria meningitidis*. *Proc Natl Acad Sci USA* **94:** 271-276

Swindle EJ, Collins JE, Davies DE (2009) Breakdown in epithelial barrier function in patients with asthma: identification of novel therapeutic approaches. *J Allergy Clin Immunol* **124:** 23-34

Taha M-K, Alonso J-M, Cafferkey M, Caugant DA, Clarke SC, Diggle MA, Fox A, Frosch M, Gray SJ, Guiver M, Heuberger S, Kalmusova J, Kesanopoulos K, Klem A-M, Kriz P, Marsh J, Mölling P, Murphy K, Olcén P, Sanou O, Tzanakaki G, Vogel U (2005) Interlaboratory comparison of PCR-based identification and genogrouping of *Neisseria meningitidis*. *J Clin Microbiol* **43:** 144-149

Tannenbaum SR, White FM (2006) Regulation and specificity of S-nitrosylation and denitrosylation. *ACS Chem Biol* **1:** 615-618

Tavares P, Pereira AS, Moura JJG, Moura I (2006) Metalloenzymes of the denitrification pathway. *J Inorg Biochem* **100:** 2087-2100

Teitzel GM, Parsek MR (2003) Heavy metal resistance of biofilm and planktonic *Pseudomonas aeruginosa*. *App Environ Microbiol* **69:** 2313-2320

Tettelin H, Saunders NJ, Heidelberg J, Jeffries AC, Nelson KE, Eisen JA, Ketchum KA, Hood DW, Peden JF, Dodson RJ, Nelson WC, Gwinn ML, DeBoy R, Peterson JD, Hickey EK, Haft DH, Salzberg SL, White O, Fleischmann RD, Dougherty BA, Mason T, Ciecko A, Parksey DS, Blair E, Cittone H, Clark EB, Cotton MD, Utterback TR, Khouri H, Qin H, Vamathevan J, Gill J, Scarlato V, Masignani V, Pizza M, Grandi G, Sun L, Smith HO, Fraser CM, Moxon ER, Rappuoli R, Venter JC (2000) Complete genome sequence of *Neisseria meningitidis* serogroup B strain MC58. *Science* **287:** 1809-1815

Thiemermann C (1997) Nitric oxide and septic shock. *Gen Pharmacol* **29:** 159-166

Titheradge MA (1999) Nitric oxide in septic shock. *Biochim Biophys Acta* **1411:** 437-455

Toledo JC, Augusto O (2012) Connecting the chemical and biological properties of nitric oxide. *Chem Res Tox* **25:** 975-989

Trotter CL, Ramsay ME (2007) Vaccination against meningococcal disease in Europe: review and recommendations for the use of conjugate vaccines. *FEMS Microbiol Rev* **31:** 101-107

Tunbridge AJ, Stevanin TM, Lee M, Marriott HM, Moir JW, Read RC, Dockrell DH (2006) Inhibition of macrophage apoptosis by *Neisseria meningitidis* requires nitric oxide detoxification mechanisms. *Infect Immun* **74:** 729-733

Turner DP, Marietou AG, Johnston L, Ho KK, Rogers AJ, Wooldridge KG, Ala'Aldeen DA (2006) Characterization of MspA, an immunogenic autotransporter protein that mediates

adhesion to epithelial and endothelial cells in *Neisseria meningitidis*. *Infect Immun* **74:** 2957-2964

Turner SM, Moir JW, Griffiths L, Overton TW, Smith H, Cole JA (2005) Mutational and biochemical analysis of cytochrome c', a nitric oxide-binding lipoprotein important for adaptation of *Neisseria gonorrhoeae* to oxygen-limited growth. *Biochem J* **388:** 545-553

van Alen T, Claus H, Zahedi RP, Groh J, Blazyca H, Lappann M, Sickmann A, Vogel U (2010) Comparative proteomic analysis of biofilm and planktonic cells of *Neisseria meningitidis*. *Proteomics* **10:** 4512-4521

van Deuren M, Brandtzaeg P, van der Meer JWM (2000) Update on meningococcal disease with emphasis on pathogenesis and clinical management. *Clinical Microbiol Rev* **13:** 144-166

van Ulsen P, Adler B, Fassler P, Gilbert M, van Schilfgaarde M, van der Ley P, van Alphen L, Tommassen J (2006) A novel phase-variable autotransporter serine protease, AusI, of *Neisseria meningitidis*. *Microbes Infect* **8:** 2088-2097

van Ulsen P, van Alphen L, ten Hove J, Fransen F, van der Ley P, Tommassen J (2003) A *Neisserial* autotransporter NalP modulating the processing of other autotransporters. *Mol Microbiol* **50:** 1017-1030

Vanasco V, Magnani ND, Cimolai MC, Valdez LB, Evelson P, Boveris A, Alvarez S (2012) Endotoxemia impairs heart mitochondrial function by decreasing electron transfer, ATP synthesis and ATP content without affecting membrane potential. *J Bioenerg Biomembr* **44:** 243-252

Vieusseux M (1805) Mémoire su la maladie qui a regné a Genêve au printemps de 1804. *J Med Chir Pharmacol* **11:** 163

Virji M (2009) Pathogenic *Neisseriae*: surface modulation, pathogenesis and infection control. *Nat Rev Microbiol* **7:** 274-286

Virji M, Alexandrescu C, Ferguson DJ, Saunders JR, Moxon ER (1992a) Variations in the expression of pili: the effect on adherence of *Neisseria meningitidis* to human epithelial and endothelial cells. *Mol Microbiol* **6:** 1271-1279

Virji M, Evans D, Hadfield A, Grunert F, Teixeira AM, Watt SM (1999) Critical determinants of host receptor targeting by *Neisseria meningitidis* and *Neisseria gonorrhoeae*: identification of Opa adhesiotopes on the N-domain of CD66 molecules. *Mol Microbiol* **34:** 538-551

Virji M, Kayhty H, Ferguson DJ, Alexandrescu C, Heckels JE, Moxon ER (1991) The role of pili in the interactions of pathogenic *Neisseria* with cultured human endothelial cells. *Mol Microbiol* **5:** 1831-1841

Virji M, Makepeace K, Ferguson DJ, Achtman M, Moxon ER (1993) Meningococcal Opa and Opc proteins: their role in colonization and invasion of human epithelial and endothelial cells. *Mol Microbiol* **10:** 499-510

Virji M, Makepeace K, Ferguson DJ, Achtman M, Sarkari J, Moxon ER (1992b) Expression of the Opc protein correlates with invasion of epithelial and endothelial cells by *Neisseria meningitidis*. *Mol Microbiol* **6:** 2785-2795

Virji M, Makepeace K, Moxon ER (1994) Distinct mechanisms of interactions of Opc-expressing meningococci at apical and basolateral surfaces of human endothelial cells; the role of integrins in apical interactions. *Mol Microbiol* **14:** 173-184

Virji M, Watt SM, Barker S, Makepeace K, Doyonnas R (1996) The N-domain of the human CD66a adhesion molecule is a target for Opa proteins of *Neisseria meningitidis* and *Neisseria gonorrhoeae*. *Mol Microbiol* **22:** 929-939

Visser JJ, Scholten RJ, Hoekman K (1994) Nitric oxide synthesis in meningococcal meningitis. *Ann Intern Med* **120:** 345-346

von Bonsdorff CH, Fuller SD, Simons K (1985) Apical and basolateral endocytosis in Madin-Darby canine kidney (MDCK) cells grown on nitrocellulose filters. *EMBO J* **4:** 2781-2792

Waage A, Halstensen A, Espevik T (1987) Association between tumour necrosis factor in serum and fatal outcome in patients with meningococcal disease. *Lancet* **329:** 355-357

Wang JF, Caugant DA, Li X, Hu X, Poolman JT, Crowe BA, Achtman M (1992) Clonal and antigenic analysis of serogroup A *Neisseria meningitidis* with particular reference to epidemiological features of epidemic meningitis in the People's Republic of China. *Infect Immun* **60:** 5267-5282

Wasser IM, de Vries S, Moenne-Loccoz P, Schroder I, Karlin KD (2002) Nitric oxide in biological denitrification: Fe/Cu metalloenzyme and metal complex NO(x) redox chemistry. *Chem Rev* **102:** 1201-1234

Weber IT, Steitz TA (1987) Structure of a complex of catabolite gene activator protein and cyclic AMP refined at 2.5 A resolution. *J Mol Biol* **198:** 311-326

Wedel B, Humbert P, Harteneck C, Foerster J, Malkewitz J, Bohme E, Schultz G, Koesling D (1994) Mutation of His-105 in the beta 1 subunit yields a nitric oxide-insensitive form of soluble guanylyl cyclase. *Proc Natl Acad Sci U S A* **91:** 2592-2596

Weichselbaum A (1887) Uber die aetiologie der akuten meningitis cerebro-spinalis. *Fortschr Med, 5***:** 573-583

Weinberg JB, Misukonis MA, Shami PJ, Mason SN, Sauls DL, Dittman WA, Wood ER, Smith GK, McDonald B, Bachus KE, et al. (1995) Human mononuclear phagocyte inducible nitric oxide synthase (iNOS): analysis of iNOS mRNA, iNOS protein, biopterin, and nitric oxide production by blood monocytes and peritoneal macrophages. *Blood* **86:** 1184-1195

Weis N, Lind I (1998) Epidemiological markers in *Neisseria meningitidis*: an estimate of the performance of genotyping vs phenotyping. *Scand J Infect Dis* **30:** 69-75

Welin-Neilands J, Svensäter G (2007) Acid tolerance of biofilm cells of *Streptococcus* mutans. *App Environ Microbiol* **73:** 5633-5638

Westall F, de Wit MJ, Dann J, van der Gaast S, de Ronde CEJ, Gerneke D (2001) Early Archean fossil bacteria and biofilms in hydrothermally-influenced sediments from the Barberton greenstone belt, South Africa. *Precambrian Research* **106:** 93-116

Whitehead RN, Overton TW, Snyder LA, McGowan SJ, Smith H, Cole JA, Saunders NJ (2007) The small FNR regulon of *Neisseria gonorrhoeae*: comparison with the larger *Escherichia coli* FNR regulon and interaction with the NarQ-NarP regulon. *BMC Genomics* **8:** 35

Wilder-Smith A, Goh KT, Barkham T, Paton NI (2003) Hajj-associated outbreak strain of *Neisseria meningitidis* Serogroup W135: estimates of the attack rate in a defined population and the risk of invasive disease developing in carriers. *Clin Infect Dis* **36:** 679-683

Wilks D, Farrington, M. & Rubenstein, D. (2003) CNS Infections. *The Infectious Diseases Manual* **2nd ed. Oxford, UK, Blackwell**

Williams JN, Jones GR, Christodoulides M, Heckels JE (2003) Serological correlates of protection against meningococci in a cohort of university students, before and during an outbreak of serogroup C infection. *J Infect Dis* **187:** 1433-1441

Wine E, Chan VL, Sherman PM (2008) *Campylobacter jejuni* mediated disruption of polarized epithelial monolayers is cell-type specific, time dependent, and correlates with bacterial invasion. *Pediatr Res* **64:** 599-604

Wink DA, Kasprzak KS, Maragos CM, Elespuru RK, Misra M, Dunams TM, Cebula TA, Koch WH, Andrews AW, Allen JS, et al. (1991) DNA deaminating ability and genotoxicity of nitric oxide and its progenitors. *Science* **254:** 1001-1003

Wong HR, Carcillo JA, Burckart G, Shah N, Janosky JE (1995) Increased serum nitrite and nitrate concentrations in children with the sepsis syndrome. *Crit Care Med* **23:** 835-842

Wu G, Morris SM, Jr. (1998) Arginine metabolism: nitric oxide and beyond. *Biochem J* **336** 1-17

Wu HM, Harcourt BH, Hatcher CP, Wei SC, Novak RT, Wang X, Juni BA, Glennen A, Boxrud DJ, Rainbow J, Schmink S, Mair RD, Theodore MJ, Sander MA, Miller TK, Kruger K, Cohn AC, Clark TA, Messonnier NE, Mayer LW, Lynfield R (2009) Emergence of Ciprofloxacin-resistant *Neisseria meningitidis* in North America. *N Eng J Med* **360:** 886-892

Xie O, Pollard AJ, Mueller JE, Norheim G (2013) Emergence of serogroup X meningococcal disease in Africa: Need for a vaccine. *Vaccine* **31:** 2852-2861

Yamakawa K, Ogura H, Koh T, Ogawa Y, Matsumoto N, Kuwagata Y, Shimazu T (2013) Platelet mitochondrial membrane potential correlates with severity in patients with systemic inflammatory response syndrome. *J Trauma Acute Care Surg* **74:** 411-418

Yan L, Wang S, Rafferty SP, Wesley RA, Danner RL (1997) Endogenously produced nitric oxide increases tumor necrosis factor-α production in transfected human U937 cells. *Blood* **90:** 1160-1167

Yang BK, Vivas EX, Reiter CD, Gladwin MT (2003) Methodologies for the sensitive and specific measurement of S-nitrosothiols, iron-nitrosyls, and nitrite in biological samples. *Free Radic Res* **37:** 1-10

Yi K, Rasmussen AW, Gudlavalleti SK, Stephens DS, Stojiljkovic I (2004) Biofilm formation by *Neisseria meningitidis*. *Infect Immun* **72:** 6132-6138

Yi K, Stephens DS, Stojiljkovic I (2003) Development and evaluation of an improved mouse model of meningococcal colonization. *Infect Immun* **71:** 1849-1855

Zabel U, Hausler C, Weeger M, Schmidt HH (1999) Homodimerization of soluble guanylyl cyclase subunits. Dimerization analysis using a glutathione s-transferase affinity tag. *J Biol Chem* **274:** 18149-18152

Zarantonelli ML, Szatanik M, Giorgini D, Hong E, Huerre M, Guillou F, Alonso JM, Taha MK (2007) Transgenic mice expressing human transferrin as a model for meningococcal infection. *Infect Immun* **75:** 5609-5614

Zech JC, Pouvreau I, Cotinet A, Goureau O, Le Varlet B, de Kozak Y (1998) Effect of cytokines and nitric oxide on tight junctions in cultured rat retinal pigment epithelium. *Invest Ophthalmol Vis Sci* **39:** 1600-1608

Zhang Z, Kolls JK, Oliver P, Good D, Schwarzenberger PO, Joshi MS, Ponthier JL, Lancaster JR, Jr. (2000) Activation of tumor necrosis factor-alpha-converting enzyme-mediated ectodomain shedding by nitric oxide. *J Biol Chem* **275:** 15839-15844

Zheng S, De BP, Choudhary S, Comhair SA, Goggans T, Slee R, Williams BR, Pilewski J, Haque SJ, Erzurum SC (2003) Impaired innate host defense causes susceptibility to respiratory virus infections in cystic fibrosis. *Immunity* **18:** 619-630

Zimmermann N, King NE, Laporte J, Yang M, Mishra A, Pope SM, Muntel EE, Witte DP, Pegg AA, Foster PS, Hamid Q, Rothenberg ME (2003) Dissection of experimental asthma with DNA microarray analysis identifies arginase in asthma pathogenesis. *J Clin Invest* **111:** 1863-1874

Zumft WG (1997) Cell biology and molecular basis of denitrification. *Microbiol Mol Biol Rev* **61:** 533-616